The molecular dissection of host manipulation by *Toxoplasma gondii* bradyzoites

Simona Seizova

0000-0002-3703-4824

Submitted in total fulfilment of the requirements of the degree of
Doctor of Philosophy

March 2020

The Walter and Eliza Hall Institute of Medical Research,
The Department of Medical Biology,
The University of Melbourne

Abstract

Toxoplasma gondii is an obligate intracellular parasite, which chronically infects one-third of the world's population. *Toxoplasma* infection severely affects immune-compromised individuals, resulting in birth defects, blindness, or brain encephalitis. Individuals often become infected through the consumption of contaminated food and water sources. *Toxoplasma* has two life stages during the lytic life cycle, the fast disease-causing tachyzoites and the chronic bradyzoites. Following host cell invasion, *Toxoplasma* tachyzoites extensively manipulate their host cell by exporting a distinct repertoire of effector proteins across the newly-established parasitophorous vacuole. This process interferes with the hosts transcriptional program and is thought to enable parasite persistence and dissemination in spite of the host's immune response. Eventually, *Toxoplasma* forms bradyzoite cysts in the visceral organs, which are a reservoir for disease reactivation. In the current scientific literature (which I review in *Chapter 1*) the disparity in our knowledge between tachyzoite- and bradyzoite-host interactions is large. Almost nothing is known on how this chronic-stage of infection persists post-cyst formation and what role host manipulation plays in latency. Therefore, in this thesis I aim to understand whether *Toxoplasma* bradyzoites modulate the host transcriptional response for their survival and, if so, what role could dense granule protein export have in this process. *Chapter 3* explores the host transcriptional profile of bradyzoite containing cells using RNA sequencing and what role host manipulation plays in latency. I show that bradyzoite-containing host cells have a unique transcriptional landscape when compared to tachyzoite infection, and, by pairing this technique with protein export deficient parasites, I show that many of these changes are dependent parasite protein export. In *Chapter 4*, I investigate whether the known tachyzoite effector proteins have a function in chronic infection. IST, an inhibitor of host IFNγ signalling, was identified as the only known tachyzoite effector to be expressed, synthesised, and exported in bradyzoites, suggesting a role for this effector protein in chronic stage. Furthermore, I demonstrate that effector proteins are critical in protecting bradyzoite infected host cells from undergoing cell death upon IFNγ-mediated cell death, thus enabling cyst persistence. To this end, I have proposed three models, outlined in *Chapter 5*, which are supported by my findings in *Chapter's 3* and *4*. This thesis explores bradyzoite-host interactions to interrogate the possible mechanism behind *Toxoplasma's* lifelong infections.

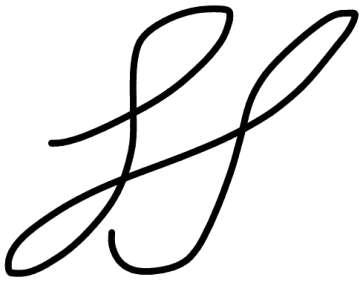
Declaration

This is to certify that:

This thesis comprises only my original work towards the degree of the Doctor of Philosophy except where indicated in the preface

Due acknowledgement has been made in the text to all other material used and provided by personal correspondence with colleagues and collaborators

The thesis is less than 100,000 words in length, exclusive of tables, figure legends, maps, bibliographies and appendices.



Simona Seizova

Preface

This work was undertaken at the Walter and Eliza Institute of Medical Research (WEHI), in the laboratory of Associate Professor Christopher Tonkin. I was supported by an Australian Postgraduate Award Scholarship through the University of Melbourne, a WEHI postgraduate scholarship, and the WEHI Edith Moffatt Scholarship.

The results in this thesis are thanks to my wonderful collaborators. These individuals have contributed the following:

Chapter 3:

Associate Professor Christopher Tonkin conceived ideas and provided guidance.

Dr. Alexandra Garnham analysed the RNA sequencing, with collaboration and guidance from me.

Dr Michael Coffey made the CRISPR/Cas9 guide for ASP5 and created the GRA24-3xMYC plasmid used.

Dr. Lachlan Whitehead developed the custom ImageJ macro for image analysis to determine MYR1 cyst area.

Dr. Stephen Wilcox provided guidance with library preparation and ran the Illumina sequencing run.

Dr. Anita Koshy kindly provided the parasite line Pru Δ*hx* toxofilin-Cre (mCherry^{+}) found in Koshy et al. (2010).

Live FACS sorting was completed by WEHI's flow cytometry team.

Chapter 4:

Associate Professor Christopher Tonkin conceived ideas and provided guidance.

Dr Michael Coffey originally haemagglutinin tagged GRA16 and IST in the Pru D*ku80* lines.

Dr. Lachlan Whitehead developed the custom ImageJ macros for image analysis used to determine export ratios.

Dr. Giel van Dooren and Dr. Azadeh Seidi made the SAG_{DGPI}APEX2-MYC plasmid.

Leon Connor used this to make the parasite line in Pru Δ*hx* toxofilin-Cre (mCherry^{+}).

Dr. Nicole McKenzie (from Assoc. Prof. Ethan Goddard-Borger's laboratory) produced biotin phenol in house.

Dr. Roberto Bonelli assisted with fitting of trendline for figure 4.7F.

All RNA sequencing data was completed by Dr. Alexandra Garnham during the data analysis in Chapter 3.

Live FACS sorting was completed by WEHI's flow cytometry team.

Data from *Chapter's 3* and *4* (including relevant methods) have been produced into an original manuscript (Seizova *et al.*[1]). This manuscript is not currently published or submitted to a peer-reviewed journal. However, it is common practice in my field to submit to bioRvix, which is an open access preprint repository for the biological sciences and involves no peer-reviewed process. I submitted my manuscript to bioRvix in June 2019 (see appendix for manuscript). I assess my contribution to this manuscript as 75%. The manuscript was written by me during my PhD, and edited by Assoc. Prof. Christopher Tonkin and Dr. Alexandra Garnham. Experimental contributions are indicated in this preface above. There are sections in *Chapter's 2, 3* and *4* that are taken from this unpublished manuscript, which have either been left unchanged (*the whole paragraph*) or edited (*majority of the paragraph)*. This is in accordance with University of Melbourne regulations regarding self-citation, which can be found on the website: https://gradresearch.unimelb.edu.au/preparing-my-thesis/thesis-with-publication, under "I want to include text in my thesis that I wrote for a publication but the publication is not appropriate to include in its entirety in my thesis. How do I include the text without self-plagiarising?"

In the following list I highlight where in my thesis I used sections from my unpublished manuscript[1]:

Chapter 2:

All the methods in this section are taken from the above mentioned manuscript.

Chapter 3:

3.1: Paragraph 1, *the majority of the paragraph*

Paragraph 4, *the third sentence*

3.2.1: Paragraph 1, *the first sentence*

Paragraph 2, *the fourth, seventh, and eighth sentences*

Paragraph 3, *the majority of the paragraph*

3.2.2 Paragraph 1, *the whole paragraph*

Paragraph 2, *the fourth, fifth, and sixth sentences*

Paragraph 3, *the majority of the paragraph*

3.2.3 Paragraph 1, *the first sentence*

Paragraph 2, *the majority of the paragraph*

3.2.4 Paragraph 1, *the first two and the tenth-to-thirteenth sentences*

Paragraph 2, *the majority of the paragraph*

Paragraph 3, *the whole paragraph*

3.3 Paragraph 1, *the whole paragraph*

Paragraph 2, *the whole paragraph*

Paragraph 3, *the first eight sentences*

Paragraph 4, *the first sentence*

Paragraph 8, *the first five sentences*

3.4 Sections: '*Bradyzoite sample collection and RNA extraction for sequencing'*

'Library preparation and transcriptome sequencing'

'Transcriptome analysis'

Chapter 4:

4.1 Paragraph 1, *the fourth sentence*

Paragraph 3, *the second, third, fourth, sixth, and seventh sentences*

4.2.2 Paragraph 1, *the majority of the paragraph*

Paragraph 2, *the first four sentences*

Paragraph 3, *the first and last sentence*

Paragraph 4, *the first, second, seventh, and eighth sentences*

4.2.3 Paragraph 1, *the second, third, and the seventh-to-eleventh sentences*

Paragraph 2, *the majority of the paragraph*

Paragraph 3, *the first sentence*

Paragraph 4, *the second, third, sixth, and seventh sentences*

4.2.4 *The whole section*

4.3 Paragraph 1,*the second and fourth sentences*

Paragraph 2, *the majority of the paragraph*

Paragraph 4, *the second and third sentences*

Paragraph 5, *the eighth and ninth sentences*

Paragraph 7, *the whole paragraph*

Paragraph 8, *the ninth sentence*

Paragraph 10, *the last sentence*

4.4 Sections: '*Interferon gamma stimulation'*

'*Live cell microscopy'*

'Flow cytometry'

'Compound 1 and BIPPO treatment'

'Statistical analysis'

Acknowledgements

I wish there was a word that could truly encompass the sheer gratitude I have for my supervisor, Associate Professor Christopher Tonkin. The encouragement and support you've given me throughout this candidature (within and out of the lab) have really made an impact on me. Your care and openness make the lab a welcoming and loving place, one that'll be sorely missed. Thank you. I'm sure you're going to miss not having a Kiwi around to make jokes about.

To Associate Professor Justin Boddey, secondary supervisor, thank you for kind words and pep talks. The many words of advice and reassurance in the corridor or as you were passing by often made my day.

A big big thank you to Dr. Alexandra Garnham, who not only put a lot of time and effort into my project but taught me so much about data analysis. You've always been accommodating to my requests and have take time to repeatedly explain things to me. I am more confident in my skills to evaluate sequencing data and for that I have you to thank.

To the Tonkin lab, past and present, thank you for making the lab and entertaining, loving and exciting place to be. I've been lucky to join a lab where you feel-like part of a family, full of culture room antics, chore disputes, and office banter. In particular, I'd like to thank Mary Lou. Starting with someone who was also new to the lab was a blessing in disguise. There is no one else I would rather make experimental mistakes with. I could not have asked for a better lab mate to 'grow up' with. Thank you to Dr. Shiraz Tyebji for being my partner-in-crime in work that never made it into this thesis. Your mentorship was something I was not expecting but am so very thankful for. And Dr. Alex Uboldi. You have seen many-a-students come through the lab, and you are to us a beacon of calm, rational thinking paired with the most magically skilled hands. You are the backbone of the lab, a constant, and I have learnt a lot from you. You are a role model of a what a skilled, reliable, and trustworthy scientist should be. Thank you.

Thank you to everyone at WEHI who has made my time the most enjoyable and inspiring place to be. From the communications team who have given me to so many opportunities, to Rosie who always welcomes me with a smile, and to Connie and Alf who clean up after me and often

feed me during my late nights. The Infection and Immunity Division has been a wonderful wider team to be a part of. The hustle-bustle and liveliness of the division have really added to the community feel. In particular, thank you to Stella Kyvetos who holds the division together, keeps everything running smoothly, and ensures we are all taken care of. Thank you to the curry crew who first welcomed me into their fold and to the multiple WESA teams who are always trying to better student lives (shout-out to WESA2018) one pizza slice at a time. Most importantly, to the friends I have made here, thank you. Our picnics, dinners and general antics have been a place of solace and pure joy. I will treasure these memories forever.

To my wonderful flatmates, Robyn, Luuk, and Ellen. Thank you for being a wonderful substitute family and listening to my rants over the kitchen sink. Your support at home feeds my success at work.

Thank you to my friends in New Zealand. Especially Elena, who, despite the physical absence and distance, has continued to be an active member in my life. I am grateful to have such an inspiring woman in my life.

To my dearest friend, Morgana. I cannot thank you enough. Truly. I could not have asked for a better friend and confidant. Your stamp is on this thesis, from editing it mere days before it was due, to the almost-weekly dinners, warm hugs, insightful discussions. Your words of love mean the world– thank you.

And finally, to my loving family. These four years have been tough for us, but I am grateful to be in it together.

There isn't a word strong enough to express my gratitude to my loving husband, Byron. Byron you are amazing. You have always kept me grounded and continue to make me laugh. Your spontaneous visits towards the end brought some much-needed light into my life. Thank you for sharing the precious time we had together on your visits so I could attend to my babies (parasites).

To my parents. Thank you for taking the leap to leave the comfort of your homes and culture to give me a better chance at life. I admire what you have done and sacrificed for this family. This thesis is evidence of not just my achievements, but also of yours. Thank you.

Abbreviations

μ	micro
α	alpha or antibody against
β	beta
Δ	Deletion/knockout
γ	gamma
λ	lamda
°C	Degrees Celsius
μm	micro meter
μM	micro molar
APEX2	Apurinic Apyrimidinic Endodeoxyribonuclease 2
ApiAP2	Apicomplexan Apetala2
ASP5	Aspartyl Protease 5
BAG1	Bradyzoite Antigen 1
BDF1	Bradyzoite Formation Deficient 1
BIPPO	5-Benzyl-3-isopropyl-1H- pyrazolo[4,3- d]pyrimidin-7(6H)-on Biotin
BP	Phenol
bp	Base pair
BSA	Bovine serum albumin
Cas9	CRISPR-associated protein 9
CO_2	Carbon dioxide
CPM	Counts Per Million
CRISPR	Clustered-regularly interspaced short palindromic repeats SAG-related
CST1	sequence SRS29B
Da	Daltons
DAPI	4’,6-diamidino-2-phenylindole
DBA	Dolichos biflorus Agglutinin
DCs	Dendritic cells
DEGs	Differentially Expressed Genes
DHFR	Dihydrofolate reductase

DNA	Deoxyribonucleic acid
DS	Data set
FACS	Fluorescence-activated cell sorting
g	gram
GBPs	Guanylate-Binding Proteins
GFP	Green Fluorescent Protein
GRA	Dense granule protein
gRNA	Guide RNA for Cas9
H_2O_2	Water
HA	Haemagglutinin
HCE1/TEEFGR	Host Cyclin E 1 / *Toxoplasma* E2F4-associated EZH2-inducing gene regulator
HMA	Host mitochondria association
HXGPRT or *hx*	Hypoxanthine phosphoribosyltransferase
ICN	inner cyst network
IFN	Interferon
IgG	Immunoglobulin G
IL	Interleukin
IMC	Inner membrane complex
IRGs	Immune Related GTPases
IST	Inhibitor of STAT1 Transcription
IVN	inner vacuolar network.
JAK	Janus Kinase
kDa	kiloDaltons
KO	Knock out
L	litre
LDH2	Lactase Dehydrogenase 2
Log	logarithm
MAF1	Mitochondrial association factor 1
MAPK	Mitogen activated protein kinase
mg	milligram
mL	millilitre
MOI	Multiplicity of infection

MYR	c-Myc-regulation
NA	North America
NF-κB	Nuclear Factor Kappa B
nm	nano meter
PBS	Phosphate-buffered saline
PEXEL	*Plasmodium* export element
Pf	*Plasmodium* falciparum
PM	Plasma membrane
Pru	Pruginaud (type II) strain of *Toxoplasma gondii*
PTEX	*Plasmodium* translocon of exported proteins
PV	Parasitophorous vacuole
PVM	Parasitophorous Membrane
QTL	Quantitative trait loci
RH	RH (type 1) strain of *Toxoplasma gondii*
RNA	Ribonucleic acid
RNAseq	Sequencing of reverse-transcribed RNA to determine abundance
ROP	Rhoptry bulb protein
RPKM	Reads Per Kilobase of transcript, per Million mapped reads
RT	Room temperature
SA	South America
SAG1	Surface Antigen 1
Spp.	Species.
SRS9	SAG-Related Sequence 9
STAT	Signal transducer and activator of transcription
TEXEL	*Toxoplasma* export element
Tg	*Toxoplasma gondii*
TGME49_	Prefix before genome accession number on https://Toxodb.org
TH1	Type 1 T helper cells
TH2	Type 2 T helper cells
WEHI	The Walter and Eliza Hall Institute of Medical Research
WIP	WAVE complex-Interacting Protein
WT	Wild type

Table of Contents

Abstract III

Declaration IV

Preface V

Acknowledgements IX

Abbreviations XI

Table of figures XVIII

List of tables XIV

1 Chapter 1: Literature review 1

1.1 *Toxoplasma gondii* 2

1.1.1 Toxoplasmosis: the disease 2

1.1.2 *Toxoplasma*'s origins and strain diversity 3

1.1.3 *Toxoplasma*'s life cycle 4

1.2 *Toxoplasma* tachyzoites 7

1.2.1 Cell compartments and morphology 7

1.2.2 Asexual lytic cycle 8

1.2.2.1 Motility 11

1.2.2.2 Invasion 11

1.2.2.3 Replication 12

1.3 *Toxoplasma* bradyzoites 13

1.3.1 The bradyzoite 13

1.3.2 Bradyzoite differentiation 14

1.3.3 The cyst wall and it's development 17

1.4 Parasite dissemination and brain infection 19

1.4.1 Parasite dissemination 19

1.4.2 Crossing the blood brain barrier 19

1.4.3 Cell tropism in the central nervous system 20

1.5 *Toxoplasma* host manipulation 21

1.5.1 Host transcriptional changes 22

1.6 *Toxoplasma*-secreted host-modifying proteins 23

1.6.1 Rhoptry proteins 23

1.6.1.1 ROP18/ROP5/ROP17 complex: inhibitors of intracellular clearance and key virulence factors 24
1.6.1.2 ROP16 and ROP38: transcription modulators 25
1.6.1.3 WIP: modulator of cell migration 26
1.6.2 Dense granule proteins 26
1.6.2.1 PV dense granule proteins 29
1.6.2.1.1 MAF1: mitochondrial recruitment factor 29
1.6.2.1.2 GRA15: NF-kB activator 30
1.6.2.2 Exported dense granule effector proteins 31
1.6.2.2.1 GRA16: cell cycle regulator 31
1.6.2.2.2 GRA24: pro-inflammatory agitator 32
1.6.2.2.3 IST: inhibitor of STAT1 transcription and immune evasion 32
1.6.2.2.4 GRA18: pro-inflammatory dampening 34
1.6.2.2.5 HCE1/TEEGR: E2F transcription modulator 34
1.6.2.2.6 GRA28: the unknown 35
1.7 Trafficking of exported effector proteins 35
1.7.1 *Toxoplasma* export signal 35
1.7.2 Tachyzoite protein trafficking 37
1.7.2.1 Protein export 37
1.7.2.2 Export machinery 38
1.7.3 Nutrient trafficking 39
1.7.4 Bradyzoite protein trafficking 42
1.8 Thesis aims 44

2 Chapter 2: General Methods and Materials 45
2.1 Host cell culture 45
2.2 Parasite culture 45
2.3 *In vitro* bradyzoite differentiation 45
2.4 Parasite transfections 46
2.5 Immunofluorescence Assays (IFA), microscopy and data quantification 46
2.6 Western blot 47
2.7 Statistical Analysis 47

3 Chapter 3: Bradyzoite-induced host cell transcriptional changes **52**

3.1 Introduction **53**

3.2 Results **55**

3.2.1 Analysing i*n vitro* differentiated bradyzoites 55

3.2.2 Bradyzoites distinctively alter the host transcriptome 64

3.2.3 ASP5 and MYR1 in bradyzoites 72

3.2.4 MYR1-dependent protein export plays a key role in host transcription modification by bradyzoites 77

3.3 Discussion **87**

3.4 Additional material and methods **93**

3.4.1 Plasmid constructs, transfections and parasites lines 93

3.4.2 Microscopy and cyst size quantification 94

3.4.3 *In vivo* infections 94

3.4.4 Quantitative PCR for *in vivo* parasites 95

3.4.5 Bradyzoite sample collection and RNA extraction for sequencing 95

3.4.6 Library preparation and transcriptome sequencing 96

3.4.7 Transcriptome analysis 96

4 Chapter 4: A bradyzoite effector protein important for parasite persistence **99**

4.1 Introduction **100**

4.2 Results **103**

4.2.1 Biotinylation of the secretory pathway 103

4.2.2 IST is expressed and exported in bradyzoites 110

4.2.3 Bradyzoites supress the Interferon gamma pathway through MYR1-dependent IST export 118

4.2.4 Protein export is important for survival of bradyzoite-containing cells upon IFNγ challenge 126

4.3 Discussion **132**

4.4 Additional material and methods **138**

4.4.1 Plasmid constructs, transfections and parasites lines 138

4.4.2 APEX2 driven biotinylation 139

4.4.3 Microscopy and export and IRF1 quantification 140

4.4.4 Interferon gamma stimulation 141

4.4.5 Reverse transcription qPCR 141

4.4.6 Live cell imaging 141
4.4.7 Flow cytometry 142
4.4.8 Compound 1 and BIPPO treatment 142
4.4.9 Statistical analysis 143

5 Chapter 5: Conclusions 144
5.1 Opening remarks 145
5.2 Models of export supporting bradyzoite survival 146
5.2.1 Model 1: Tachyzoites export effector proteins that support chronic infection 147
5.2.2 Model 2: Bradyzoites export unique proteins across the cyst wall 151
5.2.3 Model 3: Bradyzoites export proteins before the establishment of the cyst wall 152
5.3 Future directions 153

Appendix A – Seizova et al. (2019)[1] Manuscript 155
Appendix B – Data set 1: Data alignment, normalisation, filtering, and exploration 219
Appendix C – Data set 2: Data alignment, normalisation, filtering, and exploration 236
Appendix D – Data set 1 and 2, data combination process 250
References 260

Table of Figures

Figure 1.1 –	*Toxoplasma* transmission	5
Figure 1.2 –	Stages of *Toxoplasma*'s asexual life cycle	6
Figure 1.3 –	Parasite morphology	9
Figure 1.4 –	Tachyzoite host cell manipulation by rhoptry and dense granule proteins	27
Figure 1.5 –	Parasitophorous vacuole membrane (PVM) trafficking in tachyzoites	40
Figure 3.1 –	Analysing *in vitro* bradyzoite development	57
Figure 3.2 –	*In vitro* produced bradyzoites exhibit bradyzoite transcriptional markers while decreasing tachyzoite transcriptional markers	60
Figure 3.3 –	Transcriptional landscape of bradyzoite-containing host cells is different to tachyzoite infection	62
Figure 3.4 –	Bradyzoites and tachyzoites share a number of host cell gene changes	65
Figure 3.5 –	Bradyzoites and tachyzoites modulate different host pathways	68
Figure 3.6 –	ASP5 knockouts do not make functional cysts *in vitro*	73
Figure 3.7 –	MYR1 is expressed in bradyzoites	75
Figure 3.8 –	MYR1 knockouts can produce *in vitro* cysts	78
Figure 3.9 –	MYR1 plays a role in regulating host cell transcriptional changes in bradyzoite containing cells	81
Figure 3.10 –	A proportion of bradyzoite specific pathway changes are dependent on MYR1	85
Figure 4.1 –	Biotinylation of proteins in the secretory pathway and parasitophorous vacuolar (PV) space (tachyzoites).	104
Figure 4.2 –	Biotinylation of proteins in the secretory pathway and beyond in bradyzoites	107
Figure 4.3 –	Tachyzoite effector protein's expression and localisation during bradyzoite stages	111
Figure 4.4 –	IST export over time	114
Figure 4.5 –	IST is produced and exported by bradyzoites	116
Figure 4.6 –	IST and MYR1 knockouts prevent IST export in bradyzoites	119
Figure 4.7 –	Bradyzoite exported IST inhibits IRF1 expression	121
Figure 4.8 –	MYR1 affects IFN host pathways	124
Figure 4.9 –	Depletion of MYR1 prevents cyst persistence upon IFNγ stimulation	127
Figure 4.10 –	Depletion of MYR1 induces host cell death upon IFNγ stimulation	129
Figure 5.1 –	Models of export supporting bradyzoite survival	148

List of Tables

Table 1 –	CRISPR guides	48
Table 2 –	Primers for protospacer replacement	48
Table 3 –	Sequencing primers	48
Table 4 –	Oligo sequences for IST 3'prime homologous recombination	48
Table 5 –	Primers used in the amplification of knockout and HA-tag inserts, qPCR, and for sequencing CRISPR/Cas9 knockouts	49
Table 6 –	Primary antibodies used for IFA, Western blot and flow cytometry	50
Table 7 –	Secondary antibodies and conjugates used for IFA, Western blot and flow cytometry	50
Table 8 –	RIPA Lysis Buffer Composition, made up in H_2O for APEX2 experiments	51

Chapter 1: Literature Review

1.1 *Toxoplasma gondii*

Toxoplasma gondii, like all other apicomplexan species including *Plasmodium spp* (malaria), *Cryptosporidium* (cryptosporidiosis, a severe diarrheal disease) and other agricultural parasites, is a single-celled eukaryotic parasite that must invade host cells for its survival and proliferation. To infect their host, Apicomplexa use a series of apically located structures and organelles, after which the phylum is named (see *section 1.2* for more details). Unlike other genera in the phylum, *Toxoplasma* has only one species named *gondii* after the small rodent it was first discovered in, the common gundi (*Ctenodactylus gundi)*[2]. *Toxoplasma gondii* is now known to infect a diverse range of animals, including birds and mammals. *Toxoplasma* is a zootonic parasite and its lack of host specificity means it impacts are wide reaching and include conservation, agriculture, and human health.

1.1.1 Toxoplasmosis: the disease

Toxoplasma causes toxoplasmosis, which is a group of disease pathologies. *Toxoplasma* infection is determined by seroconversion, measured by anti-*Toxoplasma* IgGs[3]. Between 10-80% of the human populations globally are chronically infected, depending on the region[3,4]. In humans, the common route of infection is through the consumption of cyst contaminated food, including uncooked meat containing tissue cysts[5], and oocyst contaminated water[6]. Pathogenesis is caused by the lytic stage of the parasite where rapid and repeated rounds of invasion, replication, and egress from host cells cause damage to tissues (discussed in *section 1.2.2*).

Toxoplasma is an opportunistic parasite and the severity of infection most often depends on the individual's immune status. Immune competent individuals are often asymptomatic, but infection often results in mild flu-like symptoms before immune pressure resolves the active infection. The immune system appears unable to clear parasites that develop into dormant-encysted forms. These dormant forms enable the *Toxoplasma* to persist for the host's lifetime, which increases the risk for adults who become immune compromised, for example those that develop HIV/AIDS[7,8], cancer[9], or are on immune suppressive drugs[10]. Without immune

pressure dormant parasites can reactivate causing inflammation and tissue damage that results in progressive blindness (ocular toxoplasmosis)[11] or neurological complications[12]. Pregnant individuals are another high-risk group, in particular if they are naive to infection. Parasites can cross the blood-placental barrier resulting in major birth defects, a disease collectively known as congenital toxoplasmosis[13]. Infants that survive can develop toxoplasmic retinochoroiditis (ocular toxoplasmosis), where cycles of parasite reactivation in the eye can cause blindness due to retinal tissue damage[14]. *Toxoplasma* has a significant impact in South America (SA) communities, which have some of the highest rates of congenital infection and as a result ocular toxoplasmosis[15]. For example, in Brazil 87% of children born with congenital Toxoplasmosis will have significant visual impairments by the age of four[11]. The high rate and severity of infection in SA has been linked to the diversity of strains in the region and their virulence[15,16]. Rougier *et al.* (2017)[16] argue that the high genetic diversity in SA may also prevent a sufficient immune response to a new infection in previously infected individuals. The possibility of re-infection goes against the standing dogma of *Toxoplasma* infection: once infected, the presence of lifelong cysts results in a protective but non-sterilizing infection.

1.1.2 *Toxoplasma's* origins and strain diversity

Although the *Toxoplasma* genus has only one species, it has multiple strains which range in virulence[17,18]. *Toxoplasma's* ability to transmit between intermediate hosts without going through the primary host and sexual replication (the life cycle is discussed in *section 1.1.3*) is linked to the low strain diversity seen in North America (NA) and Europe[19]. In these regions, three main lineages (type I, II, III), labelled as typical strains, arose through clonal expansion to dominate in NA and Europe[20,21]. The three typical strains are associated with differing virulence outcomes in mice. The most virulent strains are of the type I lineage, whereas type II and III are relatively less virulent and more likely to result in chronic infection[22,23]. In contrast, SA has a wide variety of atypical strains, thought to result from a high rate of sexual reproduction and frequent recombination events[24]. Traditionally, the three typical strains are used in research which delivers homogenous experimental results between laboratories, but as a result, little is known about the virulence factors in atypical strains. Crosses between typical strains followed by Quantitative Trait Locus (QTL) has been a fruitful method of identifying virulence factors[25-

[28]. Genetic crosses were often done between type I parasites and one of the other two avirulent strains. Interestingly, the genetic cross between the two avirulent strains has produced progeny that are more virulent that their parents[24]. This suggests high levels of sexual reproduction drives virulence diversity and could explain highly virulent atypical strains in regions like SA.

The phylogenetic analysis of *Toxoplasma* isolates has also suggested that northern SA is likely the geographical origin of modern *Toxoplasma* species[29]. The re-establishment of the land bridge between NA and SA introduced *Toxoplasma* to SA. The following speciation explosion in both Felidae and Muridae families in SA likely resulted in the subsequent diversification of *Toxoplasma*[29]. The small number of founding lineages worldwide suggests diversification was likely followed by strong selection which swept through the population[30,31] before *Toxoplasma* spread upwards again to NA and later beyond to Asia, Europe and Africa[29]. Another model suggests the diversity seen in SA was also present in NA prior to a extinction event that drastically reduced primary hosts leading to a bottleneck of *Toxoplasma* strains[31,32]. As a consequence, lineages that could more easily spread between intermediate hosts dominated, and in this case it was type II. Expansions in Asia, Europe and Africa have been linked to the development of human agriculture which again favoured intermediate host transmission[17]. More recently the spread of the domestic cat and common rodent species by humans may have contributed to certain *Toxoplasma* strains[33-35]. Human aided-spread may have resulted in genetic admixture[32] and smaller founder populations[36] with a selective advantage in a more domesticated world leading to clonal expansion and establishment of the three typical strains[37].

1.1.3 *Toxoplasma's* life cycle

Like many apicomplexan parasites, *Toxoplasma* goes through a complex life cycle, transitioning between different hosts and alternating between asexual and sexual forms. *Toxoplasma* completes its sexual cycle in the small intestine of felines (Fig. 1.1). Here *Toxoplasma* invades entero-epithelial cells, where parasites undergo several rounds of replication before gametogony is initiated and oocysts are formed. Oocysts have three wall-like structures that

Figure 1.1

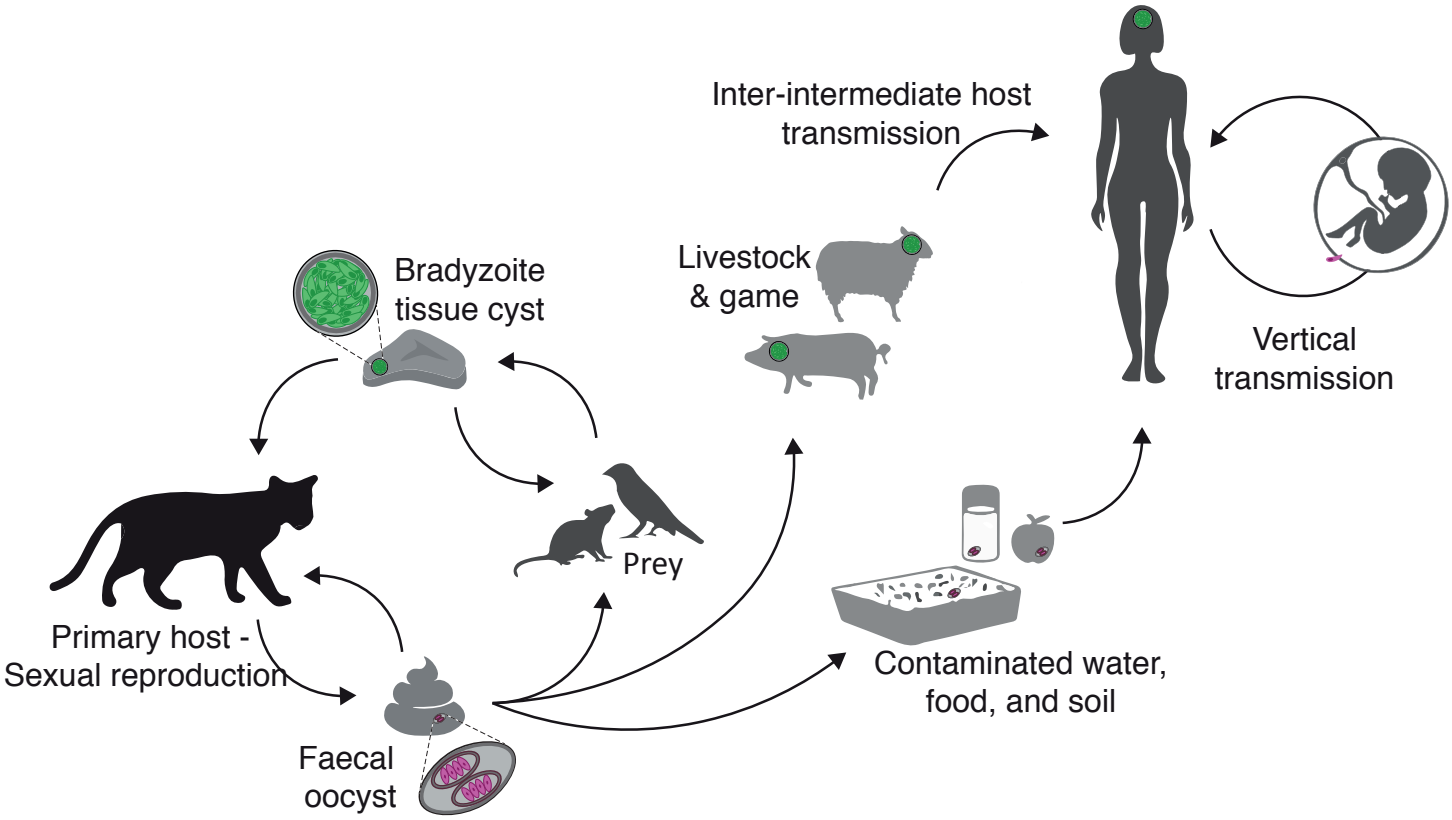


Figure 1.1 – *Toxoplasma* transmission

Felidae species infected with Toxoplasma secrete oocyst into the environment via faecal matter. These oocysts are consumed by an intermediate host, which becomes infected and forms bradyzoite tissue cysts in the muscle and brain. Toxoplasma completes the life cycle when intermediate hosts are preyed upon my felines. Humans can be infected by the consumption of contaminated water, soil and food sources or through infected livestock and game animals that carry tissues cysts. Cases of vertical transmission can occur in preg-nant individuals.

Figure 1.2

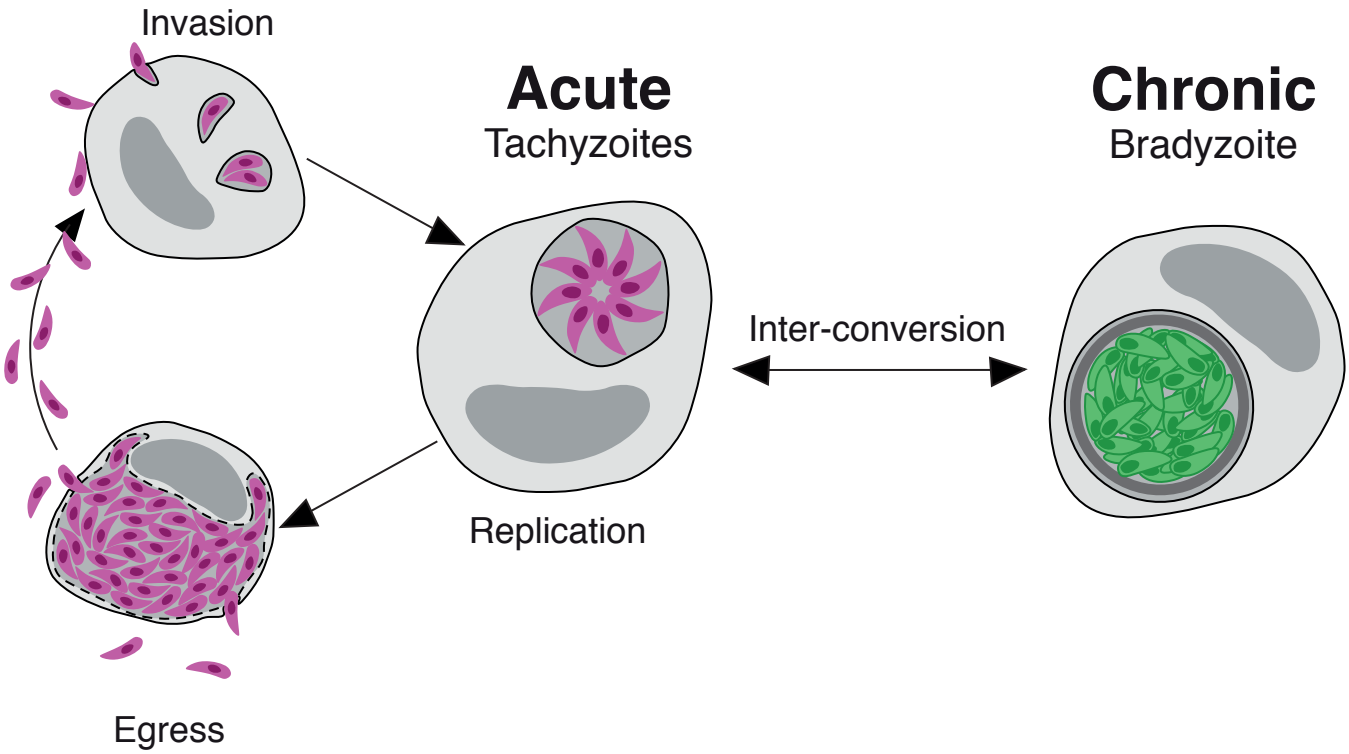


Figure 1.2 – Stages of *Toxoplasma's* asexual life cycle

Extracellular tachyzoites glide until they encounter a host cell. They attach to the host cell, re-orientate them-selves and use their apical ends to actively invade the cell. As they invade, they used the host cell membrane to form the parasitophorous vacuole (PV) and membrane (PVM). Within the PV, tachyzoites undergo multiple rounds of replication before eventually egressing out of the host cell, lysing the host cell and killing it in the process, and the cycle repeats. Some during the replicative stage, some parasites differentiate into bradyzoites and form a cyst wall underneath the PVM, which makes up the chronic stage of the life cycle.

Image inspired by Zhang, M., Joyce, B. R., Sullivan, W. J. & Nussenzweig, V. Translational control in *Plasmodium* and *Toxoplasma* parasites. *Eukaryotic cell* 12, 161-167 (2013).

enclose two sporocysts, which in turn contain four sporozoites[38]. After faecal shedding, which can last up to two weeks, the oocysts can survive up to 12 months depending on the conditions[39,40]. Oocytes can be taken up by an intermediate host or another definitive host via contaminated water or food sources[41] (Fig. 1.1). Intermediate hosts of *Toxoplasma* are vast and include terrestrial and aquatic wildlifekrishnam[42], livestock[43], and humans. Upon ingestion, *Toxoplasma* will differentiate into the fast replicating tachyzoites, which disseminate throughout the host, and leads to the formation of tissue cysts (Fig. 1.2). The exact mechanisms by which tachyzoites differentiate into bradyzoites is unknown, but they readily form in the skeletal and cardiac muscle, and in the central nervous system[39]. Here the parasites reside for the life-time of the host, unable to be cleared by the immune system, where they apparently undergo slow turnover[44]. Bradyzoite infected tissue can also be a source of transmission; whether by feline predation and completion of the lifecycle, or predation by another animal bypassing the sexual cycle completely and enabling transmission between intermediate hosts[12].

1.2 *Toxoplasma* tachyzoites

1.2.1 Cell compartments and morphology

Tachyzoites are two micrometres wide and six micrometres long with a rounded posterior end that narrows towards the anterior (Fig. 1.3A)[38,39]. *Toxoplasma* has typical eukaryotic organelles such as a nucleus, which is surrounded by the endoplasmic reticulum (ER) and a single Golgi stack that is anterior to the nucleus[39]. Each zoite form also has a single elongated and unreticulated mitochondrion that is located around the basal periphery[45]. Most Apicomplexa also have a relict non-photosynthetic plastid called the 'apicoplast'. The apicoplast is derived from a secondary endosymbiotic event in which an alga was taken up by the common ancestor the of Apicomplexa phylum[46]. Interestingly, the apicoplast has been secondarily lost in some genera like *Cryptosporidium*[47,48]. The most striking feature of all apicomplexan zoite forms is the apical organelles, which unite the phylum[49]. The dominant apical organelles are the rhoptries, which are tethered to the apical end and are required for the formation of the parasitophorous vacuolar membrane and contain effector proteins[50]. Micronemes are smaller

ovoid shaped apical organelles, that are numerous in number and contain adhesins and other factors required for motility and egress[51]. Dense granules are not apical organelles, but like the rhoptries and micronemes are secretory organelles. They are electron-dense and are found throughout the body of the parasites, and contain effector proteins and molecules required for nutrient acquisition[52].

The cytoplasm of Apicomplexan parasites are enclosed by a three-membrane structure called the pellicle. The outermost membrane is the plasma membrane (PM), and the inner two membranes are formed by a network of flattened vesicles called the inner membrane complex (IMC) (Fig. 1.3C), which are unique to Apicomplexan[38]. Placed between the PM and the IMC is the actomyosin-based glideosome, which provides the force behind parasite motility and invasion[53,54]. The IMC is situated under the PM other than small regions at the very apex and posterior of zoites[38]. The apical complex is most apically located and comprises polar rings made from microtubules, which also give rise to filaments that radiate down the body of the cell [55]. The number of these long microtubules differs depending on the species of Apicomplexa, but in the case of *Toxoplasma* there are 22 approximately 30 nm apart[56,57]. Some Apicomplexan species, including *Toxoplasma*, have a cone-like structure made up of microtubules called the conoid (Fig. 1.3C), which is extruded when parasites are extracellular[55]. Together these organelles each play important roles in motility, invasion and manipulation of host cells, which I will discuss further throughout this chapter.

1.2.2 Asexual lytic cycle

All apicomplexan parasites are obligatory intracellular parasites, to enable host nutrient scavenging during replication. Therefore a parasite's ability to engage with a host cell and invade is vital to its continued survival. Extracellular tachyzoites use a specialised complex to glide and engage with nucleated host cells before invasion. Once inside, *Toxoplasma* suppresses gliding motility and initiates asexual replication. Here the parasites synchronously and exponentially replicate, before activating cell lysis to release daughter parasites ready to infect a new host cell (Fig. 1.2). See Blader *et al.* (2015)[58] for a more in-depth review of the process.

Figure 1.3

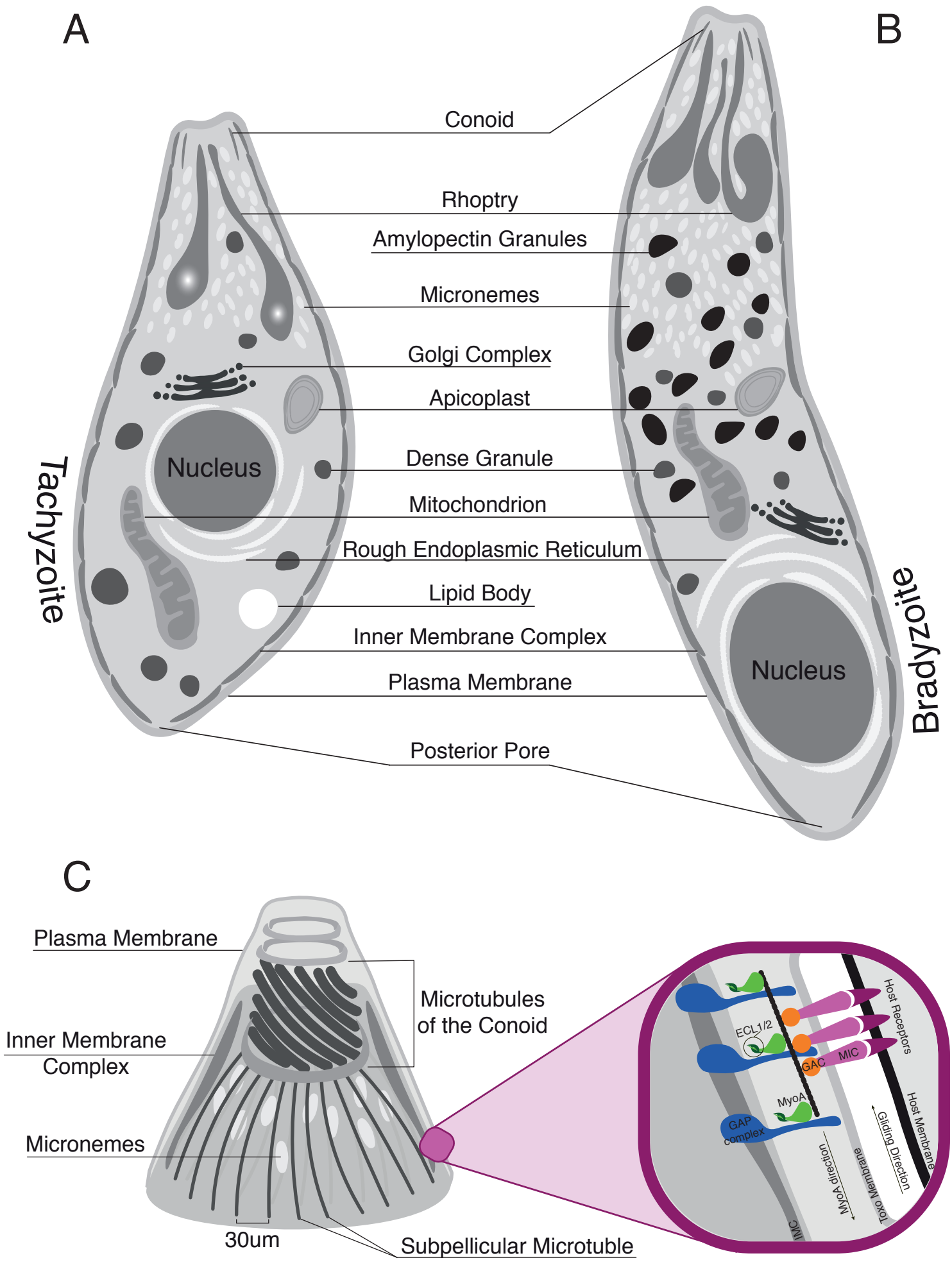

A
B
Conoid
Rhoptry
Amylopectin Granules
Micronemes
Golgi Complex
Apicoplast
Nucleus
Dense Granule
Mitochondrion
Rough Endoplasmic Reticulum
Lipid Body
Inner Membrane Complex
Plasma Membrane
Posterior Pore
Tachyzoite
Nucleus
Bradyzoite
C
Plasma Membrane
Inner Membrane Complex
Micronemes
Microtubules of the Conoid
30um
Subpellicular Microtuble
Host Receptors
ECL1/2
MIC
GAC
MyoA
GAP complex
MyoA direction
Toxo Membrane
Gliding Direction
Host Membrane
IMC

Figure 1.3 – Parasite morphology

Schematic of tachyzoites (A) and bradyzoites (B) comparing organelle compartments and features. (C) The apical complex and its microtubule structure, with a schematic of the glideosome and how MyoA and MIC work to create gliding motility.

Note: features are not to scale, and some features are adjusted for conserve space.

Image inspired by Dubey, J. P., Lindsay, D. S. & Speer, C. A. Structures of *Toxoplasma gondii* tachyzoites, bradyzoites, and sporozoites and biology and development of tissue cysts. *Clinical microbiology reviews* 11, 267-299; 0893-8512 (1998).

1.2.2.1 Motility

When encountering host tissue, *Toxoplasma* activates it's gliding motility, which is a unique form of substrate-dependent locomotion. Gliding motility powers tissue dissemination and host cell invasion and is absolutely essential for parasite survival[59]. Motility is activated upon environmental cues, causing the exocytosis of microneme organelles, resulting in release of adhesins onto the parasite surface. The glideosome, an actomyosin-based motor that lies underneath the PM and is then activated. It locks onto the short cytoplasmic tails of adhesins dragging them rearward thus driving forward motion[60]. The glideosome comprises a single-head 'type XIV' myosin heavy chain 'MyoA'[59,61] and two light chains MLC1[62] and redundant ELC1 and ELC2[63]. The motor is anchored to the parasite periphery via the glideosome associated proteins (GAPs), a set of scaffolding molecules that maintain the distance between the IMC and PM[64]. The current model suggests that filamentous actin joins to adhesins through the Gliding Associated Connector (GAC) and MyoA, stepping along actin filaments, drags adhesins backwards[65].

1.2.2.2 Invasion

In addition to the glideosome and microneme release, rhoptry secretion is also essential for invasion, but not motility, and there are several factors known to be important for this process[66-68]. During invasion, rhoptries inject Rhoptry Neck (RON) proteins into the host cell membrane and act as receptors for the micronemal proteins, like Apical Membrane Antigen 1 (AMA1). AMA1 directly binds to a C-terminal region of RON2, and complexed with RON4 and RON5, form 'the moving junction' (MJ)[60]. Using the force generated by the glideosome, the parasite is able to pull itself through the ring made by the MJ into the host cell. Although it is uncertain exactly when the rhoptry bulb (ROP) proteins are secreted during invasion, some must be injected into the host cell before commitment to invasion as delivery of ROP occurs even in the absence of invasion[69]. Many of the ROP are involved in perturbing the host cell

anti-microbial response or setting up the parasitophorous vacuole (PV), a membrane barrier separating host from pathogen[70].

The PV and its membrane (PVM) are created during the invasion process. They are thought to be formed the host cell membrane by invagination, in a process not reliant on host endocytic machinery[71]. Because of this, the PVM composition is mostly host-derived; however, during invasion the PVM is decorated with secreted ROP proteins. Proteins from the dense granules (GRA) are the last to be released, after invasion is complete[72]. GRA proteins navigate the construction of the intravacuolar network (IVN), which fills the PV lumen[73]. The IVN structure is made up of membranous tubules to connect individual parasites to each other and to the PVM [74] providing structural organisation[75], a means of sharing vesicle content and the acquisition of nutrients. GRA proteins continue to modify the PV and PVM during infection to create a niche capable of supporting the growth phase of the lytic cycle, providing control over nutrient acquisition and protection against host defence mechanisms[70].

1.2.2.3 Replication

Once the PV has been established tachyzoites start dividing by a process remarkably different from mammalian and yeast cells called endodyogeny[76]. Here, two daughter parasites form within each mother tachyzoite, where the IMC begins to form in close proximity to the duplicated centrosome[77]. Organelle division and segregation between daughters is order; the Golgi is first followed by the nucleus, apicoplast and mitochondrion[78]. The other organelles appear to be either formed *de novo* or can be recycled from the mother cell[79]. After replication is complete, some cellular material is put into the residual body, which is the remanence of the mother cell at the base of the parasite,[38]. The exact role of the residual body is unknown; however, it remains intact as the parasites replicate, leaving separate anterior ends to form the classical rosette structure[80]. Replication occurs synchronously at a doubling rate of approximately six to eight hours, and upwards to 128 parasites per vacuole, depending on the host cell's size[38]. Interestingly, synchrony appears to be reliant on the connection between parasites in the same vacuole, thought to be mediated by the basal connection between parasites within the same vacuole[81]. The mode of binary replication and method of division

means that *Toxoplasma* is able to egress and successfully reinvade at any stage of intracellular replication[82]. This is very different from *Plasmodium spp.* or *Sacocystis* which need to finish the whole replication process to be infectious[76].

1.3 *Toxoplasma* bradyzoites

1.3.1 The bradyzoite

It is during tachyzoite replication that some parasites are pushed into bradyzoite differentiation. Bradyzoites have morphological differences associated with the parasite's new physiological needs. Bradyzoites are elongated and are distinct in organelle morphology and number when compared to tachyzoites (Fig. 1.3B). Bradyzoites have electron-dense rhoptries that fold in on themselves, a posterior nucleus, a larger number of micronemes, and fewer dense granules[38]. They replicate asynchronously[44], develop amylopectin (starch) granules in the cytoplasm[83], and rely on anaerobic glycolysis for energy[84]. These physiological and morphological changes are accompanied by changes in the transcriptome and proteome with hundreds of genes differentially regulated between the two stages[85-88]. Some of these proteins have similar enzymatic functions in both stages (isoenzymes) and others are more specific to bradyzoite function (e.g. surface antigens or cyst wall proteins) because they are not required in tachyzoite stages. The differences in protein expression have enabled the field to study bradyzoites by providing markers for identification[85]. In addition, the promoters of these bradyzoites genes can be used in studies to upregulate genes of interest specifically in bradyzoites[89,90].

One of the most commonly used bradyzoite markers used is Bradyzoite Antigen 1 (BAG1) because it is highly expressed in bradyzoites[87,91]. In fact, BAG1 is one of many heat-shock proteins that are upregulated during bradyzoite differentiation[91-95]. Why bradyzoites need so many heat-shock proteins is unclear. BAG1 localises to the cytosol of bradyzoites[91] and knockout evidence suggests BAG1 is an important protein for maintaining a high cyst burden *in vivo*, despite the apparent lack of importance during development[96]. Another set of common parasite markers are surface antigens. In tachyzoites, surface antigens, such as Surface Antigen 1 (SAG1), are important for attachment, invasion, and regulating infection in tachyzoite stages[97].

Similarly, bradyzoites also express a unique composition of surface antigens. Some of these bradyzoite antigens are part of a conserved group of SAG1-Related Sequence (SRS) proteins, such as SRS9[98,99], whereas others are more structurally distinct, such as Bradyzoite Surface Antigen 4 (BSR4)[100,101]. The change in surface antigens between the two stages might assist the parasite in evading the immune system and enabling cyst persistence[102].

The differential expression of enzymatic isoforms between tachyzoites and bradyzoites has also been observed. *Toxoplasma* lactate dehydrogenase (LDH1 and LDH2) is an example of stage-specific enzymes controlled transcriptionally[103,104]. Functionally they both catalyse the reaction, converting lactate to pyruvate in anaerobic respiration (e.g. during glycolysis) with nearly identical enzyme kinetics[105]. However, LDH1 is expressed solely in tachyzoites and LDH2 is only expressed in bradyzoites. Although both are required for *in vivo* bradyzoite development, it appears LDH1 is of more importance for acute virulence[106,107]. This supports the speculation that LDH1 is replaced by LHD2 during bradyzoite development; the former is important during the early stages of infection and differentiation whereas the latter is only important for bradyzoite persistence where glycolysis is the apparent energy source used by bradyzoites. Stage specific replacement is also the case for other enzymes, like enolase proteins 1 and 2[104]. A more detailed discussion around bradyzoite markers and proteins can be found in Tu *et al.* (2018)[108]. Together, these transcriptomic and proteomic changes help define bradyzoites as a distinct entity from tachyzoites.

1.3.2 Bradyzoite differentiation

The signals that induce tachyzoite-bradyzoite conversion and the associated biological changes remain unknown. However, it is clear that these changes are accompanied by drastic alterations in the parasite's transcriptional program. For this to occur transcription factors are at the end of intracellular-signal transduction that initiate the differentiation process. A clue to what family of transcription factors could control conversion originally came from another Apicomplexan parasite, *Plasmodium*. Like *Toxoplasma*, *Plasmodium* uses a symphony of transcriptional changes as it goes through the developmental stages of its complex life cycle. A group of transcription factors containing a DNA-binding domain called Apetala2 (AP2) was found to be responsible for these stage transitions in *Plasmodium* species[109,110] and are conserved throughout the phylum[111].

These transcription factors were named Apicomplexan AP2 proteins (ApiAP2) and 68 *Toxoplasma* genes were identified as containing an AP2 domain[110,112]. T*g*AP2 proteins identified as important for bradyzoite development have been classified as either bradyzoite repressors or activators of differentiation[113]. The removal of bradyzoite repressor *tg*AP2 genes AP2IX-9[114], AP2IX-4[115], and AP2IV-4[116], results in the increase of cyst formation or the upregulation of bradyzoite specific proteins and cyst wall proteins. In contrast, knockouts of *tg*AP2 bradyzoite activators impair differentiation and results in the downregulation of bradyzoite markers. AP2XI-4[117] and AP2IV-3[113] are classified as activator proteins and both have been shown to bind to promoter regions of bradyzoite-specific genes. It appears that the balance between repressors and activators is what determines whether tachyzoites are pushed into bradyzoite development.

Despite the obvious implications of ApiAP2 proteins in bradyzoite development, no single knockout could prevent differentiation. Instead the level of differentiation was merely decreased or bradyzoite marker expression was affected. This has resulted in a differentiation model with no master transcriptional regulator[118]. However, a recent CRISPR/Cas9 screen partnered with bradyzoite differentiation identified a new transcription factor, Bradyzoite Formation Deficient 1 (BFD1)[119]. Knockouts and overexpression of BFD1 showed that it was both necessary and sufficient for differentiation both *in vitro* and *in vivo*. The authors also show that BFD1 binds to regions of the genome associated with the expression of bradyzoite markers and could potentially coordinate the expression of *Tg*AP2 proteins that results in the cascade of transcription required during differentiation. Interestingly, BFD1 mRNA is constitutively expressed but the protein is post translationally regulated, which could provide a more efficient response when differentiation is signalled. However, the key external signal that stabilises BFD1, and therefore differentiation, is still undetermined.

Understanding why and how bradyzoites differentiate is vital not only to the development of treatments, but also to the continued research in the field. Bradyzoites stages have largely been neglected due to the inefficiencies of producing bradyzoites *in vitro*. Spontaneous *in vitro* differentiation does occur at low levels with the typical lab strains (e.g. GT1 (type I) and most type II and III strains)[120]. There are reports that the spontaneous differentiation rate of atypical strain EGS is up to 70% in fibroblast and epithetical cells, as compared to levels of less than

10% for the typical lab type I and II strains[121]. Spontaneous differentiation strains are useful in *in vitro* studies when looking at a single cell level. However, for pooled data the heterogeneous sample may cause complications with data analysis and methods that can produce a more synchronised and homogenous population is also important.

Studies have identified multiple methods that can be used to increase *in vitro* differentiation to varying degrees, including heat shock, alkaline pH, small molecules and nutrient starvation[122-124]. From these studies, in conjunction with the upregulation of many heat-shock proteins, it has been suggested that bradyzoite differentiation is a stress response[120]. Whether stress is an inducer *in vivo* is unclear. Cyst development *in vivo* occurs during the host's strong pro-inflammatory response and the absence of a functioning immune system leads to reactivation of bradyzoites and uncontrolled growth of tachyzoites[118]. This implies that immune-related stress factors (e.g. immune generated nitrogen species or nutrient starvation) could play a role in triggering bradyzoite differentiation[125]. Furthermore, cyst formation appears to have a tropism for tissues where host cells are largely post-mitotic, such as the brain, heart, eyes, and muscles. Due to this tropism, some have suggested that bradyzoite conversion is linked to the cell cycle of the host cell or the unique cell host environment of specific organs[126,127]. Indeed, *in vitro* studies of neurons[128] and muscle cells[129] have shown higher spontaneous bradyzoite conversion rates over cell types in the same tissue or lineage. Despite the multitude of methods available, there are limitations to producing bradyzoites *in vitro*. Whether *in vitro* bradyzoites or cysts could be considered equal to *in vivo* bradyzoites is still an area of contention[130]. While *in vitro* studies assist in understanding bradyzoites development, late stage bradyzoite mechanisms may not be able to be elicited using these methods. There has been an observation of *in vivo* cysts containing tachyzoites as well as bradyzoites[131], although a recent *ex vivo* study has argued against such a model[44]. The field's definition of what constitutes a true bradyzoite can only be determined when we have a better understanding of how and why parasites differentiate.

1.3.3 The cyst wall and it's development

A key step during bradyzoite formation is the production and secretion of proteins that build the cyst wall. The cyst wall is thought to be important to the parasite's transmissibility and long term persistence. By adding a barrier of protection from the immune system, the cyst wall helps establish a chronic infection and may even enhance transmission, likely through shielding parasites from digestive acids (although this has not been formally proven). The cyst wall is on average 240 nm thick and is comprised of two layers that form underneath the PV membrane; the thin outermost layer abuts onto the PVM and is densely packed, whereas the thicker inner layer is composed of filamentous structures that are loosely packed, giving it a sponge like appearance[132,133]. The inner cyst network (ICN) of the cyst wall has similarities to the filamentous IVN of the tachyzoite stage and, interestingly, contains many of the known IVN dense granule proteins[132,134] thought to be involved in the early development of the cyst wall[135,136].

Although seemingly dormant when compared to tachyzoites, bradyzoites are dynamic and continue to divide slowly and asynchronously producing cysts up to 100μm in size[38,44]. To maintain the cyst wall, bradyzoites must continuously secrete protein components as they divide to enable both the cyst wall and PVM to expand as the numbers of bradyzoites increases[44,130,136]. It is likely that the ICN has a role in the transfer and incorporation of vesicles containing needed proteins. Many of the cyst wall components are either hypothetical proteins or known dense granule proteins[134]. One of the first cyst wall proteins identified was CST1, a SRS glycoprotein with a mucin domain, which is glycosylated and binds *Dolichos biflorans* lectin (DBA)[137]. The high posttranslational glycosylation of cyst wall proteins is thought to assist in immune evasion and confer structural stability[138-140]. CST1 is not required for the formation of the cyst wall, but in the absence of CST1 or the N-acetylgalactosaminyltransferases responsible for O-GalNAc glycosylation of CST1's mucin, the cyst wall becomes fragile and fewer cysts are formed *in vivo*[140,141]. However, it appears that not all cyst wall SRS-mucin glycoproteins are important for stability[142].

The cyst wall is permeable to micro-nutrients and macromolecules needed for the bradyzoites' growth and long term survival[132,143]. It is not clear how these molecules cross such a dense layer, TEM evidence shows that the cyst wall is punctuated with 30-40 nm circular openings which could be a clue to the mechanisms used[132]. Furthermore, GRA17, a key protein in trafficking of small molecules across the tachyzoite PVM (discussed in *section 1.9.3*), is important in bradyzoite conversion and viability, implicating GRA17 in the hypothetical trafficking of nutrients across the cyst wall[144]. Larger molecules might be trafficked across the PVM by the invagination and formation of uncoated vesicles that can migrate through the cyst wall into the cyst matrix[143].

1.4 Parasite dissemination and brain infection

The most common organ where bradyzoite conversion occurs is the Central Nervous System (CNS), which encompasses the retinal tissue and the brain. In this section I will briefly cover how *Toxoplasma* may reach and gain access to the CNS.

1.4.1 Parasite dissemination

Tachyzoites are responsible for dissemination throughout the body. The parasites use their gliding motility, replicative asexual cycle (discussed in *section 1.2.2*) and host cell behavioural changes induced by the parasite (discussed in *section 1.5* and *1.6*). The latter is thought to be key in the parasites distal dispersion from the initial gut infection. In this model, parasites use leukocytes recruited by chemokine-secreting enterocytes to disperse undetected in a trojan horse mechanism[16]. Infected cells become hyper-motile, enabling parasite dissemination. Macrophages and dendritic cells (DC) are thought to be the main monocytes affected and used in this manner. $CD11c^+$ and $CD11b^+$ DCs appear to be preferentially infected and, although all *Toxoplasma* strains induce migration in these cells, type II parasites exhibited a higher ability to do so[145-147]. The hyper-motility of DCs is maintained for more than 24 hours and the increased presence of $CD11c^+$ and $CD11b^+$ in the brain correlates with an increase in *Toxoplasma* infection of the brain[145-147]. Furthermore, *Toxoplasma* is able to suppress apoptosis in macrophages while also decreasing the expression of cell surface adhesion molecules to again increase motility[148,149]. This demonstrates how *Toxoplasma* uses the intrinsic migratory nature of these cells to disperse throughout the body. How *Toxoplasma* achieves these changes in cell behaviour is discussed in *section 1.8*.

1.4.2 Crossing the blood brain barrier

During dissemination, tachyzoites need to traverse physiological barriers designed to be protective and selective, including the epithelium of the gut, the placenta, and the blood-brain barrier (BBB). The BBB is a protective layer of endothelium cells that poses a

challenge to pathogen invasion into the CNS. Toxoplasma's ability to cross the BBB is vital to the parasite's ability to establish chronic infection and lifelong persistence, therefore the parasite's traversal mechanisms have been of great interest[150]. Three models for how the parasite traverses the BBB have been suggested: infiltration of infected immune cells ('Trojan horse'), transcellular migration, and paracellular entry[151]. Studies have suggested that the 'Trojan Horse' hypothesis might not only apply to the parasite's ability to disseminate to, but also traverse, the BBB. The 'Trojan Horse' model was supported by *in vitro* studies which showed that DCs can across cell monolayers and indicated that *Toxoplasma* infected DCs could pass the monolayer at a higher rate than uninfected cells[146]. However, Konradt *et al.* (2016)[152] elegantly showed that parasites traverse the BBB *in vivo* by egressing from the endothelial cells of small blood vessels in the brain releasing parasites into the brain parenchyma. Although they did find leukocytes ($CD11c^+$, $CD11b^+$, $Gr1^+$, $CD3^+$) infected with parasites in the blood, when parasite replication was inhibited no parasites were seen in the CNS, suggesting the parasite could not be transported over the BBB without replication[152]. In addition, the tachyzoites have also been shown to paracellularly cross the gut epithelia, suggesting that a similar mechanism could be used to cross the BBB and other comparable barriers[153,154]. The strategy *Toxoplasma* predominately uses to gain entry into the CNS is unknown; however, it is possible the parasite could use all these approaches.

1.4.3 Cell tropism in the Central Nervous System

Once *Toxoplasma* has traversed the BBB it goes on to form cysts in the CNS. While several *in vitro* studies have suggested that all types of resident CNS cells can be infected, *in vivo* analysis has shown that *Toxoplasma* preferentially infects neurons[128,155-157]. Tracking *Toxoplasma* infection in the brain has been notoriously difficult because of the complex cellular structure of the brain and the elaborate morphology of the residing cells. Recently technical complexities were overcome by infecting transgenic loxP-ZsGreen mice with parasites that inject cre-recombinase (during rhoptry release). LoxP-ZsGreen mice express GFP following the removal of a floxed STOP construct which allows the infection status of individual neurons *in vivo* to be determined through the expression of GFP[155,158,159]. Although

a small proportion of astrocytes were GFP+, the overwhelming majority of infected parenchymal cells were neurons[155]. In situ imaging showed that the cysts were predominantly found in the neuronal processes not the cell body as seen *in vitro*[155,160]. Interestingly, there was a population of cells, both neurons and astrocytes, that were GFP^+ but not infected. These cells have either been invaded and subsequently cleared the intracellular parasites, or, after the injection of rhoptry proteins, invasion was abandoned[155,158]. The 'injected-uninfected' population of cells outnumbered infected cells in the CNS of mice and it appears, superficially, that these host cells experienced similar physiological changes to the infected cells [155,158]. Whether the cell types infected impact the observed behavioural changes in infected mice is still unclear but continues to be an area of research in the field. Behavioural neuroscience and *Toxoplasma* is reviewed in depth by Tyebji *et al.* (2019)[161].

1.5 *Toxoplasma* host manipulation

Without the ability to manipulate their host cell, intracellular pathogens are rapidly cleared by the innate immune system. *Toxoplasma* is no exception, and over the last 10 years there has been an explosion of new discoveries of how *Toxoplasma* tachyzoites achieve this. The host cell undergoes an array of changes upon infection, which can be directly linked to the active modification by *Toxoplasma* and are important for the parasite virulence and survival. Host alterations are dependent on the host-cell type and can include organelle sequestration[162], host transcriptional modifications[163], and changes in adhesive and migratory capacity of the infected cell[164]. Host organelles, such as the mitochondria, are sequestered to the PVM[162], the reasons for which are not clear. It has been hypothesised that host organelle sequestering might be required to acquire host nutrients that are essential for parasite growth and survival. This is because interfering with mitochondria-PVM interactions stunts parasite growth, suggesting that relationships with key organelles might help the parasite scavenge essential nutrients[165]. In monocytes and dendritic cells *Toxoplasma* infection increases the motility and adhesive properties of the cells[95,150] as well as increasing the distance travelled[166] and enhancing their ability to traverse endothelial monolayers,[146] all which may aid parasite dissemination (as discussed in *section 1.4*).

1.5.1 Host transcriptional changes

The biggest change to the *Toxoplasma*-infected cell is the global rewiring of the host's transcriptome. The host cell is a hospitable environment but, by globally rewiring the host cell's transcriptional profile, *Toxoplasma* can modify the host's innate immune response and the organism's overall response to infection[163]. The first study to look at host gene expression changes by *Toxoplasma* was done using microarrays on a type II tachyzoite infection[167]. The study concluded three main classes of gene modulation: 1) genes modified by the parasite for survival and growth, 2) genes modified by the host for defence, and 3) genes modified as a consequence of the two former modification. The changes dependent on the host could account for observations that host cell transcriptional responses are largely cell-type dependent[168]. Further, time course analysis revealed two distinct gene expression profiles: rapid gene changes within one to two hours of infection associated with the immune response, and changes that occurred post six hours after infection. Overall these transcriptional changes did not represent a general response to intracellular protozoan parasite infection (as compared to *T. cruzi*) suggesting transcriptional modification was *Toxoplasma* specific[167]. Indeed, the identification of rhoptry proteins that modify the host transcription during invasion stages were identified in the following years (discussed in *section 1.6.1*)[169-172], followed a decade later by the discovery of dense granule proteins responsible for the second wave of changes[173-176]. Interestingly, microarray data showed little to no transcriptional changes of the host cell in the very early stages (44 hours post infection) of *in vitro* bradyzoite differentiation compared to tahcyzoites[177].

More recent transcriptional studies have used newer RNA sequencing methods which have a larger dynamic range compared to microarrays and is not as reliant on measuring relative differences. These are more sensitive, and are able to sequence and analyse the transcriptome of the host and pathogen (dual-transcriptomics) from the same sample[178]. The developments in RNA sequencing technology enabled *in vivo* analysis of *Toxoplasma* infected mice which showed that host transcriptional changes occurred i*n vivo* during the acute stages and continued in the chronic stages[179-181]. However, this kind of holistic approach does not disentangle the multiple factors at play as transcriptional changes observed *in vivo* could be: 1) due to the export of effector proteins from the parasite, 2) a consequence of host immune

responses (e.g. immune infiltration), or (3) the result of parasite derived rhoptry proteins injected into host cells that are not infected[69,182,183]. From *in vitro* transcription data it is evident that a majority of the acute transcriptional changes observed in infected cells is dependent on the secretion of dense granule proteins[184]; however, it is not clear how much of the chronic transcriptional changes observed *in vivo* are dependent on parasite factors.

1.6 *Toxoplasma*-secreted host-modifying proteins

Over the last decade multiple tachyzoite secreted proteins that modify the host cell have been identified. The first ROP and GRA proteins were identified by defining loci associated with virulence through genetic crosses of avirulent and virulent strains or through an *in silico* screen. These isolated virulence factors were shown to be responsible for the difference between strains. However, it did not shed light on effectors that were common between strains nor could these proteins explain all the transcriptional changes observed during infection. In this section I will discuss the tachyzoite known effector proteins, originating from both the rhoptries and DG, and their impact on the host cell.

1.6.1 Rhoptry proteins

Rhoptry (ROP) proteins are a non-related family of proteins named by their organelle of origin, the rhoptry organelle. ROP proteins mainly arising from the bulb of the rhoptry organelle, as opposed to the neck where RON proteins originate. A large proportion of ROP proteins are kinases and pseudo kinases which exported from the rhoptries during invasion. Some are responsible for the formation of the PV (as discussed in *section 1.4*) and others are involved in host manipulation. For a list of known ROP proteins associated with the PV and their function see review (table 1) Clough and Frickel (2017)[70] and Bradley *et al.* (2005)[185]. Those ROP proteins associated with virulence and host modulation are discussed below (Fig. 1.4A).

1.6.1.1 ROP18/ROP5/ROP17 complex: inhibitors of intracellular clearance and key virulence factors

The ROP18/ROP5/ROP17 complex counters the host's innate defence mechanism which enables the parasite's survival. Different alleles of ROP18 and ROP5 have been shown to confer major differences in strain virulence and enabled the discovery of this complex. ROP18 was the first competent to be identified by Quantitative Trait Locus (QTL) mapping of virulent offspring[24,25] from the cross of avirulent type III strains with either virulent type I strains[169] or semi-virulent type II strains[171]. ROP18 is an active serine-threonine kinase that is secreted during the tachyzoite invasion, localises to the PVM facing the host-cytosol, and has been associated with the control of intracellular parasite growth[186]. However, ROP18 alone could not fully account for the differences in virulence between type I and type II crosses[171], instead the loci containing rhoptry pseudo kinase ROP5 was found to accounted for a considerable amount of virulence differences between these two strains [170]. It was later found that ROP18 and ROP5, along with another rhoptry kinase ROP17, form a complex on the PVM that phosphorylates host factors activated by IFNγ to attack intracellular pathogens[187].

It was subsequently found that the ROP18/5/17 complex acts by blocking IFNγ mediated host defence mechanisms[187]. In murine cells, the IFNγ-induced recruitment of immunity-regulated GTPases (IRGs) and guanylate-binding proteins (GBPs) breaks down the PVM and either activates host cell death or autophagy to clear the parasites[188]. *Toxoplasma* targets IRGs and GBPs and inactivates them through phosphorylation to prevent the formation of active IRG/GBP oligomers, therefore protecting the PV from destruction[189,190]. Because ROP18 and ROP17 are active kinases, it is thought they are responsible for the phosphorylation of the murine IRGs, whereas ROP5 is thought to either block IRGs oligomerisation directly or indirectly by regulating ROP18, of which it is an essential co-factor [189,191-194]. Etheridge *et al.* (2014)[189] propose a model where ROP17 phosphorylates and destabilises active IRG oligomers, freeing monomers for ROP18/ROP5 to phosphorylate, preventing the IRG monomers from reforming polymers. Interestingly, humans lack the large number of IRGs found in murine cells and consequently the ROP18/5/17 complex does not affect the parasites survival in human IFN activated cells[195]. Because different strains have varying virulence capacities which means less

virulent strains (type II and III) are more likely to succumb to IFNγ in the early stages of infection.

The virulence studies were all conducted in mice and it still remains unclear how important the IRG pathway is in human infection. It is known that highly virulent strains of *Toxoplasma* are responsible for severe cases of Toxoplasmosis in humans, such as those in SA which have a wider variety of virulent strains and alleles associated with the ROP18/ROP5/ROP17 complex[196]. The parasites survival in humans may therefore also be reliant on the functioning of this complex.

1.6.1.2 ROP16 and ROP38: transcription modulators

Two other rhoptry proteins are known to be involved in modulating the host transcriptome at the early stages of invasion. ROP16 is a JAK tyrosine kinase mimic which localises to the host cell nucleus where its activity modulates the JAK/STAT pathway by phosphorylating and activating STAT3 & STAT6 to skew the innate immune response[27]. Much like ROP18, ROP16 is a virulence factor and was identified by QTL in the same virulence crosses as ROP18[171]. Type I and III ROP16 variants elicit strong host transcriptional changes; however, type II ROP16 cannot elicit the same responses[27]. Type II parasites also show an increase in NF-kB activity suggesting that the inability to activate STAT3 (a known inhibitor of NF-kB) may play a role in this observation[190] or that another parasite protein might be involved (discussed in *section 1.6.2.1.2*). On the other hand, ROP38 does not localise to the host nucleus, yet also alters the host transcriptome. Type II and type III parasites express more ROP38 compared to type I[197,198]. Data suggest that ROP38 likely acts as a transcriptional suppressor, where it downregulates MAPK signalling associated with type I infection, and may have a role in controlling apoptosis and host proliferation[198]. It has also been implicated in the parasite's ability to establish tissue cysts *in vivo*[197].

1.6.1.3 WIP: modulator of cell migration

With the development of the CRISPR/Cas9 system in *Toxoplasma,*[199-201] genetic determinants of virulence can now be identified by screening the loss of individual genes *in vitro*[202,203] and *vivo*[204,205]. A library of CRISPR guides (sgRNA), enriched for GRA proteins, was transfected into Cas9 expressing type I parasites and then were passaged multiple times *in vitro*. Genes that that were important for *in vitro* culture were therefore eliminated before injecting the remaining parasites into mice. By comparing parasites residing in the peritoneum with those at distal organs (like the lungs, brain, heart and eyes), the researchers could isolate candidates that were important for dissemination[204]. Using this method, rhoptry protein WIP (WAVE complex-Interacting Protein) was identified (along with multiple uncharacterised potential host-pathogen interacting proteins) which localises to the host cytosol and forms interactions with components of the WAVE regulatory complex (WRC)[204]. WRC can regulate actin cytoskeletal dynamics and therefore motility, adhesion, and shape of the infected cell by stimulating the Arp2/3 complex and inducing actin-nucleating sites throughout the cell[206]. The ability for the parasite to modulate the motility of monocytes and DCs has been the basis for speculations around how *Toxoplasma* disseminates and crosses cell monolayers, and WIP seems to be a key player in this process. Through WRC interactions WIP modifies host cell actin dynamics, inducing hypermotility, and has been implicated in monolayer traversal[204]. Furthermore, in the absence of WIP, the parasite's virulence and ability to disseminate to visceral organs was greatly impacted.

1.6.2 Dense granule proteins

The DG proteins (GRA) are a group of proteins that are secreted constitutively from the DG organelle as soon as three minutes post-invasion[72] and are associated with the development of the PV/PVM and host cell manipulation[70,207].

Figure 1.4

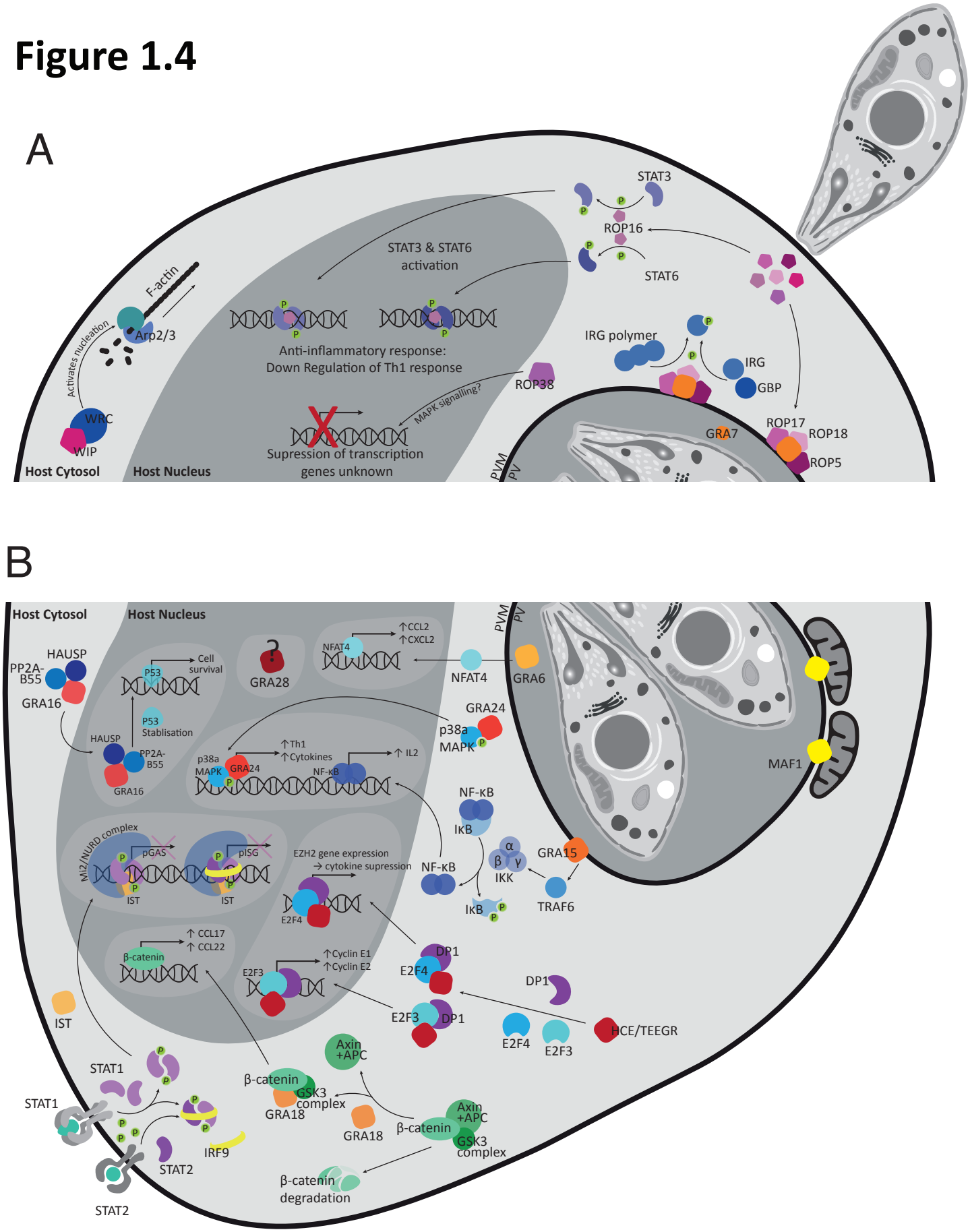

A
STAT3
ROP16
STAT6
STAT3 & STAT6
activation
F-actin
Arp2/3
Activates nucleation
WRC
WIP
Host Cytosol
Host Nucleus
Anti-inflammatory response:
Down Regulation of Th1 response
Supression of transcription
genes unknown
MAPK signalling?
ROP38
IRG polymer
IRG
GBP
GRA7
ROP17
ROP18
ROP5
PVM
PV
B
Host Cytosol
Host Nucleus
HAUSP
PP2A-
B55
GRA16
P53
Cell
survival
P53
Stablisation
GRA28
NFAT4
↑CCL2
↑CXCL2
GRA6
GRA24
p38a
MAPK
↑Th1
↑Cytokines
↑ IL2
NF-κB
IκB
α
β
γ
IKK
GRA15
TRAF6
MAF1
Mi2/NURD complex
pGAS
pISG
IST
EZH2 gene expression
→ cytokine supression
E2F4
↑ CCL17
↑ CCL22
β-catenin
E2F3
↑Cyclin E1
↑Cyclin E2
DP1
HCE/TEEGR
STAT1
STAT2
IRF9
Axin
+APC
GSK3
complex
GRA18
β-catenin
degradation

Figure 1.4 – Tachyzoite host cell manipulation by rhoptry and dense granule proteins

Tachyzoites modify the host cell using effector proteins at invasion (A) and after the PV is established (B).

(A) During invasion rhoptry proteins are injected into the host cell. ROP16 localises to the host nucleus and causes the phosphorylation of STAT3 and STAT6 to induce an anti-inflammatory response. The ROP5/17/18 complex (along with GRA7) localise to the PVM and prevent the formation of IRG polymers. ROP38 is a suppressive transcriptional element; it's host partners and mechanism are still unknown. WIP interacts with the WAVE regulatory complex (WRC) to regulate actin dynamics and host cell motility.

(B) After PV formation tachyzoites secrete dense granule proteins, of which a proportion effect the host cell response. GRA6 remains within the confines of the PVM where it induces the nuclear translocation of transcription factor NFAT4. MAF1 localises to the PVM where it recruits and interacts with the host mitochondria. PVM bound GRA15 causes the nuclear relocation of NFkB and initiates its transcriptional activity. GRA16, GRA18, GRA24, GRA28, IST and HCE/TEEGR are all exported into either the host cell nucleus or cytosol. GRA16 complexes with HAUSP/PP2A-B55 to activate cell survival and cell cycle pathways. GRA18 prevents the degradation of b-catenin activating b-catenin transcription. GRA24 causes autophosphorylation of p38a MAPK and the upregulation of the Th1 response. The function of GRA28 is still unknown. IST results in the recruitment of Mi2/NURD complex at STAT1 induced transcription sites to prevent the upregulation of IFN type I and II genes. HCE/TEEGR complexes with E2F transcription factors E2F3 (to induced upregulation of cyclins E1/2 inhibiting cell cycle) and E2F4 (to suppress cytokine expression).

Image inspired by Hakimi, M.-A., Olias, P. & Sibley, L. D. Toxoplasma effectors targeting host signalling and transcription. *Clinical microbiology reviews* 30, 615-645; 0893-8512 (2017).

1.6.2.1 PV dense granule proteins

The canonical GRA proteins have a classical or non-classical N-terminal hydrophobic signal peptide which signals their secretion through the ER and Golgi to the dense granules to be released into the PV space. GRA proteins can be associated with the PVM either directly or indirectly. For example, inside the PV GRA 2, 4, 6, 9 and 12 have roles in the biogenesis and maintenance of the IVN[207]. GRA6 and GRA12 seem to also have dual roles in parasite-host immune interactions. GRA6 re-localises host NFAT4 to the nucleus where it plays a role in the recruitment of inflammatory monocytes via the upregulation and secretion of cytokines (CCL2, CXCL2)[208]. GRA12 appears to have a role in IFN-γ activated host cell innate immunity[209]. GRA7 has multiple roles too; it is the link between the PVM and the rhoptry complex of ROP18/5/17 that destabilises IRGs as well as sequestering host tubule-structures around the PV[210,211]. Some DG proteins are exposed to the host cell cytosol where they regulate host pathogen interactions like Host Mitochondria Association (HMA) or host transcriptional modifications *(sections 1.6.2.1.1 and 1.6.2.1.1* respectively) or are involved in nutrient acquisition (*section 1.7*). Up to 40 GRA proteins have been identified as residing in the PV; the function of half are yet to be characterised[212].

1.6.2.1.1 MAF1: mitochondrial recruitment factor

The disruption of host mitochondria dynamics or mitochondria recruitment to pathogen vacuoles has been observed in multiple intracellular pathogens[213]. It is unclear whether these dynamics are pathogen driven or if it is part of the host cell response to sequester the infection. In *Toxoplasma* infection, host mitochondria become elongated and wider when associated with the PVM. The extent of HMA is strain dependent, with type II stains recruiting little to no mitochondria[165]. This meant researchers could analyse previous completed genetic crosses between HMA-positive and HMA-negative strains by QTL to map the parasite factors that are responsible for the HMA phenotype. The DG protein identified was named Mitochondrial Association Factor 1 (MAF1)[165] (Fig. 1.4B). The MAF1 locus is duplicated multiple times (lab strains have an estimated copy number of four) resulting in multiple distinct paralogs which differ in their ability to mediate HMA[214,215]. Despite strain differences, the absence of MAF1

does not correlate with virulence in type I parasites[165]; however, when a MAF1 paralog that can confer positive HMA is expressed in a type II line, it provides a competitive advantage over wildtype parasites *in vivo*[214,215]. Association might enhance the parasite's ability to scavenge fatty lipids or other nutrients, or enable the parasite to subvert the immune system via the mitochondrial antiviral-signalling protein (MAVS)[165,216]. Conversely, during early stages of infection host mitochondria compete with *Toxoplasma* for fatty acids and limits parasite growth through competition[217]. Therefore the reason why *Toxoplasma* might recruit host mitochondria is ambiguous.

1.6.2.1.2 GRA15: NF-κB activator

GRA15 was the first GRA protein identified that was shown to interact with the host and skew its response. Gene expression data indicated type II infected host cells translocated host NF-κB to the nucleus and strongly upregulated NF-κB-induced expression, both of which were not seen in type I or III to the same degree[26,218,219]. The difference between strains facilitated the discovery of GRA15. Using QTL, Rosowski *et al.* (2011)[26] identified a loci in the progeny of type II x type III crosses that induced NF-κB pathway expression. GRA15 is associated with the PVM where it is thought to activate the NF-κB pathway through the TRAF (TNF Receptor-Associated Factors)-IKK pathway, not through the MyD88/TRIF pathway[220] (Fig. 1.4B). GRA15 contains binding motifs that recruit and activate TRAF6 and TRAF2, proteins involved in NF-κB activation[220]. Both TRAF6 and TRAF2 pathways converge at the activation of the IKK complex which initiates IκBa proteasome degradation through phosphorylation[221]. Degradation releases p65/p50 heterodimers and enables nuclear translocation that initiates the transcriptional changes associated with the NF-κB pathway.

The upregulation of the NF-κB pathway is often activated during intracellular pathogen infection because it encourages a pro-inflammatory response T_H1 response. The levels of two key cytokines implicated in parasite clearance, IL-12 and INFγ, are increased in a T_H1 response[222,223]. Furthermore, cleaved IL-1b secretion is sustainably increased by type II-GRA15 NF-κB activation, adding to the inflammatory environment[224]. Why would type II strains upregulate NF-κB? Recent papers have suggested that the GRA15-dependent upregulation of

IL-1b enables parasites to proliferate in cells co-cultured with monocytes[225,226]. The authors of these studies argue that the combination of IL-1β and IFNγ produced by the monocytes upregulates inducible nitric oxide synthase (iNOS) in the co-cultured human cells, producing nitric oxide (NO). NO subsequently downregulates indole 2,3- dioxygenase 1 (IDO1), which is a protein used by the host to starve parasites of tryptophan, a crucial amino acid[227,228]. Whether inducing an inflammatory environment translates to advantages *in vivo* is yet to be determined; however, the loss of GRA15 appears not to affect the virulence of the parasite in mice or *in vitro* mouse fibroblasts[26]. GRA15 still remains as one of the only GRA proteins that can impact the host cell response from the PVM, with many of the DG proteins identified following GRA15 found to be exported across the PVM into the host cell.

1.6.2.2 Exported dense granule effector proteins

A subset of DG proteins are exported across the PVM into the host cell, where they modify signalling to manipulate the immune and pro-survival pathways[163,229] (Fig. 1.4B).

1.6.2.2.1 GRA16: cell cycle regulator

GRA16 was the first identified dense granule protein that is exported across the PVM into the host nucleus, where it affects the expression of host cell cycle and survival proteins. It was identified by an *in silico* screen that focused on characteristics that were considered requirements for altering host cell transcription[176]. In the host nucleus, GRA16 forms interactions with the phosphatase PP2A-PR55/B holoenzyme and herpesvirus-associated ubiquitin-specific protease (HAUSP), a regulator of p53[230]. The exact effect GRA16 has on these binding partners is unknown; however, the association between GRA16 and HAUSP stabilises p53 and upregulates genes implicated in arresting the cell cycle and other p53-related pathways[176]. HepG2 cells (p53-positive) expressing transfected GRA16 showed a reduction in total cell number, and growth inhibition was accompanied by arrest in the cell cycle at the G2-M phase[231], a characteristic previously observed in *Toxoplasma* infected host cells[232,233]. It has been hypothesised that cell cycle arrest could enable *Toxoplasma* to complete its lytic cycle

before the host cell divides, but this or any other hypothesis is yet to be formally proven.. Furthermore, p53 activity also regulates apoptosis[234,235], suggesting GRA16 may play a role in modulating the host's cell death response. Inhibiting apoptosis would be beneficial to the parasite; however, transfected GRA16-HepG2 cells actually showed an increase in apoptotic cell death, suggesting that arrest in cell death may not be controlled by GRA16 but by another effector protein[231]

1.6.2.2.2 GRA24: pro-inflammatory agitator

Subsequent analysis of the *in silico* data identified GRA24, another GRA protein that localises to the host nucleus[236]. GRA24 interacts with the p38α Mitogen-Activated Protein Kinase (MAPK) and induces the kinase's auto-phosphorylation activity. Phosphorylation occurs at Thr180/Tyr182 (markers of activation)[237] and helps maintain p38α in the activated state for up to 24 hours, independently of the map-kinase-kinase (MKK) cascade[173,238]. p38α activation results in the upregulation of pro-inflammatory cytokines (e.g. IL-12, IFN-γ), particularly in type II parasites, which attracts inflammatory monocytes to the site of infection. The continued activation of the GRA24-p38α complex results in the induction of Egr-1 and c-Fos regulated transcriptional changes[236]. While GRA24 appears to be an important virulence factor, it is not clear why inducing the expression of this group of cytokines is beneficial to the parasite, but it may explain type II's decrease in virulence and increased capacity to develop into bradyzoites.

1.6.2.2.3 IST: inhibitor of STAT1 transcription and immune evasion

The host's ability to initiate the T_H1 response and a cell's capacity to respond to IFNγ is crucial in controlling *Toxoplasma* infection *in vivo*[125,222,223,239]. A cell responds to IFNγ signalling through STAT1-induced transcription. Activation of STAT1 follows the binding of IFNγ to its receptor (IFNGR) which initiates STAT1 phosphorylation through JAKs[240]. Phosphorylated STAT1 dimerises and binds to Gamma Activated Sequence (GAS) sites in the nucleus, upregulating the transcription of many immunity related genes such as IRF1, GBPs, and ISGs involved in clearance. While the ROP18/5/17 complex is able to block IFNγ signalling of pre-

activated cells in some strain types, the complex does not prevent IFNγ triggering its signalling cascade. It is clear that *Toxoplasma* also has another mechanism to block IFNγ signalling [241]. It is known to suppress STAT1 dependent transcription[241-243], preventing the upregulation of iNOS[244] and Major Histocompatibility Complex (MHC) class II[245] but the molecular mechanism underlining this process was, until recently, unknown.

The inhibitor of STAT1 transcription (IST) was independently identified by two research groups and is a DG protein that localises to the host nucleus[174,175]. IST was identified *in silico*[174] by the same group that identified GRA16[176] and GRA24[173], whereas another group took a targeted approach and used STAT1 immunoprecipitation paired with mass spectrometry to find parasite-derived STAT1 interacting proteins[175]. Interestingly, STAT1-induced transcription was not inhibited through the prevention of STAT1 activation, its nuclear localisation or a decrease in STAT1's ability to bind DNA; instead, IST seems to increase STAT1-DNA interactions[174,175]. IST is thought to encourage DNA binding of STAT1 dimers by inducing the phosphorylation of STAT1 (Y701, S727). The IST-pSTAT1 complex then relocates to the host nucleus and where it recruits Mi-2/NuRD to GAS sites. Mi-2/NuRD is a repressive complex that deacetylates histones at GAS promoter regions inhibiting transcription[246-249]. Unlike the other immune-skewing effector proteins previously identified, all lineages of *Toxoplasma* appear to repress STAT1 facilitated transcription during IFNγ exposure[243,246,250]. In contrast to the effects of IST, ROP16 & GRA15 inhibit a selective number of IFNγ induced genes and are specific to type I and type II, respectively[251,252]. IST is unable to suppress the IFNγ response if host cells are pre-treated and Δ*ist* parasites treated with IFNγ are more susceptible to death[247,248,253], which is in contrast to the type I ROP18 complex that can block parasite clearance of IFNγ activated cells[195]. Importantly, *in vivo* Δ*ist* parasites show a decrease in dissemination and lethality[174]. This suggests that IST plays a more general role in immune evasion not specific to strain type.

Toxoplasma also blocks type I IFN(β) induced STAT1 transcription through IST and Mi-2/NuRD complex recruitment[241,254]. Type I interferons (α, β, λ) are secondary to IFNγ in controlling acute *Toxoplasma* both *in vitro*[255,256]and *in vivo*[257]. However, type I receptor knockout mice infected with parasites showed an increase in the number of brain cysts, suggesting that type I IFNs in the CNS do have a role in controlling CNS infection and cyst burden, implicating IST in both acute and chronic infection[254].

1.6.2.2.4 GRA18: pro-inflammatory dampening

GRA18 was originally found *in silico* with the aforementioned proteins and, unlike these proteins, localises to the host cell cytosol where it is a positive regulator of β-catenin[258]. GRA18 brings together the β-catenin destruction complex components: the glycogen synthase kinase-3 (GSK3a/b), and protein phosphatase 2A (PP2A) with its regulatory subunit B56a/b/g/d. The β-catenin destruction complex is a regulatory complex responsible for the degradation of β-catenin in the absence of Wnt signalling[259]. GSK3a/b and PP2A-B56 bind to the C-terminal end of GRA18 and, although β-catenin was associated with the N-terminus of GRA18 in pull-down experiments, the interaction is dispensable. This suggests the interaction with the destruction complex which is responsible for the positive regulation of β-catenin. Upon Wnt signalling the β-catenin destruction complex is inhibited and β-catenin accumulates at the nucleus where it controls the transcription of the Wnt target genes[260,261]. In the absence of Wnt signalling ligand (Wnt3a) β-catenin is both upregulated and localises to the host cell nucleus in *Toxoplasma* infected cells and GRA18 alone is sufficient to induce these changes[258]. The overall regulation of traditional Wnt/β-catenin target genes appears to remain unaffected despite the synthesis of type I interferon (IFN β), a known Wnt-regulated cytokine[262,263]. The host-cell pathways most impacted by GRA18 in macrophages appear to be those associated with the inflammatory response and chemotaxis. Interestingly, there is an increase in the expression and secretion of chemokines CCL17, CCL22, and CCL24[258] which are known to recruit T-regulatory cells[264]. T-regulatory cells amplify the T_H2 response and dampen the pro-inflammatory T_H1 response, which is critical to parasite control and clearance suggesting the early secretion of T_H2 cytokines favours the parasites survival and dissemination[222,223,258]

1.6.2.2.5 HCE1/TEEGR: E2F transcription modulator

Two independent groups identified *Toxoplasma* gene ME49_239010 and both implicated the protein in the modulation of two pathways controlled by E2F transcription factors (TF): host cell cycle and NF-κB signalling, named Host Cyclin E (HCE1)[265] and *Toxoplasma* E2F4-associated EZH2-inducing Gene Regulator (TEEGR) respectively[266]. The HCE1/TEEGR localises to the host cell nucleus and interacts with E2F-DP (E2F-dimerization partner) complexes, which includes

DP1 complexed with E2F proteins, E2F4 and E2F3 TF (among other TF)[265,266]. Further, the enrichment of specific Transcription Factor Binding Sites (TFBS) associated with E2F4 and E2F3 TFs, and the enrichment of differentially expressed genes in the E2F transcription pathways supports such interactions[265,266]. Cyclin E1 and cyclin E2, initiators of G1/S phase, are known downstream targets of E2F transcription factors and both are upregulated during *Toxoplasma* infection. This suggests that the parasites induce host cells into S phase, before inhibiting G2/M phase via GRA16[176,265]. Why the S phase is important for the parasites survival remains unclear. E2F4 complexed with HCE1/TEEGR also upregulates EZH2 gene expression, a regulator of histone methylation[267]. EZH2 interferes with the induction of NF-kB activity by GRA15 to supress the release of NF-κB induced inflammatory chemokines (IL-8) and cytokines (e.g. IL-1B, IL-6), while not affecting the production of others (IL-12, IL-18)[266]. Like GRA18, HCE1/TEEGR's secondary role might be striking a balance between causing a severe prolonged inflammatory response (e.g. cytokine release from the activation of NF-κB by GRA15) from the host and preserving the host to enable parasite survival.

1.6.2.2.6 GRA28: the unknown

GRA28 was discovered by biotinylation of PV and PVM proteins via a biotin ligase fused to the PVM protein GRA17 and the subsequent streptavidin immunoprecipitation and mass spectrometry[212]. This process identified upwards of 100 new proteins, of which only 15 were used for localisation studies. Only GRA28 was found to be exported to the host nucleus and no further analysis on the role of GRA28 has been discussed in the literature to date[212].

1.7 Trafficking of exported effector proteins

1.7.1 *Toxoplasma* export signal

For decades, it has been known that *P. falciparum* remodels its host cell via the export of parasite proteins, which is central to the survival of blood-stage parasites. For this reason, post-invasion protein export has been the centre of many *P. falciparum* studies. As both *Toxoplasma*

and *Plasmodium* require nutrient uptake and systems to evade the immune system, it seemed possible that *Toxoplasma* could also export host-modifying proteins post-invasion. Previous *Plasmodium* export studies gave *Toxoplasma* researchers a place to start and continues to be used as a comparison for *Toxoplasma* export[268].

P. falciparum completely transforms the erythrocyte, by exporting and installing protein machinery to enable nutrient exchange and prevent immune detection. Proteins that are destined for export are directed by an N-terminal signal peptide (SP) that targets proteins for translocation into the ER[268]. Subsequently, these proteins are cleaved by the membrane bound aspartyl protease, Plasmepsin V (PMV), which permits translocation across the PVM. PMV recognises the *Plasmodium* export element motif (PEXEL; RxL*xE/Q/D, *indicates cleavage) typically found a short distance from the SP cleavage site[269-271]. All proteins that are cleaved are directed to the *Plasmodium* translocon of exported proteins (PTEX), which mediates transport across the PVM and into the host cell[272,273]. *Toxoplasma* too has a PEXEL-like motif (coined TEXEL: *Toxoplasma* Export Element) and a homologue of the PMV, called aspartyl serine protease 5 (ASP5)[274-277] (Fig. 1.5A). The TEXEL's consensus motif is 'RRL*xx'[274], a common motif identified by Hsiao *et al.* (2013)[277].

Like PMV, ASP5 loss results in a complete block in protein export, whereas the loss of the TEXEL in individual proteins is not as severe. Unlike the PEXEL, not all TEXEL containing DG proteins processed by ASP5 are exported into the host cell[278-281]. Some require both ASP5 and TEXEL cleavage for the maturation and localisation to the PV and PVM[282]; others do not require ASP5 for their localisation to the PV[279]. All *Toxoplasma* proteins known to localise to the host nucleus require ASP5 despite not all having a TEXEL. Three independent groups identified a TEXEL in GRA16 (RRLAE) and showed that the cleavage of GRA16 by ASP5 is required for its export into the host cell[274-276]. Similarly, IST contains a TEXEL and ASP5 cleavage is required for export into the host nucleus[247,248], and GRA18 also has N-terminal TEXEL motifs[258]. GRA24 and HCE/TEEGR have no obvious TEXEL motifs and undergo no processing, and yet they require ASP5 for export, suggesting direct TEXEL cleavage is not the signal for export and may lie in another sequence or structural signal yet to be identified[266,274-276]. Similarly, MAF1 has no TEXEL but upon ASP5 knockout host mitochondrial association (HMA) is reduced[280]. This suggests that ASP5 acts indirectly on GRA24, HCE/TEEGR, MAF1 and potentially other GRA proteins lacking

a TEXEL motif; ASP5 likely acts on a protein component of the *Toxoplasma* translocon. In fact protein components of the theoretical *Toxoplasma* translocon complex (MYR1, GRA44, GRA45; discussed in *section 1.7.2.2*) have TEXELs and are cleaved by ASP5, but ASP5 cleavage is not essential for their role in protein translocation[278,280]. It is clear that we have no consensus on the export signal in *Toxoplasma* and gaining a better understanding on what directs a protein to the translocon will be vital in identifying novel exported proteins in a more targeted and efficient fashion.

1.7.2 Tachyzoite protein trafficking

1.7.2.1 Protein export

Proteins destined for export are transported across the PVM by the *Plasmodium* Translocon of Exported Proteins (PTEX), which unfolds and refolds proteins to facilitate export. The PTEX is comprised of three essential proteins transmembrane protein Exported Protein 2 (EXP2), the ATPase Heat Shock Protein 101 (HSP101), and PTEX150[283]. There are no homologs of PTEX proteins in *Toxoplasma* outside of small molecule traffickers, GRA17 and GRA23 (whose functions are discussed in *section 1.9.3*), despite the need for a protein complex with a similar function and role. Similar to *Plasmodium*, a key requirement for protein export in *Toxoplasma* is an unfolded protein. Whereas *Plasmodium* has unfolding and refolding mechanisms as part of the export process[283]*, Toxoplasma's* exported effector proteins are all are highly disordered and often contain Short Linear Motif (SLiM), characteristics now used to help define a exported dense granule protein[258,265,284], suggesting that they might not need a unfolding a refolding mechanism.

The use of intrinsically disordered regions and SLiMs is not unique to *Toxoplasma*, multiple organisms use such peptides to enable pathogen-host interactions because: 1) the structural simplicity is suggested to aid in an organisms ability to acquire and tolerate mutations in said peptide, enabling pathogens to evolve quickly in response to the consistent evolutionary arms race[284-286], and 2) traditionally eukaryotic interacting motifs are found in highly disordered areas of structured proteins[286-288]. For example B56 (the PP2A regulatory subunit)

binds to a SLiM (LxxLxE) onto the β-catenin destruction complex scaffolding protein (Axin)[286,289] and GRA18 has two SLiM motifs suggesting this is the mechanism for PP2A-B56 recruitment to GRA18[258] with a similar SLiM mechanism also shown to be the case with GRA24 and GRA16[238,284]. Furthermore, peptide disorder in *Toxoplasma* is required for functional export where the addition of a structured protein domain (dihydrofolate reductase, DHFR) to GRA16 prevents export of not only the fused protein but also other effector proteins[290]. It appears large, highly ordered proteins block the export machinery, suggesting there is no active unfolding at the translocon unlike *Plasmodium*. However, there are indications that smaller folded proteins fused to dense granule protein GRA16 can be exported[291], including proteins often used for genetic modification like Cre (personal correspondence with Dr. Antia Koshy) and FKBP (unpublished Tonkin data), suggesting some structure is tolerated in the export system. The exact mechanical process of export remains an unanswered but important question, which could lead to a better understanding of the types of machinery proteins responsible for export.

1.7.2.2 Export machinery

With only two PTEX homologs in *Toxoplasma* and no evidence that they were required for protein export, other experimental means had to be used to identify the translocon components. The first *Toxoplasma* protein identified as having a role in protein export was Myc Regulator 1 (MYR1)[279]. MYR1 was identified through a random mutagenesis screen that looked for genes that prevented the upregulation of host c-Myc, a phenotype previously seen in *Toxoplasma* infected cells. The next three proteins were identified by data from the same screen, two novel proteins, MYR2 and MYR3, and ROP17[290,292]. Finally, by pulling down MYR1 and investigating interacting proteins two more novel proteins, designated MYR4 and GRA45, and one previously identified protein, GRA44[281,282], were identified and characterised as important in *Toxoplasma* protein export. The exact function of these proteins in protein export is unknown. All are membrane associated and localise to the PVM and their absence prevents protein export[203,265,278,279,281]. However, host cell modifications that do not require protein export, such as host mitochondrial association (MAF1) and induction of NF-kB (GRA15), remain uninfected by the loss of MYR1[293].

These studies only work to identify players involved in protein export but do not explore the exact function of these proteins (Fig. 1.5B). It is still unclear what each protein's exact role is in export. MYR1 is the most studied protein of the seven identified. It is a proposed homologue of TatC, a protein that is involved in translocating folded proteins[294], which was the first suggestion that MYR1 is part of a putative *Toxoplasma* translocon complex[279]. The absence of MYR1 abolishes host c-Myc induced transcription by *Toxoplasma*, and prevents the export of all known GRA effector proteins. Further, MYR1 is essential for a large portion of transcriptional changes observed in *Toxoplasma* infected host cells, supporting its key role in the export of parasite effector proteins[184], and (at least in type II parasites) is a key virulence factor *in vivo*[279]. MYR1 must be able to form stable interactions, and may even complexes with the MYR3, MYR4, GRA44 and GRA45 as they easily co-precipitate[278,290]. In contrast, MYR2's interaction with MYR1 and MYR3 is either transient or absent[290]. Which proteins make up the pore and which are accessories or chaperones to export is unclear. Additionally, it appears the phosphorylation of a translocon component by ROP17 is key to protein export but what competent is phosphorylated, when phosphorylation occurs, and how long phosphorylation confers function remains undetermined[292]. There is still a lot of work to be done if our understanding of *Toxoplasma* protein export is to ever reach that of *Plasmodium*.

1.7.3 Nutrient trafficking

As mentioned above, *Toxoplasma* has two homologs of *Pf*EXP2, the PTEX pore forming protein[295]. These homologs were named GRA17 and GRA23 and both localise to the PVM, although their localisation is not dependent on each other[295,296]. *Pf*EXP2 functions in both nutrient acquisition and protein export, likely changing the pore function depending on interactions with other factors[297]. In contrast, GRA17 and GRA23's roles are more specific to nutrient acquisition and neither is thought to be involved with protein export[295]. GRA17 is responsible for the influx and efflux of small molecules (<3000 Daltons) across the PVM. These small molecules are likely vital for *Toxoplasma* as parasite growth is stunted in GRA17 knockout lines and overexpression increases parasite numbers; neither phenotype was observed in GRA23 knockouts to the same degree. However, dual GRA17 and GRA23 parasite knockouts do not survive *in vitro* suggesting a compounding effect of these two proteins. A model offered

Figure 1.5

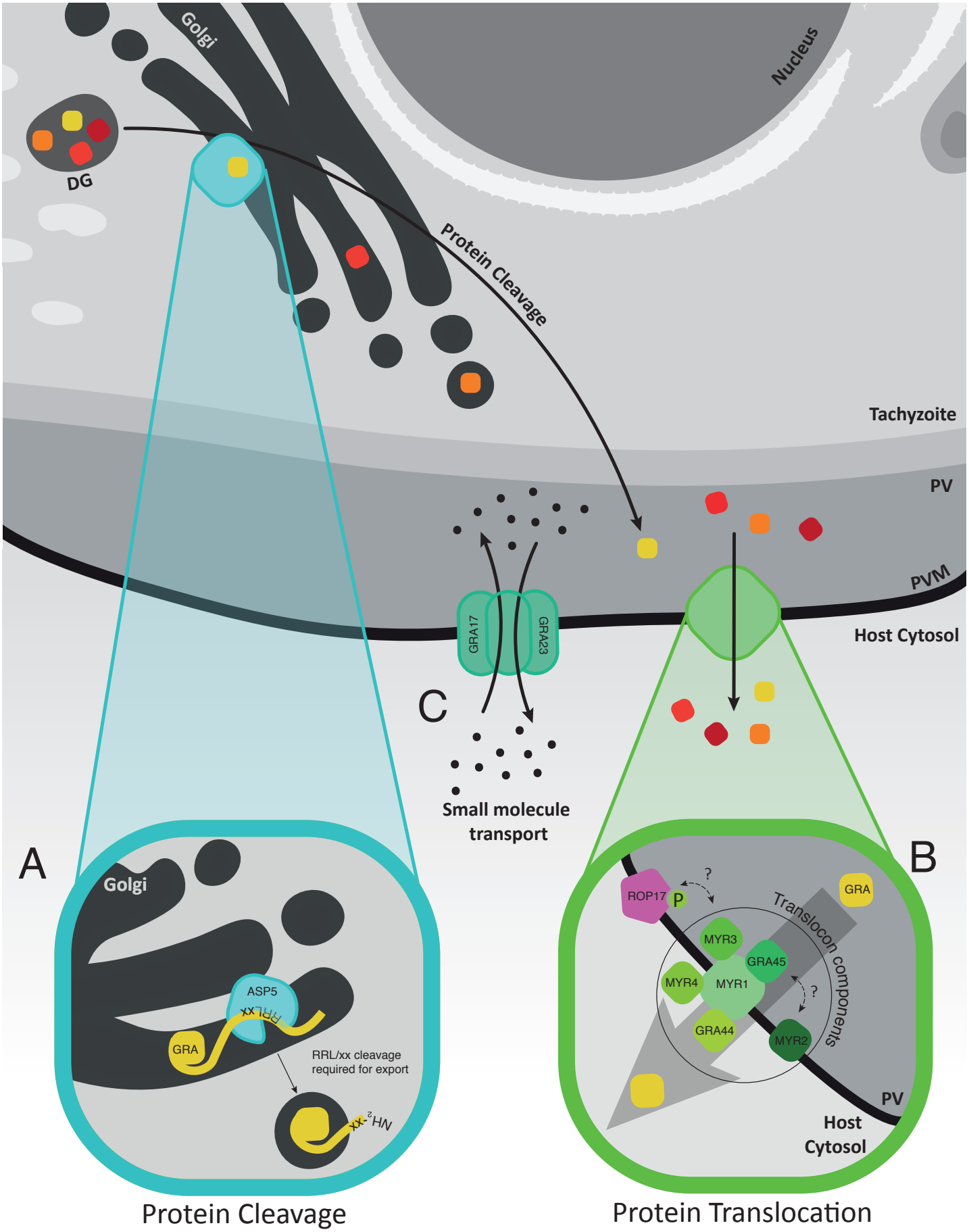

Golgi
Nucleus
DG
Protein Cleavage
Tachyzoite
PV
PVM
Host Cytosol
GRA17
GRA23
C
Small molecule transport
A
Golgi
ASP5
RRL-xx
GRA
RRL/xx cleavage required for export
NH2-xx
Protein Cleavage
B
ROP17
P
?
GRA
Translocon components
MYR3
GRA45
MYR4
MYR1
?
GRA44
MYR2
PV
Host Cytosol
Protein Translocation

Figure 1.5 – Parasitophorous vacuole membrane (PVM) trafficking in tachyzoites

Exported dense granule (GRA) proteins (reds, oranges, and yellows) are produced in the dense granule (DG) and go through the Golgi as part of the secretory pathway where they are cleaved by ASP5 (blue) and exported by the MYR1 translocon complex (green).

(A) GRA proteins that contain the RRLxx motif are cleaved by ASP5 after the lysine and are transported to the PV space or PVM. Cleavage is required for export, but not all exported proteins have the RRLxx motif.

(B) The exact translocon proteins, composition of the complex and the mechanism of export is unclear. MYR1-4, GRA44 and 45 are required for export. MYR2 does not interact with MYR1 and MYR2's relationship with the translocon complex is undetermined. Phosphorylation by ROP17 appears to be required, although what component of the complex is phosphorylated is unknown.

(C) Small molecules are transported across the PVM via protein pores (aqua) made from either GRA17, GRA23 or a combination of both.

Image inspired by Hakimi, M.-A., Olias, P. & Sibley, L. D. Toxoplasma effectors targeting host signalling and transcription. *Clinical microbiology reviews* 30, 615-645; 0893-8512 (2017).

is that GRA17 and GRA23 form a variety of homo- and/or hetero-multimers with differing small molecule affinities that enable them to compensate for the loss of the other[295] (Fig. 1.5C). Whether GRA17 and GRA23 have overlapping roles with the translocon complex (like *Pf*EXP2) is unknown. Both proteins co-precipitate with MYR1, and with GRA23 in the top 25 enriched proteins it could suggest a potential interaction with the translocon complex, an interaction that should be investigated further[278].

1.7.4 Bradyzoite protein trafficking

In comparison to all that I describe above, we know very little about if and how protein export occurs in *Toxoplasma* bradyzoites. As discussed previously (*section 1.5.2*) GRA17 has been implicated in the trafficking of nutrients across the cyst wall[144] which appears to be vital for bradyzoite differentiation. This could explain the size restriction in the passive movement of small molecules observed previously[132] and larger macromolecules may need to be trafficked in via vesicle invagination[143]. These studies focus on the movement of nutrients into the cyst wall, but neither look at protein export, which is likely an active and selective process. To do specifically probe protein export, one study tested the capacity for encysted bradyzoites to export GRA16 and GRA24 by using a tetON conditional-promoter system that activated the expression of these proteins post-differentiation[298]. Both GRA16 and GRA24 were confined to the cyst wall, indicates that protein export may be prohibited in bradyzoite stages[298]. The authors speculate that protein export is not essential for encyst bradyzoites and that the cyst wall is impenetrable, likely due to the lack of a function translocon complex. However, MYR1 along with many of the other known hypothetical translocon complex proteins are expressed in bradyzoites stages and are at high enough levels in the cyst wall to be detected by mass spectrometry[134,278]. Whether these proteins are in a functional complex or if ROP17 phosphorylation continues to be a requirement in protein export remains unclear. Furthermore, the exact signal for protein export is unknown, and the signal might differ between stages meaning proteins such as GRA16 or GRA24 are not exported simply because they do not have the right signals for bradyzoite export. It is also likely that there are many yet unidentified exported proteins, some of which could be bradyzoite exported effectors or components of the translocon and are differentially expressed between stages. These are all

questions that remain unanswered but could provide a greater insight into how bradyzoites persist.

1.8 Thesis aims

Bradyzoite-host pathogen interactions remain largely unknown, despite the recent advances the field has made in understanding *Toxoplasma* host manipulation in tachyzoite stages. This is likely due to the technical difficulties with working on *in vitro* bradyzoite differentiation; *in vitro* differentiation is a balancing act between preventing bradyzoites conversion to tachyzoites and host cell viability. Consequently, this makes segregating and obtaining sufficient bradyzoite material difficult. In contrast, *in vivo* work does not lend itself to the study of individual cells and signal pathways, making disentangling pathogen contributions from host responses difficult. The last decade of research has made it evident that tachyzoites use host modification to enable persistence and that these proteins are often drivers of virulence. It is equally likely that bradyzoites export proteins to skew the host's transcriptional response to infection in order to remain undetected thus enabling long term persistence within the host.

Therefore, my thesis aims to understand whether *Toxoplasma* bradyzoites modulate the host transcriptional response for their survival and, if so, what role does dense granule protein export plays during bradyzoite stages. Specifically, the thesis focuses on:

- Understanding the transcriptional profile of bradyzoite-infected host cells and determining whether the profile is similar or different to tachyzoites
- Determining if parasite protein export plays a role in these transcriptional changes.
- Identifying dense granule proteins that may be exported at the bradyzoite stages.
- And, discovering what importance bradyzoite host modification may have on bradyzoite persistence.

Chapter 2: General Methods and Materials

2.1 Host cell culture

Primary human foreskin fibroblasts (HFFs) were grown to confluency in DME supplemented with 1% v/v Glutamax (Invitrogen) and 10% v/v cosmic calf serum (GE Healthcare, New Zealand) (D10). Cells were incubated at 37°C with 10% CO_2. HFFs were passaged by trypsin de-attachment, and kept for a maximum of 15 passages before new HFFs were acquired.

2.2 Parasite culture

All *Toxoplasma* parental parasite lines used are of the 'type II' Prugniaud (Pru) unless otherwise indicated. D10 media was replaced with D1 (DME supplemented with 1% v/v Glutamax (Invitrogen) and 1% v/v cosmic calf serum (GE Healthcare, New Zealand)) prior to parasite inoculation. Inoculated HFF were incubated at 37°C with 10% CO_2 until the monolayer lysed or, if required prior to lysis, host cells were scraped and passed through a 27G needle to release parasites.

2.3 *In vitro* bradyzoite differentiation

Bradyzoite differentiation was achieved by inoculating tachyzoites onto confluent HFFs at an MOI of 0.1 (for IFA) or 0.2 (for RNA sequencing, western blots and FACS) and cultured in RPMI-HEPES supplemented with 5% v/v fetal calf serum (FCS) (Invitrogen, Australia) at pH 8.1-8.2 and allowed to differentiate at 37 °C with ambient CO_2[299]. The media was changed every 2 days (to prevent acidification) for at least 7 days prior to assays.

2.4 Parasite Transfections

Parasites were needle passed and $2x10^6$ cells were resuspended in 20 uL P3 solution (Lonza) containing plasmid or DNA fragments, before being transfected by the Amaxa 4D Nucleofector (Lonza) using the code FI-115 (Human Unstimulated T-cells). Parasites were cloned out immediately or, for drug selectable transfections, parasites were on drug selection for a minimum of two cycles prior to being serially cloned out and screened either by, sequencing, western blot or IFA. Specific plasmid design, construction and used primers are indicated in the relevant chapter's Methods.

2.5 Immunofluorescence Assays (IFA), microscopy and data quantification

Parasites were fixed in 4% v/v paraformaldehyde (Sigma) in PBS for 10 minutes; permeabilised in 0.1% v/v Triton X-100 in PBS and blocked in 3% w/v BSA (Sigma) in PBS for 1hr. Primary antibodies were diluted in the bovine serum albumin (BSA)/PBS solution for 1hr, washed, and then incubated with Alexa Fluor-conjugated secondary antibodies (Invitrogen) for 1hour, 5 µg/ml DAPI was added in the penultimate wash for 10 minute and samples were mounted onto microscope slides with Vectashield (Vector Labs) and kept at 4 degrees until imaged. Samples were imaged using either the Zeiss AxioLive Cell Observer, or the Zeiss LSM 880 for quantification. Quantification was automated using an FIJI (ImageJ)[300] macro developed in house (available on request). Briefly, the mean grey value (MGV) of the protein of interested was measured both within the parasite vacuole and the host nucleus. MGV for non-specific background was subtracted for all analyses before the ratio of export (nucleusMGV/vacuoleMGV) or ratio of IRF1 expression (IRF1infectedMGV/ IRF1uninfectedMGV) was calculated. Also measured was size area for both nucleus and parasite and GFP intensity.

2.6 Western blot

Immunoblot samples were pelleted then lysed for 30 minutes at 4 °C in 1% v/v Triton-X 100 (BioRAD), 1 mM $MgCl_2$ in PBS (Gibco) supplemented with final 1 x cOmplete protease inhibitors (Roche) and 0.2 % v/v Benzonase (Merck). Samples were then combined with an equal volume of non-reducing or reducing (β-mercaptoethanol) 2x Sample buffer and 15 µl was loaded onto a 4-12% Bis-Tris NuPAGE Protein gel (Invitrogen) and run in 1x MOPS (Thermo Fisher) for a minimum of 60 minutes at 200V. Proteins were transferred onto nitrocellulose by running in western transfer buffer (25 mM Tris, 192 mM glycine, 20% (v/v) MeOH in water) for minimum of 90 minutes at 110V. The transfer was then blocked in 5 % w/v milk in 0.05 % Tween 20-supplemented PBS (PBS-T). Primary and secondary antibodies were diluted in milk/PBS-T. Nitrocellulose membranes were either imaged using a chemiluminescent process or an infrared fluorescence imaging (LiCOR). The former used antibodies conjugated to HRP followed by ECL (GE Healthcare) incubation; the latter was imaged on an Odyssey Fc imager (LI-COR Biosciences) using IRDye 800CW goat α-rat, IRDye 800CW goat α-mouse or IRDye 680RD goat α-rabbit antibodies.

2.7 Statistical Analysis

Statistical analyses were conducted with Prism 7 (GraphPad). Samples were tested for normal (Gaussian) distribution prior to statistical testing. For groups of three or more, the test for significance was performed using either a parametric one-way analysis of variance (ANOVA) if all samples were normally distributed, or a non-parametric Kruskal-Wallis test for non-normal distributions. Both test were accompanied with the indicated post-test analysis for multiple comparison correction. Groups of two were analysed using unpaired Student's *t* test (parametric) or the non-parametric test indicated. In all cases, significance was determine by $p \leq 0.05$. Specific statistical tests used are identified in each figure legend. Specialised or extra testing that differ from these methods are included in the corresponding chapter's methods section.

G#	ToxoDB Gene ID (ME49_)	Gene Target	Function	Sequence
1	254470	MYR1	KO	gatggattggcctggtcttgt
2	242720	ASP5	KO	gggtcctgttctgggcagat
3	254470	MYR1	3'tag	gaaaagcaggagaacgtgcc
4	208830	GRA16	3'tag	gatcagatgtgactaaccaga
5	230280	GRA24	3'tag	gtgtgttcaaagtgccctat
6	240060	IST	3'tag	gtagtgaacggcgggtctag
7	240060	IST	KO	actgtgacggcctctgcccg

Table 1 – CRISPR guides

P #	Direction	Target	Sequence	For Guide #
1	Reverse	All	aacttgacatccccatttac	All
2	Forward	MYR1	gatggattggcctggtcttgtgttttagagctagaaatagcaag	1
3	Forward	ASP5	gggtcctgttctgggcagatgttttagagctagaaatagcaag	2
4	Forward	MYR1	gaaaagcaggagaacgtgccgttttagagctagaaatagcaag	3
5	Forward	GRA16	gatcagatgtgactaaccagagttttagagctagaaatagcaag	4
6	Forward	IST	gtagtgaacggcgggtctaggttttagagctagaaatagcaag	6
7	Forward	GRA24	gtgtgttcaaagtgccctatgttttagagctagaaatagcaag	5
8	Forward	IST	actgtgacggcctctgcccggttttagagctagaaatagcaag	7

Table 2 – Primers for protospacer replacement

SeqP #	Direction	Target	Sequence
1	5' →	U6 promoter	cgagacactgggatatgtagagccaagg
2	5' →	U6 promoter	gcttcctccctgtgcgctcttcgaagg
3	5' →	MYR1	gccgccacagaatcgtaacgag
4	5' →	ASP5	gcagagcagggaacagagagg

Table 3 – Sequencing primers

OligoP #	Direction	Target	Sequence
3	5' →	IST	cgccggccgccgagtagtgaacggcgggtctatccttacgatgttccagattatgcctag
4	3' →	IST	aattctgcccgcaaatgcatccacccactaggcataatctggaacatcgtaaggatagac

Table 4 – Oligo sequences for IST 3' prime homologous recombination

AmpP #	Direction	Target	Function	Sequence
1	Forward	MYR1	KO confirmation	gccgccacagaatcgtaacgag
2	Reverse	MYR1	KO confirmation	gcacacgagatcgccgtggctg
3	Forward	ASP5	KO confirmation	gggggctcttcgttcctcagtttctcc
4	Reverse	ASP5	KO confirmation	ggtcggattcattgaataaagggtacttgg
5	Forward	MYR1	HA 3'tag	gaccgtcatttccgtcagtcacataattcgtacccgtacgacgtcccggactacgctggc
6	Reverse	MYR1	HA 3'tag	gggatttcccctggcCcgttctcctgctttaccacacggcagtgcggagcactgctctga
7	Forward	*Tg*Repeat	qPCR	aggagagatatcaggactgtag
8	Reverse	*Tg*Repeat	qPCR	gcgtcgtctcgtctagatcg
9	Forward	*m*GAPDH	qPCR	aggtcggtgtgaacggatttg
10	Reverse	*m*GAPDH	qPCR	tgtagaccatgtagttgaggtca
11	Forward	GRA24	HA 3'tag	tccgccgctacgcatcgttaaaccacccactaagggtaattacccgtacgacgtcccgga
12	Reverse	GRA24	HA 3'tag	atAcggcactttgaacacacattcgctgcccctaaaacAAacgggaccacacggcagtgc
13	Forward	MYR1	DHFR-KO	cgacatgaattctctagaccgacattaagtgaatagagaccaggccaatccatcggagcc
14	Reverse	MYR1	DHFR-KO	ggctccgatggattggcctggtctctattcacttaatgtcggtctagagaattcatgtcg
15	Forward	IST	DHFR-KO	gccctctagccgtatatgcaaggactgtgacggcctctgcgtaaaacgacggccagtgaa
16	Reverse	IST	DHFR-KO	gacaagagcctctctctgggaccagtgagttccaccgcggataatacgactcactatagg
17	Forward	*h*IRF1	qPCR	catgagaccctggctagagatgc
18	Reverse	*h*IRF1	qPCR	atgcttggcagcatgcttccatgg
19	Forward	*h*HPRT	qPCR	ggaaagggtgtttattcctcatggac
20	Reverse	*h*HPRT	qPCR	acacagagggctacaatgtgatgg

Table 5 – Primers used in the amplification of knockout and HA-tag inserts, qPCR, and for sequencing CRISPR/Cas9 knockouts

Origin	Target	CAT#	Dilution	Source
Mouse	SAG1	DG52	1:1000	
Rabbit	GAP45		1:1000	
Rabbit	SRS9		1:1000	John Boothroyd
Rabbit	cMyc	Ab32072	1:1000	abcam
Rabbit	IRF1	D5E4	1:200	Cell signalling
Rat	HA	3F10	1:1000	Sigma-Aldrich
Rabbit	CST1		1:1000	John Boothroyd
Mouse	BAG1		1:500	John Boothroyd
DBA – Rhodamine	N-Acetylgalactosamine	RL-1032	1:200	Vector Laboratories
DBA – Fluorescein	N-Acetylgalactosamine	RL-1031	1:200	Vector Laboratories
Streptavidin, Alexa Fluor 488 conjugate	Biotin	S11223	1:1000	Invitrogen
Avidin, NeutrAvidin-HRP	Biotin	A2664	1:10,000	Invitrogen

Table 6 – Primary antibodies used for IFA, Western blot and FACS

Conjugate	Target	CAT#	Dilution	Source
Alexa Fluor 488	Rat IgG	A11006	1:1000	Invitrogen
Alexa Fluor 568	Rat IgG	A11077	1:1000	Invitrogen
Alexa Fluor 594	Rat IgG	A11007	1:1000	Invitrogen
Alexa Fluor 647	Rat IgG	A21247	1:1000	Invitrogen
Alexa Fluor 488	Rabbit IgG	A11008	1:1000	Invitrogen
Alexa Fluor 594	Rabbit IgG	A11037	1:1000	Invitrogen
Alexa Fluor 647	Rabbit IgG	A21245	1:1000	Invitrogen
Alexa Fluor 488	Mouse IgG	A11001	1:1000	Invitrogen
Alexa Fluor 594	Mouse IgG	A21201	1:1000	Invitrogen
Alexa Fluor 647	Mouse IgG	A31571	1:1000	Invitrogen
HRP	Rabbit IgG	AP307P	1:2000	Merck Millipore
HRP	Mouse IgG	1031-05	1:2000	Southern Biotech
HRP	Rat IgG	3010-05	1:2000	Southern Biotech
IR-800 dye	Mouse IgG	925-32210	1:4000	LiCOR Biosciences
IR-800 dye	Rat IgG	925-32219	1:4000	LiCOR Biosciences
IR-680 dye	Rabbit IgG	925-68071	1:4000	LiCOR Biosciences

Table 7 – Secondary antibodies and conjugates used for IFA, Western blot and FACS

Chemical	Final Concentration
Tris (pH 8.0)	50 mM
Sodium Chloride	150 mM
NP40	1%
Deoxycholate	0.5%
EDTA	2 mM
SDS	0.1%
Sodium L-Ascorbate	10 mM
Sodium Azide	10 mM
Trolox	5 mM
Complete Protease Inhibitor Cocktail (Sigma)	1x

Table 8 – RIPA Lysis Buffer Composition, made up in H_2O for APEX2 experiments

Chapter 3:

Bradyzoite-induced host cell transcriptional changes

There are sections in the following chapter that are taken from Seizova *et al.*[1], a manuscript written by me during my PhD, and edited by Assoc. Prof. Christopher Tonkin and Dr. Alexandra Garnham. It has been submitted to bioRxiv, but is still in progress and has not been submitted at a journal. Please see preface for more details.

3.1 Introduction

Like many pathogens, *Toxoplasma*'s ability to survive within its host can be attributed to its capacity to avoid immune detection[5]. This is achieved, in part, by its ability to export parasite effector proteins that interfere with host cell programs[163]. *Toxoplasma*-host manipulation investigations have largely focused on tachyzoites, whereas bradyzoite-host cell interactions and manipulation has largely been neglected. It is highly likely that host cell manipulation does differ between tachyzoites and bradyzoites to accommodate the different lifestyles and requirements of the different biological stages: tachyzoites are responsible for the parasites dissemination and virulence, whilst bradyzoites remain quiescent for long periods of time. Bradyzoite dependent transcriptional changes could take place either when setting up a latent infection (i.e. upon differentiation from tachyzoites to bradyzoites) or in ongoing maintenance to allow for persistence of the latent forms over long time periods. Whether such modifications even occur during bradyzoite stages is currently unclear.

In understanding host-parasite interactions, transcriptional analysis of the host cell (originally in the form of microarrays[167] and, more recently, RNA sequencing[184]) has become a very powerful tool. Although there are likely non-transcriptional-based mechanisms used by the parasites to skew the host response, an unbiased, global transcriptional analysis of infected cells is a good starting point in understanding the complex nature of host-parasite interactions as it provides an impartial view of the landscape. Global[179] and more specific *in vitro*[184] transcriptional studies focusing on the host cell upon infection have shown that tachyzoites have a large impact on the host transcription. In contrast, little significant transcriptional changes were observed in *in vitro* bradyzoite samples analysed by microarray[177]; conversely, *in vivo* chronic infection does change the host transcriptome[88,181,253]. However, a *in vivo* holistic analysis does not enable us to pull apart the multiple factors associated with parasite-driven modification from the subsequent host immune response due to infection. Host driven transcriptional responses can also occur in *in vitro* studies, and this may account for differences in the cell-specific responses seen in tachyzoite infection [168,184]. However, with the discovery of ASP5 and MYR1 there is now the ability to prevent a large proportion of parasite effector proteins from either being exported[278-280,290] or maturing to the host-parasite interface[282], thus enabling parasite and host driven factors to be separated. Mutants of MYR1 and ASP5 in

combination with *in vitro* RNA sequencing has been used effectively to probe at tachyzoite-host interactions[184] and will be used in this chapter to probe bradyzoite-host interactions.

Key to understanding bradyzoite-host interactions is obtaining bradyzoite rich samples. The tachyzoite-bradyzoite differentiation process is poorly understood, and, as a result, makes *in vitro* differentiation difficult. Currently, there is a lack of a good *in vitro* differentiation model (discussed in *section 1.5*). Stress induced *in vitro* differentiation models are a balancing act, easily tipped to favour either tachyzoite development or host cell death over bradyzoite formation, which consequently makes segregating and obtaining sufficient material difficult[118]. Furthermore, there are questions around how representative *in vitro* stressed and differentiated bradyzoites are to those developed naturally *in vivo*[130]. Nevertheless, work at the cellular level is essential in order to comprehend how *Toxoplasma* bradyzoites can establish and maintain the clinically relevant reservoir, and whether bradyzoite-host modification occurs even at the early stages.

Therefore, in this first results chapter I focused on understanding the host cell's transcriptional response to *Toxoplasma* bradyzoites and whether any transcriptional changes observed are parasite driven. To do this I differentiated samples for seven days before concentrating wildtype or *myr1* knockout bradyzoite-containing cells and completed dual RNA-sequencing on the samples. I found that at seven days post differentiation, bradyzoite-containing host cells have a unique transcriptional landscape when compared to tachyzoite-infected cells, and demonstrated that parasite protein export via MYR1 is involved in many of the transcriptional patterns seen, suggesting parasite driven modifications during bradyzoites stages.

3.2 Results

3.2.1 Analysing *in vitro* differentiated bradyzoites

I first determined the best time point to take bradyzoite samples after inducing differentiation. Primary human foreskin fibroblasts (HFF) were used in all the analyses as these cells are amendable to bradyzoite differentiation, are of human origin, and are the most commonly used host cell type for RNA sequencing in the *Toxoplasma* field, enabling simpler comparisons between studies[184]. Two strains of the type II parasite strain Pruganid was used in all the experiments because the strain is easy to grow *in vitro* and differentiation has been extensively characterised in this strain. In particular, I use strains Pru Δ*hx* toxofilin-Cre (mCherry^{+}) (kindly gifted by Dr. Anita Koshy) and Pru Δ*ku80* Δ*hx*. The former was chosen for RNA sequencing as it has mCherry expression which enabled sorting of both stages and could later be used *in vivo*[301]; the latter was used mainly for HA-protein tagging and imaging as deletion of DNA repair protein KU80 easily enables homologous recombination[89].

I first wanted to determine the best time point to analyse bradyzoites. This should be the latest time possible as to ensure that they are differentiated, whilst still remaining healthy in order to prevent stress or death of host cells and to minimise unwanted parasite lysis. I tested two multiplicities of infection (MOI; 0.1 and 0.2), visually analysed bradyzoite development through protein expression, and determined the number of infected cells over time. Seven days post alkaline-induction at a MOI of 0.2 (Fig 3.1A) was the longest period of time and the highest density of parasites that could be used without visibly compromising the health of bradyzoite-infected host cells. After seven days of differentiation Pru Δ*hx* toxofilin-Cre (mCherry^{+}) parasites (which will from now be referred to as Pru Δ*hx* (WT)) have accumulated amylopectin granules, built a cyst wall and express bradyzoite markers, like SRS9 (Fig 3.1B). If cultures were continued for 21 days, there was a significant loss of parasite-infected cells (Fig 3.1C) and host cells looked unhealthy (not shown). Such a significant drop in parasite-infected cells suggests that three weeks in differentiation media results in unhealthy host cells (potentially host cell death) and freed parasites maybe unable to reinvade or grow in these cells. However, after seven days the number of parasite-infected host cells does not significantly differ from 24 hours (Fig 3.1C). The persistent numbers at day seven suggest that the host cells remained

healthy enough to support parasite persistence during alkaline-induction. To determine bradyzoite purity at day seven, parasite samples were co-probed with anti-SRS9 antibodies and DBA, and the number of double positive vacuoles were counted by microscopy (no single positives were observed in the frames chosen at random for counting). Quantitation showed at least 90% of the population was positive for SRS9 and DBA under the differentiation conditions used (Fig. 3.1D; consistent with Fouts and Boothroyd[177]). To further characterise bradyzoites produced by the alkaline method, I then examined the expression level of other bradyzoite markers over time using confocal microscopy, quantitating average fluorescence (pixel) intensity as a marker of the level of protein production. Bradyzoite marker CST1 increases during differentiation and by day three protein levels have stabilised, whereas bradyzoite protein markers SRS9 and BAG1 peak at day three, slightly decreasing at day seven (3.1E, F, and G).

Looking at tachyzoite marker SAG1 provides another assessment of the degree of differentiation. In contrast to the bradyzoite markers mentioned above, the time series of tachyzoite protein marker SAG1 shows a decrease over time in differentiation media (Fig. 3.1H). To determine whether the expression level of SAG1 at day seven was background noise or a true signal, I looked at the localisation and intensity of individual parasites representative of the population. On day one, there is a strong SAG1 signal localised to the parasite periphery, whereas SRS9 is lowly expressed (Fig 3.1I). By day seven the majority of SAG1 has lost its parasite membrane localisation and is more diffuse, and SRS9 is strongly expressed on the parasite's periphery (3.1J). This suggests that SAG1 expression at day seven is likely either background noise or the anti-body is cross-reacting with other SRSs proteins, both of which could be tested in the future by repeating the experiment with SAG1 negative parasites.

Confident with the degree and quality of the bradyzoite samples I then proceed to analyse the global effect of bradyzoites on the host transcriptome using RNA sequencing. Bradyzoite-containing host cells were separated from uninfected 'bystander' cells by FACS based on the presence of mCherry (Fig. 3.2A and B). Tachyzoites were also harvested at 24 hours (under normal growth conditions) and sorted on mCherry. RNA was then extracted and sequenced using Illumina chemistry on a NextSeq platform. The parasite data was analysed for the differentially expressed genes between tachyzoites and bradyzoites, which showed that

Figure 3.1

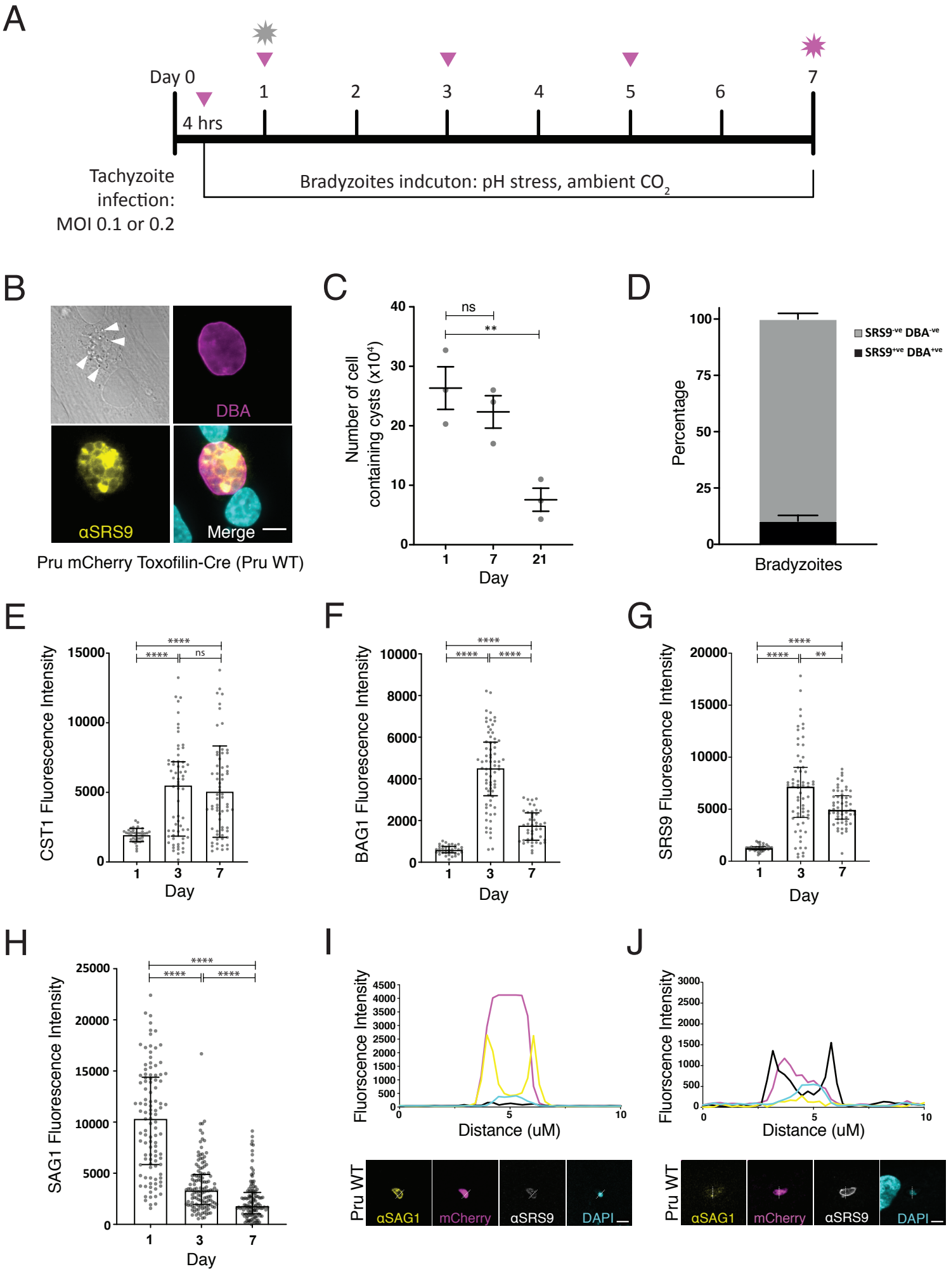

A
Day 0
1
2
3
4
5
6
7
4 hrs
Tachyzoite infection: MOI 0.1 or 0.2
Bradyzoites indcuton: pH stress, ambient CO2
B
DBA
αSRS9
Merge
Pru mCherry Toxofilin-Cre (Pru WT)
C
Number of cell containing cysts (x10⁴)
ns
**
Day
D
Percentage
SRS9-ve DBA-ve
SRS9+ve DBA+ve
Bradyzoites
E
CST1 Fluorescence Intensity
Day
F
BAG1 Fluorescence Intensity
Day
G
SRS9 Fluorescence Intensity
Day
H
SAG1 Fluorescence Intensity
Day
I
Fluorscence Intensity
Distance (uM)
Pru WT
αSAG1
mCherry
αSRS9
DAPI
J
Fluorscence Intensity
Distance (uM)
Pru WT
αSAG1
mCherry
αSRS9
DAPI

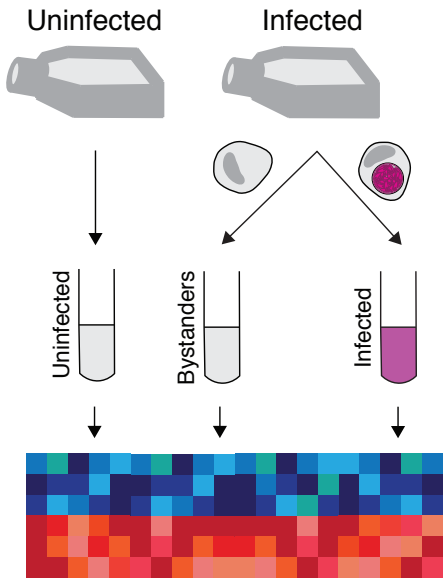
Figure 3.1 -Analysing *in vitro* bradyzoite development

(A) A timeline of *in vitro* differentiation using Pru Δ*hx* toxofilin-Cre (mCherry^{+}) parasites. Magenta arrowheads indicate when the differentiation media was replaced. Tachyzoite samples are taken at 24 hours (grey star) and bradyzoite samples are taken at seven days post inoculation (magenta star). (B) After seven days being in differentiation media amylopectin granules can be seen (white arrows), a cyst wall is developed (DBA, magenta), and parasites are expressing bradyzoite markers (SRS9, yellow). Scale bar = 10μm. Brightness and contrast was edited on single colour channels prior to merging (C) The number of cells containing WT (Pru) parasites cells after 24 hours, seven day and 21 days of differentiation, analysed by FACS (mean ± SEM, minimum of n = 3 per experiment, unpaired, parametric ANOVA with Tukey's test for multiple comparisons, **p=0.008) (D) The percentage of SRS9^{+} (grey) and SRS9^{-} (black) parasites in bradyzoite samples (n = 3 experiments). Over the seven days of differentiation (E) CST1 protein expression (measured by imaging and analysing the fluorescence intensity) grew and plateaued at day three, whereas BAG1 (F) and SRS9 (G) peaked at day three before levels dropped on day seven. In contrast SAG1 (H) steadily decreased over time. (I) After 24 hours of infection, express SAG1 (yellow) is expressed and localises to the parasite's (mCherry, magenta) periphery, whereas SRS9 (white) expression almost at background levels. (J) In contrast after seven days in differentiation media, SAG1 (yellow) expression is at background levels and labelling is diffused, whereas SRS9 is strongly expressed and localises to the parasite's (mCherry, magenta) periphery. Parasite and host nuclei indicated in blue. White dotted line shows path of fluorescence measurement. Scale bar = 5μm

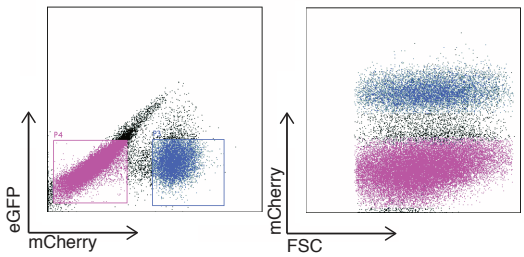
quintessential bradyzoite markers were enriched in the sample (Fig 3.2C and D) whereas the expression of tachyzoite marker transcripts were depleted (Fig. 3.2C and E). Together, this data suggests that our preparations are highly enriched for bradyzoites, thus validating the experimental procedure and previous imaging results.

Figure 3.2

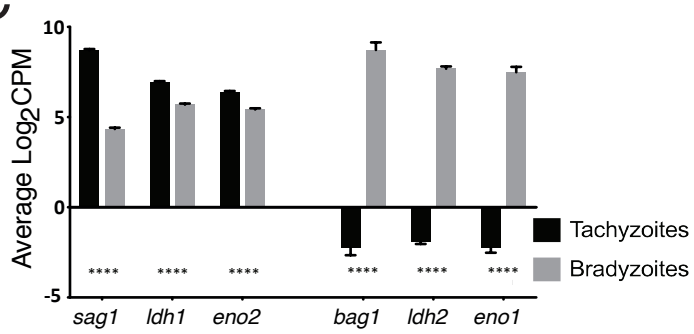
A



B



C



D

Gene ID	Gene and protein description	logFC	AveExpr	adj.P.Val
TGME49_259020	bradyzoite antigen BAG1	10.9612627	3.24411489	2.18E-14
TGME49_202020	DnAK-TPR	10.8448814	3.17240446	2.59E-20
TGME49_216140	tetratricopeptide repeat-containing protein	10.4187181	2.64150134	7.02E-19
TGME49_280570	SAG-related sequence SRS35A	10.1201039	2.90965239	3.36E-13
TGME49_268860	enolase 1	9.72784034	2.62965797	2.29E-15
TGME49_291040	lactate dehydrogenase LDH2	9.59392051	2.88568999	7.02E-19
TGME49_221550	CMGC kinase2C MAPK family2C MEK kinase-related (incomplete catalytic triad)	8.72701853	1.8840233	4.81E-16
TGME49_207160	SAG-related sequence SRS49D	8.64207925	1.70190377	3.34E-15
TGME49_221840	hypothetical protein	8.58413126	1.28878704	1.86E-16
TGME49_209755	hypothetical protein	8.58205695	3.130199	2.28E-19
TGME49_278080	Toxoplasma gondii family A protein	8.5635678	1.78609207	4.27E-16
TGME49_252640	P-type ATPase PMA1	8.49668397	1.45103457	4.81E-16
TGME49_309930	melibiase subfamily protein	8.04909378	2.67128056	3.05E-13
TGME49_275790	EGF family domain-containing protein	7.74735256	0.87039769	2.09E-15
TGME49_207210	hypothetical protein	7.59607083	3.37241376	2.27E-17
TGME49_272590	hypothetical protein	7.45643616	1.10908223	8.09E-14
TGME49_243470	hypothetical protein	7.39538398	1.662399	5.19E-13
TGME49_220560	hypothetical protein	7.30962788	1.15253551	6.64E-13
TGME49_320190	SAG-related sequence SRS16B (SRS9)	7.27065029	2.14975579	1.20E-16

E

Gene ID	Gene and protein description	logFC	AveExpr	adj.P.Val
TGME49_244280	hypothetical protein	-4.9628531	4.3458943	2.09E-18
TGME49_233460	SAG-related sequence SRS29B (SAG1)	-4.3610612	6.51570795	2.28E-19
TGME49_261740	hypothetical protein	-3.6464746	6.7462156	8.50E-20
TGME49_291890	microneme protein MIC1	-3.572769	6.03922932	2.28E-19
TGME49_291960	rhoptry kinase family protein ROP40 (incomplete catalytic triad)	-3.2466874	4.21816409	2.41E-15
TGME49_319350	SAG-related sequence SRS17B	-3.0708961	4.87812627	6.67E-17
TGME49_294990	hypothetical protein	-2.9348111	1.56141381	2.57E-09
TGME49_280670	hypothetical protein	-2.9201819	2.84248143	2.51E-10
TGME49_277270	NTPase II	-2.9155687	4.79929314	3.04E-16
TGME49_266970	hypothetical protein	-2.9116828	1.80450381	2.35E-10
TGME49_205250	rhoptry protein ROP18	-2.9065015	5.70469219	5.66E-17
TGME49_233480	SAG-related sequence SRS29C	-2.8801171	8.00470784	6.55E-19
TGME49_297070	hypothetical protein	-2.8384911	4.73535726	1.60E-15
TGME49_262730	rhoptry protein ROP16	-2.836856	4.14630882	4.73E-15
TGME49_271050	SAG-related sequence SRS34A	-2.7395091	7.72872773	3.76E-18
TGME49_208830	hypothetical protein	-2.6805929	3.90491466	2.58E-10
TGME49_235370	hypothetical protein	-2.6575665	4.61043309	2.41E-14
TGME49_308840	SAG-related sequence SRS51	-2.6548756	5.01742409	4.61E-16
TGME49_201230	kinesin motor domain-containing protein	-2.6540803	1.70162198	1.33E-09
TGME49_279350	hypothetical protein	-2.6217305	1.42510672	5.30E-07
TGME49_256030	hypothetical protein	-2.6137306	3.57727924	3.71E-12

Figure 3.2- *In vitro* produced bradyzoites exhibit bradyzoite transcriptional markers while decreasing tachyzoite transcriptional markers

(**A**) Schematic of sample collection for RNA sequencing indicating uninfected, infected, and bystander populations. (**B**, *left*) a representative FACS plot of the sorting gates used to sort infected and bystander host cells defined as $mCherry^{+}eGFP^{-}$ (blue) and $mCherry^{-}eGFP^{-}$ (magenta) respectively; discarded cells indicated in black. (**B**, *right*) a FACS plot showing a shift towards a $mCherry^{+}$ population after inoculation (**C**) The expression levels in log_2CPM (counts per million) of tachyzoite markers *sag1, ldh1, eno2* and bradyzoite markers *bag1, ldh2, eno1* in tachyzoite (black) and bradyzoite (grey) infected samples **** < 0.0001 (**D**) Top 20 genes that are upregulated and (**E**) the top 20 downregulated genes in bradyzoite samples versus tachyzoite samples (from dataset 1), including the associated log fold change (LogFC), average expression levels in log_2RPKM (AveExpr), and adjusted p-value (adj. P. val).

Figure 3.3

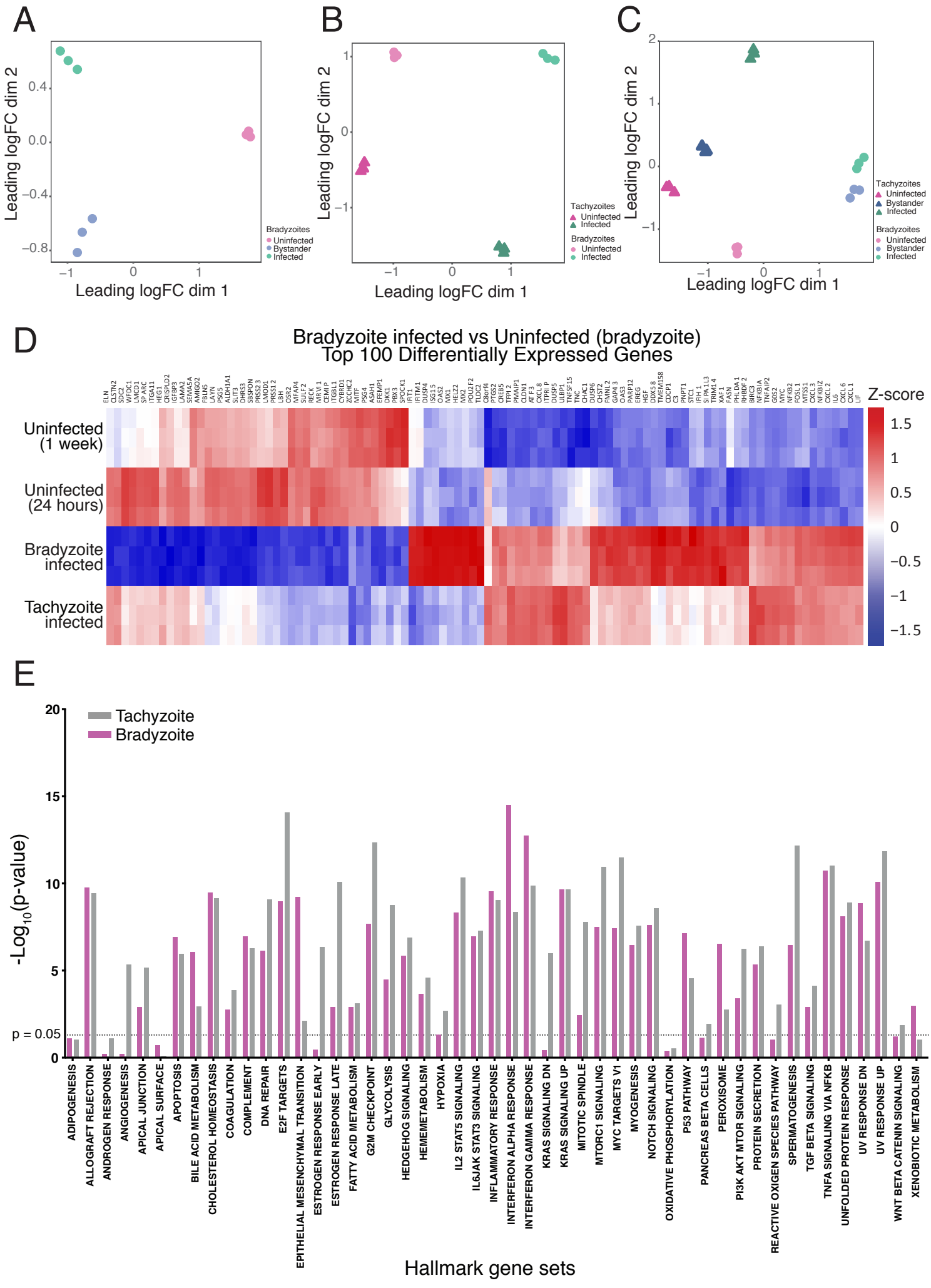

A
B
C
Leading logFC dim 1
Leading logFC dim 2
Bradyzoites
Uninfected
Bystander
Infected
Tachyzoites
Uninfected
Infected
Tachyzoites
Uninfected
Bystander
Infected
D
Bradyzoite infected vs Uninfected (bradyzoite)
Top 100 Differentially Expressed Genes
Z-score
Uninfected (1 week)
Uninfected (24 hours)
Bradyzoite infected
Tachyzoite infected
E
Tachyzoite
Bradyzoite
-Log10(p-value)
p = 0.05
ADIPOGENESIS
ALLOGRAFT REJECTION
ANDROGEN RESPONSE
ANGIOGENESIS
APICAL JUNCTION
APICAL SURFACE
APOPTOSIS
BILE ACID METABOLISM
CHOLESTEROL HOMEOSTASIS
COAGULATION
COMPLEMENT
DNA REPAIR
E2F TARGETS
EPITHELIAL MESENCHYMAL TRANSITION
ESTROGEN RESPONSE EARLY
ESTROGEN RESPONSE LATE
FATTY ACID METABOLISM
G2M CHECKPOINT
GLYCOLYSIS
HEDGEHOG SIGNALING
HEMEMETABOLISM
HYPOXIA
IL2 STAT5 SIGNALING
IL6JAK STAT3 SIGNALING
INFLAMMATORY RESPONSE
INTERFERON ALPHA RESPONSE
INTERFERON GAMMA RESPONSE
KRAS SIGNALING DN
KRAS SIGNALING UP
MITOTIC SPINDLE
MTORC1 SIGNALING
MYC TARGETS V1
MYOGENESIS
NOTCH SIGNALING
OXIDATIVE PHOSPHORYLATION
P53 PATHWAY
PANCREAS BETA CELLS
PEROXISOME
PI3K AKT MTOR SIGNALING
PROTEIN SECRETION
REACTIVE OXIGEN SPECIES PATHWAY
SPERMATOGENESIS
TGF BETA SIGNALING
TNFA SIGNALING VIA NFKB
UNFOLDED PROTEIN RESPONSE
UV RESPONSE DN
UV RESPONSE UP
WNT BETA CATENIN SIGNALING
XENOBIOTIC METABOLISM
Hallmark gene sets

Figure 3.3 - Transcriptional landscape of bradyzoite-containing host cells is different to tachyzoite infection.

Dataset 1: Inoculated HFF cells (human foreskin fibroblast) were FACS sorted into infected and uninfected samples before RNA extraction and sequencing (as per figure 3.2B) (n = 3 experiments, each with 3 replicates). (A) Multi-dimensional scaling (MDS) plot between uninfected, bystander and infected bradyzoite samples. Dimension 1 (dim1) measures the logFC of the top 500 genes between the uninfected-flask and infected-flask samples, whereas dimension 2 (dim2) looks at the differences between host cells from the infected-flask: bystanders and infected/ Plot shows replicates in each sample clustering together away from other groups. (B) MDS plot between tachyzoite infected, bradyzoite infected and corresponding uninfected samples. Dim1 indicates difference between uninfected and infected samples. Dim2 indicates differences between tachyzoite and bradyzoite samples. (C) MDS plot of the above-mentioned samples. Dim1 measures the differences between tachyzoites and bradyzoites. Dim2 measures the difference between samples of the same stage e.g. uninfected, bradyzoite infected, tachyzoite infected. (D) Heat map of expression values for the top 100 differentially regulated genes between bradyzoite-infected (7 days *in vitro*) vs uninfected host cells (7 days). Top 100 DEGs expression are also shown for the tachyzoite-infected (24 hours) and uninfected host cells (24 hours) samples. Expression values are Log_2 reads per kilobase per million (RPKM), scaled to have mean 0 and standard deviation 1 for each gene. The plots show that bradyzoites change the transcriptional profile of the host cell, and this appears to be somewhat different to the profile of tachyzoite infected host cells. (E) Pathways enriched during both tachyzoite and bradyzoite infection. Over-representation analysis results for tachyzoite vs uninfected (grey) and vs uninfected DEGs (magenta) for each Hallmark gene set displayed as the negative Log_{10} of the p-value, dotted line p = 0.05.

3.2.2 Bradyzoites distinctively alter the host transcriptome

Confident with the quality of the samples the global effect of bradyzoites on the host transcriptome was then analysed. To identify if bradyzoite-containing host cells had a unique transcriptional profile and whether their profile differed from tachyzoite-containing host cells, parasite-infected host cells were compared with host cells from uninfected flasks. When bradyzoite-containing cells were compared with the uninfected HFF (after one week), 5804 host genes had significantly changed out of 13,793 expressed genes detected (~42%), suggesting the presence of bradyzoites alters host cell transcription. This is slightly less than the number of differentially expressed genes upon tachyzoite infection (7209, ~52%).

To more quantitatively assess these changes, a multidimensionally scaling (MDS) plot of the top 500 differentially expressed genes (DEG) between bradyzoite-containing, bystander, and control cell samples was generated. The MDS plot indicates that the transcriptional profile of bradyzoite-containing cells are unlike uninfected cells and bystander cells (Fig. 3.3A). Bradyzoite-containing cells are also distinct from tachyzoite infected samples (Fig. 3.3B and C). The relative expression of the top 100 differentially expressed genes (DEGs) between bradyzoite-containing cells and uninfected cells (bradyzoites) was compared to all samples (bradyzoites, tachyzoites, and respective uninfected controls). From the heat map generated using these 100 DEGs, the similarities and differences in bradyzoite-containing and tachyzoite-containing host cells were evident (Fig. 3.3D). Some bradyzoite-induced changes were similar to those observed in tachyzoite infected host cells, whilst other changes appeared to be less pronounced or in the opposite direction, suggesting distinct transcriptional patterns between these two developmentally different stages.

To further understand how host cells containing bradyzoites differ from tachyzoite infected cells, the changes in gene expression were used to analyse how infection impacted host biological pathways. DEGs of both bradyzoite- and tachyzoite-containing cells were analysed via over-representation analyses with the Molecular Signatures Database (MSigDB) Hallmark gene sets[302] (gene sets commonly used in *Toxoplasma* RNA sequencing studies[184])(Fig. 3.3E). Overall there is a high perturbation across all biological pathways, suggesting a significant re-wiring of the host transcriptome in both stages. However, some of these transcriptional changes may be secondary to parasite presence e.g. responses to endogenously released

Figure 3.4

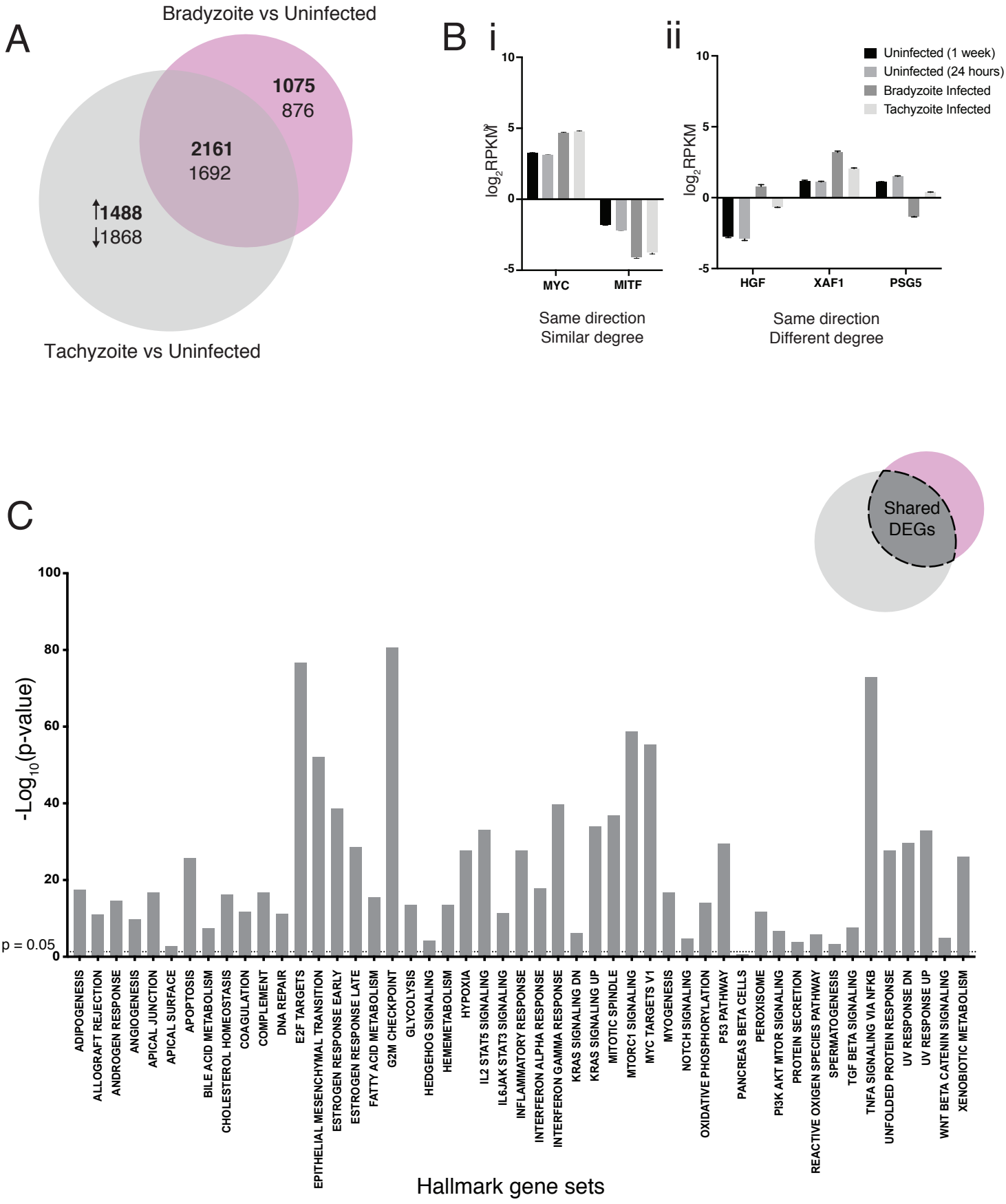

A
Bradyzoite vs Uninfected
1075
876
2161
1692
↑1488
↓1868
Tachyzoite vs Uninfected
B i
ii
Uninfected (1 week)
Uninfected (24 hours)
Bradyzoite Infected
Tachyzoite Infected
log2RPKM
10
5
0
-5
MYC
MITF
HGF
XAF1
PSG5
Same direction
Similar degree
Same direction
Different degree
C
Shared
DEGs
-Log10(p-value)
100
80
60
40
20
0
p = 0.05
ADIPOGENESIS
ALLOGRAFT REJECTION
ANDROGEN RESPONSE
ANGIOGENESIS
APICAL JUNCTION
APICAL SURFACE
APOPTOSIS
BILE ACID METABOLISM
CHOLESTEROL HOMEOSTASIS
COAGULATION
COMPLEMENT
DNA REPAIR
E2F TARGETS
EPITHELIAL MESENCHYMAL TRANSITION
ESTROGEN RESPONSE EARLY
ESTROGEN RESPONSE LATE
FATTY ACID METABOLISM
G2M CHECKPOINT
GLYCOLYSIS
HEDGEHOG SIGNALING
HEMEMETABOLISM
HYPOXIA
IL2 STAT5 SIGNALING
IL6JAK STAT3 SIGNALING
INFLAMMATORY RESPONSE
INTERFERON ALPHA RESPONSE
INTERFERON GAMMA RESPONSE
KRAS SIGNALING DN
KRAS SIGNALING UP
MITOTIC SPINDLE
MTORC1 SIGNALING
MYC TARGETS V1
MYOGENESIS
NOTCH SIGNALING
OXIDATIVE PHOSPHORYLATION
P53 PATHWAY
PANCREAS BETA CELLS
PEROXISOME
PI3K AKT MTOR SIGNALING
PROTEIN SECRETION
REACTIVE OXIGEN SPECIES PATHWAY
SPERMATOGENESIS
TGF BETA SIGNALING
TNFA SIGNALING VIA NFKB
UNFOLDED PROTEIN RESPONSE
UV RESPONSE DN
UV RESPONSE UP
WNT BETA CATENIN SIGNALING
XENOBIOTIC METABOLISM
Hallmark gene sets

Figure 3.4 - Bradyzoites and tachyzoites share a number of host cell gene changes.

(**A**) Venn diagram of tachyzoite vs uninfected DEGs (24 hours post infection; grey) and bradyzoite vs uninfected DEGs (7 days post infection; magenta); the number of up-regulated genes are identified in **bold** and down-regulated genes in regular font. (**B**) Examples of host gene changes that are changed in the same direction (e.g. DEGs are shared) for both bradyzoite and tachyzoite infected samples. (i) MYC and MITF expression changes in the same to the same degree in both tachyzoite and bradyzoite samples. (ii) The expression changes of HGF, XAF1 and PSG5 go in the same direction for tachyzoite and bradyzoite infected cells but to a significantly different degree. (**C**) Host cell pathways enriched in shared DEGs. Over-representation analysis results for tachyzoite and bradyzoite shared DEGs (grey) for each Hallmark gene set displayed as the negative Log_{10} of the P-value, dotted line p = 0.05.

cytokines or non-specific disturbances. In order to tease out biological processes related to the presences of bradyzoites, DEGs were first separated by a Venn diagram (Fig. 3.4A) that compared DEGs from bradyzoite-containing cells versus uninfected cells (bradyzoites), and DEGs from tachyzoite-infected cells versus uninfected cells (tachyzoites). By separating the DEGs, we were able to isolate DEGs that were either shared between the different parasite stages or specific to a stage. Here we found that 3853 DEGs are shared between tachyzoite infected cells and bradyzoite infected cells (41%; 2161 up-regulated, 1692 down-regulated.), leaving 3356 tachyzoite specific DEGs (1488 up-regulated, 1868 down-regulated), and 1951 DEGs specific to bradyzoite infection (1075 up-regulated, 876 down-regulated) (Fig. 3.4A).

To further understand how similar the changes were in the shared group, I looked at the relative expression of the genes in each sample. I found that shared DEGs may have differing degrees of expression despite sharing directionality. Whilst some bradyzoite-induced DEGs had similar patterns to those observed in tachyzoite-infected host cells e.g. gene expression changed in the same direction to the same degree (e.g MYC, MITF; fig 3.4B (i)), others changed in the same direction but to a different degree (e.g. HGF, XAF1, PSG5; fig 3.4B (ii)). Nevertheless, we completed an over-representation analysis of the shared DEGs and showed that the majority of pathways in the Hallmark series were significantly enriched in the number of genes altered by both bradyzoites and tachyzoites (e.g. shared; Fig. 3.4C). However, when the analyses for bradyzoite and tachyzoite specific DEGs were compared, certain pathways are more enriched beyond the shared pathways (Fig. 3.5A). For example, the E2F- and Myc-targets pathways were altered by tachyzoite infection (overall upregulation; visualised by heatmaps Fig. 3.5B (i) and (ii)), but no significant changes were seen in bradyzoite-containing cells over shared DEGs (Fig. 3.5A). On the other hand, cells containing bradyzoites show a greater enrichment of DEGs in immune pathways, including the IFN alpha- and IFN gamma-response pathways, over what is already shared with tachyzoite infected cells (Fig. 3.5A and C). Overall, this implies that the presence of bradyzoites results in unique modulations of the host cell transcriptome when compared to tachyzoites.

Figure 3.5

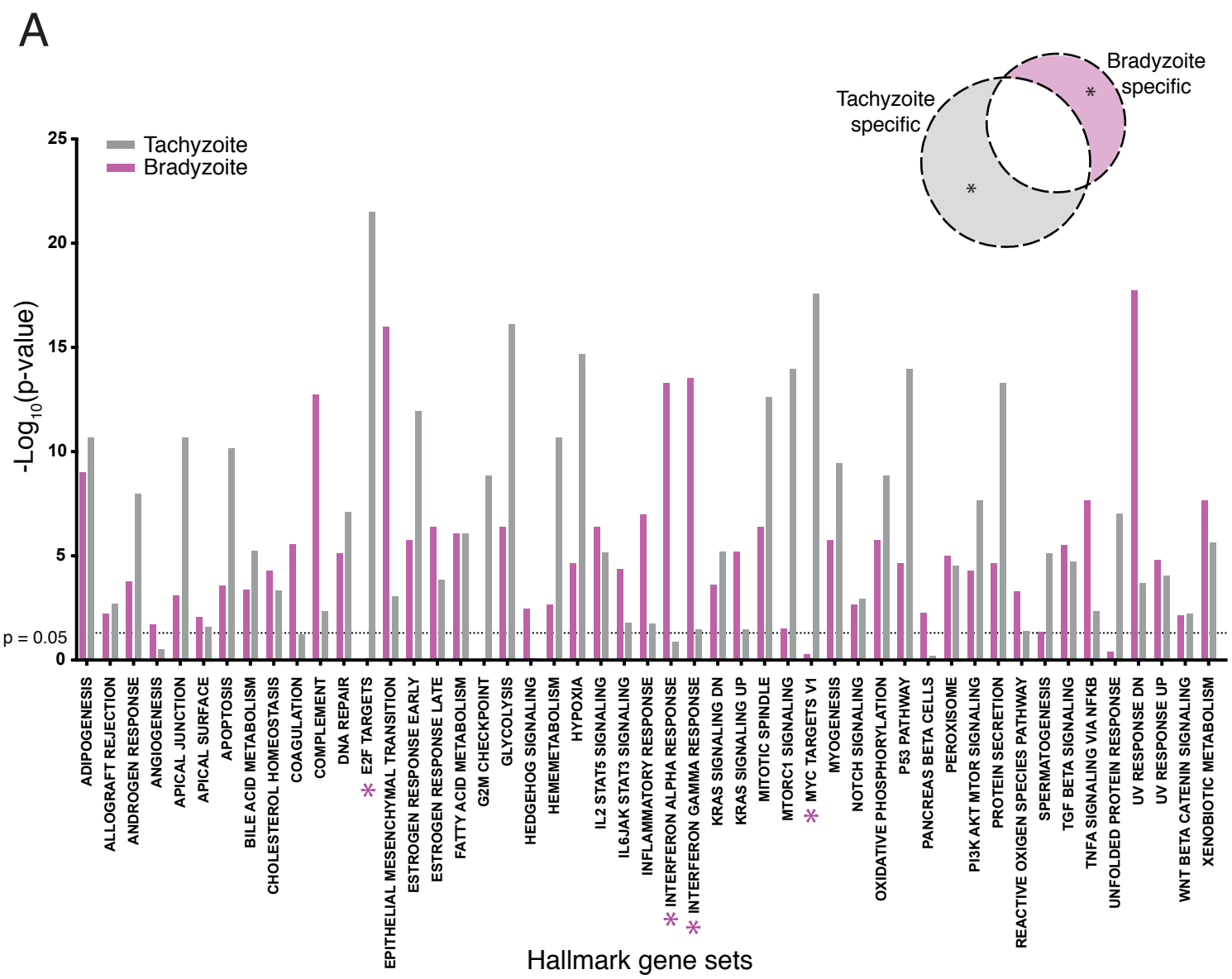

A
Tachyzoite
Bradyzoite
Tachyzoite specific
Bradyzoite specific
*
*
-Log10(p-value)
25
20
15
10
5
0
p = 0.05
ADIPOGENESIS
ALLOGRAFT REJECTION
ANDROGEN RESPONSE
ANGIOGENESIS
APICAL JUNCTION
APICAL SURFACE
APOPTOSIS
BILE ACID METABOLISM
CHOLESTEROL HOMEOSTASIS
COAGULATION
COMPLEMENT
DNA REPAIR
* E2F TARGETS
EPITHELIAL MESENCHYMAL TRANSITION
ESTROGEN RESPONSE EARLY
ESTROGEN RESPONSE LATE
FATTY ACID METABOLISM
G2M CHECKPOINT
GLYCOLYSIS
HEDGEHOG SIGNALING
HEMEMETABOLISM
HYPOXIA
IL2 STAT5 SIGNALING
IL6JAK STAT3 SIGNALING
INFLAMMATORY RESPONSE
* INTERFERON ALPHA RESPONSE
* INTERFERON GAMMA RESPONSE
KRAS SIGNALING DN
KRAS SIGNALING UP
MITOTIC SPINDLE
MTORC1 SIGNALING
* MYC TARGETS V1
MYOGENESIS
NOTCH SIGNALING
OXIDATIVE PHOSPHORYLATION
P53 PATHWAY
PANCREAS BETA CELLS
PEROXISOME
PI3K AKT MTOR SIGNALING
PROTEIN SECRETION
REACTIVE OXIGEN SPECIES PATHWAY
SPERMATOGENESIS
TGF BETA SIGNALING
TNFA SIGNALING VIA NFKB
UNFOLDED PROTEIN RESPONSE
UV RESPONSE DN
UV RESPONSE UP
WNT BETA CATENIN SIGNALING
XENOBIOTIC METABOLISM
Hallmark gene sets

Figure 3.5 continued

B

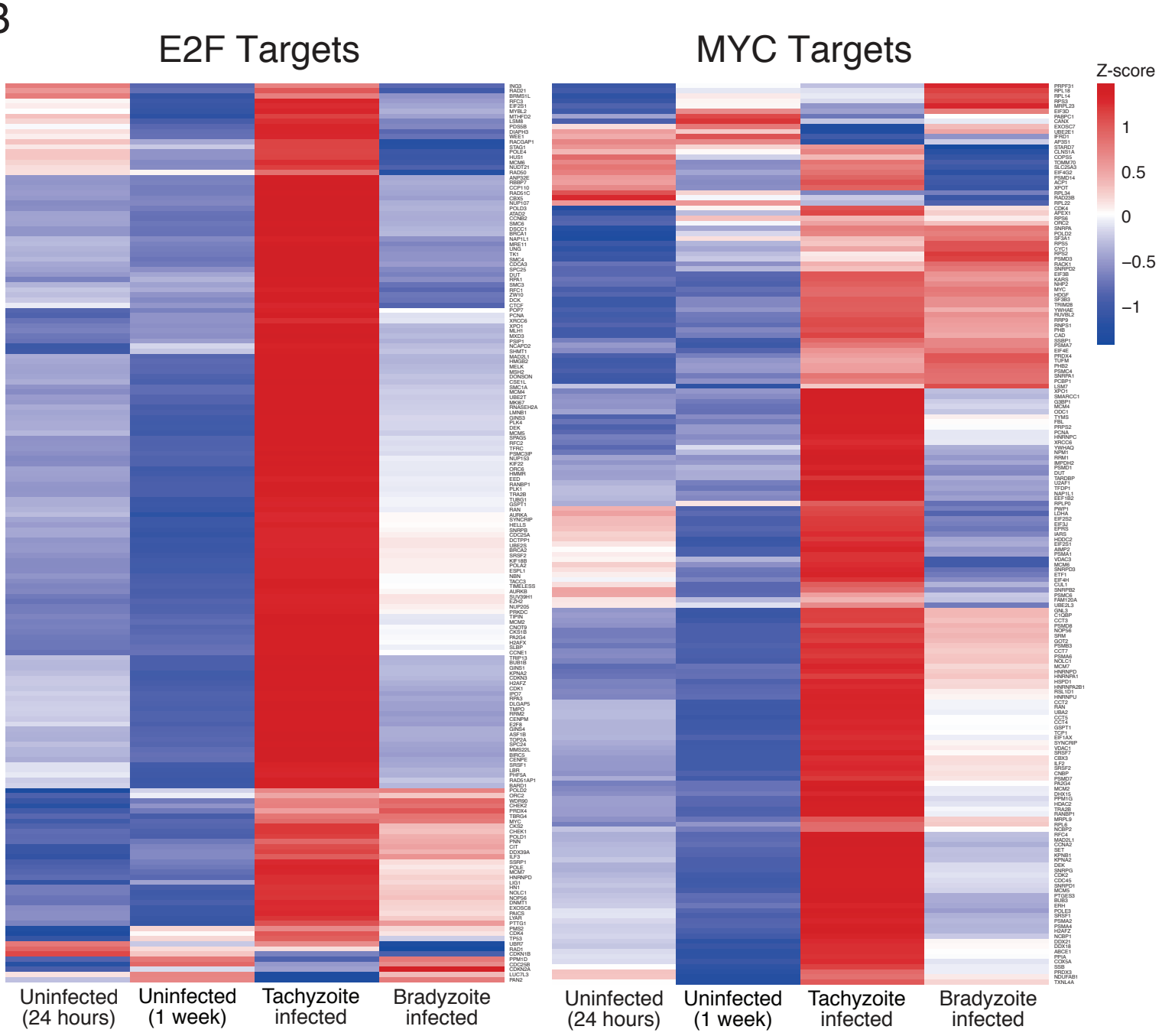


Figure 3.5 continued

C

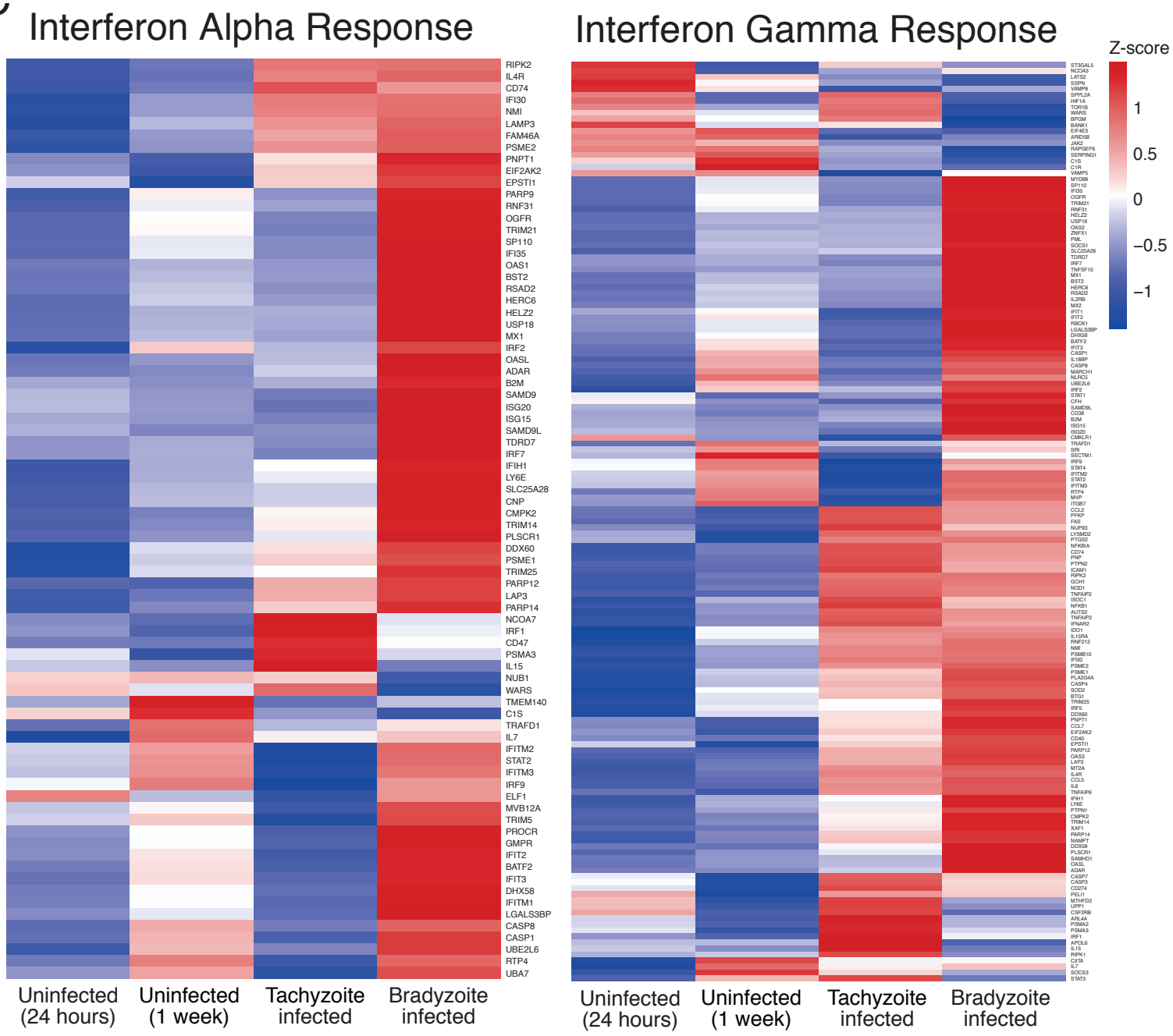


Figure 3.5 - Bradyzoites and tachyzoites modulate different host pathways.

(A) Tachyzoites (grey) and bradyzoite (magenta) over-representation analysis results for each Hallmark gene set displayed as the negative $\log_{10}$ of the p-value, dotted line p = 0.05. Black stars on Venn diagram schematic indicate DEGs used. Magenta stars indicate pathways with largely different profiles between tachyzoite and bradyzoites, which are shown in Figure 3.5 (B) and (C). (B) Pathways enriched during tachyzoite infection. Heat map of expression values for the genes that make up the *E2F target* and *MYC target* pathways. Expression values are Log_2 RPKM, scaled to have mean 0 and standard deviation 1 for each gene. The plots show that tachyzoites alter the transcriptional profile of pathways *E2F target* and *MYC target* more so than bradyzoites. (C) Pathways enriched during bradyzoites infection. Heat map of expression values for the genes that make up the *Interferon Alpha Response* and *Interferon Gamma Response* pathways. Expression values are Log_2 RPKM, scaled to have mean 0 and standard deviation 1 for each gene. These plots show that bradyzoite-containing cells have more changes in the transcriptional profile of these pathways on top of tachyzoite induced changes.

3.2.3 ASP5 and MYR1 in bradyzoites

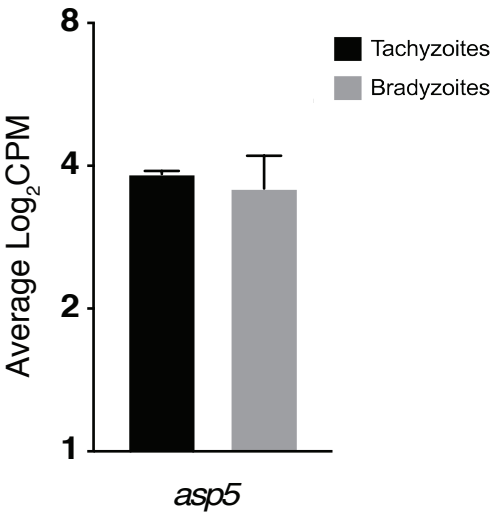
Transcriptional changes can be imparted directly by pathogen effectors or as a result of downstream signalling after immune activation. To specifically identify transcriptional changes induced by bradyzoites and to determine the overall effect of protein export on the host I prevented the export of effector proteins. To do this I knocked-out ASP5 and MYR1 as both have key roles in the export of effector proteins[279,280].

ASP5 cleaves and licences proteins for export and is expressed at both tachyzoite and bradyzoite stages (Fig. 3.6A). Previous data suggests that ASP5 presence is vital for the formation of healthy cysts[303], so to validate these findings and determine whether or not a ASP5 knock-out could be a good model for understanding host-pathogen transcriptional modifications, I knocked-out ASP5 in Pru WT (mCherry). Using CRISPR/Cas9 I targeted the first exon which resulted in a single Thymine base insertion 1137bp after the start codon. This insertion caused a frame shift and multiple early stop codons, including one disrupting the catalytic trio (Fig. 3.6B). All the stop codons are prior to the catalytic triad, ensuring that even if a truncated version of the protein was expression, it would have no proteolytic activity. To functionally validate ASP5 loss I looked at the parasite's capacity to export effector protein GRA24. GRA24-Myc was transiently expressed in WT and Δ*asp5* tachyzoites, and knockout parasites showed a complete inhibition of GRA24-Myc export (Fig. 3.6C). As previously shown, upon differentiation Δ*asp5* parasites were unable to make morphological healthy cysts. The cyst wall, marked by DBA, did not form a consistent structure around the bradyzoites and appears compromised (Fig. 3.6D). ASP5 is further upstream in the secretion pathway and is known to disrupt the final destination of non-exported dense granule proteins as well as exported proteins, therefore to target export more specifically I turned my focus to the translocon complex.

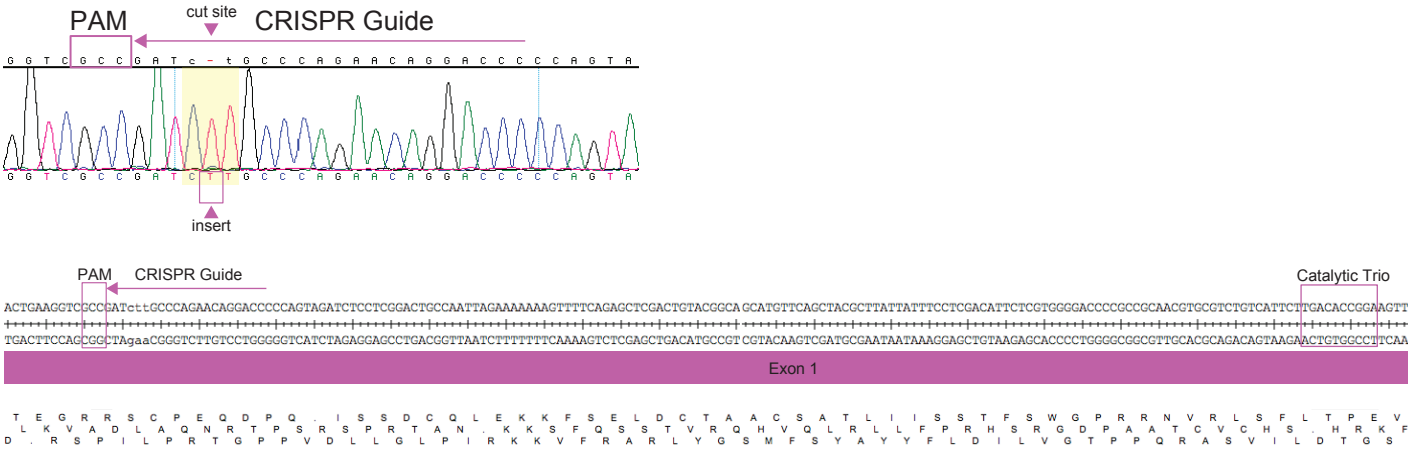
MYR proteins are putative components of the PVM translocon complex and are required for effector export, but it is unclear if these proteins continue to be functionally present in bradyzoites. To start answering this question, I first determined whether the MYR genes are expressed in bradyzoites by interrogating my transcriptional data. The relative expression of *myr1*, *2* and *3* in bradyzoites and tachyzoites from my RNAseq data shows that *myr1*, *2* and *3*

Figure 3.6

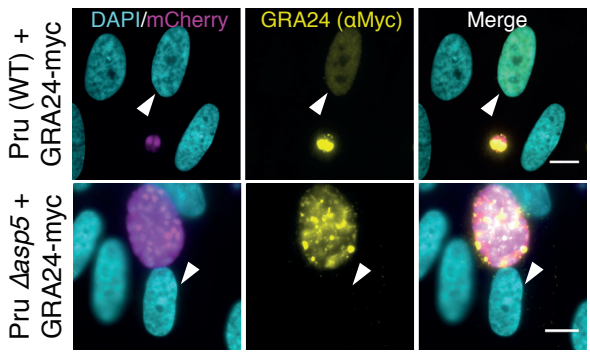
A



B



C



D

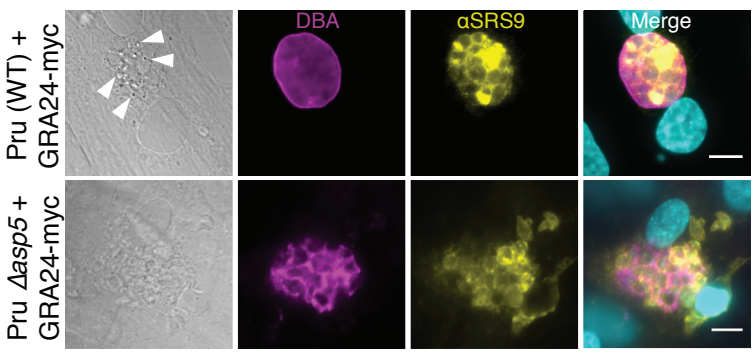


Figure 3.6 - ASP5 knockouts do not make functional cysts *in vitro*.

(**A**) There are no differences in the expressional profile (Log_2CPM) of ASP5 between tachyzoites (24 hours) and bradyzoites (7 days *in vitro*). (**B**) Location of the PAM (magenta square), CRISPR guide (magenta arrow), cut site (magenta arrowhead/yellow highlight) and sequencing of knockout clone. One thymine bp addition (magenta arrowhead) causes a frameshift in the ASP5 gene resulting in multiple stop codons (highlighted in yellow). (**C**) Δ*asp5* tachyzoites (mCherry: magenta) are unable to export transiently transfected GRA24-myc3 (αMyc; yellow) into the host nucleus (DAPI: blue). White arrows indicate location of host nucleus. (**D**) WT and D*asp5* parasites were fixed after 7 days of differentiation under alkaline conditions. Δ*asp5* were unable to form intact cysts (DBA; magenta) despite expressing bradyzoite markers (αSRS9; yellow). WT bradyzoites had an intact cyst wall filled with SRS9 expressing bradyzoites and had amylopectin granules (white arrows). Scale bar = 10μm. Brightness and contrast was edited on single colour channels prior to merging.

Figure 3.7

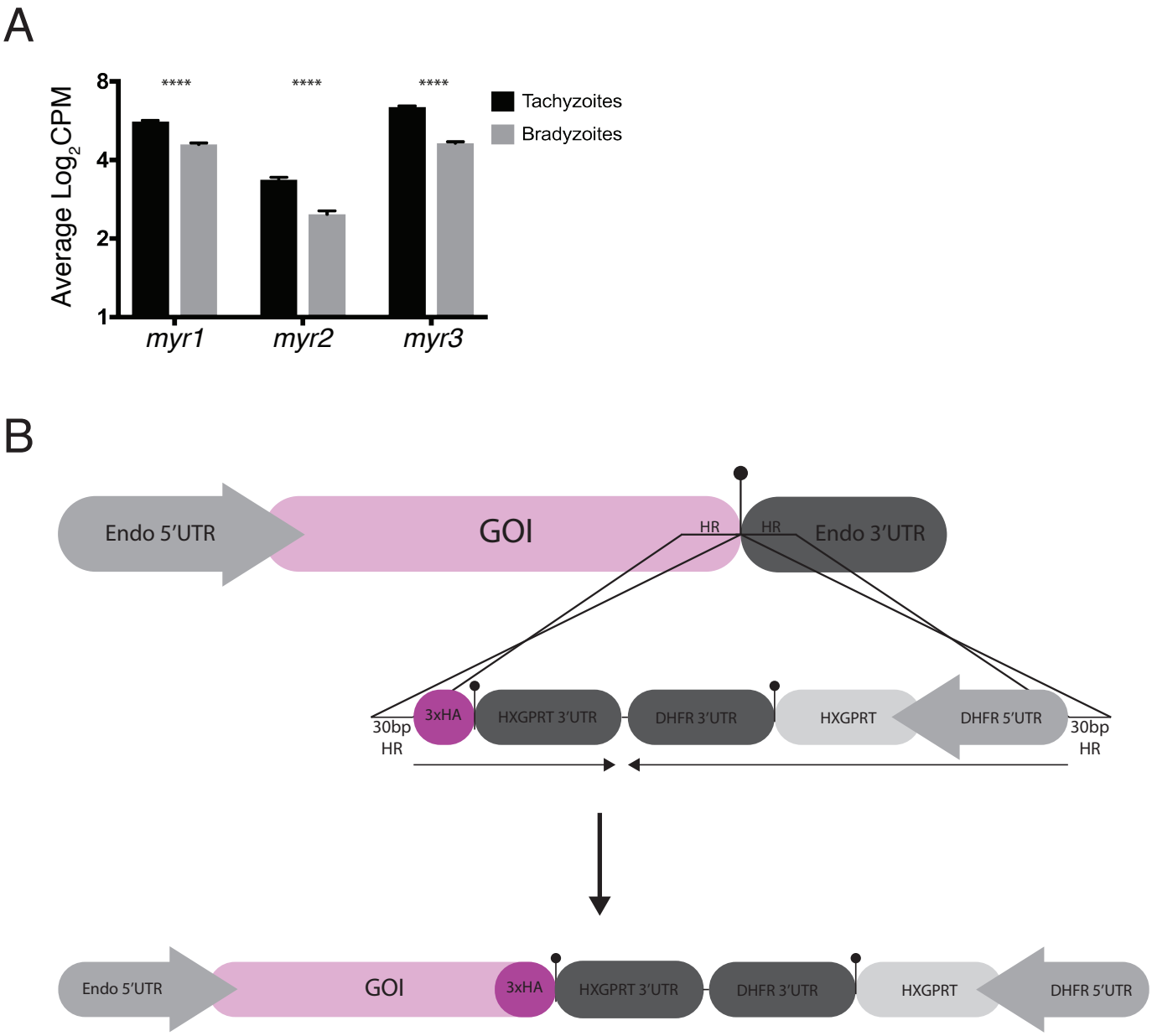

A
Average Log2CPM
8
4
2
1
****
****
****
Tachyzoites
Bradyzoites
myr1
myr2
myr3
B
Endo 5'UTR
GOI
HR
HR
Endo 3'UTR
30bp HR
3xHA
HXGPRT 3'UTR
DHFR 3'UTR
HXGPRT
DHFR 5'UTR
30bp HR
Endo 5'UTR
GOI
3xHA
HXGPRT 3'UTR
DHFR 3'UTR
HXGPRT
DHFR 5'UTR
C
Pru Δku80 (WT)
Pru Δku80 MYR1-HA
αGAP45
αHA (MYR1)
Merge
D
Pru Δku80 (WT)
Pru Δku80 MYR1-HA
pLDH2-eGFP
αCST1
αHA (MYR1)
Merge

Figure 3.7 - MYR1 is expressed in bradyzoites.

(A) Differences in the expressional profile (Log_2CPM) of *myr1*, *myr2*, and *myr3* between tachyzoites (24 hours) and bradyzoites (7 days *in vitro*). Expression drops during bradyzoite stages for all proteins. (B) Schematic of endogenous HA-epitope tagging of *myr1* PruΔ*ku80* in using the 3xHA-HXGPRT construct. (C) PruΔ*ku80* tachyzoites (αGAP45; green) express MYR1 (αHA; white) which localises to the PV and within the PV space. (D) PruΔ*ku80* and PruΔ*ku80* MYR1-HA parasites were induced under alkaline conditions for 7 days before fixation. MYR1-HA (αHA; white) in bradyzoites (pLDH2-eGFP; green) is localised to the PV space and co-localises to cyst wall marker CST1 (αCST1; magenta). Scale bar = 10μm. Brightness and contrast was edited on single colour channels prior to merging.

reduction in expression equals total protein loss in bradyzoites and to further functionally assess this complex during chronic stages, I genetically tagged MYR1 with HA in a Pru*Δku80* background (Fig. 3.7B). MYR1 protein was easily detectable via microscopy and localises between individual bradyzoites within the confines of the cyst wall, as marked by CST1 (Fig. 3.7D), similar to tachyzoites (Fig. 3.7C). I then knocked-out MYR1 in Pru WT (mCherry) using CRISPR/Cas9 by targeting the first exon to ensure disruption. This resulted in a random 69 bp insertion leading to three stop codons (Fig. 3.8A) and was functionally confirmed by the inability of parasites to export transiently expressed GRA24-Myc in tachyzoites (Fig. 3.8B)[280].

Next, I assessed differentiation capacity and morphology of Δ*myr1* bradyzoites by inducing bradyzoite formation *in vitro* using a the high pH-stress method for seven days. There were no obvious differences in morphology as measured by DBA staining for the cyst wall, compact parasites expressing SRS9, and the presence of amylopectin granules (Fig. 3.8C). Cyst size was not altered by the absence of MYR1 (Fig. 3.8D); however, the number of cyst-containing host cells was significantly less in Δ*myr1* samples (Fig. 3.8E). Next I wanted to determine if MYR1 loss was important for cyst formation *in vivo*. I infected mice with Δ*myr1* parasites and no parasite genomic material could be identified (via qPCR) four weeks later, as compared to WT and uninfected controls (Fig. 3.8F). Overall, this suggests that cyst development is not critically reliant on MYR1 in tissue culture, but that MYR1 plays an important role for the parasite's dispersal to the CNS or for the bradyzoite's persistence in an immune competent scenario. This is in contrast to deletion of ASP5, which results in defects in cyst wall biosynthesis[303].

3.2.4 MYR1-dependent protein export plays a key role in host transcription modification by bradyzoites

With the ability to form apparently healthy Δ*myr1* cysts *in vitro* I then went on to determine whether transcriptional changes are specifically caused by potential bradyzoite effectors in the early stages of chronic infection (seven days), compared to indirect effects such as host defence signals. Following the procedure laid out in figure 3.2A, uninfected, bradyzoite-containing and uninfected bystander cells were collected.

Figure 3.8

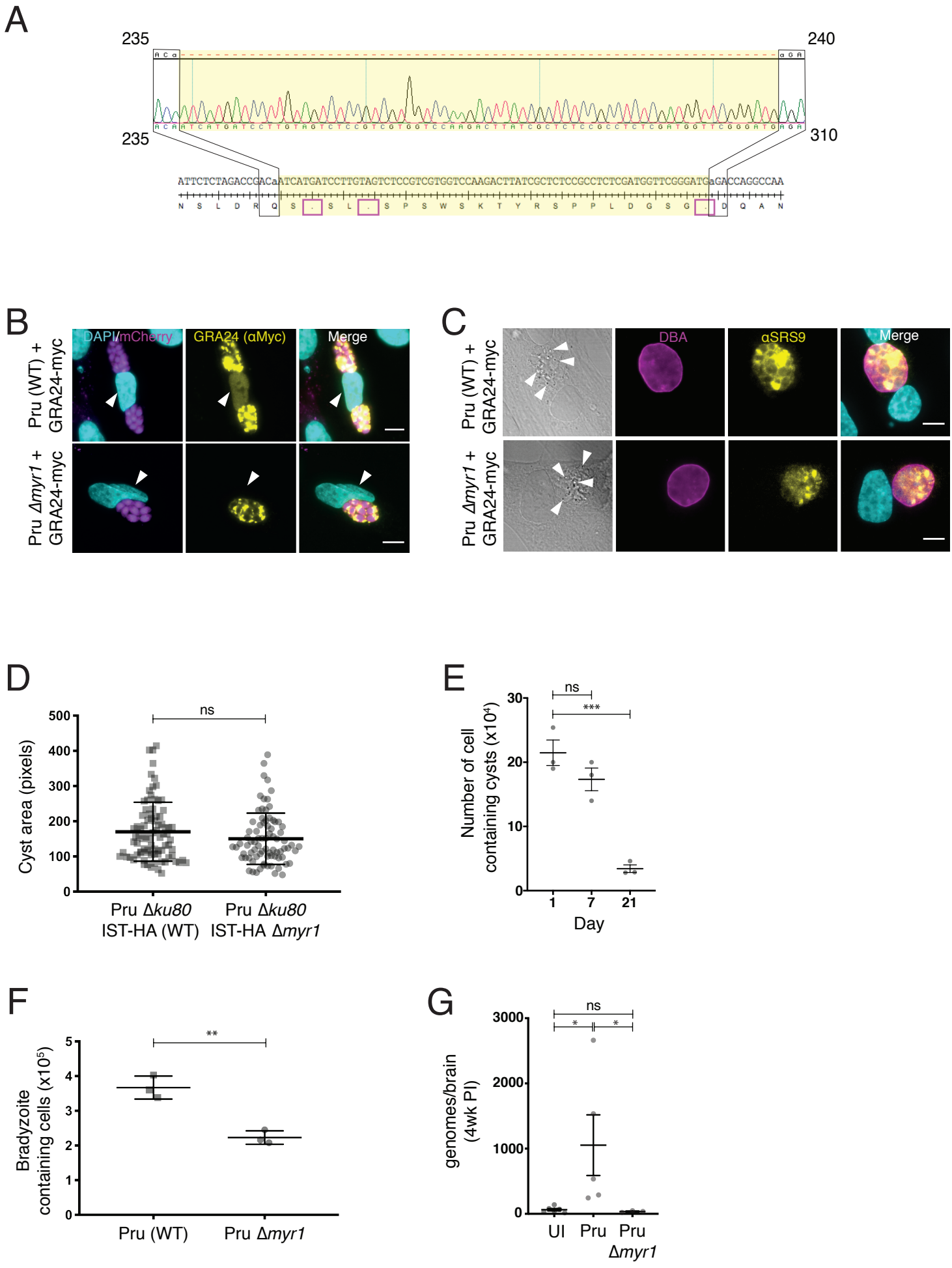

A
235
240
235
310
ATTCTCTAGACCGACaATCATGATCCTTGTAGTCTCCGTCGTGGTCCAAGACTTATCGCTCTCCGCCTCTCGATGGTTCGGGATGaGACCAGCCCAA
N S L D R Q S . S L . S P S W S K T Y R S P P L D G S G . D Q A N
B
Pru (WT) + GRA24-myc
Pru Δmyr1 + GRA24-myc
DAPI/mCherry
GRA24 (αMyc)
Merge
C
Pru (WT) + GRA24-myc
Pru Δmyr1 + GRA24-myc
DBA
αSRS9
Merge
D
Cyst area (pixels)
500
400
300
200
100
0
ns
Pru Δku80 IST-HA (WT)
Pru Δku80 IST-HA Δmyr1
E
Number of cell containing cysts (x10⁴)
30
20
10
0
ns
***
1
7
21
Day
F
Bradyzoite containing cells (x10⁵)
5
4
3
2
1
0
**
Pru (WT)
Pru Δmyr1
G
genomes/brain (4wk PI)
3000
2000
1000
0
ns
*
*
UI
Pru
Pru Δmyr1

Figure 3.8 - MYR1 knockouts can produce *in vitro* cysts.

(**A**) A random 69 bp insertion in Pru (WT) between the CRISPR cut site at bp 237-238 results in three stop codons (**B**) Transiently transfected GRA24-myc3 (αMyc; yellow) export into the host nucleus (DAPI; blue) is inhibited in Δ*myr1* tachyzoites (mCherry; magenta). White arrows indicate location of host nucleus. (**C**) WT and Δ*myr1* parasites were fixed after 7 days of differentiation under alkaline conditions. Both WT and Δ*myr1* were able to form intact cysts (DBA; magenta) containing health bradyzoites (αSRS9; yellow) and showed the presence of amylopectin granules (white arrows). Scale bar = 10μm. Brightness and contrast was edited on single colour channels prior to merging. (**D**) The size of PruΔ*ku80* Δ*myr1* cysts were compared to WT by quantification of from immuno-fluorescence images (mean ± SD, data points come from 3 different experiments, each experiment analysed on average between 15-30 bradyzoite cysts, unpaired, non-parametric Mann-Whitney test) (**E**) The number of cells containing Δ*myr1* parasites cells after 24 hours, seven days and 21 days of differentiation, analysed by FACS (mean ± SEM, minimum of n = 3 per experiment, unpaired, parametric ANOVA with Tukey's test for multiple comparisons, **p=0.0005) (**F**) The number of bradyzoite containing cells after 7 days of differentiation between WT (Pru) and Δ*myr1* was analysed by FACS (mean ± SD, n = 3 experiments, unpaired, Student's t-test with Welch's correction; **p=0.0058). (**G**) Brain tissue was harvested from uninfected, WT (Pru) infected and Δ*myr1* infected mice 4 weeks post inoculation. gDNA was extracted and number of of bradyzoite genomes was determined by qPCR. Δ*myr1* are not significantly different to uninfected mice (mean ± SEM, minimum of n = 3 per experiment, unpaired, non-parametric Kruskal-Wallis test with Dunn's correction for multiple comparisons; *<p=0.05).

When WT-infected cells were compared with Δ*myr1*-infected cells, the difference in gene expression was observed. Like for data set one (DS1; *section 3.2.2*, fig. 3.3C) a multidimensionally scaling (MDS) plot of the top 500 DEGs between all the samples was generated for data set two (bradyzoite *myr1*-knockout RNA sequencing; DS2), which grouped uninfected samples away from samples exposed to parasites (Fig. 3.9A). Bystander cells clustered more closely to each other and, again, the WT bradyzoite-containing cells' transcriptional profile was dissimilar to uninfected cells and bystander cells (Fig. 3.9A). Interestingly, Δ*myr1* bradyzoite-containing cells are in a similar dimension to infected samples, but are closer to bystander cells than WT bradyzoite-containing cells. This indicates a significant difference between WT- and Δ*myr1* bradyzoite-containing cells and potentially a role for bradyzoite protein export in transcriptional changes.

When both data sets (DS1 and DS2) were combined and the sequencing run batch effect was removed, the MDS plot shows DS2 samples clustering with corresponding samples from DS1. The tight clustering indicates these transcriptional profiles are similar (Fig. 3.9B). It is of interest that Δ*myr1* bradyzoite-containing cells overlap with bystander samples to form a group separate from WT and UI samples (Fig. 3.9B). The Δ*myr1*/bystander similarity is also demonstrated in the heatmap generated of the top 100 DEGs identified between WT-infected and Δ*myr1*-infected cells, which shows that the loss of MYR1 results in a transcriptional profile that closely mirrors the transcriptional changes seen in bystander cells (Fig. 3.9C). Reinforcing this concept, Δ*myr1*-infected cells cluster with bystander cells in the hierarchical heatmap (whereas bradyzoite-WT-containing and uninfected cells are excluded from the Δ*myr1*/bystander cluster). Moreover, bystander cells are vastly different when compared to uninfected cells, implying that uninfected bystander cells are impacted by the presence of bradyzoites in culture. Together these data suggest that transcriptional changes observed in the presence of bradyzoites are actively modulated and that protein export via MYR1 plays a role in altering the transcriptional program during early establishment of chronic infection.

Next I wanted to investigate the role protein export might have in altering the biological function of bradyzoite-containing cells. Before we could do a pathway analysis to examine this, we had to determine which DEGs were dependent on MYR1 (and therefore dependent on protein export). We first created a Venn diagram that compared the DEG analysis of WT-

Figure 3.9

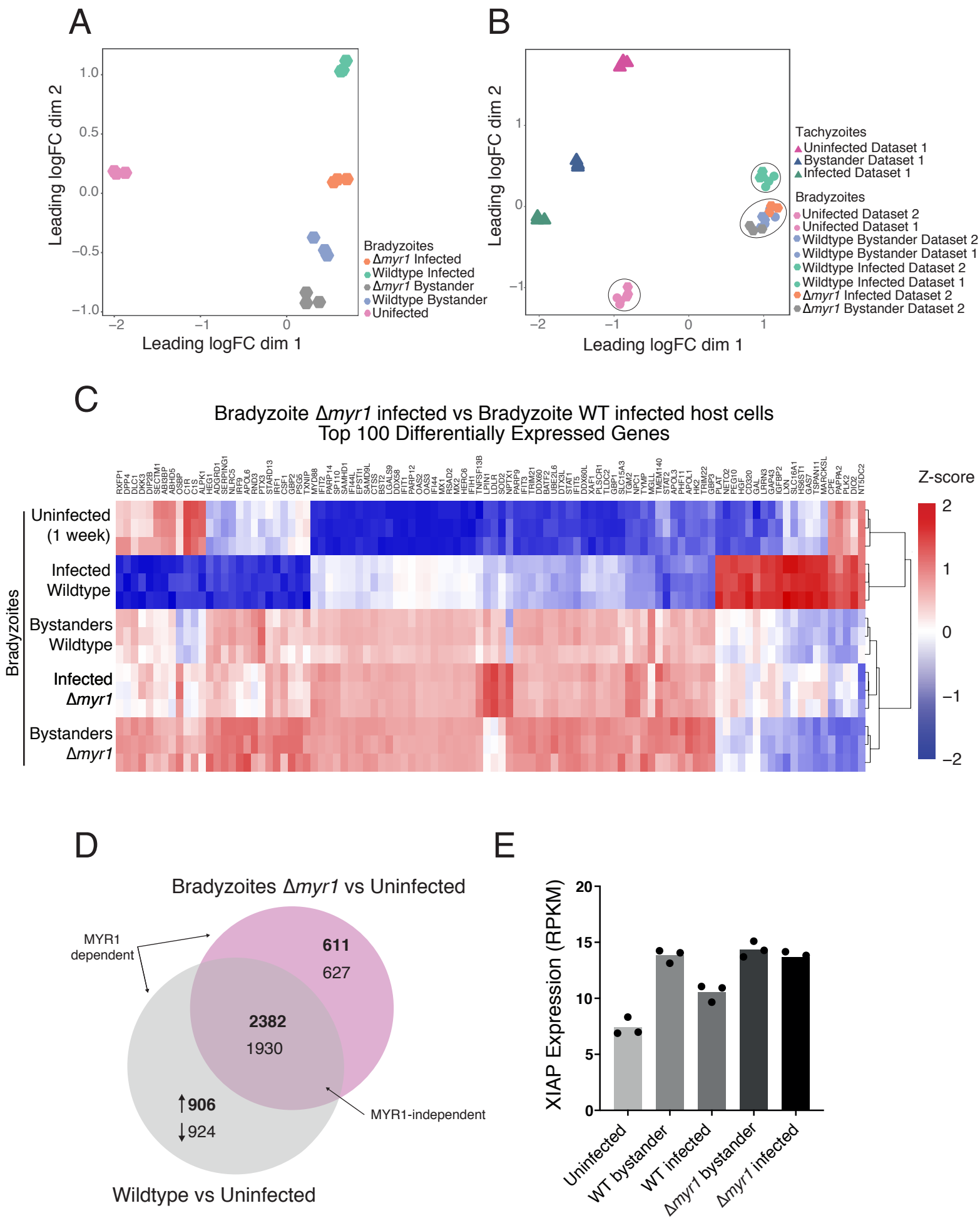

A
Leading logFC dim 2
Leading logFC dim 1
Bradyzoites
Δmyr1 Infected
Wildtype Infected
Δmyr1 Bystander
Wildtype Bystander
Unifected
B
Leading logFC dim 2
Leading logFC dim 1
Tachyzoites
Uninfected Dataset 1
Bystander Dataset 1
Infected Dataset 1
Bradyzoites
Unifected Dataset 2
Unifected Dataset 1
Wildtype Bystander Dataset 2
Wildtype Bystander Dataset 1
Wildtype Infected Dataset 2
Wildtype Infected Dataset 1
Δmyr1 Infected Dataset 2
Δmyr1 Bystander Dataset 2
C
Bradyzoite Δmyr1 infected vs Bradyzoite WT infected host cells
Top 100 Differentially Expressed Genes
Z-score
Bradyzoites
Uninfected (1 week)
Infected Wildtype
Bystanders Wildtype
Infected Δmyr1
Bystanders Δmyr1
D
Bradyzoites Δmyr1 vs Uninfected
MYR1 dependent
611
627
2382
1930
906
924
MYR1-independent
Wildtype vs Uninfected
E
XIAP Expression (RPKM)
Uninfected
WT bystander
WT infected
Δmyr1 bystander
Δmyr1 infected

Figure 3.9 - MYR1 plays a role in regulating host cell transcriptional changes in bradyzoite containing cells.

Dataset 2: WT (Pru) and Δ*myr1* inoculated human foreskin fibroblast (HFF) cells were FACS sorted into infected and uninfected samples before RNA extraction and sequencing (as per figure 3.2A & B) (A) Multi-dimensional scaling (MDS) plot between bystander and infected bradyzoite samples of WT and Δ*myr1* and the corresponding uninfected control. Dimension 1 (dim1) measures the logFC of the top 500 genes between the uninfected-flask and infected-flask samples, whereas dimension 2 (dim2) looks at the differences between host cells from WT and Δ*myr1* infected-flask: bystanders and infected. Plot shows replicates in each sample clustering together away from other groups (B) Dataset 1 and dataset 2 samples are merged together and, after corrections, are replotted on an MDS plot. All tachyzoite samples separate from bradyzoite samples. Uninfected bradyzoite samples and infected WT bradyzoite samples from both datasets overlap. WT and Δ*myr1* bystanders group together along with Δ*myr1* infected samples. (**C**) Heat map of $\log_2$RPKM expression for the top 100 differentially regulated genes between WT bradyzoite infected and Δ*myr1* bradyzoite infected cells. Expression has been scaled to have mean 0 and standard deviation 1 for each gene. In the absence of MYR1, bradyzoite specific host expression appears to somewhat mimic the bystander cell population (from both WT and Δ*myr1*). (**D**) Venn diagram of bradyzoite WT infected vs uninfected DEGs (grey) and bradyzoite Δ*myr1* infected vs uninfected DEGs (magenta); the number of up-regulated genes are identified in **bold** and down-regulated genes in regular font. Shared DEGs are deemed as independent of MYR1. (**E**) RPKM values for XIAP protein expression

infected versus uninfected with Δ*myr1*-infected versus uninfected (Fig. 3.9D). This identified 3068 host genes (~42%), whose expression changes are dependent on MYR1 (Fig. 3.9D). The remaining genes (4312) were altered in the same direction in both comparisons suggesting these genes are independent of MYR1 and therefore their expression changes does not depend on protein export. However, as for figure 3.4A, a limitation with the two-way Venn diagram is that it cannot distinguish between the degree of change. For an example, XIAP expression is significantly upregulated in both WT-infected cells and Δ*myr1*-infected cells when compared to uninfected host cells, placing it in the MYR1-independent section of the Venn diagram. However, the degree to which XIAP is upregulated is different between the comparisons; it is the degree of expression change which is seemingly dependent on MYR1 (Fig. 3.9E). To counter the degree problem and enable us to pull out DEGs that are truly dependent on MYR1, a third factor was added to the comparison: WT-infected cells verses Δ*myr1*-infected cells. This comparison takes into account the degree of change between WT- and Δ*myr1*-infected cells and enabled the separation of MYR1-independent DEGs (purple), from those truly dependent on MYR1 (all other grey regions) (Fig. 3.10A).

To discern if certain biological pathways were altered by exported proteins, we performed an over-representation analysis with the Hallmark gene sets on the designated MYR1-dependent (grouped grey regions) and MYR1-independent (purple) DEGs. It is clear that the presence of bradyzoites results in a multitude of changes in the host transcriptome that consequently influences all the Hallmark pathways (Fig 3.10B), in accordance with the pathway analysis of DS1 (Fig. 3.3E). All the pathways examined contain a significant number of genes that change in expression following the loss of MYR1; however, the modulation of some pathways is less dependent on MYR1 than others. For example, pathways *TNF-alpha signalling via NFκB* and *Epithelial Mesenchymal Transition* are highly enriched in the MYR1 independent gene set, whereas the manipulation of other pathways such as *Adipogenesis* and *Glycolysis* are more dependent on MYR1 (Fig 3.10B). These data represents all the gene expression changes during bradyzoite infection, including those that are present in tachyzoite infection. In order to determine what role protein export plays specifically in bradyzoite host manipulation, the Hallmark pathways that saw a significant enrichment of DEGs specific to bradyzoites (Fig. 3.5A) were examined for dependence on MYR1. All pathways that were enriched in bradyzoite samples from DS1 were significantly altered by the absence of MYR1 (Fig. 3.10C). In the

majority of the pathways examined, the proportion of MYR1 dependent gene changes were equal to or less than MYR1-independent gene changes. However, three key pathways stand out as MYR1-dependent pathways: Notch signalling (44%), IFN alpha- (69%), and IFN gamma-response (49%) pathways. These data show that a large proportion of bradyzoite induced host transcriptional changes requires the presence of MYR1, and implicates active protein export in bradyzoites.

Figure 3.10

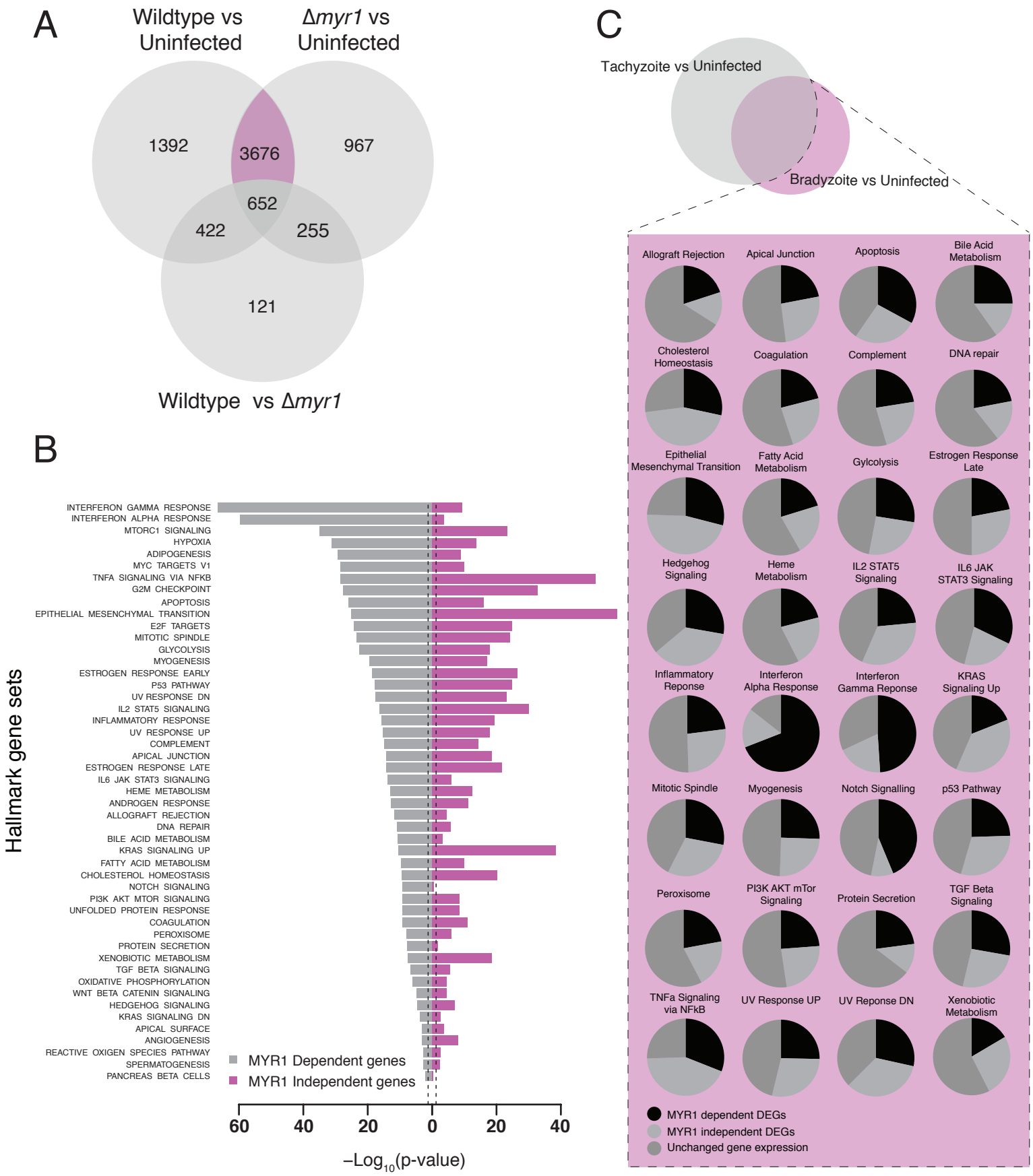

A
Wildtype vs Uninfected
Δmyr1 vs Uninfected
1392
3676
967
652
422
255
121
Wildtype vs Δmyr1
B
Hallmark gene sets
INTERFERON GAMMA RESPONSE
INTERFERON ALPHA RESPONSE
MTORC1 SIGNALING
HYPOXIA
ADIPOGENESIS
MYC TARGETS V1
TNFA SIGNALING VIA NFKB
G2M CHECKPOINT
APOPTOSIS
EPITHELIAL MESENCHYMAL TRANSITION
E2F TARGETS
MITOTIC SPINDLE
GLYCOLYSIS
MYOGENESIS
ESTROGEN RESPONSE EARLY
P53 PATHWAY
UV RESPONSE DN
IL2 STAT5 SIGNALING
INFLAMMATORY RESPONSE
UV RESPONSE UP
COMPLEMENT
APICAL JUNCTION
ESTROGEN RESPONSE LATE
IL6 JAK STAT3 SIGNALING
HEME METABOLISM
ANDROGEN RESPONSE
ALLOGRAFT REJECTION
DNA REPAIR
BILE ACID METABOLISM
KRAS SIGNALING UP
FATTY ACID METABOLISM
CHOLESTEROL HOMEOSTASIS
NOTCH SIGNALING
PI3K AKT MTOR SIGNALING
UNFOLDED PROTEIN RESPONSE
COAGULATION
PEROXISOME
PROTEIN SECRETION
XENOBIOTIC METABOLISM
TGF BETA SIGNALING
OXIDATIVE PHOSPHORYLATION
WNT BETA CATENIN SIGNALING
HEDGEHOG SIGNALING
KRAS SIGNALING DN
APICAL SURFACE
ANGIOGENESIS
REACTIVE OXIGEN SPECIES PATHWAY
SPERMATOGENESIS
PANCREAS BETA CELLS
MYR1 Dependent genes
MYR1 Independent genes
60
40
20
0
20
40
−Log10(p-value)
C
Tachyzoite vs Uninfected
Bradyzoite vs Uninfected
Allograft Rejection
Apical Junction
Apoptosis
Bile Acid Metabolism
Cholesterol Homeostasis
Coagulation
Complement
DNA repair
Epithelial Mesenchymal Transition
Fatty Acid Metabolism
Gylcolysis
Estrogen Response Late
Hedgehog Signaling
Heme Metabolism
IL2 STAT5 Signaling
IL6 JAK STAT3 Signaling
Inflammatory Reponse
Interferon Alpha Response
Interferon Gamma Reponse
KRAS Signaling Up
Mitotic Spindle
Myogenesis
Notch Signalling
p53 Pathway
Peroxisome
PI3K AKT mTor Signaling
Protein Secretion
TGF Beta Signaling
TNFa Signaling via NFkB
UV Response UP
UV Reponse DN
Xenobiotic Metabolism
MYR1 dependent DEGs
MYR1 independent DEGs
Unchanged gene expression

Figure 3.10 - A proportion of bradyzoite specific pathway changes are dependent on MYR1.

(A) Venn diagram from figure 3.9(D) (bradyzoite WT infected vs uninfected DEGs, bradyzoite Δ*myr1* infected vs uninfected DEGs) updated to include bradyzoite WT infected vs bradyzoite Δ*myr1* infected DEGs to isolate truly MYR1 dependent gene changes (grey) from MYR1 independent changes (magenta). (B) DEGs separated by the Venn diagram in 3.10(A) to MYR1 dependent (grey) and MYR1 independent genes (magenta) were used in a pathway enrichment analysis using the hallmark pathways. (C) The proportion of genes dependent (black), independent (light grey) and not changed (dark grey) in pathways previously determined from dataset 1 to be enriched for bradyzoite specific changes.

3.3 Discussion

My data shows, for the first time, that parasite driven manipulation of the host cell occurs in bradyzoites stages. I have established that host cells containing seven day-old bradyzoites have a transcriptional profile that is different from acute-stage tachyzoite forms. Furthermore, I show that MYR1 (a component of the export machinery) is expressed in bradyzoites and that its absence leads to an inability to induce the same transcriptional changes seen in bradyzoite-containing cells.

The lifestyles of tachyzoites and bradyzoites are vastly different and thus they have distinct requirements of their host cell. Tachyzoites are fast growing and disseminate around the body. Bradyzoites, on the other hand, are slow growing and persist for the life of their host, seemingly avoiding immune clearance. Here I show that bradyzoite-containing host cells have a distinct transcriptional landscape, which differs from acute stage tachyzoites, perhaps reflecting specific survival requirements. Tachyzoites appear to impact the host's cell cycle and survival pathways (such as c-Myc targets, PI3K/AKT/mTOR signalling, p53, mitotic spindle, G2M checkpoints, E2F targets, DNA repair, apoptosis, unfolded protein response), and metabolism (mTORC1 signalling, glycolysis, heme metabolism). In contrast, bradyzoite infection appears to more heavily impact immune pathways (complement, IL6/JAK/STAT3 signalling, inflammatory response, interferon gamma response, interferon alpha response), in addition to pathways that are also altered by tachyzoites.

It is interesting to note that known targets of tachyzoite effectors are differentially affected in bradyzoite. HCE1/TEEGR targets E2F-dependent genes (including cyclins and NF-κB targets)[265,266] and these are clearly not affected in bradyzoite-containing cells to the same degree, thus I would predict that HCE1/TEEGR is not expressed or exported in latent forms. GRA16 is known to be a key player in host cell cycle regulation by modulating p53 signalling, DNA replication, and DNA repair[176]. In my data, these pathways appear to be regulated to a lower degree in bradyzoites when compared to tachyzoites. Furthermore, tachyzoites are known to induce DNA replication and block G2M, transition preventing mitosis in host cells, thus increasing the ploidy of the host cells[232,233]. These observations complement my data which shows the regulation of both the G2M and mitosis pathways in tachyzoites but not

bradyzoites. The differential ability for *Toxoplasma* zoites to control cycle cell pathways could reflect the type of host cell the parasites reside in. Tachyzoites can replicate in rapidly dividing cells, whilst bradyzoites appear to predominantly develop in post-mitotic cells, such as neurons, myocytes and cardiomyocytes, and thus may have no need to modulate the cell cycle[38]. IST suppresses the IFNγ and IFNα signalling pathways of tachyzoite infected cells when stimulated[174,175,254]. As my samples are not exogenously stimulated with neither type I nor type II IFN it is not surprising to see no differences in the transcriptional profile between tachyzoite infected and uninfected cells (as described previously). In contrast, both pathways are largely upregulated in bradyzoite-containing cells, which could be explained by two scenarios: either bradyzoites are not actively suppressing these pathways and there is enough endogenous IFN in the system (likely produced by bystander cells) resulting in the upregulation of the pathways, or bradyzoites are actively upregulating these pathways by effector proteins (exported or otherwise).

Previous microarray data used to explore the expression profile of bradyzoite-containing host cells concluded that, when the effects of the stress on the host were taken into account, there was little to no transcriptional difference compared to tachyzoite infected host cells[177]. There are multiple reasons why these results contrast with my study. Firstly, I have shown that bystander cells have a different transcriptional profile to bradyzoite-containing cells. By concentrating and enriching bradyzoite-containing cells prior to RNA extraction, I was able to minimise the transcriptional signal from bystander cells which outnumber bradyzoite-containing cells five to one, and therefore expose potentially hidden signals from bradyzoite-containing cells. Pairing the enrichement experimental set up with the enhanced sensitivity and depth of RNAseq, my study has the power to detect a wider range of host transcriptional changes previously undetected by microarray. Finally, in Fouts and Boothroyd (2007)[177], bradyzoite samples were taken 44 hours post infection, whereas in samples in this thesis were harvested after seven days. Although sampling earlier during the differentiation process *in vitro* minimises unwanted lysis and cell death signals, it puts into question whether the transcripts detected in the Fouts and Boothroyd (2007) study are truly indications of bradyzoite modification. Residual tachyzoite effects may still be in play at earlier time points during bradyzoite development (e.g. >48 hours), from both tachyzoite specific GRA and ROP proteins

injected during invasion. This could result in a larger overlap of host transcripts with tachyzoites, and may explain the differences between the two studies findings[177].

Despite the longer differentiation period and clear differences between the transcriptional profiles of the samples, my experimental design cannot guarantee the host cell effects observed in this chapter are truly specific to bradyzoites. The transcriptional patterns observed could be remnants from tachyzoites or a result of the absence of tachyzoite effector proteins. There is no indication how long the transcriptional changes caused by known tachyzoite effectors lasts in the host cell e.g. are the effector proteins required to be present for their effects to continue to impact the host or are some changes permanent. A majority of known effector proteins indirectly regulate transcriptional changes by imparting their effects at the protein level (e.g. GRA16, GRA15, GRA24) and therefore the impact of these effector proteins could be tied to their half-life and continued presence. Effector proteins that have a more direct interaction with DNA, such as IST, have the potential to have long lasting impacts on the host. IST recruits the host cell's Mi-2/NuRD complex to GAS promoter regions[174,175]. Mi-2/NuRD is thought to inhibit transcription by condensing the chromatin structure through deacetylating histones using complexed HDAC1/2 (histone deacetylases 1 & 2)[304,305]. Chromatin structural changes could remain in effect even after IST has been degraded. A limitation of using RNAseq to gain an agnostic view of parasite manipulation is that it ignores non-transcriptional modifications. Because there are fewer bradyzoite-specific transcriptional changes when compared to tachyzoite infection, I cannot exclude the potential that mechanisms used by bradyzoites to manipulate the host cell might not be directed at the host transcription and could be working at the protein level, by either inhibition, activation, stabilisation or degradation of host proteins. These manipulation methods are used by other intracellular pathogens such as citrobacter[306], salmonella[307], and various viruses[308-310], which secrete pathogen proteins that interfere with important cell death proteins, resulting in the survival of the host.

Furthermore, the different tachyzoite effector sub-types could play a role in the expression profile differences between tachyzoites- and bradyzoite-containing host cells. Tachyzoites are known to inject several ROP effectors (and likely more unknown) into the host cell during invasion, which are independent of MYR1[172]. Unfortunately, my study cannot address what

role these injected proteins have on the transcriptional profile of bradyzoite-containing host cells. Furthermore, while it is not known if any ROP are injected in during bradyzoite invasion it is highly likely that this also occurs, and consequently their effects remain unknown. A recent study suggests that MYR1-dependent GRA proteins suppress or counter ROP effects early on in infection[183]. It could be that the effects of injected ROP are short-lived. Therefore, it is probable that the longer period of bradyzoite intracellular growth results in the loss of transcriptional patterns associated with rhoptry proteins during chronic infection, leading to differences between tachyzoite and bradyzoite effects.

The only known route for post-invasion secretion occurs via the MYR1-dependent translocon complex, which up until now has only been studied in tachyzoites[183,184,278,279]. As my first data set implicates a role for parasite effector export in bradyzoite stages, I wanted to examine the overall effect of protein export on the host during chronic infection. I used MYR1 knockouts to detangle what proportion of the changes observed are parasite driven. In general, bradyzoites have lower mRNA levels of translocon-complex components; however, the MYR1 protein is still seen in seven-day-old *in vitro* bradyzoites, and previous analysis of the cyst wall by proteomics has identified MYR1 and other translocon components[134], implying a role for export during these stages. In tachyzoites, MYR1 is a limiting factor in the modification of many host genes (even more so than ASP5)[184] and, from my data, it appears that MYR1 continues to have a functional role into chronic stages. The loss of MYR1 during bradyzoite stages does not hamper the ability of parasites to differentiate *in vitro*. However, Δ*myr1* parasites are attenuated *in vivo*[279] and it is easy to speculate that the combined loss of the GRA effectors and corresponding host modifications leaves tachyzoites susceptible to the immune system, resulting in early clearance which prevents dissemination and consequently cyst development in visceral organs. This is supported by the recent *in vivo* CRISPR screen which identified WIP. Parasites lacking MYR1 were unable to establish an infection in visceral organs, but were still found in the peritoneum[204] and, in another study, fewer cysts were found in the brain of mice[311]. In the future a conditional system with MYR1 could be used to study parasite driven interactions with the host *in vivo,* which are often concealed by the host's severe transcriptional response to infection[181,253]. However, as Δ*myr1* parasites can produce cysts *in vitro*, *in vitro* culture can be used as a proxy in the study of bradyzoite-host interactions.

All the hallmark pathways that were altered specifically in bradyzoites had a significant proportion of DEGs dependent on MYR1. In the heatmap WT-infected cells are grouped with uninfected cells, whereas Δ*myr1*-infected cells cluster with bystander cells, suggesting that bradyzoites actively skew the host transcriptional response via a MYR1-dependent pathway. A good example of this pattern is the IFNγ and IFNα hallmark pathways that become active in an inflammatory environment. In cells containing WT-bradyzoites, the expression of IFNγ and IFNα related genes are globally suppressed when compared to all the samples, more closely mimicking uninfected cells despite the slight increase in IFN signalling. Upon the loss of MYR1, the manipulation of IFNγ- and IFNα-mediated gene expression is lost, and bradyzoite-containing cells mimic bystander cells from the same culture. As IFNγ and IFNα are important mechanisms in controlling *Toxoplasma* infection *in vivo*[125,222,255,256], it is not unexpected to see these pathways being controlled in both stages. As discussed previously, IST is a MYR1-dependent effector in tachyzoites that suppresses these pathways, and it has also been implicated as an important protein in the persistence of cysts *in vivo* in relation to type I IFN signalling[174,254]. The role of IST, and other effector proteins, in bradyzoite infection is investigated further in *Chapter* 4.

In this chapter, I have shown that bradyzoite-containing host cells have a different transcriptional profile to tachyzoites, and many of these changes are MYR1-dependent. Taking into account my data along with the current literature, I have concluded that there are three potential explanations for transcriptional changes seen in bradyzoite-containing host cells. One, bradyzoites are exporting bradyzoite specific effector proteins across the cyst wall, using the same MYR1 dependent pathway. Two, tachyzoites and non-encysted bradyzoites setup the host cell for chronic infection by exporting proteins to cause prolonged transcriptional changes to enable continued survival even in the absence of parasite protein export after the cyst wall is established. And three, the absence of early secreted rhoptry proteins or GRA proteins could diminish over time resulting in an increase of host's susceptibility to defence signals, consequently changing the transcriptome of cells harbouring developing bradyzoites.

The identification of bradyzoite effectors and their function in host cell manipulation will be important in determining what cellular pathways are important in chronic stages verses tachyzoites stages. Without any known differences in bradyzoite-induced transcriptional

patterns between strains, other methods could be employed including a candidate based approach as used by the Boothroyd[265] and Hakimi[173,175,176,258] laboratories, CRISPR/Cas9 screens[203-205] or using biochemical approaches, such as the recently described LOPIT strategy to identify dense granule proteins that could also be exported into the host cell (unpublished data: can be accessed via ToxoDB[312]). Moreover, limitations on the amount of true bradyzoite material produced *in vitro* appears to no longer be a barrier. The discovery of BDF1 enables a way to genetically induce the differentiation of large amounts of the encysted bradyzoites without the stressors of alkaline induction[119]. In addition, it provides a clearer defined bradyzoite population with better conversion rates and less risk of tachyzoite contamination or reversion to tachyzoites. However, due to the timing of this project, I was unable to employ these strategies; therefore, in *Chapter 4*, I investigate known tachyzoite effectors in bradyzoites.

3.4 Additional methods and materials

3.4.1 Plasmid constructs, transfections and parasites lines

Candidate genes were targeted in all cases by the CRISPR/Cas9 system, which has been adapted for use in *Toxoplasma*[199,200]. EuPaGDT (http://grna.ctegd.uga.edu)[313] was used for guide selection. The UPRT protospacer in CRISPR-Cas9 plasmid pSAG1::Cas9-U6::sgUPRT[200] and pU6-Universal::mCherry[199,280] were replaced with gene-specific guides by Q5 site-directed mutagenesis (NEB) using a common reverse primer (P#1)[201] paired with a gene-specific forward primer (FP). Q5 reactions were confirmed by Sanger sequencing (AGRF, Victoria, Australia) using either primer SeqP#1 or SeqP#12 which bind in the U6 promoter upstream of the protospacers [199,200]. See *section 2.4* for more details on parasite transfections.

Producing MYR1 and ASP5 knockouts

Knockouts were made in Pru-Toxofilin-Cre[4301] (Pru) background lines or Pru Δ*ku80* Δ*hx*[89] *(*Pru Δ*ku80*; the latter is covered in *section 4.4*). PruΔ*myr1* and PruΔ*asp5* were created by CRISPR-Cas9 facilitated cutting within the first exon and errors during non-homologous recombination lead to disruption. The UPRT protospacer in the pU6-Universal::mCherry plasmid was replaced with guides targeting *myr1* (G#1) and *asp5* (G#2)[280] using the forward primers 2 and 3, respectively. 20 μg of plasmids were transfected as per the protocol laid out in *section 2.4* and followed by drug-free cloning. Clones were grown up and a region of approximately 500 bp surrounding the cut site was amplified by PCR (*myr1*: AmpP#1 & AmpP#2; *asp5*: AmpP#3 & AmpP#4) before being sequenced (myr1: SeqP#3, asp5: SeqP#4) (Fig. 3.8 A and 3.6 B, respectively). *myr1* and *asp5* knockouts were functionally confirmed by the transient transfection of the GRA24-Myc$_3$-expressing plasmid[280].

MYR1-HA epitope tagging

The C-terminal tagging of MYR1 was made in the Pru Δ*hxgprt* Δ*ku80* (PruΔ*ku80*)[89] background. The UPRT in pSAG1::Cas9-U6::sgUPRT [200] was replaced by a guide targeting myr1 (G#3) at the 3'prime end of the gene (P#4). P#4 plasmid was co-transfected with a pLIC-3xHA-HXGPRT[282,314] amplicon with 30 bp of complementarity (underlined) on either side of the CRISPR/Cas9 cut

site (AmpP#5 & AmpP#6) (Fig. 3.7B). The homology arms of the primers are engineered to remove the original stop codon and introduces a point mutation at the fourth bp after the PAM (NGG) sequence to prevent unwanted continuous cutting. 10 μg of CRISPR/Cas9 plasmid was combined with up to 30 μg of amplicon, ethanol and sodium acetate precipitation and resuspended in 20 μL P3 solution (Lonza) before transfection. Transfected populations were selected with three rounds of 50 μg/mL xanthine and 25 μM/mL mycophenolic acid[315] before cloning. Positive clones were determined by immunofluorescent imaging.

3.4.2 Microscopy and cyst size quantification

See *section 2.5* for immunofluorescence assays, imaging and data quantification details.

In addition, images for figures 3.1 I & J were analysed using the Plot Profile tool in Fiji (ImageJ)[300]. Only single invaded parasites were used, and the intensities of the fluorescence markers were measured along a 10 μm cross-section (indicated by the dotted line) that centred in the middle of the parasite nucleus.

3.4.3 *In vivo* infections

All procedures involving mice were completed in compliance with Walter and Eliza Hall Institute's animal ethics application (2018.048). C57BL/6 mice were infected via intraperitoneal injection (IP) with $5x10^4$ Pru WT or Δ*myr1*. Day five post-infection, mice were orally treated with sulfadiazine at 100 mg/100 mL via the drinking water which was replaced with drug free water after seven days. Mice were weighed daily for four weeks to help determine if any reach the ethical endpoint. Mice that had reached the ethical endpoint outlined in the animal ethics application (2018.048) before the four-week time point were euthanised and no organs were harvested. Mice were euthanised using CO_2 exposure prior to organ removal.

3.4.4 Quantitative PCR for *in vivo* parasites

The following procedure was modified from Di Christina *et al.* (2017)[316]

One-quarter of the brain was collected and weighed prior to the addition of 3x w/v of PBS was added. Samples were homogenised using TissueLyser II (Qiagen) for 60 seconds at a frequency of 30/second. 100 μL of the homogenate (equals to approximately 25 mg of brain tissue) was spun down to remove excess PBS. gDNA was extracted from the tissue pellet using the DNeasy Blood & Tissue Kit (Qiagen) following the manufacture's procedure. A 529 bp repeat element[317] in the *Toxoplasma* genome was amplified (AmpP#7 & AmpP#8) to measure parasite load, and the housekeeping mouse gene, GAPDH, was used as a loading control (AmpP#9 & AmpP#10). Primers were used at 2 μM in a final reaction volume of 10 μL, which contained 2 μL of brain gDNA (50 ng) and 1x SYBR green (Applied Biosystems). Samples were run for 40 cycles on a C100 Thermal Cycler (BioRAD).

For the standard curve, the gDNA of 10^7, 10^6, 10^5 and 10^4. tachyzoites were extracted using the DNeasy Blood & Tissue Kit (Qiagen) and resuspended in 1 mL of water. These stock extractions were then used to 'spike' 30 μL of mouse gDNA (final volume 50 μL) and used to create a standard curve. This ensures the background signal from the mouse DNA present in the brain samples is taken into account in the standard curve. Cq values were compared to the standard curve and, using brain weight, values were extrapolated to determine parasite genomes per brain.

3.4.5 Bradyzoite sample collection and RNA extraction for sequencing

HFFs were passaged and grown in D10 media until they reached confluency. Following this, HFFs were transferred into D1 media (for tachyzoites; 24 hours) or differentiation media (for bradyzoites; 7 days) and left as uninfected (no parasites) or infected at an MOI of 0.2 with either Pru-Toxofilin-Cre (Pru (WT)) or Pru-Toxofilin-Cre Δ*myr1* (Pru Δ*myr1*) tachyzoites. Prior to RNA extraction, HFFs were washed with PBS, dislodged with trypsin, and sorted into infected ($mCherry^+$) and uninfected ($mCherry^-$) cells using the BD Influx (361) cell sorter (BD

Biosciences). Samples were kept on ice before, during, and after the sorting process. Total host and parasite RNA was extracted immediately after sorting using the RNeasy kit (Qiagen). Three independent biological replicates of each condition were obtained. Cell sorting data (raw values) from both experiments were used to determine the number of infected cells in the populations (Fig. 3.1C and 3.8E).

3.4.6 Library preparation and transcriptome sequencing

An input of 100 ng of total RNA was prepared and indexed separately for Illumina™ sequencing using the TruSeq RNA Sample Prep Kit (Illumina) as per the manufacturer's instructions. Each library was quantified using the Agilent Tapestation and the Qubit™ DNA BR assay kit for Qubit 3.0® Fluorometer (Life technologies). The indexed libraries were pooled and diluted to 1.5pM for paired-end sequencing (2x 81 cycles) on a NextSeq 500 instrument using the v2 150 cycle High Output kit (Illumina) as per manufacturer's instructions (generating 80 bp paired-ends). The base calling and quality scoring was determined using Real-Time Analysis software v2.4.6, while the FASTQ file generation and de-multiplexing utilised bcl2fastq conversion software v2.15.0.4.

3.4.7 Transcriptome analysis

Before differential expression (DE) analysis occurs, the samples go through alignment and quality checks. This will be briefly described here; however, for a more in-depth look at the pre-DE analysis pipeline used please see appendices B for DS1, C for DS2 and D for the combined analysis.

The RNA sequencing reads were simultaneously aligned to the human and parasite genomes, builds hg38 and ME49 respectively, using the Rsubread aligner version 1.24.1 (tachyzoite and bradyzoite infection dataset) and version 1.27.4 (WT-Δ*myr1* bradyzoite infection dataset)[318]. For this alignment, a reference was first built that contained both human and parasite genomic sequences. In all instances, greater than 89% of the reads mapped to this combined genome.

The number of fragments overlapping each human Entrez gene and parasite gene were summarized using FeatureCounts[318] and NCBI RefSeq annotation. Differential expression analyses were then undertaken using the edgeR[319] and limma[320] software packages. The analysis of each data set was performed independently, details as follows.

DS1: Tachyzoite and bradyzoite infected data.

For the analysis of the human count data, any gene which did not achieve a counts per million mapped reads (CPM) greater than 1 in at least 3 samples were deemed to be unexpressed and filtered from the data. Additionally, all genes without current annotation were also removed. The parasite count data (infected samples only) was filtered using edgeR's filterByExpr function with default settings. Compositional differences between libraries for both human and parasite data were normalised using the trimmed mean of log expression ratios (TMM) method[321]. All counts were then transformed to $\log_2$CPM. Differential expression between the experimental groups in both instances was assessed relative to a fold-change threshold of 1.1 using linear models and empirical Bayes moderated t-statistics with a trended prior variance[322,323].

DS2: WT and Δmyr1 bradyzoite infection data.

For dataset 2, only the human count data were analysed. All genes which did not achieve a CPM greater than 0.7 in at least 3 samples were filtered from the data together with all genes with no current annotation. TMM normalisation was then applied to alleviate compositional differences between libraries. All counts were transformed to $\log_2$CPM. Differential expression between all groups was then evaluated relative to a fold-change threshold of 1.1 using linear models and robust empirical bayes moderated t-statistics with a trended prior variance.

In both data sets, the false discovery rate (FDR) was controlled below 5% using the Benjamini and Hochberg method. All MDS plots were created using limma's plotMDS function with default settings. For the MDS plot that shows both datasets (*DS1* & *DS2*), the data sets were first merged and the genes filtered. To be kept, all genes were required to show a CPM greater than 1 in at least 3 samples. TMM normalization was then applied and the data corrected to remove the sequencing run batch effect using limma's removeBatchEffect function prior to creating the MDS plot. The Venn diagrams were made using limma's vennDiagram function.

Analysis of the Hallmark gene sets from the Molecular Signatures Database was performed using limma's kegga function and the bar chart of Hallmark gene sets (Fig. 3.10B) was made using the R barchart function. Any other bar or pie chart was made using Prism 8 using data from the gene sets. To make the heatmaps of the top 100 differential expressed genes, the expression of each gene was summarized as $\log_2$ reads per kilobase per million mapped reads (RPKM) with a prior count of 2. For the heatmaps of the Hallmark gene sets, gene expression was summarised as average $\log_2$ RPKMs. The plots themselves were created using the pheatmap software package and limma's coolmap function.

Chapter 4:

A bradyzoite effector protein important for parasite persistence.

There are sections in the following chapter that are taken from Seizova *et al.*[1], a manuscript written by me during my PhD, and edited by Assoc. Prof. Christopher Tonkin and Dr. Alexandra Garnham. It has been submitted to bioRxiv, but is still in progress and has not been submitted at a peer-reviewed journal. Please see preface for more details.

4.1 Introduction

Host manipulation is a key method used by intracellular pathogens to aid infection and survive the host's immune system. Host manipulations can occur in multiple forms, including pathogen-host protein interactions that interfere with host protein function, to modulators of the host transcriptional response. Identified *Toxoplasma* exported effectors all impact the host transcription, with many changes observed in tachyzoite infection[163]. Tachyzoites are able to modulate the host using two distinct temporally separated pathways. The first wave of effectors are injected into the host cell during the invasion process (rhoptry proteins), whilst the second occurs during intracellular growth (dense granules)[72] (refer to *Chapter 1* for details).

In the past, methods of identifying host-parasite interacting proteins have included the genomic mapping of virulence loci by crossing virulent and avirulent strains[26,165,169,171], random mutagenesis paired with phenotypic screening[279,290,292] or bioinformatic candidate-based approaches where exported effector characteristics are used to identify potential candidates[173,175,176,258,265,266] . Each method has benefits and biases. Virulence crosses are exploratory and have identified multiple novel tachyzoite effector proteins that change the host transcriptional response. However, virulence crosses also introduce bias into the analysis by focusing efforts on responses and proteins that are different between the strains. Random mutagenesis requires a previously identified phenotype to be used in the screen, making it a more targeted search for effector proteins of known host-pathogen interactions. And candidate-based approaches require knowledge around the protein characteristics. In the case of *Toxoplasma*, few effector proteins have been identified. There is no homology between the effector proteins, not all have signs of export (such as signal peptides and TEXEL cleavage sites), and there are many proteins that fit these characteristics but are not exported[282]. Because of these reasons, generating a consensus that can be used in bioinformatic analysis is difficult and following up on hits is inefficient and costly. To date, no studies have focused on identifying effector proteins of bradyzoites and hence it is not known if bradyzoites need effector proteins for their survival.

Of the multiple tachyzoite exported effector proteins characterised, many are geared towards skewing the host's defence mechanisms to facilitate the parasite's survival. *Toxoplasma* is tightly controlled by the innate and adaptive immune responses, and IFNγ plays a vital role controlling acute *Toxoplasma* infection and prevents reactivation of latent bradyzoites[324]. Previous studies have used murine cell lines to understand how IFNγ can control tachyzoite infection and induce parasite clearance. It has been shown that IFNγ stimulated Guanylate-Binding Proteins (GBPs)[324,325] and Immune Related GTPases (IRGs)[326] are recruited to the tachyzoite PVM, but the downstream clearance mechanism that follows remains elusive[188]. The effector protein IST is one mechanism tachyzoites use to prevent IFNγ signalling of infected cells (see *section 1.6.1.1* which discusses the effector protein used to shut down cells pre-stimulated with IFNγ)[174,175,242,246]. As discussed in *Chapter 1*, IST is exported via the MYR1 pathway where it inhibits IFNγ and IFNα induced STAT1 transcription through chromatin remodelling[174,175], thus blunting transcriptional changes when the host cell encounters these cytokines. In *Chapter 3*, I show IFNγ and IFNα are the most altered pathways by bradyzoites, suggesting that out of the three known tachyzoite effector proteins, IST likely has the largest impact on bradyzoite survival. Although, it is not known if IFNγ has any capacity to affect bradyzoite clearance, even though it has consistently been shown to have an important role in immune defence *in vivo* and to prevent reactivation into acute stages[125,223,239].

In this results chapter I focus on identifying *Toxoplasma* bradyzoite effector proteins, what role such proteins could have on host transcription, and how effector protein absence could impact the parasite's long term persistence. As the bradyzoite stage is not responsible for the *Toxoplasma's* virulence, crosses would not be a suitable method. Similarly, there is no clear phenotype that can be used in a mutagenesis screen, and with an undetermined effector-export consensus signal in tachyzoites a candidate-based approach could be ineffective. I trialled a localised biotinylation method to identify bradyzoite effectors which was unsuccessful. Because many of the transcriptional changes observed in bradyzoites from *Chapter 3* were also found in tachyzoites, I decided to focus on the known exported-effector proteins (GRA16, GRA24 and IST). I tagged known effector proteins and looked at their expression and export during *in vitro* bradyzoite differentiation and in the absence of MYR1. I found that at seven days post differentiation, bradyzoites export IST but not GRA16 or GRA24, and that IST export is at similar levels to tachyzoites. I have also shown the export of effector

proteins is important for the parasite's survival in the face of immune attack (IFNγ stimulation), suggesting that early bradyzoite export is important for the parasite's and host's survival.

4.2 Results

4.2.1 Biotinylation of the secretory pathway.

Given the findings in *Chapter 3*, I hypothesised that *Toxoplasma* may have effector proteins that are exported into the host during bradyzoite stages. Because multiple biotin studies have been effectively used in *Toxoplasma* and there was already a system in place at in Tonkin Laboratory, I decided to use a biotin tagging approach that was spatially restricted to the secretory pathway to identify possible exported proteins. At that point in time, although there had been multiple studies in tachyzoites[212,327-330], no studies had used such a system in bradyzoites. The BioID system was commonly used in *Toxoplasma* studies, and often the biotin ligase (BirA) is fused to a protein of interest where it catalyses the biotinylation of interacting proteins or surrounding proteins. However, BirA has poor specificity, likely a consequence of the long biotin incubation period required for enzyme kinetics (18-24 hours)[331]. Instead we use another biotinylation protein called APEX2, a modified soybean ascorbate peroxidase[332,333] that biotinylates proteins within a 20 nm region. Unlike BirA, APEX2 does not use biotin for the reaction; instead, APEX2 rapidly catalyses the oxidation of biotin-phenol into biotin-phenoxyl (a highly-reactive free-radical) only in the presence of hydrogen peroxide (Fig. 4.1A). The speed of the reaction means the reaction period can be reduced resulting in less promiscuity and more specificity. A study published during my PhD showed that APEX2 is four time fewer false positives when compared to BirA, making APEX2 a more reliable system[327].

To target secreted dense granule proteins, APEX2 had to be confined to the dense granules and traffic through the secretory pathway. In order to do this, APEX2 was MYC-epitope tagged and fused to a SAG1 construct that lacked the GPI-anchor and driven by a tubulin promoter to ensure expression at all stages (Fig 4.1B). The plasmid was kindly gifted to the Tonkin Laboratory by Dr. Giel van Dooren and Dr. Azadeh Seidi (Australian National University). By removing the GPI-anchor but keeping the signal peptide, SAG1 would no longer be localised to the parasite membrane, instead it would localise to the dense granules in extracellular parasite (the default pathway of secreted proteins) or be secreted into the PV space of intracellular parasites. In the PV space, upon the addition of biotin-phenol and H_2O_2, APEX2 could then biotinylate proteins that are not membrane bound and identify candidates for export (Fig.

Figure 4.1

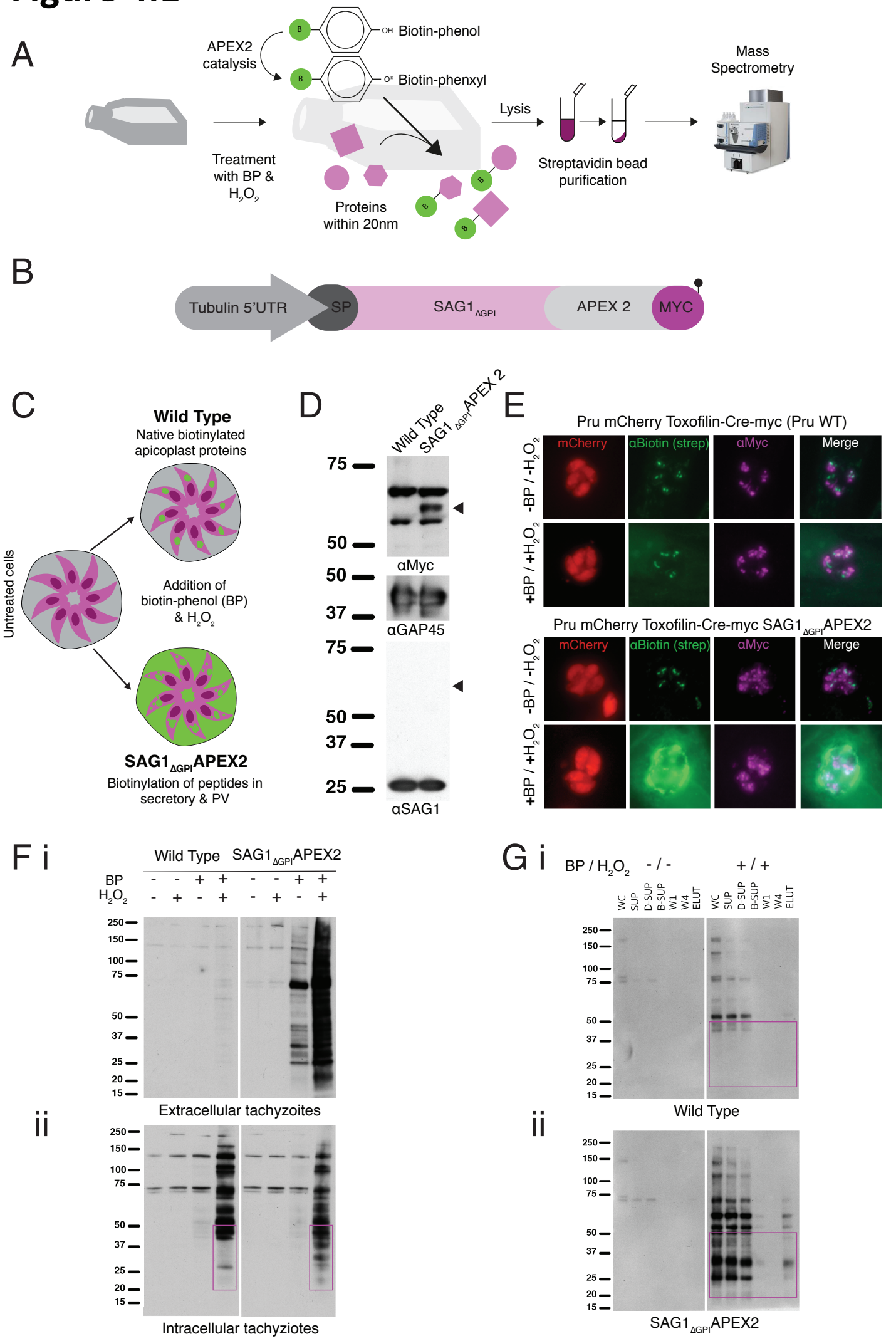

A
APEX2 catalysis
Biotin-phenol
Biotin-phenxyl
Treatment with BP & H_2O_2
Proteins within 20nm
Lysis
Streptavidin bead purification
Mass Spectrometry
B
Tubulin 5'UTR
SP
SAG1 ΔGPI
APEX 2
MYC
C
Wild Type
Native biotinylated apicoplast proteins
Untreated cells
Addition of biotin-phenol (BP) & H_2O_2
SAG1 ΔGPI APEX2
Biotinylation of peptides in secretory & PV
D
Wild Type
SAG1 ΔGPI APEX 2
75
50
50
37
75
50
37
25
αMyc
αGAP45
αSAG1
E
Pru mCherry Toxofilin-Cre-myc (Pru WT)
mCherry
αBiotin (strep)
αMyc
Merge
-BP / -H_2O_2
+BP / +H_2O_2
Pru mCherry Toxofilin-Cre-myc SAG1 ΔGPI APEX2
F i
Wild Type
SAG1 ΔGPI APEX2
BP
H_2O_2
Extracellular tachyzoites
ii
Intracellular tachyziotes
G i
BP / H_2O_2
- / -
+ / +
WC
SUP
D-SUP
B-SUP
W1
W4
ELUT
Wild Type
ii
SAG1 ΔGPI APEX2

Figure 4.1 - Biotinylation of proteins in the secretory pathway and parasitophorous vacuolar (PV) space (tachyzoites).

(**A**) Schematic of the overall APEX biotinylation process: upon the addition of biotin-phenol (BP) and hydrogen peroxide (H_2O_2), APEX2 catalyses BP into biotin-phenxyl and biotinylates (green) surrounding proteins (magenta). Biotinylated proteins can then be pulled down and analysed using mass spectrometry (**B**) Schematic of the SAG1$_{\Delta GPI}$APEX2-myc construct, driven by the tubulin promoter. (**C**) Schematic of the expected localisation of biotinylated proteins, shown in green, in WT lines and APEX2 expressing lines after the addition of BP and H_2O_2. (**D**) Western blot confirming the expression of the SAG1$_{\Delta GPI}$APEX2-myc construct. SAG1 and GAP45 are used as loading controls. (**E**) After 24 hours, tachyzoite (red) samples were treated with or without biotin-phenol and hydrogen peroxide, before fixation. Streptavidin labelling (green) shows there was a strong biotinylation of the PV space in SAG1$_{\Delta GPI}$APEX2-myc expressing parasites, whereas in WT parasites or untreated SAG1$_{\Delta GPI}$APEX2-myc lines biotinylation only occurs in the apicoplast. Strong toxofilin-Cre-myc expression prevents visual localisation of the SAG1$_{\Delta GPI}$APEX2-myc fusion protein (αMYC; magenta). (**F**) Western blot showing total biotinylated proteins (probed with NeutrAvidin-HRP) after the addition of either BP, H_2O_2, or both as compared to untreated samples. APEX2 dependent biotinylation appears to be more active in (i) extracellular parasites than (ii) intracellular parasites. Magenta boxes indicate areas of increase, in biotinylated in intracellular parasite samples, between WT and SAG1$_{\Delta GPI}$APEX2-myc. (**G**) Western blot showing the process of biotin-protein pull down in intracellular parasite samples treated with or without BP and H_2O_2. Samples were probed with NeutrAvidin-HRP. Magenta boxes show sizes where biotinylation is enriched between WT and SAG1$_{\Delta GPI}$APEX2-myc. WC, whole cell; SUP, superannuant; D-SUP, superannuant after dialysis; B-SUP, bead superannuant; W1, wash 1; W4, wash 4; ELUT, elute. Brightness and contrast was edited on single colour channels prior to merging.

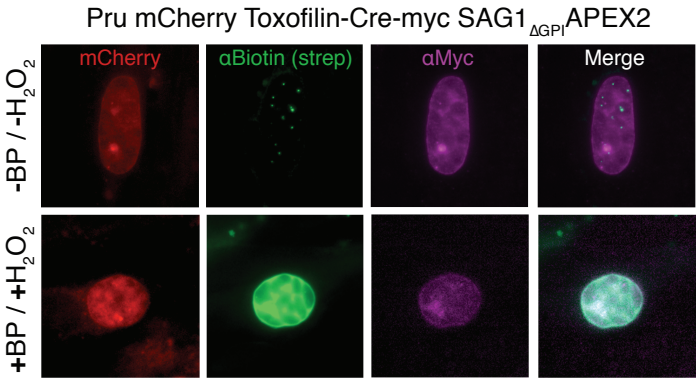
4.1C). Samples could then be compared to APEX2-negative parasite lines or untreated samples to control for endogenously biotinylated proteins found in the apicoplast[328,334](Fig. 4.1C). This plasmid was then transfected into the previously described Pru-Toxofilin-Cre (Pru) line and the expression of SAG1$_{\Delta GPI}$APEX2-MYC could be seen via western blot using only anti-myc antibodies, running at the expected approximate size (~62kDa; black arrow) between the MYC-epitope tag of the Toxofilin-Cre-MYC fusion protein (Fig. 4.1D). Toxofilin-Cre-MYC prevented the localisation of the SAG1$_{\Delta GPI}$APEX2-MYC protein to be easily detected via immunofluorescence imaging; however, there was a slight visual increase in that channel (Fig. 4.1E). Upon biotin-phenol treatment and H_2O_2 stimulation, biotinylation was labelled using streptavidin conjugated with Alexa-488 and only observed in APEX2 expressing parasites (Fig. 4.1E) localising to the PV space suggesting the protein fusion was trafficking correctly.

Although the goal was to identify bradyzoite specific proteins, I first wanted to test the protocol up to but not including the mass spectrometry in tachyzoites (Fig. 4.1A). Because bradyzoites would be intracellular during biotin-phenol treatment and I wanted to find secreted proteins in the PV, I tested intracellular tachyzoites in addition to extracellular tachyzoites. Furthermore, intracellular tachyzoite samples could be used as a comparison to bradyzoite samples. To observe the degree of protein biotinylation, Pru WT and Pru APEX2 expressing parasites (both intra- and extra- cellular) were either not treated, or were exposed to biotin-phenol only, H_2O_2 only, or both. Samples were run on an SDS-PAGE gel and biotinylated proteins were visualised with horse radish peroxidase (HRP)-conjugated neutravidin (Fig. 4.1F). In the extracellular samples, WT parasites had little to no biotinylated proteins on top of the two endogenous biotinylated proteins (Fig. 4.1F (i)). In contrast, extracellular APEX2 parasites had an increase in biotinylation in the biotin-phenol only treatment and an even more significant increase in the dual treatment (Fig. 4.1F (i)). This suggests that the system is working, despite the fact that there might be some APEX2 activity in the absence of H_2O_2, potentially from endogenous H_2O_2.

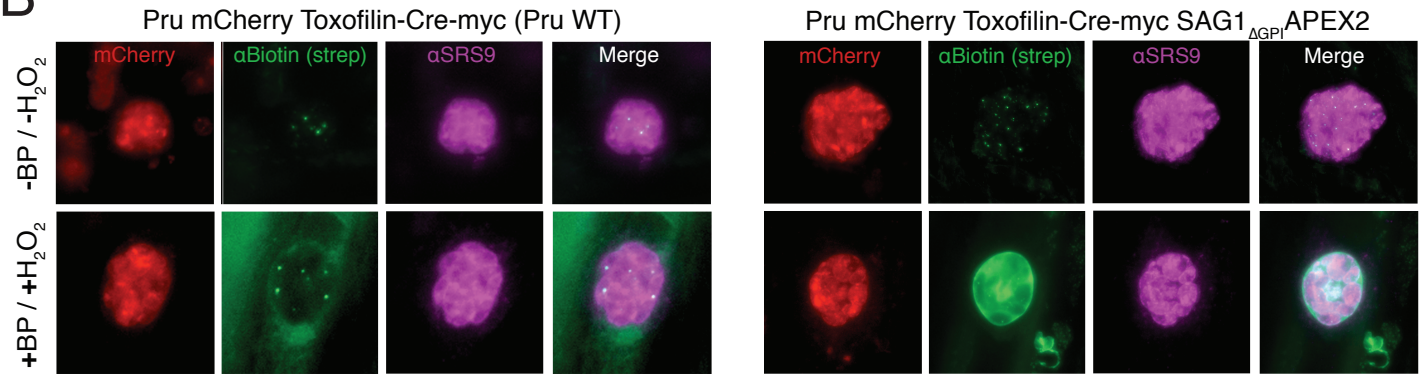
When the same experiment was performed with intracellular parasites there were stark differences. Intracellular WT parasite samples had a notable increase in the number of biotinylated proteins when treated with both biotin-phenol and H_2O_2, and the protein pattern did not appear considerably different from the biotinylation protein profile of APEX2

Figure 4.2

A



B



C

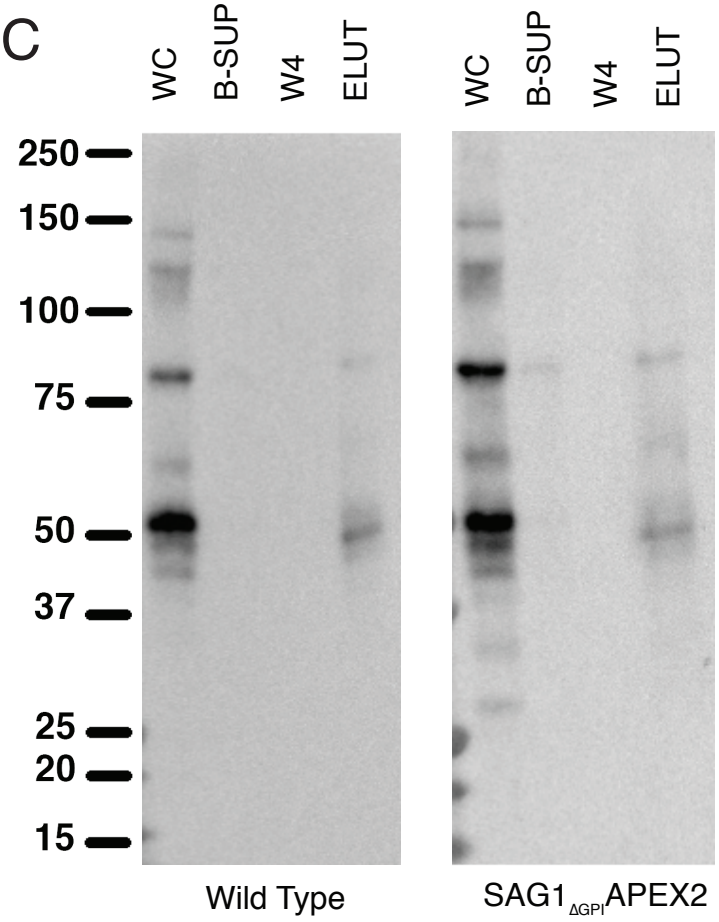


Figure 4.2 -Biotinylation of proteins in the secretory pathway and beyond in bradyzoites.

(**A**) SAG1$_{\Delta GPI}$APEX2-myc expressing parasites (red) were differentiated for 7 days before samples were treated with or without biotin-phenol (BP) and hydrogen peroxide (H_2O_2) and fixed. APEX2 (αMYC; magenta) localises around parasites in the cyst wall and cyst matrix. Streptavidin labelling (green) shows strong biotinylation colocalised with APEX2 in the cyst wall and matrix. (**B**) WT and SAG1$_{\Delta GPI}$APEX2-myc expressing parasites (red) were differentiated for 7 days before samples were treated with or without BP and H_2O_2 and fixed. Only SAG1$_{\Delta GPI}$APEX2-myc expressing bradyzoite (αSRS9; magenta) were able to biotinylate (green) proteins that appear to localise at the cyst wall and between parasites in the cyst matrix. (**C**) Western blot showing the process of biotin-protein pull down in bradyzoite samples treated with BP and H_2O_2. Not a significant increase in biotinylation in SAG1$_{\Delta GPI}$APEX2-myc expressing bradyzoites when compared to WT samples. Samples were probed with NeutrAvidin-HRP. WC, whole cell; SUP, superannuant; B-SUP, bead superannuant; W4, wash 4; ELUT, eluted sample. Scale bar =5μm. Brightness and contrast was edited on single colour channels prior to merging.

expressing parasites (Fig. 4.1F (ii)) This could be explained by the presence of an intact host cell that may have enzymes which catalyse the same reaction as APEX2 resulting in host proteins that are also biotinylated. Host biotinylated to a degree can be observed in the immunofluorescence images (Fig. 4.1E (ii)) with an increase in signal coming from the host cell surrounding the parasite vacuole. Despite the unexpected WT biotinylation, there is a slight increase in biotinylated proteins at molecular weights lower than 50kDa (magenta square). Low molecular weight proteins are clearly evident in figure 4.1G, which shows the pulldown and purification of biotinylated proteins using streptavidin beads for both WT (Fig. 4.1G (i)) and APEX2 expressing parasites (Fig. 4.1G (ii)). It is unclear why such a strong biotinylated signal that was observed in the IFAs (Fig. 4.1E (ii)) is not translated in the western blot or pulldown experiments. Nevertheless, there were some differences in the biotinylated-protein profile indicating the experimental set up was working for intracellular parasites, and therefore the next step was to move the experiment to bradyzoite samples.

To determine the localisation and function of APEX2 in bradyzoites, I first differentiated parasites for seven days before treating with biotin-phenol and H_2O_2. The biotin-phenol incubation period was doubled for bradyzoites to allow for cyst wall penetration. It was clear that APEX2 was localising to the cyst wall and space (Fig. 4.2A). It is likely that the SAG1$_{\Delta GPI}$APEX2-MYC fusion protein has been integrated into the cyst wall, an occurrence that can happen with other PV dense granule proteins[134,135,143]. However, cyst wall integration did not seem inhibit the ability of the APEX-fusion protein to catalyse biotinylation (Fig. 4.2B). Interestingly, biotinylation signals observed in fluorescence imaging again did not translate to western blot or pulldown experiments (Fig. 4.2C). The biotinylation profile of WT bradyzoites looked remarkably similar to intracellular WT tachyzoites (Fig. 4.1G (i)) but unlike the tachyzoite experiments, there was no additional biotinylation in bradyzoites expressing APEX2 (as per western blot). This was the case for all five independent experimental repeats. Furthermore, if APEX2 was indeed incorporated into the cyst wall, it is likely mass spectrometry analysis would result in an enrichment of cyst wall proteins rather than potential exported proteins. It was clear, from this data, that biotinylation was not the way forward.

4.2.2 IST is expressed and exported in bradyzoites

Due to the unsuccessful biotinylation experiment and the fact that some of the transcriptional changes observed in *Chapter 3* overlapped with tachyzoites, I decided to focus on known tachyzoite effector proteins, GRA16, GRA24 and IST. I first compared the proportion of reads between the infected bradyzoite and tachyzoites samples from the data in the first RNAseq analysis. There was a significant drop in the expression of GRA16 (log_2 fold change -2.681) and GRA24 (log_2 fold change -2.159) in bradyzoite samples, whereas IST appeared to be slightly more expressed in bradyzoites (log_2 fold change +0.374) (Fig. 4.3A). To validate that mRNA expression changes were translatable to protein expression, I HA-epitope tagged these proteins at the endogenous locus in PruΔ*ku80* using either HXGRPT selection (Fig. 4.3B (i)) or homologous recombination without selection (Fig. 4.3B (ii)). GRA16, GRA24 and IST proteins were all expressed in tachyzoites, whereas bradyzoites (classified by SRS9 expression and absence of SAG1) expressed GRA16 and IST (Fig. 4.3C) by western blot. This experiment indicated that potentially two known effectors are translated into protein in *in vitro* bradyzoite stages.

In order to establish if GRA16 and IST were exported in bradyzoite-containing host cells, I quantitated the expression and localisation by microscopy (Fig. 4.3D). GRA24 is consistently not expressed in 7-day-old bradyzoites; accordingly, the presence of GRA24 in the host nucleus is comparable to un-tagged WT controls (Fig. 4.3D and 4.3E). Interestingly, there appears to be some GRA16 present within the bradyzoite PV, but it is undetectable in the host nucleus (Fig. 4.3D and 4.3E). In contrast, IST was observed in the host nucleus by bradyzoites (Fig. 4.3D and 4.3E) which were also expressing cyst wall marker CST1. To explore IST export in more detail I looked at the level of protein export as compared to tachyzoites. First I quantitated the amount of IST export in tachyzoites during intracellular replication and found that the amount of IST remains consistent as the parasites grow within the host cell (Fig. 4.4A). I then quantitated the level of IST export during bradyzoite differentiation and found that it appears to decrease over the first three days (albeit a mild difference) but by day seven the export levels are comparable to tachyzoites (Fig 4.4B).

Figure 4.3

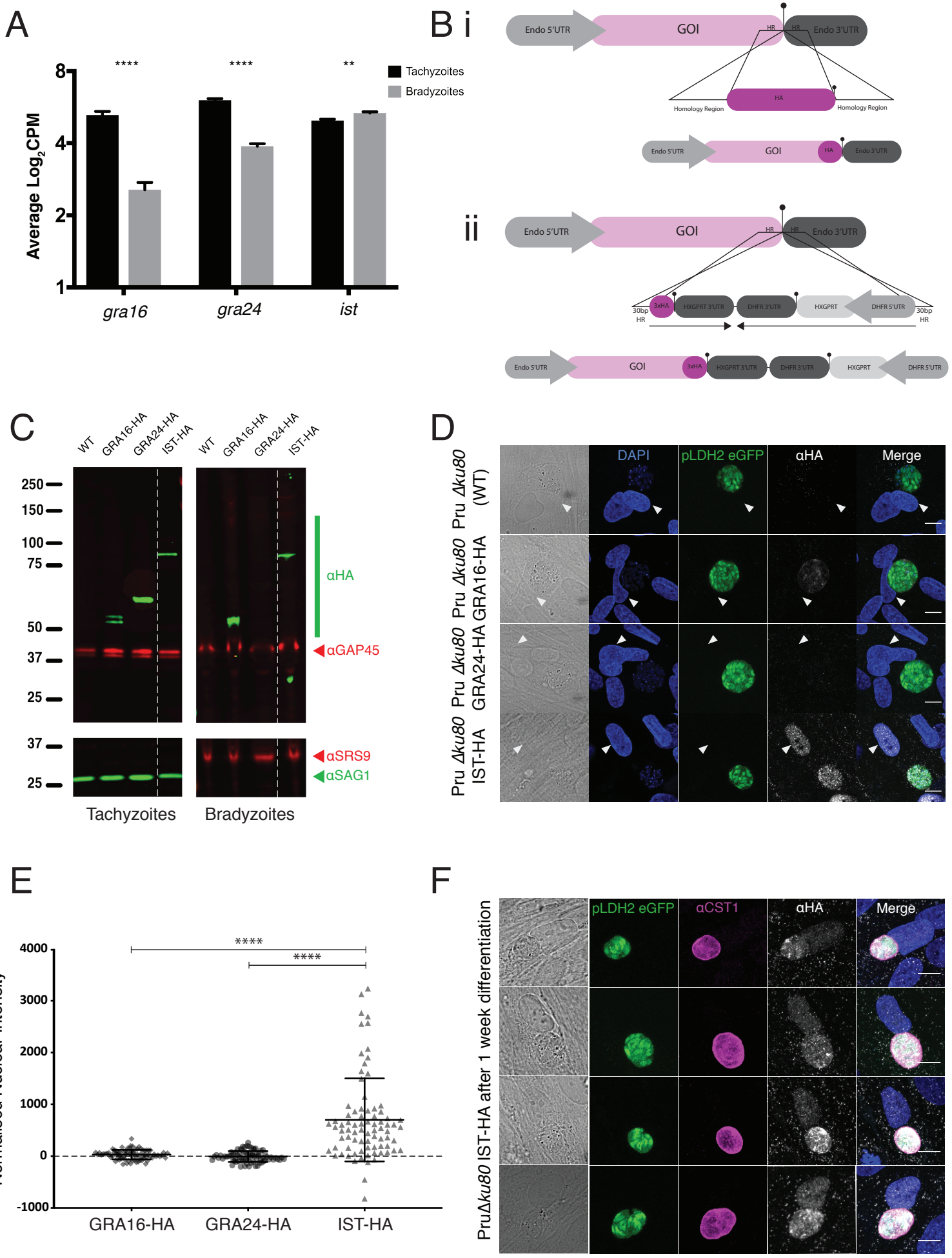

A
Average Log2 CPM
Tachyzoites
Bradyzoites
****
****
**
gra16
gra24
ist
B i
Endo 5'UTR
GOI
HR
HR
Endo 3'UTR
HA
Homology Region
Homology Region
ii
3xHA
HXGPRT 3'UTR
DHFR 3'UTR
HXGPRT
DHFR 5'UTR
30bp HR
C
WT
GRA16-HA
GRA24-HA
IST-HA
αHA
αGAP45
αSRS9
αSAG1
Tachyzoites
Bradyzoites
D
Pru Δku80 (WT)
Pru Δku80 GRA16-HA
Pru Δku80 GRA24-HA
Pru Δku80 IST-HA
DAPI
pLDH2 eGFP
αHA
Merge
E
Normalised Nuclear Intensity
GRA16-HA
GRA24-HA
IST-HA
F
PruΔku80 IST-HA after 1 week differentiation
pLDH2 eGFP
αCST1
αHA
Merge

Figure 4.3 - Tachyzoite effector protein's expression and localisation during bradyzoite stages

(**A**) Differences in the expressional profile (log_2CPM) of *gra16*, *gra24*, and *ist* between tachyzoites (24 hours) and bradyzoites (7 days *in vitro*). *gra16* and *gra24* reads drop during bradyzoite stages, whereas *ist* levels slightly increase (n = 3 experiments, each with 3 replicates; ****p<0.0001) (**B**) (i) Schematic of HA epitope tagging of GRA16 and IST using doubled stranded oligo primers (ii) Schematic of 3xHA-HXGPRT epitope tagging used for GRA24 (**C**) Western blot indicates GRA16-HA, GRA24-3xHA and IST-HA (PruΔ*ku80* background) are expressed in tachyzoites (lysed), whereas only GRA16-HA and IST-HA are expressed in bradyzoites (7 days *in vitro*). αGAP45 is used as a loading control, αSAG1 and αSRS9 are used as tachyzoite and bradyzoite controls respectively. (**D**) PruΔ*ku80* WT, GRA16-HA, GRA24-3xHA and IST-HA parasites were differentiated under alkaline conditions for 7 days before fixation. GRA24-3xHA (αHA; white) was not produced by bradyzoites (pLDH2-eGFP; green) or exported into the host nucleus. In contrast, bradyzoites were able to produce GRA16-HA and IST-HA; however, only IST-HA was exported into the host nucleus. White arrows indicate location of host nucleus (DAPI; blue). (**E**) Quantification of the intensity of nuclear GRA16-HA, GRA24-3xHA and IST-HA (normalised to untagged PruΔ*ku80* WT controls) of bradyzoites infected host cells from immuno-fluorescence imaging (Figure 4.3D) (mean ± SD, data points come from 3 different experiments, each experiment analysed on average between 20-50 bradyzoite cyst; unpaired, non-parametric Kruskal-Wallis test with Dunn's test to correct for multiple comparisons; ****p<0.0001) (**F**) PruΔ*ku80* IST-HA parasites were differentiated under alkaline conditions for 7 days before fixation. The presence of a strong CST1 (αCST; magenta) labelling does not prevent IST-HA export (αHA; white) into the host nucleus (DAPI; blue). Scale bar = 10μm. Brightness and contrast was edited on single colour channels prior to merging.

Next I had to resolve whether the presence of IST in the host nucleus is residual protein from tachyzoite stages, or if it is synthesised and exported in bradyzoites during development or after maturation is complete. I first wanted to understand the progression of *in vitro* differentiation over time in my samples in a rudimentary way. To do this, I analysed the mean fluorescence intensity of GFP as a marker of differentiation because, in the PruΔ*ku80* parasite line used, GFP expression is driven by the bradyzoite specific promoter of LDH2[89]. Ideally multiple markers would have been used; however, attempts to use other markers, in particular CST1, to further analyse differentiation were unsuccessful. Technical fluorescent limitations prevented the signal from the two channels visualising IST and CST1 (or other markers) from being separated. Therefore, GFP intensity was the only marker of bradyzoite development used in these studies. The mean GFP intensity steadily increased over time during *in vitro* stimulated differentiation with the highest average intensity at day seven (Fig. 4.4C). In addition there is a significant positive correlation between the vacuole size and the mean GFP intensity at all time points (days one, three and seven), suggesting larger vacuoles are likely further along in bradyzoite development (Fig 4.4D (i), (ii), (iii)). I then used GFP expression and vacuole size as a proxy for the degree of differentiation and looked to see if there was a negative or positive relationship between bradyzoite maturation and IST export. If the IST observed in the nucleus is from tachyzoites I expect exported levels to decrease as GFP intensity and vacuole size increases. However, I observed no change in export levels as the size (Fig. 4.4E (i) and (iii)) or GFP intensity (Fig. 4.4F (i) and (iii)) of the developing cyst increases. At day three there was a weak negative correlation between IST export and both size (Fig. 4.4E (ii)) and GFP intensity (4.4F (ii)). To verify if IST is indeed synthesised and exported by bradyzoites, week-old *in vitro* differentiated bradyzoites were extracted via needle passage and used to inoculate new host cells (Fig. 4.5A). Although I was unable to obtain enough extracellular bradyzoites to quantify export, it was clear at both 24 hours (Fig. 4.5B) and one week after the second inoculation IST was present in the host nucleus of infected cells (Fig. 4.5C). This strongly suggests that IST is produced in and exported by bradyzoites.

Following the identification of IST as a bradyzoite exported effector protein, I sought to determine whether MYR1 was also responsible for IST export in bradyzoite stages and whether IST was functional in controlling IFNγ-dependent responses. To investigate this, I created knockouts of both *myr1* and *ist* (as a negative control) in the PruΔ*ku80* IST-HA line by coupling

Figure 4.4

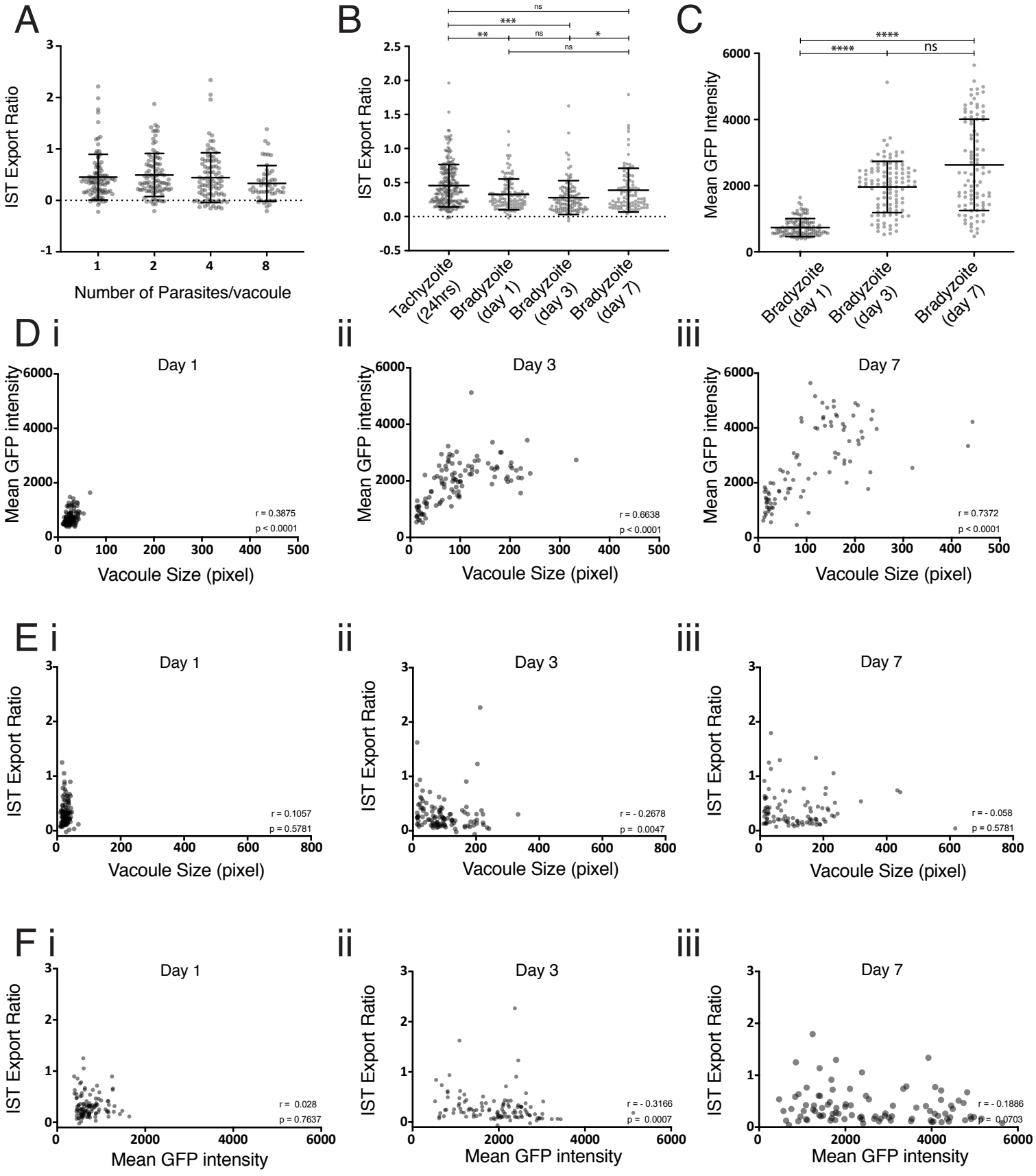
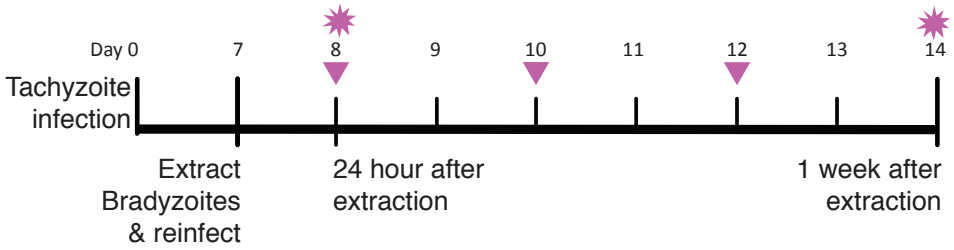

A
IST Export Ratio
Number of Parasites/vacoule
B
IST Export Ratio
Tachyzoite (24hrs)
Bradyzoite (day 1)
Bradyzoite (day 3)
Bradyzoite (day 7)
C
Mean GFP Intensity
D i
ii
iii
Day 1
Day 3
Day 7
Mean GFP intensity
Vacoule Size (pixel)
r = 0.3875
p < 0.0001
r = 0.6638
p < 0.0001
r = 0.7372
p < 0.0001
E i
ii
iii
IST Export Ratio
r = 0.1057
p = 0.5781
r = - 0.2678
p = 0.0047
r = - 0.058
p = 0.5781
F i
ii
iii
Mean GFP intensity
r = 0.028
p = 0.7637
r = - 0.3166
p = 0.0007
r = - 0.1886
p = 0.0703

Figure 4.4 - IST export over time

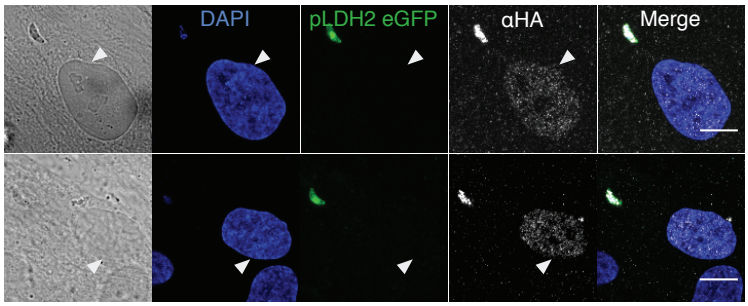
(A) There is no change in the ratio (nuclear intensity/vacuolar intensity) of IST export as the number of parasites grows. Tachyzoite samples were fixed after 24 hours post inoculation and probed with αGAP45 and αHA (IST). Stacked 4x4 tiles were taken and processed using ImageJ. One host cell containing one parasite vacuole were measured and the separated by parasite number. (mean ± SD, data points come from 3 different experiments, each experiment analysed on between 60-100 tachyzoite vacuoles; non-parametric Kruskal-Wallis test with Dunn's test to correct for multiple comparisons) (B) Time series of IST export measured by the ratio of export (nuclear intensity/vacuolar intensity). IST export decreases over time during bradyzoite development, but by day 7 levels of export return to levels of tachyzoites. Tachyzoite samples were fixed at 24 hours and bradyzoite samples were fixed at day 1, 3, and 7 of being in differentiation media. Tachyzoite samples were labelled with αGAP45 and αHA (IST) and bradyzoite samples were probed only with αHA (IST). Stacked 4x4 tiles were taken and processed using ImageJ. Only host cells containing one parasite vacuole/cyst was considered in the measurement levels. (mean ± SD, data points come from 3 different experiments, each experiment analysed on between 20-50 bradyzoite cysts and 60-100 tachyzoite vacuoles; non-parametric Kruskal-Wallis test with Dunn's test to correct for multiple comparisons. *p=0.0285, **p=0.0017, ****p<0.0001) (C) The mean GFP intensity increases over time during bradyzoite differentiation. (mean ± SD, experimental data was used from Figure 4.4B; non-parametric Kruskal-Wallis test with Dunn's test to correct for multiple comparisons. ****p<0.0001) (D) As vacuole size significantly (****p<0.0001) increases as the mean GFP intensity increases for days 1 (I), 3 (ii), and 7 (iii). Correlation was tested using the non-parametric Spearman's rank correlation coefficient (r). Experimental data was used from Figure 4.4B. (E) IST-HA export does not significantly (p>0.5) increase as vacuole size increases for days 1 (i), 3 (ii), and 7 (iii). Correlation was tested using the non-parametric Spearman's rank correlation coefficient (r). Experimental data was used from Figure 4.4B. (F) IST-HA export does not significantly (p>0.05) increase as vacuole size increases for day 1 (i) and 7 (iii). However, during day 3 (ii) IST-HA significantly decreases as mean GFP intensity increases. Correlation was tested using the non-parametric Spearman's rank correlation coefficient (r). Experimental data was used from Figure 4.4B.

Figure 4.5

A

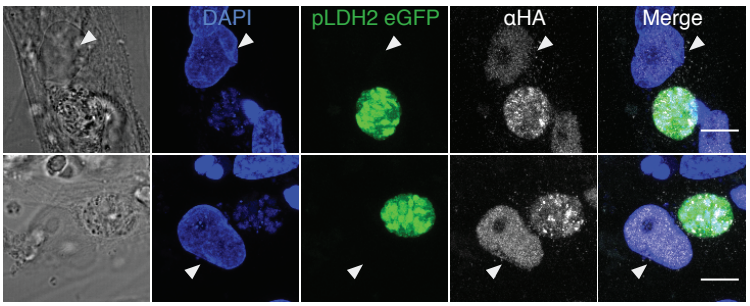


B



PruΔ*ku80* IST-HA 24 hours after extraction

C



PruΔ*ku80* IST-HA 1 week after extraction

Figure 4.5 - IST is produced and exported by bradyzoites

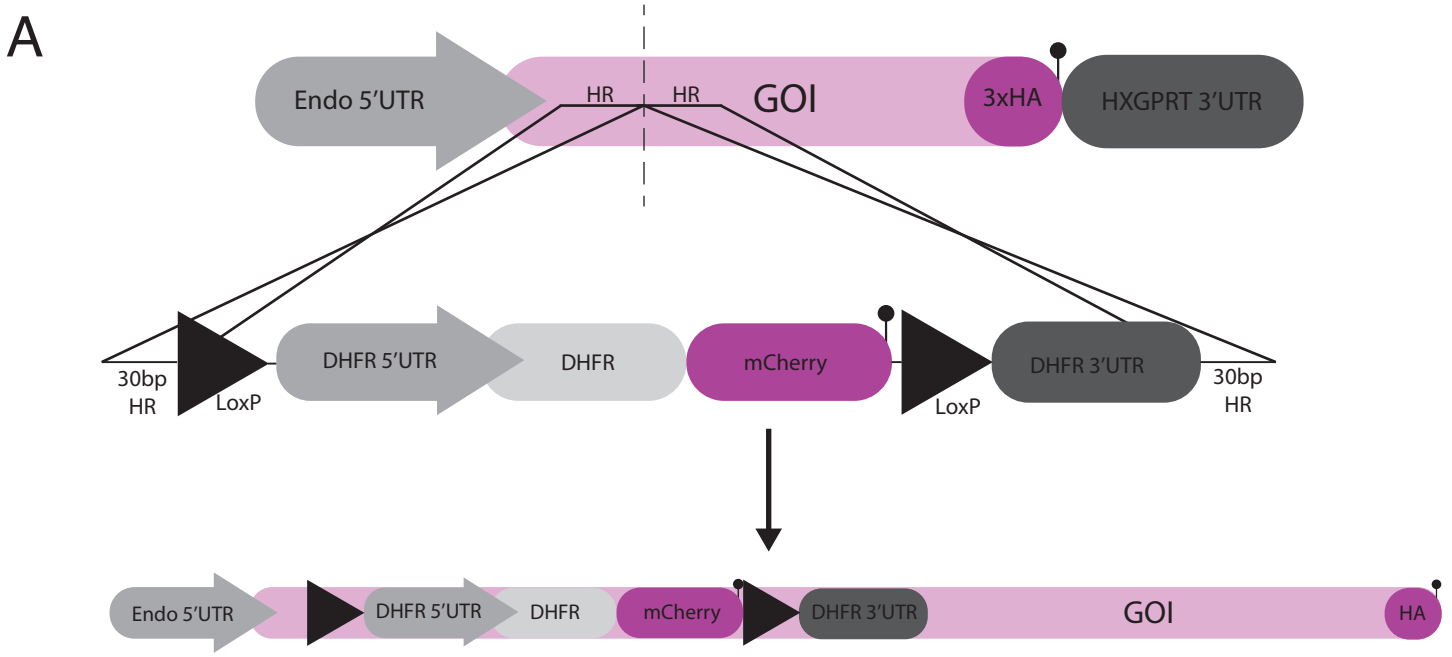
(A) Pru Δ*ku80* IST-HA parasites were differentiated under alkaline conditions for 7 days before being extracted and reinoculated. Magenta arrowheads indicate when the differentiation media was replaced during the second 7-day period of differentiation. Magenta stars indicate that samples were fixed on either (B) day 8, 24 hours post reinfection, or (C) day 14, 7-days after reinfection. IST (αHA; white) is consistently exported into the host cell nucleus (DAPI; blue) during bradyzoite (pLDH2-GFP; green) infection. Scale bar = 10μm. Brightness and contrast was edited on single colour channels prior to merging.

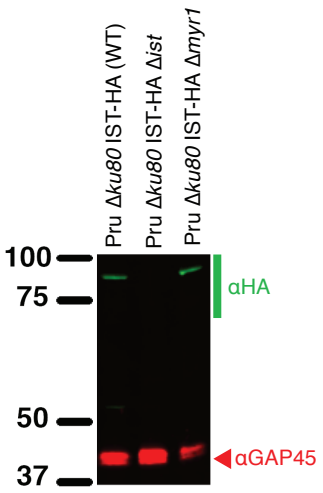
CRISPR/Cas9 with an homologous template containing a mCherry and DHFR selectable marker floxed by two LoxP sites, so that these markers could be excised in the future if needed (Fig 4.6A). Knockout parasite lines were verified by western blot and microscopy in tachyzoites (Fig. 4.6B and C, respectively). Western blot data showed IST expressed in both PruΔ*ku80* IST-HA and Δ*myr1* but no expression in Δ*ist* as expected (Fig. 4.6B). Similarly, no IST was observed in the host nucleus or parasites of Δ*ist* samples by microscopy, whereas in Δ*myr1* samples IST was confined to the tachyzoite vacuole and not observed in the nucleus unlike PruΔ*ku80* IST-HA parasites (Fig. 4.6C). To test if this was also the case in bradyzoites, nuclear IST levels were measured after seven days of bradyzoite differentiation and normalised to WT untagged lines. Similar to tachyzoites, the amount of IST in the nucleus (white arrows) of Δ*myr1* bradyzoite infected cells is significantly reduced when compared to PruΔ*ku80* IST-HA infected cells and is comparable to background levels of cells infected with Δ*ist* and WT PruΔ*ku80* levels (Fig. 4.6D and 4.6E(i)). Moreover, the export of IST in Δ*myr1* bradyzoites infected cells is significantly inhibited (Fig. 4.6E (ii)). Together, these data suggest that bradyzoites express and actively export known effector proteins, IST, via MYR1-dependent translocation mechanisms in bradyzoites.

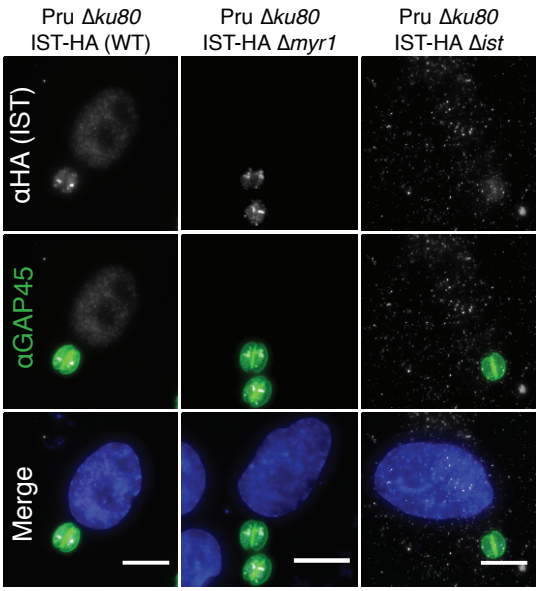
4.2.3 Bradyzoites supress the Interferon gamma pathway through MYR1-dependent IST export

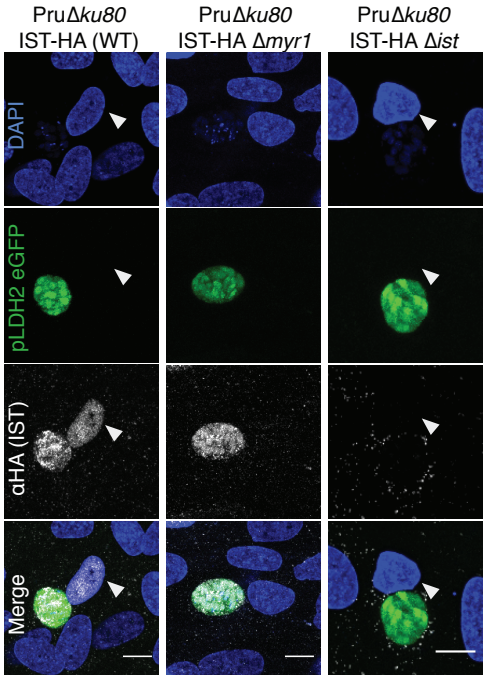
To further understand the role of protein export in bradyzoites I sought to understand whether IST was functional in these stages. In tachyzoite infection, IST has been shown to inhibit the host cell response to IFNγ stimulation[174,175]. To determine if bradyzoite infection also inhibits IFNγ signalling, I stimulated bradyzoite-containing cells with IFNγ and determined if IRF1 is expressed. IRF1 is one of many proteins that are upregulated in response to IFNγ stimulation. IFNγ activates transcription factor STAT1 which results in the translocation and binding of pSTAT1 homodimers to gamma-activated sites (GAS) in promoter regions of genes like IRF1. In tachyzoites, IRF1 is downregulated by the presence of IST upon IFNγ stimulation, and in the absence of IST, either through IST knockouts[174,175] or blocking export[279], IRF1 levels are restored to that of surrounding uninfected cells. As is the case in tachyzoites, IRF1 expression

Figure 4.6


A
Endo 5'UTR
HR
HR
GOI
3xHA
HXGPRT 3'UTR
30bp HR
LoxP
DHFR 5'UTR
DHFR
mCherry
LoxP
DHFR 3'UTR
30bp HR
Endo 5'UTR
DHFR 5'UTR
DHFR
mCherry
DHFR 3'UTR
GOI
HA


B
Pru Δku80 IST-HA (WT)
Pru Δku80 IST-HA Δist
Pru Δku80 IST-HA Δmyr1
100
75
50
37
αHA
αGAP45


C
Pru Δku80 IST-HA (WT)
Pru Δku80 IST-HA Δmyr1
Pru Δku80 IST-HA Δist
αHA (IST)
αGAP45
Merge


D
PruΔku80 IST-HA (WT)
PruΔku80 IST-HA Δmyr1
PruΔku80 IST-HA Δist
DAPI
pLDH2 eGFP
αHA (IST)
Merge

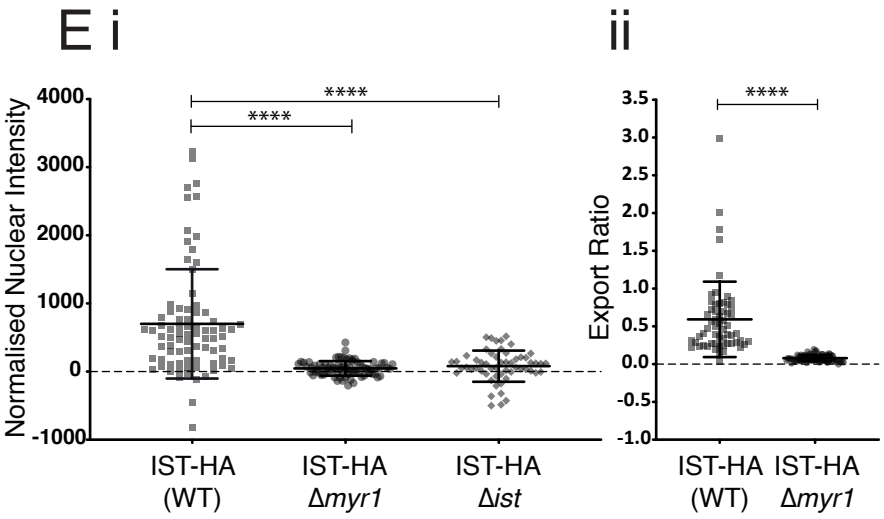

E i
ii
Normalised Nuclear Intensity
4000
3000
2000
1000
0
-1000
****
****
IST-HA (WT)
IST-HA Δmyr1
IST-HA Δist
Export Ratio
3.5
3.0
2.5
2.0
1.5
1.0
0.5
0.0
-0.5
-1.0
****
IST-HA (WT)
IST-HA Δmyr1

Figure 4.6 - IST and MYR1 knockouts prevent IST export in bradyzoites

(A) A schematic of the process used to insert the LoxP-DHFR-mCherry-LoxP cassette to knockout both MYR1 and IST. (B) Western blot indicates IST (αHA) is expressed in WT and Δ*myr1* tachyzoites but is absent in Δ*ist*. αGAP45 is used as a loading control. (C) Immuno-fluorescence images of tachyzoite (αGAP45; green) PruΔ*ku80* IST-HA (WT), PruΔ*ku80* IST-HA Δ*myr1*, and PruΔ*ku80* IST-HA Δ*ist* infected cells. WT can export IST-HA (αHA; white) into the host nucleus (DAPI; blue), whereas there is a loss of export in Δ*myr1* and no expression in Δ*ist* infected cells. (D) PruΔ*ku80* IST-HA (WT), PruΔ*ku80* IST-HA Δ*myr1*, and PruΔ*ku80* IST-HA Δ*ist* parasites were differentiated under alkaline conditions for 7 days before fixation. The absence of MYR1 in bradyzoites (pLDH2-eGFP; green) inhibits the export of IST-HA (αHA; white) into the host nucleus. White arrows indicate location of infected host nucleus (DAPI; blue). (E) (i) The increase in IST-HA mean fluorescence intensity in the host nuclei of WT infected cells is lost in Δ*myr1* and Δ*ist* infected host cells (normalised to PruΔ*ku80* untagged controls). Analysed from immuno-fluorescence imaging (Figure 4.6D) (mean ± SD, data points come from 3 different experiments, each experiment analysed on average between 20-40 bradyzoite cysts; unpaired, non-parametric Kruskal-Wallis test with Dunn's test to correct for multiple comparisons. ****p<0.0001). (ii) The ratio (nuclear intensity/vacuolar intensity) of IST drops in Δ*myr1* when compared to WT. Analysed from immuno-fluorescence imaging (Figure 4.6D) (mean ± SD, n = data points come from 3 different experiments, each experiment analysed on average between 20-40 bradyzoite cysts; unpaired, non-parametric Mann-Whitney test; ****p<0.0001). Scale bar = 10μm. Brightness and contrast was edited on single colour channels prior to merging.

Figure 4.7

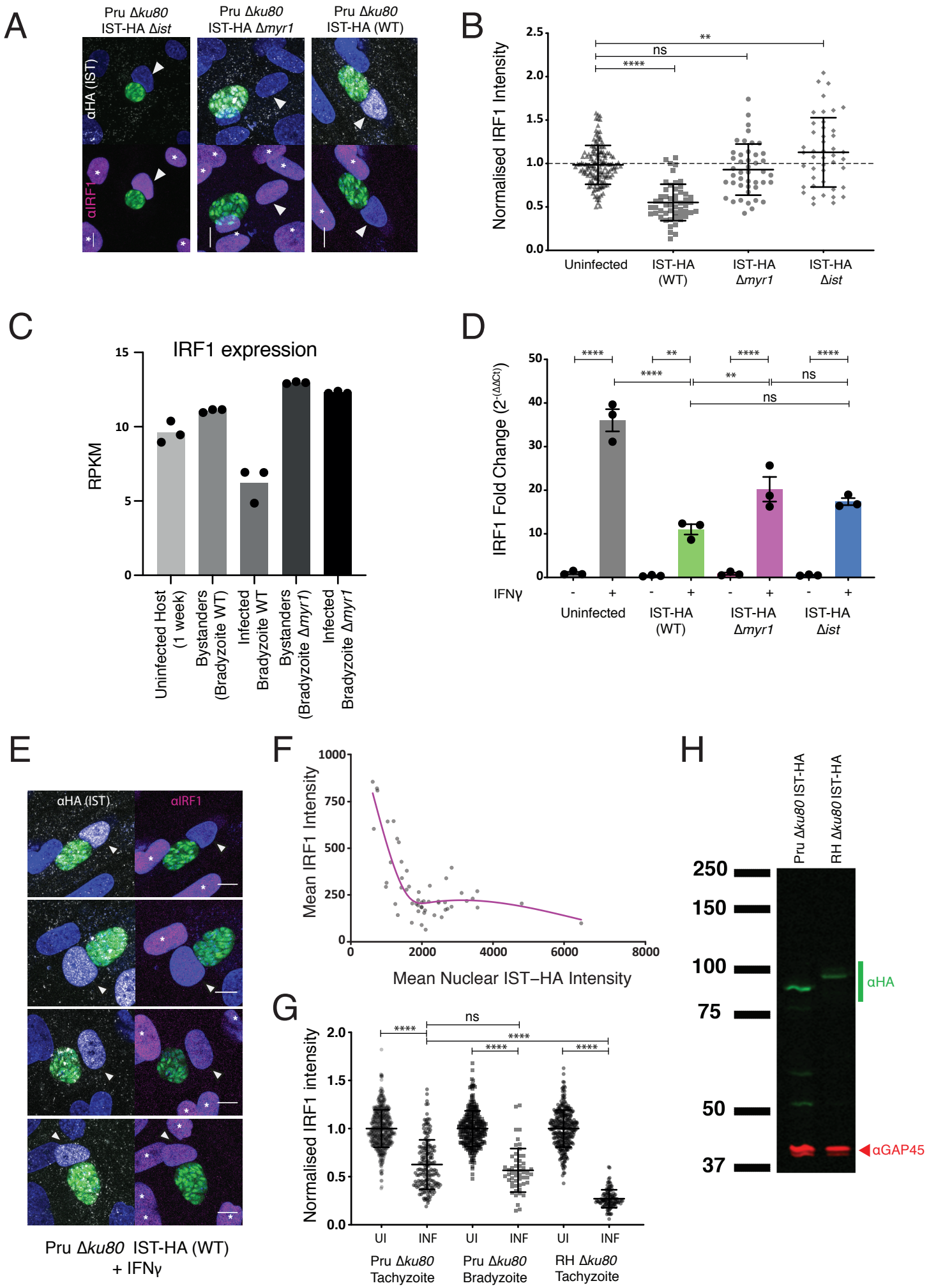

A
Pru Δku80 IST-HA Δist
Pru Δku80 IST-HA Δmyr1
Pru Δku80 IST-HA (WT)
αHA (IST)
αIRF1
B
Normalised IRF1 Intensity
ns
****
**
Uninfected
IST-HA (WT)
IST-HA Δmyr1
IST-HA Δist
C
IRF1 expression
RPKM
Uninfected Host (1 week)
Bystanders (Bradyzoite WT)
Infected Bradyzoite WT
Bystanders (Bradyzoite Δmyr1)
Infected Bradyzoite Δmyr1
D
IRF1 Fold Change (2-(ΔΔCt))
IFNγ
Uninfected
IST-HA (WT)
IST-HA Δmyr1
IST-HA Δist
E
αHA (IST)
αIRF1
Pru Δku80 IST-HA (WT) + IFNγ
F
Mean IRF1 Intensity
Mean Nuclear IST–HA Intensity
G
Normalised IRF1 intensity
UI
INF
Pru Δku80 Tachyzoite
Pru Δku80 Bradyzoite
RH Δku80 Tachyzoite
H
Pru Δku80 IST-HA
RH Δku80 IST-HA
250
150
100
75
50
37
αHA
αGAP45

Figure 4.7 - Bradyzoite exported IST inhibits IRF1 expression

(A) PruΔ*ku80* IST-HA (WT), Δ*myr1*, and Δ*ist* parasites were differentiated under alkaline conditions for 7 days before being treated with 50ng/ml of human-IFNγ for 15 hours and fixed. Nuclear IRF1 (αIRF1; magenta) protein levels drop to varying degrees in WT infected cells, and this inhibition is lost in Δ*myr1* and Δ*ist* bradyzoite (pLDH2-eGFP; green) infected host cells. White arrows indicate location of host nucleus (DAPI; blue). White stars indicate location of un-infected host nuclei. (B) The inhibition of IRF1 by WT bradyzoites is reversed by the knockout of *myr1* and IRF1 levels return to similar levels when compared to uninfected and Δ*ist* infected cells. Analysed from immuno-fluorescence imaging and normalised to surrounding uninfected cells (Figure 4.7A) (mean $\pm$ SD, data points come from 3 different experiments, each experiment analysed on average between 20-40 bradyzoite infected host cells; unpaired, parametric one-way ANOVA test with Dunnett's multiple comparison; **p<0.002, ****p<0.0001). (C) RPKM values for IRF1 from *data set 2*. (D) Fold change of IRF1 expression in uninfected (grey), WT (green), Δ*myr1* (magenta), Δ*ist* (blue) bradyzoite-containing cells with and without IFNγ (as compared to uninfected, unstimulated samples). (E) Range of IRF1 inhibition in PruΔ*ku80* IST-HA (WT) sample from previous figure 4.7A fluorescence imaging data. (F) The relationship between the intensity of IRF1 and the intensity of nuclear IST-HA (WT) was modelled with a non-linear curve (magenta) using natural splines with 3 degrees of freedom. This could significantly explain the relationship between IST-HA and IRFI ($p=1.042x10^{-12}$) (G) PruΔ*ku80* IST-HA parasites, that were either differentiated under alkaline conditions for 7 days (bradyzoites) or grown in D1 for 15 hours (tachyzoites), and RHΔ*ku80* IST-HA tachyzoites, were treated with 50ng/ml of human-IFNγ for 15 hours. Samples were fixed and probed with αIRF1 and DAPI. Nuclear IRF1 protein intensity levels were measure as a proportion of surrounding uninfected cell intensity for both uninfected and infected cells (mean $\pm$ SD, data points come from 3 different experiments, each experiment analysed on average between 15-30 bradyzoite cysts or 100-200 tachyzoite vacuoles; unpaired, non-parametric Kruskal-Wallis test with Dunn's test to correct for multiple comparisons. ****p<0.0001). There was no difference in IRF1 expression between PruΔ*ku80* tachyzoites and bradyzoites (p>0.9999). However, there is a significant difference between PruΔ*ku80* and RHΔ*ku80* tachyzoites. (H) Western blot indicates that IST (αHA; green) from PruΔ*ku80* IST-HA has a smaller molecular weight than RHΔ*ku80* IST (isolated from lysed tachyzoites). Loading control is αGAP45 (red) Scale bar = 10μm. Brightness and contrast was edited on single colour channels prior to merging.

is significantly inhibited in cells containing WT cysts as compared to bystander cells (white arrows; Fig. 4.7A (i) and (ii)). On the other hand, Δ*myr1* and Δ*ist* bradyzoites are unable to inhibit IRF1 expression and are comparable to uninfected bystander cells (Fig. 4.7A (i) and (ii)).

To further analyse the role of MYR1 (and therefore indirectly IST) in the host cell's response to bradyzoite infection, I returned to the second dataset in *Chapter 3*, derived from Δ*myr1* bradyzoites. Whilst in these experiments additional IFNγ was not added during the preparation of these samples, I observed a difference in the expression of IRF1 between WT-infected and Δ*myr1*-infected cells. In the absence of *myr1*, the transcript levels of IRF1 is comparable to that of uninfected bystander cells (Fig. 4.7B). To verify this, I sorted bradyzoite-infected cells on GFP before and after IFNγ treatment (15 hours), followed by qPCR for IRF1 to monitor transcription of the gene. Here it could be observed that IRF1 levels are significantly higher in Δ*myr1*-infected cells after treatment when compared to WT; however, unlike the RNA sequencing data, IRF levels are not to the same degree as uninfected cells (Fig. 4.7C). The lower levels of IRF1 expression in Δ*myr1*-infected (compared to uninfected cells) could be an underestimate, explained by host cell death observed by Δ*myr1*-infected cells upon IFNγ stimulation, as discussed in *section 4.2.3*.

Next I wanted to investigate the degree to which bradyzoites were able to inhibit IRF1 and whether inhibition was comparable to tachyzoites. First I looked at the ability of an individual cyst to inhibit IRF1 expression (white arrows) and noticed this varied widely between host cells, from having no effect to complete inhibition (Fig. 4.7D). I checked whether the variation could be explained by the correlation between the amount of IST in the nucleus and the subsequent expression of IRF1. The data could be modelled by fitting a hyperbolic curve (blue; Fig. 5e (p = 1.042×10^{-12})). As the hyperbolic curve indicates, the level of IRF1 decreases as the amount of IST-HA in the nucleus increases; however, there is a point at which high levels of IST cannot further decrease IRF1 expression. The variability in parasite induced IRF1 inhibition was also noted in the tachyzoite stages of the PruΔ*ku80* strain, with no significant difference in the degree of inhibition between the two stages (Fig. 4.7F; range 1.069-0.133). Interestingly, the type I strain, RHΔ*ku80*, showed a stronger ability to suppress IRF1 with less variability (Fig. 4.7G). To understand why these differences might have occurred I compared IST from both RHΔ*ku80* and PruΔ*ku80* by running on a western blot. I observed a significant size difference

Figure 4.8

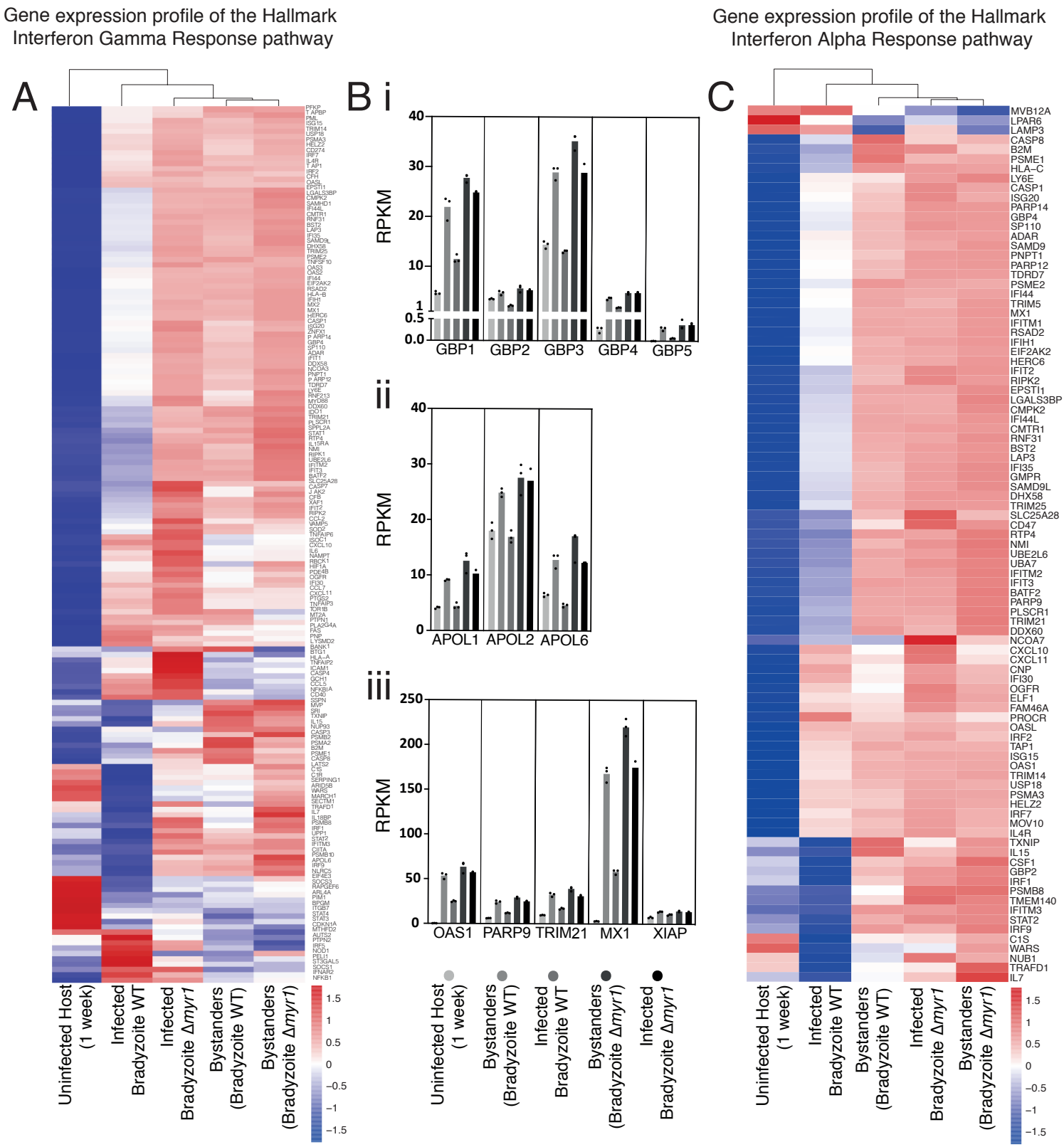


Figure 4.8 - MYR1 affects IFN host pathways

(**A**) A gene heat map of log_2RPKM expression for the Hallmark gene set *IFN gamma response* showing all samples from *data set 2* pathway analysis. Expression has been scaled to have mean 0 and standard deviation 1 for each gene. (**B**) RPKM values for protein expression of IFNγ-pSTAT1-GAS induced transcripts from *data set 2*. Genes include GBP family proteins (i), APOL family proteins (ii) and others (iii). (**C**) A gene heat map of log_2RPKM expression for the Hallmark gene set *IFN alpha response* showing all samples from *data set 2* pathway analysis. Expression has been scaled to have mean 0 and standard deviation 1 for each gene.

between RH-derived IST (bigger) and Pru-derived IST (smaller), suggesting there might be variations in splicing or a post translation event that could be responsible for the differences observed above (Fig. 4.7H). Therefore, the differences in the ability to supress IFNγ signalling between different strains might be a result of IST differences. Clearly transcript sequencing and allelic swap experiments would help discern what causes the size difference of IST and if it is biologically meaningful.

In *Chapter 3* (*section 3.2.4*) the *Interferon gamma response* pathway was one of three Hallmark gene sets to be observed as highly altered by bradyzoites and dependent on MYR1 and now, given the IRF1 data, I wanted to determine the wider impact MYR1 has on the IFNγ pathway. A gene expression heat map of the *Interferon gamma response* pathway (Fig. 4.8A) illustrates that Δ*myr1*-infected cells generally have a higher expression of IFNγ-related genes and cluster more closely with uninfected bystander cells than with WT-infected cells, suggesting that the majority of transcriptional changes that occur within the *Interferon gamma response* pathway are dependent on MYR1 in bradyzoites. I then chose several genes previously identified via CHIP-Seq analysis as IFNγ-induced pSTAT1-GAS transcripts[335] (Fig. 4.8B) and explored their gene expression in the bradyzoite RNA sequencing data. I observed the same expression pattern as IRF1 (Fig. 4.8B), where expression is suppressed in bradyzoite WT-infected cells but not in bradyzoite Δ*myr1*-infected cells. To visualise the extent of IFNγ gene suppression by bradyzoites, samples (WT, Δ*myr1* and Δ*ist*) would need to be treated with IFNγ prior to sequencing. However, it may be difficult to get enough material for RNA, from Δ*myr1* samples in particular, considering the cell death phenotype observed. As Matta et al. (2019)[254] identified type I interferons important for *in vivo* bradyzoite development, I looked further at the Hallmark gene set: *Interferon alpha response* pathway using a heat map (Fig. 4.8C). Interferon alpha also sees Δ*myr1*-infected cells cluster more closely with uninfected bystander cells than with WT-infected cells, and can be explained by the shared intracellular signal transducer protein STAT1 and the function of IST. Overall, this work indicates that bradyzoites are altering the host cell's response to IFNγ stimulation via the export of IST through the MYR1 pathway that persists for at least seven days post differentiation.

4.2.4 Protein export is important for survival of bradyzoite-containing cells upon IFNγ challenge

During the IFNγ stimulating experiments, I noticed that the number of intact Δ*myr1* cysts was greatly reduced after IFNγ treatment, suggesting IFNγ may cause the death of infected host cells. To further investigate the drop in cyst numbers, I performed live cell imaging of WT, Δ*myr1* and Δ*ist* over 15 hours following IFNγ treatment (Fig. 4.9A) and monitored host cell death by Propidium Iodide (PI) uptake. Upon IFNγ treatment I observed that there was a significant decrease in the survival of infected host cells when compared to negative controls (Fig. 4.9B). Cells containing Δ*myr1* cysts had the largest decrease in cell survival (87%), whereas WT and Δ*ist* saw a drop of 28% and 37%, respectively. This equated to no significant difference between IFNγ treated WT and Δ*ist* cyst numbers at the end of the 15 hour incubation period of IFNγ, whilst loss of MYR1 was significantly different from both WT and Δ*ist*, suggesting a role for other unknown MYR1-dependent exported protein/s in blocking IFNγ-induced host cell death. Analysing the same samples using FACS and monitoring GFP expressed from the bradyzoite-specific LDH2 promoter also showed a similar outcome (Fig. 4.9C & D). In stark contrast, IFNγ treatment of cells infected with Δ*myr1*-tachyzoites did not have a significant cell death phenotype, strongly supporting the notion that bradyzoite-infected cells are functionally different from tachyzoite-infected cells (Fig. 4.9E). These data suggest that IST alone is not accountable for the large volume of cell loss seen by Δ*myr1*-bradyzoite-containing cells, implying other factors contribute to prevent cell death.

To further investigate the mode of cell death, I observed the morphology of the cysts over the filming period and tracked how long it took for cell death to occur. Here I could see that cell death was accompanied by PI uptake, which was observed as staining of the host nucleus and debris. During cell death, host cells contracted before lysis or cell death occurred (Fig. 4.9A). Although some bradyzoites are released from the cyst during the death process, a majority remain within the dying cell and in some cases parasites are also observed taking up PI (Fig. 4.9A; white arrows). For Δ*myr1* infected cells, cell death occurred earlier, at approximately 9 hours post IFNγ stimulation, and was significantly earlier than those WT-infected cells that died (13.65 hours) (Fig. 4.9F). Interestingly, the time of death for Δ*ist*-infected cells was between

Figure 4.9

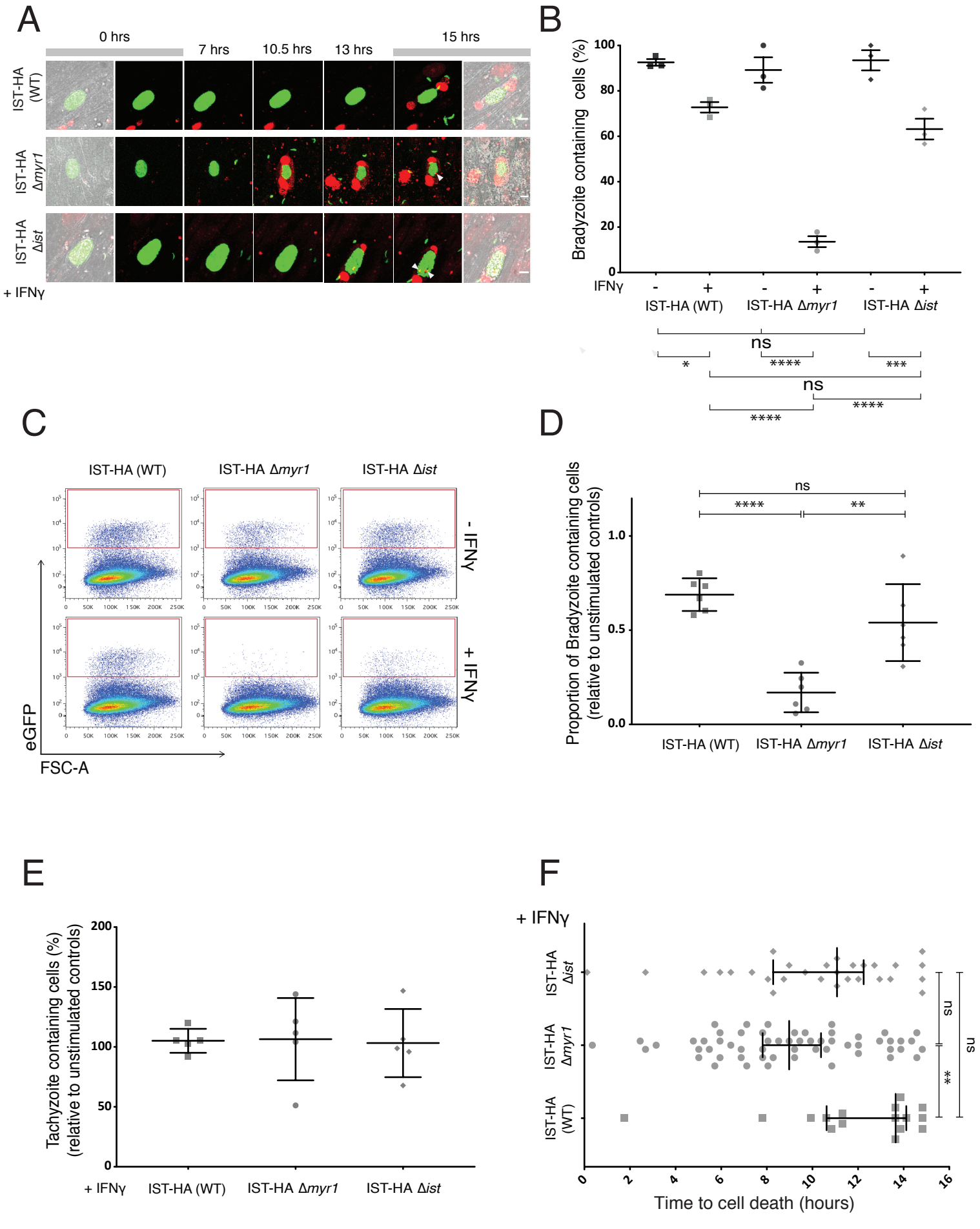
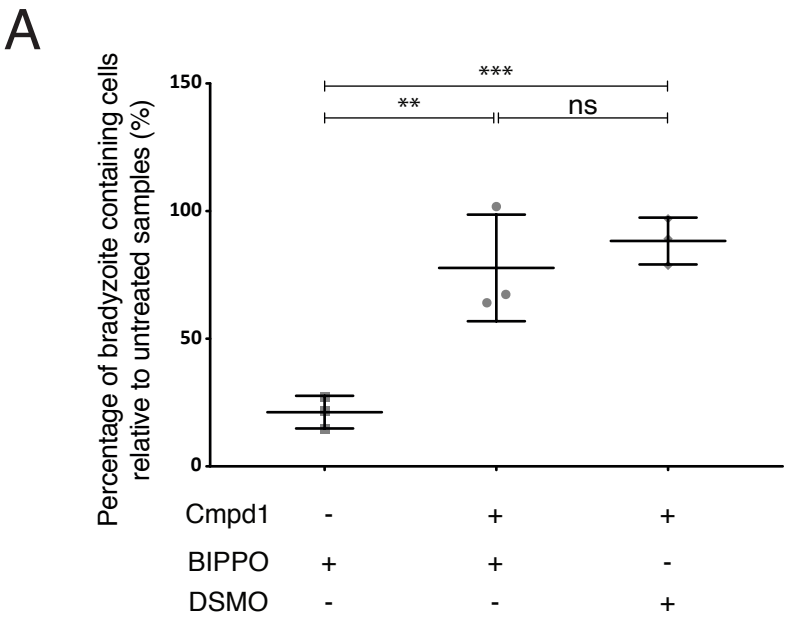
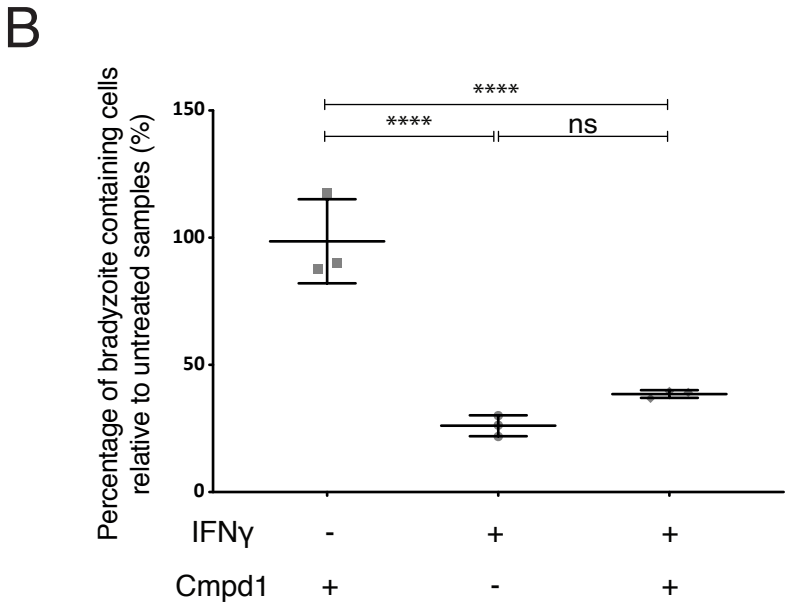

A
0 hrs
7 hrs
10.5 hrs
13 hrs
15 hrs
IST-HA (WT)
IST-HA Δmyr1
IST-HA Δist
+ IFNγ
B
Bradyzoite containing cells (%)
IFNγ
IST-HA (WT)
IST-HA Δmyr1
IST-HA Δist
ns
*
****
***
ns
****
****
C
IST-HA (WT)
IST-HA Δmyr1
IST-HA Δist
- IFNγ
+ IFNγ
eGFP
FSC-A
D
Proportion of Bradyzoite containing cells (relative to unstimulated controls)
ns
****
**
IST-HA (WT)
IST-HA Δmyr1
IST-HA Δist
E
Tachyzoite containing cells (%) (relative to unstimulated controls)
+ IFNγ
IST-HA (WT)
IST-HA Δmyr1
IST-HA Δist
F
+ IFNγ
IST-HA Δist
IST-HA Δmyr1
IST-HA (WT)
ns
**
ns
Time to cell death (hours)

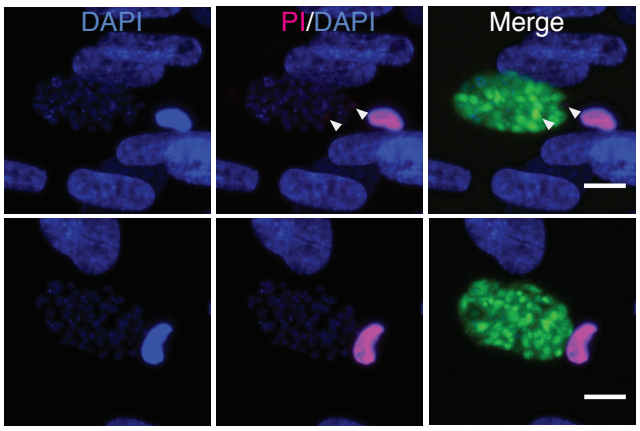
Figure 4.9 - Depletion of MYR1 prevents cyst persistence upon IFNγ stimulation.

(A) PruΔ*ku80* IST-HA (WT), IST-HA Δ*myr1*, and IST-HA Δ*ist* parasites were differentiated under alkaline conditions for 7 days before imaging. During each experiment (n = 3), between 15-35 parasite cysts were imaged every 14 minutes for 15 hours after the addition of PI (red) and 50ng/ml of IFNγ. PI can be seen entering the host cell and bradyzoites (pLDH2-eGFP; green) are released. Some PI enters bradyzoites (white arrow) Scale bar = 10μm. Brightness and contrast was edited on single colour channels prior to merging. (B) The percentage of cyst infected cells that survived the 15 hours treatment of IFNγ drops by almost 90% in Δ*myr1* infected cells, significantly more than both WT and Δ*ist* (mean ± SD, n = 3 experiments, each experiment tracked between 15-30 bradyzoite cysts; unpaired, one-way ANOVA test with Sidak's multiple comparison test; *p=0.0234, ***p=0.0008, ****p<0.0001). (C) PruΔ*ku80* IST-HA (WT), Δ*myr1*, and Δ*ist* parasites were differentiated under alkaline conditions for 7 days before being treated with 50ng/ml of human-IFNγ for 15 hours, trypinised and FACS sorted. FACS plot showing gating of $eGFP^+$ cells (red) of WT, Δ*myr1*, and Δ*ist* bradyzoite infected host cells. (D) Proportion of bradyzoite $eGFP^+$ cells compared to unstimulated samples shows a similar pattern to the live imaging data from Figure 4.9B. (mean ± SD, n = 6 experiments, unpaired, one-way ANOVA test with Tukey's multiple comparison test; **p=0.0011, ****p<0.0001). (E) PruΔ*ku80* IST-HA (WT), Δ*myr1*, and Δ*ist* tachyzoites were grown for 15 hours before being treated with IFNγ for 15 hours and dextran sulfate. HFFs were washed, trypinised and fixed, before probed with αGAP45. Samples were analysed using FACS and there was no difference between knockout lines and WT (mean ± SD, n = 5 experiments, unpaired, one-way ANOVA test with Tukey's multiple comparison test). (F) Time to cell death in hours from live cell imaging 4.9A; Δ*myr1* infected cells died earlier than both WT and Δ*ist* (median ± 95% CI, n = 3 experiments, each experiment tracked between 15-30 bradyzoite cysts; unpaired, non-parametric Kruskal-Wallis test with Dunn's multiple comparison; **p<0.01).

Figure 4.10







Pru*Δku80 Δmyr1* + IFNγ + Compound 1

Figure 4.10 - Depletion of MYR1 induces host cell death upon IFNγ stimulation.

(A) Compound 1 does not inhibit the parasites ability to egress. Compound 1 (2μM) was added to 7-day-old PruΔ*ku80* IST-HA Δ*myr1* bradyzoites for 16 hours prior to the addition of BIPPO or vehicle (DMSO). Samples were trypinised and fixed, FACS analysed. The proportion of bradyzoite-eGFP^{+} cells compared to DSMO only treated samples (mean ± SD, n = 3 experiments, unpaired, one-way ANOVA test with Sidak's multiple comparison test; **p=0.0012, ***p=0.0004). (B) The addition of compound 1 does not result in cell death recovery. Compound 1 (2μM) was added to 7-day-old PruΔ*ku80* IST-HA Δ*myr1* bradyzoites for an hour prior to the IFNγ addition for 15 hours. Samples were fixed, FACS analysed. The proportion of bradyzoite-eGFP^{+} cells compared to untreated samples (mean ± SD, n = 3 experiments, unpaired, one-way ANOVA test with Sidak's multiple comparison test; ****p<0.0001). (C) Intact cysts contain PI (red) positive host cell nuclei (blue) indicating host cell death. Compound 1 (2μM) was added to 7-day-old PruΔ*ku80* IST-HA Δ*myr1* bradyzoites (green) for an hour prior to the IFNγ addition for 15 hours. PI was added for 10 minutes before samples were washed and fixed. White arrows indicated PI positive parasites. Scale bar = 10μm. Brightness and contrast was edited on single colour channels prior to merging.

Δ*myr1*- and WT-infected cells (at approximately 11 hours), further implying that IST alone cannot account for the host cell response to IFNγ during infection.

Next I wanted to determine if the host cell death was host cell driven or if it was caused by the egress of parasites from host cells. The latter would suggest bradyzoites can sense a change in the environment upon IFNγ treatment resulting in egress activation, whereas the former implies the host cell initiates cell death in the absence of parasite modulation. To disentangle these two pathways I used compound 1, which has been shown to prevent egress by inhibiting PKG[124,336]. I hypothesised that if parasite egress was responsible for the cell death, then the addition of compound 1 would result in the recovery of the phenotype. Bradyzoite samples were incubated with compound 1 for an hour prior to the addition of IFNγ (to give compound 1 sufficient time to diffuse through the cyst wall) and 15 hours later checked for the levels of bradyzoite-containing host cells. As a control, I first established that compound 1 was functional and able to inhibit bradyzoite egress by inducing egress through BIPPO stimulation (Fig. 4.10A). Indeed, compound 1 was able to inhibit bradyzoite egress; however, when compound 1 was added to IFNγ cell death experiments, there was no significant difference in cell survival between cells treated with and without compound 1 (Fig. 4.10B). Furthermore, PI uptake was observed in bradyzoite-containing cells treated with compound 1 and IFNγ suggesting cell death was still occurring in the absence of parasite lysis (Fig 4.10C; white arrows indicate PI-positive parasites). These data indicate that one or more MYR1-dependent effectors protect bradyzoite-containing host cells from undergoing IFNγ-mediated cell death, demonstrating the importance of host cell modification during immune challenge, at least in early bradyzoite forms.

4.3 Discussion

Secreted and exported effector proteins have been observed during tachyzoite infection, yet few have looked into whether such proteins are produced during bradyzoite stages and if they are important for infection and persistence. Here I show that IST, expressed from its native promoter, is exported by bradyzoites into host cells in a MYR1-dependent fashion, suggesting that at least early-stage bradyzoites are capable of protein export and modification of their host cell. Furthermore, I show that not only is MYR1 important in export, it is vital for the parasites persistence in the face of IFNγ stimulation. Given that IST represses STAT1 signalling during IFNγ stimulation[174,175], these data suggest that IST could be important for bradyzoite persistence in muscle and CNS tissue, a line of enquiry future *in vivo* studies could focus on.

It has recently been reported, using a conditional expression system, that encysted bradyzoites are incapable of exporting proteins[298], which appears contradictory to my work. Here the authors tested protein export in bradyzoites by turning on the expression of tachyzoite proteins GRA16 and GRA24 using the tetON regulation system[187], five days post *in vitro* differentiation. These effectors accumulated within the boundaries of the cyst wall, suggesting that protein export might not occur at bradyzoite stages. The authors suggest this could be because GRA16 and GRA24 are either not required during chronic stages, or the cyst wall creates a physical barrier to protein export, or that bradyzoites lack a function translocation complex[298]. In contrast, I monitored all protein export from native promoters and showed that GRA24 is not expressed at all in bradyzoite stages, whilst GRA16 appears to be lowly expressed but not exported. In the case of GRA16, the experiments reported in my thesis are in line with the Krishnamurthy and Saeij (2018)[298] study. Conversely, in bradyzoites I see an increase in IST expression by RNAseq and a similar level of export in seven-day-old bradyzoites when compared to tachyzoites. IST was detected in host cells that were both infected with tachyzoites and subsequently differentiated into bradyzoites, and in samples where isolated bradyzoites were re-infected onto new host cells at both early and late time points. Together with the transcriptional data showing increased expression of IST I am confident that early stage bradyzoites are capable of producing and exporting IST into the host cell nucleus.

The capacity for bradyzoites to export IST was validated by another study that focuses on host nuclear levels of GRA16, GRA24, GRA28 and IST[337]. In the Mayoral *et al.* (2020)[337] study parasites were pre-differentiated *in vitro* and lysed bradyzoites were then inoculated onto new coverslips before protein levels were measured via microscopy. In agreement with my data, Mayoral *et al.* (2020)[337] found that IST was exported in newly infected cells, but, in conflict with my data, nuclear IST levels decreased over time, although levels were still statistically higher than uninfected samples. The difference between the two studies may be due to the different post-microscopic analysis. Mayoral *et al.* (2020)[337] normalise the levels of IST in the nucleus to uninfected nuclei, whereas I take a ratio of the amount of IST in the nucleus verses the amount of IST in the vacuole. By taking a ratio, I am able to account for an overall change in IST expression over time and normalise IST variation between the parasite's differing intrinsic IST production, which both Mayoral *et al.* (2020)[337] and I have shown.

Neither Mayoral *et al.* (2020)[337] data or my data truly addresses is whether translocation of IST occurs across the cyst wall. It remains possible from my experiments that all IST observed in the host cell nucleus of 7 day old bradyzoites is exported before the production of the cyst wall. For this to be true IST would have to be extremely stable and have a low turnover rate; which would enable IST to stay at the levels we observed in tachyzoites after 7 days of differentiation. A long half-life is not unheard of with some structural proteins lasting decades[338,339]. From our current knowledge, IST is an intrinsically disordered protein (IDP)[175] and evidence suggests a protein's overall degree of disorder is correlated with higher a turnover rate[340]. However, during infection IST is found in a complex with STAT1 dimers and Mi-2/NuRD[174], and evidence shows that complex formation increases the half-life of IDPs by concealing the IDP from degradation machinery[341]. Radioactive pulse-chase[342] or fluorescence bleaching[343] experiments can be used to determine a protein's half-life. In the context of IST, there remains several technical hurdles to overcome before the half-life can be addressed using these methods. For example, IST has host protein binding partners and previous pulldown experiments show that some of these binding partners (in particular STAT1 and pSTAT1) run at the similar molecular weight as IST[174], making it difficult to distinguish host proteins from IST. Fluorescence bleaching experiments would require the binding of a fluorophore to IST; however, fluorophores, like GFP, are structured proteins and previous data on protein export via MYR1 shows that highly structured proteins fused to the end of GRA16

block the export process[290]. Blockage would prevent the recovery stage of the experiment and one could not be sure if export was inhibited because of the cyst wall or because of the fusion protein.

Mayoral *et al.* (2020)[337] use a Di-Cre based system to tackle the half-life of IST. In their study IST is flanked by two LoxP sites in a DiCre expressing parasite line. After 24 hours in differentiation media, rapamycin is added and enables DiCre to excise IST from the genome. Four days post rapamycin addition all protein production is lost and there is no IST in the host nucleus. Their data indicates that the half-life of IST is at the most four days, suggesting that the IST in my analysis must be either be continuously exported or newly produced. Newly produced IST could be due to bradyzoite lysis, which can occur during the *in vitro* differentiation process. Lysis would result in new cell infections and subsequently IST export before the cyst wall is established. If lysis and reinfection did occur, IST export would be negatively correlated with an increase in the cyst size or parasite GFP intensity, which I do not observe. The other possibility is that there is something unique about IST that allows for its export across the cyst wall in bradyzoites but not GRA16 and GRA24. The only known trafficking element in some exported proteins is the TEXEL motif[268,280], but this cannot explain the export differences observed given the motif is present in both GRA16 and IST[175,176]. Furthermore, Krishnamurthy and Saeij (2018)[298] enforced expression of two proteins (GRA16 and GRA24) that are, according to my data not produced by bradyzoites, whereas it is apparent that IST is produced. This might cause unknown problems and may help to explain the export inhibition observed in the study. The best way to determine if IST can cross the cyst wall is to create a conditional system, either through an inducible promoter or promoter replacement with a bradyzoite specific promoter, which is now a focus of the lab.

If IST is not exported beyond the cyst wall, its continued expression in bradyzoites and the ability for lysed bradyzoites to export IST could be important for the parasite to establish new bradyzoite infections by continued immune evasion. IST is effective in inhibiting IFNγ signalling when it is delivered prior to IFN-γ activation, therefore it may be especially important during infection of naïve cells[174]. Bradyzoites encounter naïve cells at two points in *Toxoplasma's* lifecycle: 1) during reactivation where free bradyzoites may be released in to the surrounding tissue and invade new host cells, and 2) after cysts have been consumed by a new host, where

bradyzoites will encounter naïve epithelial cells. The bradyzoite's ability to skew the immune system at the initial stages of infection might be key to *Toxoplasma's* capacity to infect new a host. In addition, IST interacts with DNA and recruits the Mi-2/NuRD complex[174,175]. Altering the chromatin structure could result in long lasting inhibitory effects long after IST has diminished.

To determine if the export of IST from bradyzoites continues to impact its host, I looked at the expression of transcription factor IRF1, which is expressed in a IFNγ dependent fashion. IRF1 is blocked by the presence of IST, which implies that, at least at the early timepoints (7 days), bradyzoites continue to have the ability to block IFNγ signalling just as well as tachyzoites. From *Chapter 3*, RNA sequencing data shows that expression of IFNγ- and IFNα-related genes globally decreases in bradyzoite-containing cells when compared to uninfected bystanders (presumably by exported IST). Upon the loss of MYR1, the manipulation of both IFNγ- and IFNα-mediated gene expression is lost, and bradyzoite-containing cells mimic uninfected cells from the same culture. However, my data also indicates that IST alone does not appear to protect bradyzoite-containing host cells from IFNγ-mediated cell death.

The parasite's ability to interfere with the IFNγ-axis is important because it is the host's key mechanism in controlling *Toxoplasma* infection *in vivo*[125,239]. The mechanism by which IFNγ does this *in vivo* is not fully understood. Through *in vitro* analysis of human and murine cells, it has been suggested that IFNγ induced cell death or nutrient depletion might play a role during acute stages[188,228]. My data suggests that during chronic infection IFNγ may also play a role initiating cell death as an anti-microbial defence mechanism. Fibroblasts containing MYR1-knockout bradyzoites undergo cell death upon IFNγ stimulation, whereas cell death is not observed in tachyzoites. Furthermore, I show cell death occurs in the absence of parasite egress, suggesting the process is host cell driven. This implies that bradyzoites may work to block IFNγ-mediated host cell death. It is speculated that in tachyzoite-infected macrophages cell death may occur by pyroptosis initiated by the release of PAMPs following GBP-induced PVM breakdown in human cells[188], but the type of cell death observed in IFNγ-primed HFFs[344] remains undetermined and apoptosis could be equally likely. Although type II tachyzoites lacking IST are more susceptible to clearance after and before the addition of IFNγ in murine

macrophages[174,175], the death phenotype I observed is not solely controlled by IST. This implies that there could be other parasite effectors in play during chronic stages.

Alternatively, the cell death of Δ*myr1*-bradyzoite-containing host cells could be explained by the absence of tachyzoite effector export during the early stages of infection. By knocking out MYR1 I remove the entire repertoire of MYR1-dependent effector proteins at all stages, not just potential export at bradyzoite stages. Key effector proteins (like IST or GRA16) may need to be exported at tachyzoite or early-bradyzoite stages, potentially before the cyst wall is formed, for the parasite to benefit from their protection long into chronic stages. Tachyzoites have a range of available host manipulators other than MYR1 exported GRA proteins, including rhoptry proteins and PVM-localised cytosol-facing GRA proteins, that are unlikely to impact the host cell after differentiation. For example, it has been shown that GRA15 inhibits IFNγ cell death in macrophages infected with type II tachyzoites[26,224], but GRA15 is not found within the cyst wall[134], and its expression levels are significantly lower in bradyzoite stages (RNA sequencing, *Chapter 3*). The absence of GRA15 (and other effector proteins) during bradyzoite stages may not severely impact the survival of WT parasites unless it is also paired with the loss of MYR1, leaving host cells susceptible to cell death. It may simply be the collective absence of parasite-derived effector proteins from all areas in Δ*myr1*-bradyzoites that results in host cell death upon IFNγ stimulation.

The afore described model can also explain the different response to IFNγ stimulation between Δ*myr1*-tachyzoites and Δ*myr1*-bradyzoites, because Δ*myr1*-tachyzoites continue to be protected from cell death by other host-manipulation avenues (e.g. ROP effects) unlike Δ*myr1*-bradyzoites. Further studies should look into whether IFNγ-induced cell death occurs in physiologically important bradyzoite reservoirs such as neurons. The neuron signalling response to IFNγ is not well understood[345]; however, *in vitro* studies of primary neurons (murine) show neurons can respond in both canonical (STAT1-dependent) and non-canonical (STAT1-indepedent) ways to IFNγ[346]. Furthermore, there are reports of IFNγ induced neural clearance of pathogens in a non-lytic manner[347-349], suggesting IFNγ-induced cell death as an anti-microbial tool in neurons is not out of the realm of possibility.

In comparison to IFNγ, type I IFNs appear have a secondary role in managing tachyzoite growth[241,255,256]. However, recent evidence suggests type I IFNs could be more important in controlling chronic infection[254]. Type I IFN(a, b, l) signalling and transcription is induced by the dimerization of STAT1 with STAT2 after the phosphorylation of both[240]. A recent study looking into the effects of IST on type I signalling during *Toxoplasma* infection showed that IST can also bind STAT1/STAT2 dimers and, through the same mechanism described for IFNγ, blocks the expression of IFNβ induced genes[254]. Matta *et al*. (2019)[254] show that mice lacking the type I IFN receptor, IFNAR1, have a higher cyst burden in the brain and *in vitro* experiments with CNS immune cells lacking IFNAR1 are unable to control parasite growth. This implies IST may have an important role in the *Toxoplasma*'s ability to establish and maintain a chronic infection in the brain.

To further understand how much protection is provided by tachyzoite effectors verses hypothetical bradyzoite effectors, a conditional-system controlling the transcription of MYR1 will need to be used. Not only could a conditional MYR1 line help determine the importance of stage-specific export, it also enables further *in vivo* studies. Parasite lines lacking MYR1 are avirulent in acute stages[279] and have a lower cyst burden in the brain[311]. Without a conditional system it is unclear what proportion of the low cyst count is due to fewer tachyzoites reaching the brain and what proportion is due to Δ*myr1*-cyst-containing neurons succumbing to an inflammatory environment[204]. If bradyzoites need MYR1 (and therefore protein effector export) to persist during chronic stages, I would expect to see a decline in the cyst burden over time with a conditional-system that switches off bradyzoite MYR1 expression. By uncovering the cell death pathway initiated upon IFNγ stimulation in neurons and how the parasite inhibits this is important in understanding how the chronic stages persist *in vivo*.

4.4 Additional Methods and Materials

4.4.1 Plasmid constructs, transfections and parasites lines

As per *Chapter 3*, all genes were modified at the endogenous locus using the CRISPR/Cas9 system in Pru Δ*ku80* Δ*hx* (PruΔ*ku80*) only. Briefly, protospacers in the pSAG1::Cas9-U6::sgUPRT[200] and pU6-Universal::mCherry[199,280] plasmids were replaced with gene-specific guides targeting either at the 3' end of the gene (epitope tagging) or within the first exon (knockout generation).

HA-epitope tagging target genes

PruΔ*ku80* Δ*hx* GRA16 and IST were previously HA-tagged at the endogenous locus by a previous PhD student in the lab but were not used in his work, but similar methods can be seen in his published work[280,282]. Briefly, parasites were co-transfected with 10 μg of CRISPR/Cas9 guide plasmids (pSAG1::Cas9-U6::sgGRA16 (G#4) and pSAG1::Cas9-U6::sgIST (G#6) and 80 μg of homologous repair (HR) constructs that contained an HA-epitope and a minimum of 30 bp homology on the 3' ends of the dsDNA fragment (Fig. 4.3B (i)). HR constructs for GRA16 were made following the procedure outlined in Coffey et al. (2015)[280]. For IST, HR constructs were made by annealing two complementarity oligos (OligoP#3 & OligoP#4) together in IDT-duplex buffer and heating to 98°C for two minutes and cooled to room temperature[199]. In both cases, these procedures resulted in HA epitope tagged parasites lines with no drug selectable markers.

I tagged GRA24 using the same method as for MYR1-HA in *Chapter 3*. A CRISPR guide targeting the 3' end of the gene (G#5) was inserted into the pSAG1::Cas9-U6::sgUPRT plasmid using the forward primer P#7 by Q5 sitedirected mutagenesis (NEB). The pSAG1::Cas9-U6::sgGRA24 plasmid was co-transfected with a pLIC-3xHA-HXGPRT[282,314] amplicon with 30 bp HR (underlined) on either side of the CRISPR/Cas9 cut site (AmpP#11 & AmpP#12) (Fig. 4.3B (ii)). 10 μg of CRISPR/Cas9 plasmid was combined with up to 30 μg of amplicon for transfection. Transfected populations were selected with three rounds of 50 μg/mL xanthine and 25 μM/mL mycophenolic acid[315] before cloning. Positive clones were determined by immunofluorescent imaging.

Generating myr1 and ist knockouts.

Both myr1 and ist were knocked out in the PruΔ*ku80* Δ*hx i*st-HA parasite by homologous recombination paired with CRISPR/Cas9 which targets the first exon in myr1 and within the first 350 bp of IST (a 2532 bp sequence). For MYR1 the same guide and plasmid was used as described in *section 3.4* but this round it was co-transfected with up to 30 μg of pLoxP::pDHFR::mCherry (Fig. 4.6A)[201] DNA, amplified by PCR to incorporate 30 bp of homology on either end (AmpP#13 & AmpP#14). IST was knocked out in the same manner; the guide (G#7) was integrated into the pSAG1::Cas9-U6::sgUPRT plasmid by Q5 site-directed mutagenesis (NEB) using P#8, and co-transfected with 30 μg of pLoxP::pDHFR::mCherry amplified using AmpP#15 & AmpP#16 which incorporate 30 bp of homology to either side of the cut site in IST. After transfection, both lines were selected with 1 μM pyrimethamine[350] for a minimum of 2 cycles and cloned out.

APEX2 construct

The pBTM::TUB::sag1$_{\Delta gpi}$-apex2-myc plasmid was designed, crafted and kindly gifted to us by Dr. Giel van Dooren and Dr. Azadeh Seidi (Australian National University). In this construct, APEX2 is tagged with a MYC epitope and this is attached to the SAG1 gene lacking its GPI anchor; the resulting fusion protein is driven by the Tubulin promoter. This plasmid was transfected into the Pru-Toxofilin-Cre (Pru) line and selected on Ble using the protocol previously set out for phleomycin[351].

4.4.2 APEX2 driven biotinylation

The overall process was adapted from Seidi *et al.* (2018)[327]. Extracellular tachyzoites were harvested from a full lysed T25 culture flask, filtered using a 5 μM filter (Sartorius stedim) and resuspended in D1. An MOI of 1 was used to inoculate intracellular tachyzoite samples and 24 hours later biotin-phenol was added to the flask. Bradyzoite samples were inoculated with an MOI of 0.2 and differentiated *in vitro* for seven days before biotin-phenol addition. Biotin-phenol was produced in house by Dr. Nicole McKenzie from Assoc. Prof. Ethan Goddard-

Borger's laboratory, diluted in DSMO and added to samples to a final concentration of 1mM. Tachyzoites were incubated for 1 hour and bradyzoites were incubated for 2 hours, both at 37°C. After the incubation period, biotinylation was initiated by the addition of H_2O_2 at a final concentration of 1mM and incubated at RT for 45 seconds. To quench the reaction, samples were immediately spun at 12,000g for 30 seconds to pellet parasites and remove the supernatant, which was quickly followed by four rounds of five-minute washes with quenching solution (10 mM sodium azide, 10 mM sodium ascorbate, and 5 mM Trolox in PBS). Imaging samples were quenched in the culture dish using the same process before fixation and followed by the standard IFA protocol (*section 2.5*) using Streptavidin conjugated with Alexa-488 to probe for biotin. Cell pellets are washed with PBS before being lysed in RIPA lysis buffer (Table 8) which was supplemented with quenching agents. Protein concentration was determined by Pierce BCA Protein Assay Kit (Thermo Fisher Scientific) as per manufactures instructions. From here samples can be used for western blot analysis or to the pulldown step. For the pulldown, 500 μl of Pierce™ Streptavidin Magnetic Bead (concentration of 4-5 mg/mL; NEB) slurry was washed with RIPA lysis buffer twice before 4 mg of total protein sample was added to a final volume of 1 mL. Samples were incubated on a gentle rotation for 1 hour at RT. Using a magnetic stand, samples were washed twice with RIPA lysis buffer, once with 2 M urea (in 10 mM Tris-HCl pH 8.0), and one more time with RIPA lysis buffer before being eluted in 10mM Tris-Cl (pH 8.5 in water). Samples were collected for western blot (see *section 2.6* for western blot process) analysis at every step and probed with NeutrAvidin-HRP.

4.4.3 Microscopy and export and IRF1 quantification

See *section 2.5* for immunofluorescence assay (IFA), imaging and data quantification details.

Specific to *Chapter 4* is the IFA for IFNγ cell death using compound 1 (Fig. 4.10C). For this IFA, treated cells were incubated with Propidium Iodide (PI) for 10 minutes in a final concentration of 0.05mg/ml (Merck). Samples were washed three times (with PBS) prior to fixation and permeabilised as described in *section 2.5*. Other than the addition of DAPI, no other markers were used in this experiment.

4.4.4 Interferon gamma stimulation

Human IFNγ 285-IF (R&D systems) was added from a 50 μg/μL stock solution to a final experimental concentration of 50 ng/μL. Tachyzoites samples were inoculated for 20 hours before a 15 hour stimulation in D1. Bradyzoites were stimulated for 15 hours after 7 days in differentiation media.

4.4.5 Reverse transcription qPCR

Bradyzoites were differentiated for seven days before IFNγ stimulation. Prior to RNA extraction, HFFs were washed with PBS, dislodged with trypsin, and GFP^+ cells were collected by sorting on a BD Influx (361) cell sorter (BD Biosciences). Uninfected cells also went through this process. Total host and parasite RNA was extracted using the RNeasy kit (Qiagen) and reversed transcribed to cDNA using SensiFAST cDNA Kit (Bioline) following the manufacturer's instructions on a T100 Thermal Cycler (BioRAD).

Host IRF1 was amplified using previously validated primers (AmpP#17 & AmpP#18)[174] and the human housekeeping gene, HPRT, was used as the reference gene (AmpP#19 & AmpP#20). Primers were used at 2 μM in a final reaction volume of 10 μL, which contained 2uL cDNA and 1x SYBR green (Applied Biosystems). Samples were run for 40 cycles on a C1000 Thermal Cycler (BioRAD).

Relative IRF1 expression was normalised against HPRT expression using the efficiency-corrected ΔΔCt method[352] and is presented as fold change in expression levels as compared to uninfected, unstimulated samples. Three independent biological replicates of each condition were obtained.

4.4.6 Live cell microscopy

Parasites were cultured and differentiated as described above in a 35mm polymer coverslip dish (Ibidi) for 7 days. 100 μL of Propidium Iodide (PI: 1 mg/mL; Merck) was added to 2 mL of fresh differentiation media and either 50 ng/μL of human IFNγ 285-IF (R&D systems) was added

or not. Between 15-25 cysts were tracked every 14 minutes for 15 hours (overnight) on a Lecia SP8 confocal using resonant scanning.

4.4.7 Flow cytometry

Bradyzoites were differentiated as described in *section 2.3* and after 7 days in differentiation media cells were stimulated for 15 hours with IFNγ 285-IF (R&D systems), prior to being dislodged with trypsin, fixed with 4% v/v paraformaldehyde in PBS for 10 minutes and resuspended in PBS for flow cytometry. A minimum of $1x10^3$ cells were analysed using a BD LSR WII cell analyser (BD Biosciences) and the proportion of $eGFP^+$ between unstimulated and stimulated cells was calculated. In addition to IFNγ stimulation, Tachyzoites were also treated with 25 mg/mL dextran sulphate (Sigma) to prevent reinvasion[353]. Tachyzoite samples were dislodged with trypsin, fixed with 4% v/v paraformaldehyde/PBS for 10 minutes and permeabilised in 0.1% v/v Triton X-100/PBS and blocked in 3% w/v BSA/PBS for 1 hour at RT. Samples were incubated in primary antibody, αGAP45[53], overnight at 4°C, PBS washed, and incubated at RT for 1 hour with α-rabbit Alexa-594 conjugated secondary antibody (Invitrogen) before analysis.

4.4.8 Compound 1 and BIPPO treatment

Compound 1 was added to a final concentration of 2 μM an hour before the addition of IFNγ and left in the solution for the remainder of the IFNγ treatment period[124]. This is the same procedure used for immunofluorescence images of compound 1 treated cells. BIPPO (5-Benzyl-3-isopropyl-1H- pyrazolo[4,3- d]pyrimidin-7(6H)-on) was added to a final concentration of 1μM and incubated for 7 minutes before cells were harvested[354].

4.4.9 Statistical analysis

The relationship between the intensity of IRF1 and the intensity of nuclear IST-HA was modelled with a non-linear curve (polynomial) using natural splines with 3 degrees of freedom using RStudio.

Chapter 5: Conclusions

5.1 Opening Remarks

As an intracellular pathogen, *Toxoplasma* is continuously encountering hostile environments induced by the host's defence mechanism. Over the last two decades, the field has worked to elucidate the consequences of *Toxoplasma* infection on the host cell and the molecular mechanisms used by the parasite to mitigate the host's defences. It was clear that the parasite inhibited some host cell responses while activating others, including subverting the immune system[355] and modifying the cell's morphology[162] and behaviour [150,356]. Underpinning many of these changes were alterations in the host's transcriptional response, which is immense[167,184]. The degree of parasite interference was not fully understood until the identification of parasite proteins that directly affected the host's transcript profile[355]. Specific transcriptional alterations were linked to virulence[23,171,242,252] and initial studies focused on finding parasite factors responsible for the difference in strain virulence. By studying the progeny of avirulent and virulent strains using QTL[28], multiple discoveries were made that expanded the field's understanding on the mechanisms around host-pathogen interactions and the extent of host manipulation during *Toxoplasma* infection. It became clear that *Toxoplasma* secreted effector proteins into the host cell at different stages of the lytic life cycle: rhoptry proteins were injected during invasion, and the dense granules secreted and exported proteins for the remainder of the cycle[72]. Both groups of proteins interacted with host proteins, some altering the host transcriptome, and often these effector proteins were responsible for the subversion of the host's immune response[163].

Due to the nature of *Toxoplasma* virulence, proteins identified in strain crosses were limited to tachyzoite-specific host interactions because bradyzoites do not influence virulence. Virulence studies led to a considerable expansion in the field's understanding of tachyzoite infection and the mechanisms used for tachyzoite's survival. In contrast, knowledge around bradyzoites and their interactions with the host cell has been largely neglected, despite being an important reservoir for transmission and reactivation. Neglect was likely driven by three main factors. Firstly, the dogma that bradyzoites were dormant, and therefore did not interact with the host, plagued the field until a study by Watts *et al.* (2015)[44] showed once again that bradyzoites were indeed dynamic, both replicating and lysing during this long stage of infection. Secondly, the straightforward nature of tachyzoite culture *in vitro* meant tachyzoite-

host investigations could proceed without the complexities and reservations that often accompanied *in vitro* bradyzoite differentiation[118]. In fact, our molecular understanding of bradyzoite differentiation and how it could be manipulated *in vitro* for research was, until this year[119], an enigma. Despite the BDF1 advancement, true *in vitro* differentiation is still in its infancy. Finally, the cyst wall is quoted as being impenetrable[229]; however, it seems unlikely that a parasite that scavenges nutrients for its survival develops an insurmountable wall. It is easy to speculate that bradyzoites also need a permeable wall to enable protein secretion across into the host cell to influence the host response and support their long-term persistence, much like tachyzoites.

Therefore, the aim of my thesis was to obtain a more comprehensive understanding of host-pathogen interactions between the host cell and *Toxoplasma* bradyzoites by determining the mechanisms bradyzoites use to establish and maintain life-long infection. Specifically, my thesis has focused on characterising the host transcriptional changes induced by bradyzoite infection, resolving if and what parasite export factors could be responsible, and determining the relevance of these changes it the context of bradyzoite persistence. To this end, I have concluded that:

- Bradyzoite impacts on host transcription are distinct from tachyzoites, as presented in *Chapter 3*
- Bradyzoites produce and export effector protein IST to skew IFN responses, as shown in *Chapter 4*
- And that export of effector proteins is important in bradyzoite stages for their survival, as discussed in *Chapters 3* and *4*

My thesis has shed light the importance of exported parasite proteins in *Toxoplasma* and the role these proteins have on the parasite's capacity to modify the host cell for its benefit, not only during the tachyzoite lytic cycle but also into the long-lived bradyzoite stages. Transcriptional data of MYR1 knockouts indicate that export is important in modulating host cell responses to bradyzoite infection, especially in immune related pathways like type I and II IFN. This is further validated by data from *Chapter 4* which shows the presence of MYR1 is important in preventing host cell death upon IFNγ signalling and that the potent inhibitor of STAT1, IST, continues to be produced and exported by bradyzoites.

5.2 Models of export supporting bradyzoite survival

What my thesis has been unable to tease out is at exactly what point protein export is critical for bradyzoite survival. To help answer this question, I propose three models to explain how protein export could impact the bradyzoite's long-term survival. These ideas have been informed by my data (and others) and parts have been mentioned throughout my thesis as likely explanations for observations, but I have merged these models here to form three cohesive ideas. The first model focuses on tachyzoites as the only source of exported proteins and host modification, the second explores the idea bradyzoite-specific exported proteins being trafficked across the cyst wall, and the final model considers a position somewhere between these two extremes. These models are all underpinned by the debate around cyst wall permeability to parasite proteins, where the first and last models assume no protein export occurs across the cyst wall, while the second explores the idea that export can occur across the cyst wall.

5.2.1 Model 1: Tachyzoites export effector proteins that support chronic infection (fig. 5.1A)

During infection, tachyzoites disseminate and infect tissues that will eventually harbour bradyzoite cysts. Therefore, it's highly likely that tachyzoites modify the host cell to setup the environment the continued growth and survival of bradyzoites. During tachyzoite infection three groups of effector proteins are employed: injected ROP proteins, PV/M bound GRA proteins and exported GRA proteins. To prevent clearance, rhoptry proteins may be needed instantaneously to counter the rapid first line defence of the host. The single secretion of these proteins could be either because the proteins are so efficient in their function only one secretion event is required, or that ROP effects on the host are not required in the long term once DG proteins have started to secret. On the other hand, GRA proteins appear to be required for the length of tachyzoite infection as they are observed through-out the three-day infection. GRA effector proteins that are confined to the PV and its membrane might not be exported because these proteins have secondary roles, like within the IVN network (e.g GRA12 & 6)[135,208,209]. Whereas GRA exported proteins have only one function; to modify the host cell

Figure 5.1

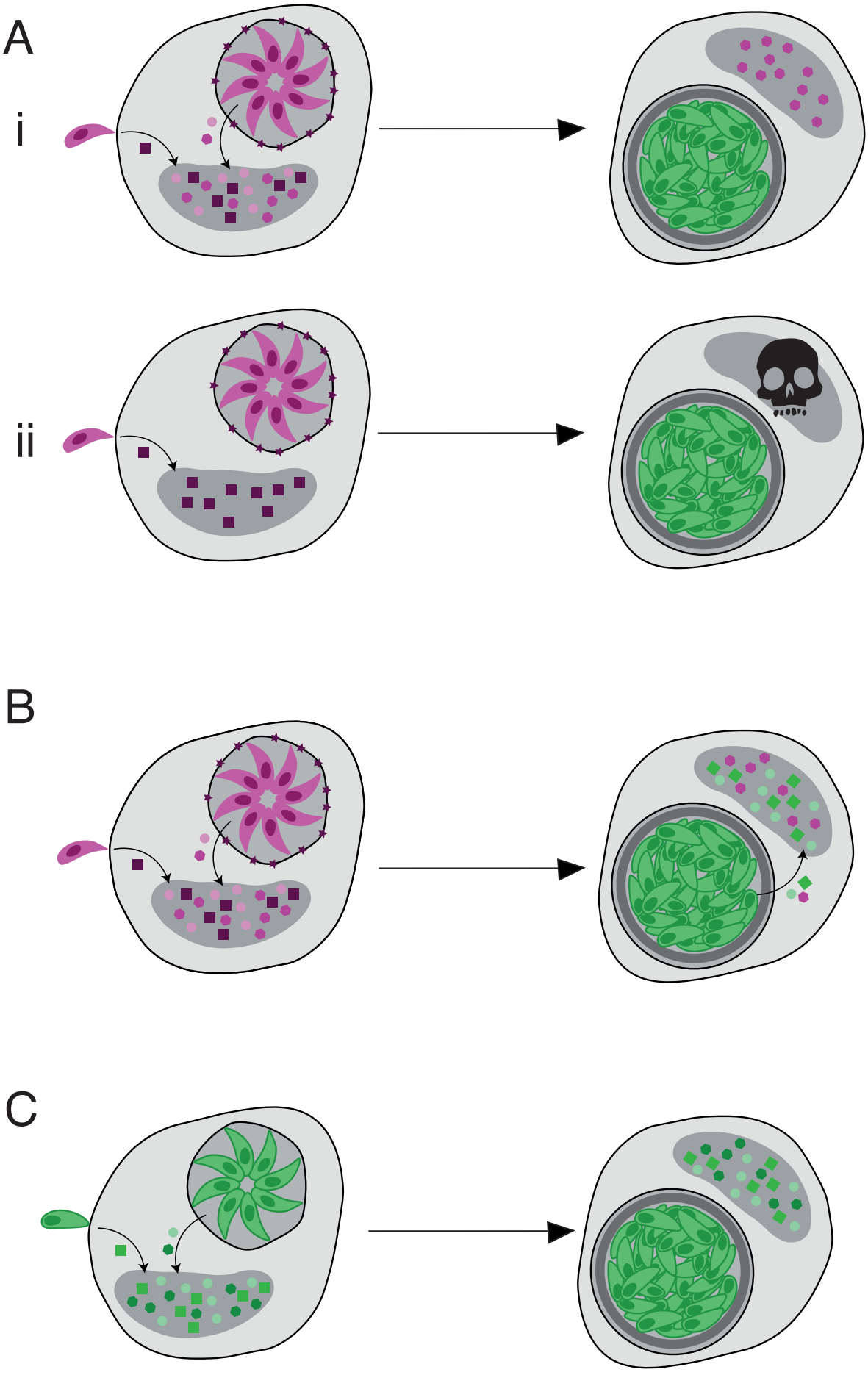


Figure 5.1 – Models of export supporting bradyzoite survival

The three models discussed in section 5.2 in a schematic presentation.

(A) *Model 1 - Tachyzoites export effector proteins that support chronic infection*. Rhoptry (dark pink square), dense granule PVM proteins (dark pink stars) and exported effector proteins (hot pink and baby pink) are present during tachyzoites stages (parasites). (i) Some of these proteins have short half-lives or are integrated into the cyst wall and their effects are diminished when parasites develop into bradyzoites (green). Some exported dense granule proteins may have long term effects on the host enabling continued bradyzoite survival despite no bradyzoite export of effector proteins. (ii) When tachyzoite export is inhibited (e.g. MYR1 knockout), the loss of both short term and long-term effectors during bradyzoite stages prevents parasite persistence.

(B) *Model 2 - Bradyzoites export unique proteins across the cyst wall.* Both tachyzoites and bradyzoites are able to export effector proteins across their host-pathogen barriers. Some of these proteins are stage specific (baby pink, dark pink squares & stars, green square and light green circle) and others are expressed in both stages (hot pink).

(C) *Model 3 - Bradyzoites export proteins before the establishment of the cyst wall.* Bradyzoites are unable to export effector proteins across the cyst wall; however, they are able to export proteins during invasion (green square) and initial stages of infection (dark green, and light green circle). These proteins are likely bradyzoite specific proteins.

and their continued secretion prevents protein turnover, guaranteeing a sufficient amount of effector protein within the host cell.

Both the absence of early secreted ROP, and/or the diminishing effects of GRA proteins over time could result in an increase in the host's susceptibility to defence signals, consequently changing the transcriptome of cells harbouring developing bradyzoites. When a tachyzoite infection develops into a longer infection, we could hypothesise that it's less likely the transcriptome effects originating from rhoptry proteins still impact the host cell. As the chronic infection progresses and the cyst wall becomes established, GRA protein effects start to become impacted. PV/M GRA proteins could be incorporated into the matrix and can no longer function as effector proteins, further decreasing the transcriptional changes observed in tachyzoites. Finally, the decrease of functional ROP17[278,292] and the potential incorporation of MYR1 (and other translocon complex proteins) into the cyst wall matrix[134,135] would prevent the export of effector proteins. Inhibiting protein export by building a cyst wall could be a mechanism used by the parasites to remain hidden in the cyst, leaving the cyst wall as a physical barrier to internal cell defence mechanisms. The combined loss of all of these effector proteins, contributes to the overall decrease of transcriptional changes during bradyzoite infection observed in *Chapter 3*. Furthermore, the lack of tachyzoite effector protein expression and export in bradyzoite stages could consequently change the host transcript profile to one that looks unique to bradyzoites, as seen in my data.

However, there are overlaps between the two stages in the transcriptional profile, specifically in IFN pathways. I show that IST is indeed still present in the host nucleus and functional in bradyzoite stages. Although in this model there is no export in bradyzoite stages, IST could be from tachyzoite stages and result in the continued alteration of these pathways. In tachyzoites, IST export levels are steady as parasites numbers increase. A consistent level of IST could suggest that either IST is exported in one burst and remains in the host cell for the remainder of the three-day infection, or a decrease in the surface to volume ratio as the PV grows means the translocation is the limiting factor despite an increase in overall IST. It is possible that IST has a half-life of three days[337] but a protein with a half-life of seven days is unheard of in Apicomplexa (to my knowledge). An extremely long half-life is not unheard of in other eukaryotes, with some cell types that have proteins with half-lives in the range of 21 days and

some structural proteins with turnover rates in the range of years[343]. However, the more likely explanation is that IST causes prolonged host transcriptional modulation as a result of the recruitment of the Mi-2/NuRD complex and the consequence of Mi-2/NuRD driven chromatin modifications. This would enable continued survival even in the absence of parasite protein export after the cyst wall is established, like what is seen in WT-bradyzoite containing cells when treated with IFNγ (Fig. 5.1A(i)).

When GRA protein export is blocked at tachyzoites, these long-term protective effects are no longer present in bradyzoite-containing cells which can now respond to death and immune signals. This is characterised by the similarity of the transcriptional profile between host cells harbouring bradyzoites and uninfected bystanders, and the ability of host cells to initiate cell death processes. This again is observed heavily in IFN pathways, which supports the idea that IST's effects continue to impact the host cell into bradyzoite stages. Unlike bradyzoites, tachyzoites lacking export continue to be protected by the effects of rhoptry proteins and PV/M bound dense granules, but the collective absence of all parasite derived effector proteins in bradyzoites results in host cell death upon stimulation (Fig. 5.1A(ii)).

5.2.2 Model 2: Bradyzoites export unique proteins across the cyst wall (fig. 5.1B)

Alternatively, bradyzoites could be exporting bradyzoite specific effector proteins across the cyst wall, using the same MYR1 dependent pathway. It's been consistently shown that bradyzoites express proteins unique to this stage, including isoforms of tachyzoite proteins that have a similar (if not the same) function[105,357]. Bradyzoites and tachyzoites have different lifestyles (slow growing and long-lived versus fast growing and destructive, respectively) and thus may require unique strategies to manipulate the host's response. The export of unique bradyzoite proteins beyond the cyst wall could explain the unique transcriptional profile seen in bradyzoite-containing cells. Although, cyst wall export has been controversial, evidence around the cyst wall's permeability has not excluded export nor has it been definitive against export[132,298,337]. Translocon components, like MYR1, are expressed in bradyzoites stages and are present with the cyst wall which could allow for protein translocation[134,337]. The export signal remains undefined for both tachyzoite and potential bradyzoite exported proteins. This

opens the possibility of a bradyzoite specific signal that targets proteins for continued export during bradyzoite stages, including those that are also present in tachyzoites. IST could be one of these proteins, as IFN pathways continue to be impacted during bradyzoite stages, it continues to be expressed in bradyzoites and is exported at the same levels as tachyzoites. With a potential half-life of between three-four days[337] IST would need to be continuously exported across the cyst wall to keep protein levels at a critical mass for function during chronic infection.

It is likely IST is not the only bradyzoite exported protein, as its absence does not fully account for the host cell death phenotype observed with IFNγ stimulation. This suggests there might be unknown bradyzoite proteins in addition to IST that inhibit IFNγ signalling and/or cell death. I should mention that, throughout this thesis, I have continuously used transcription as a marker of effector protein export and host manipulation; however, transcription modification is not the only means of parasite manipulation. Proteins that mechanically block death pathways, rather than altering the host's transcripts, do exist in other pathogens[285,294,306,310]. If this is the case in *Toxoplasma*, the expression of such proteins in bradyzoites may explain the lower levels of transcriptional changes in WT bradyzoite-containing cell, but still account for continued protection. If these hypothetical proteins are also specific to bradyzoites, it could account for the differences seen in cell death between tachyzoites and bradyzoites. The absence of MYR1 in bradyzoites would prevent the export of these unique effectors resulting in cell death, whereas in tachyzoites the collective impact of other effector proteins (ROP and PV/M proteins) could lend protection in the absence of exported proteins.

5.2.3 Model 3: Bradyzoites export proteins before the establishment of the cyst wall (fig. 5.1C)

As discussed previously, the permissibility of the cyst wall to parasite proteins is still in question. If indeed the cyst wall is not surmountable, I propose a similar model to Model 1; however, in addition to tachyzoites, freshly lysed bradyzoites are also able to modify the host cell and establish an environment that supports the long-term survival of the cyst. *In vivo* cysts have been shown to lyse throughout chronic infection and enough lysed bradyzoites have to reinvade to maintain a consistent number of cysts [44,358]. The time between a newly invaded

bradyzoite and the completion of the cyst wall is a potential gap where effector protein export could occur. Reinvasion would also allow for freshly secreted ROP17 to phosphorylate the required translocon components[265,278], which have been observed in bradyzoite stages[134,337], to enable export.

The repertoire of effector proteins exported by bradyzoites might differ from tachyzoites, explaining both the transcriptional and cell death differences. There is already evidence that the curated list of proteins exported differs between the two stages. GRA16 and GRA24 are not produced by bradyzoites, and transcriptional data suggests this might also be the case for HCE1/TEEGR. Plainly, IST is produced in bradyzoites and is exported at early stages[337]. Its continued expression in mature bradyzoites (despite the lack of export across the cyst wall) might assist parasites in evading the immune system of a naïve host after ingestion or during the invasion of naïve cells. Furthermore, it is equally likely that bradyzoites produce unidentified effector proteins unique to the bradyzoite's lifestyle, which further alters the composition of the export proteins. In addition, the injection of bradyzoite-specific host-modifying rhoptry proteins may also play a role in setting up chronic infection. As mentioned in the second model, the effects of these unique bradyzoite exported proteins could account for the transcriptional and phenotypic difference seen in my data.

5.3 Future directions

Over the last couple of years, bradyzoite research has gained traction and with new techniques and discoveries bradyzoites research will likely continue to grow. If our goal is to cure high-risk individuals of chronic *Toxoplasma* infection, further research will be needed to better understand the interplay between bradyzoites and the host. From this thesis, I have concluded that the problems at the forefront of bradyzoite-host interactions are: 1) determining whether bradyzoites can export proteins across the cyst wall and gaining a fuller picture on *Toxoplasma* mechanism of export, 2) identifying any potential bradyzoite effector proteins, and 3) investigating the consequences of removing export and effector proteins in chronic infection.

Both *in vitro* and *in vivo* experiments will be an important part of this process. This year's BDF1 discovery has opened the door to a potentially easier and more efficient method for *in vitro* differentiation[119]. This is vital, because by turning on differentiation without the complexities of host and parasite stress provides a means to do valuable bradyzoite experiments in a controlled manner which was previously unattainable. Combining controlled *in vitro* differentiation with a conditional system that regulates proteins like IST or MYR1 in different stages (e.g. promoter swaps, inversible stage dependent knockouts or mRNA degradation) is the next step to build a more accurate model bradyzoite export. Furthermore, an efficient differentiation model would increase the volume of bradyzoites that could be produced, facilitating methods like LOPIT that could add in bradyzoite effector identification.

Conditional systems of translocon components would also be helpful *in vivo* where a protein's function in tachyzoites needs to be isolated from the function in bradyzoites. This would allow *in vitro* studies to be paired with *in vivo* experimental evidence that will provide a better understanding of how protein export plays a role in the persistence of chronic stages in a more physiological setting. Some *in vivo* experimental studies that might assist in this endeavour could include looking for the presence of IST in the nuclei of chronically infected mice and measuring cyst burden over time in mice infected with conditionally controlled MYR1. Whether or not export occurs across the cyst wall will guide future research into either identifying bradyzoite effector proteins and their functions or towards other potential mechanism of persistence.

Appendix A -

1. Seizova, S. et al. *Toxoplasma gondii* bradyzoites induce transcriptional changes to host cells and prevent IFNγ-mediated cell death. bioRxiv, 669689, doi:10.1101/669689 (2019)

bioRxiv preprint doi: https://doi.org/10.1101/669689. The copyright holder for this preprint (which was not peer-reviewed) is the author/funder. It is made available under a CC-BY 4.0 International license.

Toxoplasma gondii bradyzoites induce transcriptional changes to host cells and prevent IFNγ-mediated cell death

Simona Seizova[1,2], Alexandra L Garnham[1,2], Michael J Coffey[1,2], Lachlan W Whitehead[1,2], Kelly L Rogers[1,2], Christopher J Tonkin[1,2]

[1]The Walter and Eliza Hall Institute of Medical Research, Parkville, Melbourne, Victoria, Australia

[2]Department of Medical Biology, The University of Melbourne, Melbourne, Victoria, Australia

Correspondence to:
Chris Tonkin
Division of Infection and Immunity,
The Walter and Eliza Hall Institute of Medical Research,
1G Royal Pde, Parkville, 3052,
Phone: +613 9345 2926,
tonkin@wehi.edu.au

bioRxiv preprint doi: https://doi.org/10.1101/669689. The copyright holder for this preprint (which was not peer-reviewed) is the author/funder. It is made available under a CC-BY 4.0 International license.

Summary

Toxoplasma gondii, the causative agent of toxoplasmosis, lies dormant for life and is a reservoir for disease reactivation, causing blindness, encephalitis and congenital birth defects. Acute-stage tachyzoites extensively manipulate their host cell by exporting a repertoire of proteins across the parasitophorous vacuolar membrane (PVM). This interferes with the hosts transcriptional program, allowing for persistence during immune attack. It is unknown how bradyzoites persist and what role host manipulation plays in latency. Here we show that bradyzoite-containing host cells have a unique transcriptional landscape when compared to tachyzoite infection. We demonstrate that many of these changes are dependent parasite protein export. Furthermore, we show that bradyzoite effector proteins protect host cell's from IFNγ-mediated cell death, thus highlighting the functional importance of host manipulation. Together, our work provides the first understanding of how *Toxoplasma* sets up latency to persist in its host.

Keywords: Toxoplasma gondii, bradyzoites, interferon gamma, chronic, Myc-regulation 1 (MYR1), cell death

bioRxiv preprint doi: https://doi.org/10.1101/669689. The copyright holder for this preprint (which was not peer-reviewed) is the author/funder. It is made available under a CC-BY 4.0 International license.

Introduction

Toxoplasma gondii is an obligate intracellular parasite that can infect many warm-blood animals causing toxoplasmosis. *Toxoplasma* infects one third of the human population and is contracted by eating undercooked meat that harbour the cysts forms or consumption of food contaminated with oocysts shed in cat faeces[1]. Acute toxoplasmosis results in a life-long chronic infection, whereby bradyzoites establish tissues cysts in the central nervous system and muscle tissue (Dubey et al., 1998). Chronic infection in healthy individuals is largely asymptomatic; however, severe complications can arise in immune-compromised individuals from the reactivation of encysted bradyzoites. Furthermore, reactivation of tissue cysts in retinal tissue is a major cause of blindness in some countries[2, 3]. In recent years, chronic infection has also been associated with a several psychiatric disorders, suggesting that latent *Toxoplasma* may subtly effect the brain in unappreciated ways[4]. There are currently no treatments to clear the bradyzoite reservoir to prevent reactivation and associated diseases, or an understanding of how latent forms manipulate the brain to survive and cause alterations to brain physiology.

Like many pathogens, *Toxoplasma's* ability to survive within its host can be attributed to its capacity to avoid immune detection[5], achieved, in part, by their ability to export parasite effector proteins that interfere with host cell programs. Acute stage tachyzoites are able to modulate the host using two distinct temporally separated pathways. The first wave of effectors is injected into the host cell during the invasion process, whilst the second occurs during intracellular growth[6]. During invasion, tachyzoites inject rhoptry (ROP) proteins into the host cell, which can traffic to the outer side of the parasitophorous vacuolar membrane (PVM)[7] and host cell nucleus[8]. Characterised ROP effectors act by interfering with the immune response by either altering host gene expression[9] by directly disrupt signalling pathways (e.g. STAT3 and STAT6)[8, 10, 11] or preventing destruction of the vacuole by interfering with function of key host proteins induced by IFNγ signalling (e.g. IRGs and GBPs)[7, 12, 13].

After invasion is completed, tachyzoites activate a second wave of protein export by secreting proteins from the parasite's dense granule (DG; DG proteins annotated by GRA) organelles. Some of these proteins sit at the host interface, often interacting with

bioRxiv preprint doi: https://doi.org/10.1101/669689. The copyright holder for this preprint (which was not peer-reviewed) is the author/funder. It is made available under a CC-BY 4.0 International license.

host proteins in order to modulate their activity[14-16]. For example, GRA15 localises to the host cytosolic face of PV/PVM, where it manipulates NFκB signalling, initiating IL-12 secretion and interferon gamma (IFNγ) production[14], whereas MAF-1 protrudes from the vacuolar membrane and sequesters the host mitochondria to surround the PVM[15]. Additionally, a subset of dense granule proteins are translocated across the PVM into the cytosol or nucleus of the host. These include cell cycle regulator GRA16[17], p38α MAPK activator GRA24[18], Inhibitor of STAT1 Transcription (IST)[19, 20], GRA28 (effects on host are unknown)[21], β-catenin signalling modulator GRA18 is associated with anti-inflammatory responses[22] and, more recently, HCE1/ TEEGR, which has been shown to affect the cyclin proteins[23] and host immune regulation by the suppression of NF-κB-regulated cytokines[24]. Interestingly, all the exported dense granule proteins are predicted to be disordered, which could be essential to the translocation process[25].

All known effector proteins traffic via *Toxoplasma's* secretory pathway[26] and are translocated across the PVM using parasite-derived machinery[25, 27, 28]. Upon trafficking through the parasite secretory pathway, some effectors are matured by a resident Golgi Aspartyl Protease, ASP5. ASP5 cleaves proteins at the TEXEL (*Toxoplasma Export Element*) 'RRL' motif, and is required for PVM translocation of all tested DG effector proteins[19, 22, 27, 29, 30]. This has similarities with the export process of proteins in *Plasmodium* spp.[31-34]; however, unlike *Plasmodium* spp., it appears that not all TEXEL-containing protein are exported[18, 27, 35] Recent evidence suggests a protein complex, consisting in part of MYR1, MYR2 and MYR3, is required for the translocation of proteins across the PVM[25, 28], but the exact mechanism it yet to be defined. Furthermore, MYR1-dependent transcriptional changes account for a large portion of the changes in host transcription induced by tachyzoite infection, consistently affecting immune response pathways[36]

Despite its extensive ability to shut down defence mechanisms, *Toxoplasma* is tightly controlled by the innate and adaptive immune responses. IFNγ is vital in controlling acute *Toxoplasma* infection and prevents reactivation of latent bradyzoites[37]. Previous studies have used murine cell lines to understand how IFNγ can induce tachyzoite clearance. It has been shown that IFNγ stimulated guanylate-

bioRxiv preprint doi: https://doi.org/10.1101/669689. The copyright holder for this preprint (which was not peer-reviewed) is the author/funder. It is made available under a CC-BY 4.0 International license.

binding proteins (GBPs)[38, 39] and immune related GTPases (IRGs)[40] are recruited to the tachyzoite PVM, but the downstream clearance mechanism that follows remains elusive[41]. *Toxoplasma* has developed mechanisms to prevent IFNγ activation of infected cells[9, 42, 43]. One mechanism is DG protein IST, which is exported via the MYR1 pathway where it inhibits IFNγ induced STAT1 signalling and transcription by modifying the GAS (Gamma Activated Sequence) sites through the recruitment of the Mi-2/NuRD chromatin remodelling complex[19, 20], thus blunting transcriptional changes when the host cell encounters this cytokine. It is not known if IFNγ has any capacity to affect bradyzoite clearance, even though it has consistently been shown to have an important role in immune defence *in vivo* [44-46].

In fact, most investigations into *Toxoplasma* host manipulation have been performed with acute stage tachyzoites, whereas bradyzoite-host cell interaction and manipulation has been largely neglected. Indeed, it is highly likely that host cell manipulation does differ between tachyzoites and bradyzoites to accommodate their different lifestyles and requirements. This must occur both when setting up a latent infection (ie. upon differentiation from tachyzoites to bradyzoites) as well as ongoing changes that must exist to allow for latent forms to persist over long time periods. Here we tackle the former to understand the differences between transcriptional changes between tachyzoites and seven-day-old bradyzoite forms. Our study shows that, at 7 days post differentiation, bradyzoite-containing host cells have a unique transcriptional landscape when compared to tachyzoite-infected cells. We demonstrate that many of these changes are imparted by both the presence of bradyzoite effector proteins, including IST, and likely the absence of tachyzoite effector proteins, which are not expressed/exported at this dormant stage. Furthermore, we show that bradyzoite effector proteins protect host cell's from IFNγ-mediated cell death, thus highlighting the functional importance of host manipulation. Together, our work provides the first understanding of how *Toxoplasma* sets up latency to persist in its host.

bioRxiv preprint doi: https://doi.org/10.1101/669689. The copyright holder for this preprint (which was not peer-reviewed) is the author/funder. It is made available under a CC-BY 4.0 International license.

Experimental Procedures

Host cell and parasite cultures and differentiation

All *Toxoplasma* parental parasite lines used in this study are of the 'type II' Prugniaud (Pru) background, either Pru-Toxofilin-Cre[47], or Pru Δ*hxgprt* Δ*ku80* (PruΔ*ku80*)[48]. These parasites, and all subsequently derived lines, were cultured in primary HFFs (American Type Culture Collection, ATCC) in Dulbecco's Modified Eagle medium (DME) supplemented with 1% v/v fetal calf serum (FCS) (Invitrogen, Australia) and 1% v/v Glutamax (Invitrogen) (D1). Prior to infection HFFs were grown to confluency in DME supplemented with 10% v/v cosmic calf serum (GE Healthcare, New Zealand) (D10). Cells were incubated at 37 °C with 10% CO_2.

Bradyzoite differentiation was achieved by inoculating tachyzoites onto confluent HFFs at an MOI of 0.1 (for IFA and FACS) or 0.2 (for RNA sequencing and western blots) and cultured in RPMI-HEPES supplemented with 5% v/v fetal calf serum (FCS) (Invitrogen, Australia) at pH 8.1-8.2 and allowed to differentiate at 37 °C with ambient CO_2 [49]. The media was changed every 2 days (to prevent acidification) for at least 7 days prior to assays.

DNA, plasmids and transfection

Candidate genes were targeted in all cases by the CRISPR/Cas9 system, which has been adapted for use in *Toxoplasma*[50, 51]. EuPaGDT (http://grna.ctegd.uga.edu)[52] was used for guide selection and CRISPR-Cas9 target plasmids were made by Q5 mutagenesis (NEB) using pU6_Universal_Cas9_mCherry[27, 51].

PruΔ*myr1* was created by transfection of *myr1* CRISPR guide and followed by serial dilution cloning and sequencing. PruΔ*myr1* knockouts were confirmed by the transient transfection of the GRA24-Myc3-expressing plasmid[27]. Candidate genes in PruΔ*ku80* were tagged with a DNA sequence encoding the HA epitope tag to allow for monitoring of protein expression during the generation of knockouts[53]. Briefly, CRISPR guide plasmids were co-transfected with either HA containing dimerised oligo primers, pLIC-3xHA-HXGPRT[35] or, for knockouts, pLoxP-DHFR-mCherry[54] amplicon and selected with 6-thiozanthine and mycohenolic acid, and pyrimethamine respectively (Fig.

bioRxiv preprint doi: https://doi.org/10.1101/669689. The copyright holder for this preprint (which was not peer-reviewed) is the author/funder. It is made available under a CC-BY 4.0 International license.

S5a)[55, 56]. 10 ug of Cas9 plasmid was combined with up to 80 ug of amplicon and resuspended in 20 uL P3 solution (Lonza), before being transfected by the Amaxa 4D Nucleofector (Lonza) using the code FI-115 (Human Unstimulated T-cells).

IFA and antibodies

Parasites were fixed in 4% v/v paraformaldehyde in PBS for 10 min; permeabilized in 0.1% v/v Triton X-100 in PBS and blocked in 3% w/v BSA (Sigma) in PBS for 1 hr. For samples with Propidium Iodide, cells were incubated for 10mins in a final concentration of 0.05mg/ml (Merck). Samples were washed three times prior to fixation and permeabilized as described above. The following antibodies were used in this study: αGAP45[57], αSAG1 DG52[58], αHA 3F10 (Roche), αSRS9[59], αCST1[59], Fluorescein-Dolichos Biflorus Agglutinin (DBA; Vector Labs), αIRF1 D5E4 (Cell Signalling Technologies) and αMyc 9E10 (Sigma). Primary antibodies were diluted in the bovine serum albumin (BSA)/PBS solution for 1 hr, washed, and then incubated with Alexa Fluor-conjugated secondary antibodies (Invitrogen) for 1 hr. 5 µg/ml DAPI was added in the penultimate wash for 10 min and samples were mounted onto microscope slides with Vectashield (Vector Labs). Parasites were imaged using either the Zeiss AxioLive Cell Observer, or the Zeiss LSM 880 for quantification. Quantification was automated using an Image J macro developed in house (available on request). Briefly, the mean grey value (MGV) of the protein of interested was measured both within the parasite vacuole and the host nucleus. MGV for non-specific background was subtracted for all analyses before the ratio of export (nucleusMGV/vacuoleMGV) or ratio of IRF1 expression (IRF1infectedMGV/ IRF1uninfectedMGV) was calculated.

Western Blots

Immunoblot samples were pelleted then lysed for 30 mins at 4 °C in 1% v/v Triton-X 100 (brand), 1 mM $MgCl_2$ in PBS (Gibco) supplemented with final 1 x cOmplete protease inhibitors (Sigma) and 0.2 % v/v Benzonase (Merck). Samples were then combined with an equal volume of non-reducing 2x Sample buffer and 15 µl loaded onto a gel. Proteins were transferred onto nitrocellulose then blocked in 5 % w/v milk in 0.05 % Tween 20-supplemented PBS (PBS-T). Primary and secondary antibodies were diluted in milk/PBS-T. Nitrocellulose membranes were imaged on an Odyssey Fc imager (LI-COR Biosciences) using IRDye 800CW goat α-rat, IRDye 800CW goat

bioRxiv preprint doi: https://doi.org/10.1101/669689. The copyright holder for this preprint (which was not peer-reviewed) is the author/funder. It is made available under a CC-BY 4.0 International license.

α-mouse and IRDye 680RD goat α-rabbit antibodies. Antibodies used in this study were: αGAP45[57], αSAG1 DG52[58], αHA 3F10 (Roche), αSRS9[59].

IFN-gamma Stimulation

Human IFNγ 285-IF (R&D systems) was added from a 50 µg/µl stock solution to a final experimental concentration of 50 ng/µl. Tachyzoites were inoculated for 20 hours before a 15 hour stimulation in D1 supplemented with 25mg/ml dextran sulfate (Sigma)[60]. Bradyzoites were stimulated for 15 hours after 7 days in differentiation media.

Compound 1 and BIPPO treatment

Compound 1 was added to a final concentration of 2µM an hour prior to the addition of IFNγ and left for indicated treatment period[55, 61]. BIPPO (5-Benzyl-3-isopropyl-1H-pyrazolo[4,3- d]pyrimidin-7(6H)-on) was added to a final concentration of 1µM and incubated for 7 mins before cells were harvested[62].

Live Imaging

Parasites where cultured and differentiated as described above in a 35mm polymer coverslip dish (Ibidi) for 7 days. 100ul of Propidium Iodide (1mg/ml; Merck) was added to 2mL of fresh differentiation media and either 50 ng/µl of human IFNγ 285-IF (R&D systems) was added or not. Between 15-25 cysts were tracked every 14 mins for 15 hours (overnight) on the Lecia SP8 confocal using resonant scanning.

Flow Cytometry

Bradyzoites were differentiated as described above and treated as indicated prior to being washed with PBS and dislodged with trypsin. A minimum of $5x10^3$ cells were analysed live using a BD FACSAria Fusion cell sorter (BD Biosciences). The proportion of $eGFP^+$ between unstimulated and stimulated cells was calculated. Compound 1 samples were fixed in 4% v/v paraformaldehyde/PBS before being analysed. Tachyzoite samples were treated with IFNγ as described above before being fixed in 4% v/v paraformaldehyde/PBS, permeabilized in 0.1% v/v Triton X-100/PBS and blocked in 3% w/v BSA/PBS for 1 hr. Samples were incubated in primary antibody, αGAP45[57], overnight at 4°C, washed, and then incubated with Alexa-594-

bioRxiv preprint doi: https://doi.org/10.1101/669689. The copyright holder for this preprint (which was not peer-reviewed) is the author/funder. It is made available under a CC-BY 4.0 International license.

conjugated secondary antibody (Invitrogen) for 1 hr. All fixed samples were run on a BD LSR WII.

Library Preparation and Transcriptome Sequencing

HFFs were passaged and grown in D10 media until they reached confluency. Following this, HFFs were transferred into D1 media (for tachyzoites; 24 hours) or differentiation media (for bradyzoites; 7 days) and left as uninfected (no parasites) or infected at a MOI of 0.2 with either Pru-Toxofilin-Cre (Pru (WT)) or Pru-Toxofilin-Cre∆*myr1* (Pru∆*myr1*) tachyzoites. Prior to RNA extraction, HFFs were washed with PBS, dislodged with trypsin, and sorted into infected ($mCherry^+$) and uninfected ($mCherry^-$) cells using the BD Influx (361) cell sorter (BD Biosciences). Total host and parasite RNA was extracted using the RNeasy kit (Qiagen). Three independent biological replicates of each condition were obtained.

An input of 100ng of total RNA was prepared and indexed separately for Illumina™ sequencing using the TruSeq RNA sample Prep Kit (Illumina) as per manufacturer's instruction. Each library was quantified using the Agilent Tapestation and the Qubit™ DNA BR assay kit for Qubit 3.0® Fluorometer (Life technologies). The indexed libraries were pooled and diluted to 1.5pM for paired end sequencing (2x 81 cycles) on a NextSeq 500 instrument using the v2 150 cycle High Output kit (Illumina) as per manufacturer's instructions (generating 80bp paired-ends). The base calling and quality scoring were determined using Real-Time Analysis on board software v2.4.6, while the FASTQ file generation and de-multiplexing utilised bcl2fastq conversion software v2.15.0.4.

Transcriptome analysis

The RNA sequencing reads were simultaneously aligned to the human and parasite genomes, builds hg38 and ME49 respectively, using the Rsubread aligner version 1.24.1 (tachyzoite and bradyzoite infection dataset) and version 1.27.4 (WT-∆*myr1* bradyzoite infection dataset)[63]. For this alignment a reference was first built that contained both human and parasite genomic sequences. In all instances greater than 89% of the reads mapped to this combined genome. The number of fragments overlapping each human Entrez gene and parasite gene were summarized using FeatureCounts[64] and NCBI RefSeq annotation. Differential expression analyses were

bioRxiv preprint doi: https://doi.org/10.1101/669689. The copyright holder for this preprint (which was not peer-reviewed) is the author/funder. It is made available under a CC-BY 4.0 International license.

then undertaken using the edgeR[65] and limma[66] software packages. The analysis of each data set was performed independently, details as follows.

Tachyzoite and bradyzoite infected samples.

For the analysis of the human count data, any gene which did not achieve a counts per million mapped reads (CPM) greater than 1 in at least 3 samples were deemed to be unexpressed and filtered from the data. Additionally, all genes without current annotation were also removed. The parasite count data (infected samples only) was filtered using edgeR's filterByExpr function with default settings. Compositional differences between libraries for both human and parasite data were normalised using the trimmed mean of log expression ratios (TMM) method[67]. All counts were then transformed to $\log_2$CPM. Differential expression between the experimental groups in both instances was assessed relative to a fold-change threshold of 1.1 using linear models and empirical Bayes moderated t-statistics with a trended prior variance[68, 69].

WT-Δ*myr1* bradyzoite infection data.

For this dataset, only the human count data was analysed. All genes which did not achieve a CPM greater than 0.7 in at least 3 samples was filtered from the data together with all genes with no current annotation. TMM normalisation was then applied to alleviate compositional differences between libraries. All counts were transformed to $\log_2$CPM. Differential expression between all groups was then evaluated relative to fold-change threshold of 1.1 using linear models and robust empirical bayes moderated t-statistics with a trended prior variance.

In both datasets the false discovery rate (FDR) was controlled below 5% using the Benjamini and Hochberg method. Analysis of the Hallmark gene sets from the Molecular Signatures Database was performed using limma's kegga function. To make the heatmaps of the top 100 differential expressed genes, the expression of each gene was summarized as $\log_2$ reads per kilobase per million mapped reads (RPKM) with a prior count of 2. For the heatmaps of the Hallmark gene sets, gene expression was summarised as average $\log_2$ RPKMs. The plots themselves were created using the pheatmap software package and limma's coolmap function.

Statistical Analysis

bioRxiv preprint doi: https://doi.org/10.1101/669689. The copyright holder for this preprint (which was not peer-reviewed) is the author/funder. It is made available under a CC-BY 4.0 International license.

Statistical analyses were conducted with Prism 7 (GraphPad). For groups of three or more, the test for significance was performed using a one-way analysis of variance (ANOVA) with the indicated post-test for correction. Groups of two were analysed using the unpaired Student's t test and significance was determine $p \leq 0.05$. The relationship between the intensity of IRF1 and the intensity of nuclear IST-HA was modelled with a non-linear curve (polynomial) using natural splines with 3 degrees of freedom using RStudio.

bioRxiv preprint doi: https://doi.org/10.1101/669689. The copyright holder for this preprint (which was not peer-reviewed) is the author/funder. It is made available under a CC-BY 4.0 International license.

Results

Bradyzoites distinctively alter the host transcriptome

We sought to identify if bradyzoite-containing host cells had a unique transcriptional profile and whether this profile differed from tachyzoite-containing host cells. We first determined the best time point to take bradyzoite samples after inducing differentiation. We found that approximately 7 days post alkaline-induction at an MOI of 0.2[70] was the longest period of time and density we could take the cultures without visibly compromising the health of bradyzoite-infected host cells. We then harvested corresponding tachyzoites at 24 hrs (under normal growth conditions) before infected cells were separated from uninfected 'bystander' cells by FACS based on the presence of mCherry (Fig. 1A and B). To determine bradyzoite purity, parasite samples were probed with anti-SRS9 antibodies and the number of positive vacuoles were counted by microscopy[59]. Quantitation demonstrated at least 90% of the population was positive for SRS9 under the differentiation conditions used (Fig. 1C (i); consistent with Fouts and Boothroyd 2007)[70]. RNA was then extracted and sequenced using Illumina chemistry on a NextSeq platform. We analysed the data for levels of BAG1[71] and SAG1[72], quintessential bradyzoite and tachyzoite markers, and this showed the expected enrichment and depletion in each sample respectively (Fig. 1C (ii)). We also interrogated other known stage-specific transcripts in our bradyzoites samples, which also showed the expected pattern of up- and down-regulation of genes associated with this stage (Fig. 1C (iii))[73, 74, 75]. This suggests that our preparations are highly enriched for bradyzoites, thus validating our experimental procedure.

Confident with the quality of our samples we then analysed the global effect of bradyzoites on the host transcriptome. This was done by comparing parasite-infected host cells with host cells from uninfected flasks. When bradyzoite-containing cells were compared with the uninfected HFF (after 1 week) we identified that 5804 host genes had significantly changed out of 13,793 expressed genes detected (~42%), suggesting the presences of bradyzoites alters host cell transcription. This is slightly less than the number of differentially expressed genes upon tachyzoite infection (7209, ~52%). To more quantitatively assess these changes we generated a heat map of the top 100 differentially expressed genes (DEG) for bradyzoite-infected cells

bioRxiv preprint doi: https://doi.org/10.1101/669689. The copyright holder for this preprint (which was not peer-reviewed) is the author/funder. It is made available under a CC-BY 4.0 International license.

verses uninfected host (1 week) and compared these to transcriptional profiles of the tachyzoite samples (Fig. 1D, see Table S1). From this set alone, similarities and differences in bradyzoite-containing and tachyzoite-containing host cells were evident. Some bradyzoite-induced changes were similar to those observed in tachyzoite infected host cells, whilst others appeared to be less pronounced or opposing, suggesting distinct transcriptional patterns between these two developmentally different stages (Fig. 1D, see Table S1, and Fig. 1E).

To further understand how host cells containing bradyzoites differ from tachyzoite infected cells, we wanted to determine how the changes in gene expression impacted host biological pathways. We first analysed all DEG of both bradyzoite- and tachyzoite-containing cells via over-representation analyses on the Molecular Signatures Database (MSigDB) Hallmark gene sets. (see Fig. S1A). Overall we could see a high perturbation across all biological pathways, suggesting re-wiring of the host transcriptome in both stages. However, some of these transcriptional changes may be secondary to parasite presence e.g. responses to endogenously released cytokines or non-specific disturbances. In order to tease out biological processes related to the presences of bradyzoites, we separated DEG into those that are specific to either developmental stage and those that are shared (Fig. 2A and see Fig. S1B respectively). Here we found that 3853 DEGs are shared between tachyzoite infected cells and bradyzoite infected cells (41%; 2161 up-reg., 1692 down-reg.), leaving 3356 tachyzoite specific DEGs (1488 up-reg., 1868 down-reg.), and 1951 DEGs specific to bradyzoite infection (1075 up-reg., 876 down-reg.) (Fig. 1E). We then performed over-representation analyses on each group. The majority of pathways in the Hallmark series showed a significant enrichment in the number of genes altered by both bradyzoites and tachyzoites (see Fig. S1B and Table S2). However, when the analyses for bradyzoite and tachyzoite specific DEG were compared, certain pathways are more enriched beyond the shared pathways (Fig. 2A, see Table S2). For an example, the *E2F*- and *Myc-targets* pathways were altered by tachyzoite infection, but no significant changes were seen in bradyzoite-containing cells over those that are shared (Fig. 2A and 2B, see Table S3). On the other hand, cells containing bradyzoites show a greater enrichment of DEGs in immune pathways, including the *IFN alpha*- and *IFN gamma*- response pathways, over what is already shared with tachyzoite infected cells (Fig. 2A and C, see Table S3). Overall, this

bioRxiv preprint doi: https://doi.org/10.1101/669689. The copyright holder for this preprint (which was not peer-reviewed) is the author/funder. It is made available under a CC-BY 4.0 International license.

implies that the presences of bradyzoites results in modulations of the host cell transcriptome, which is unique when compared to tachyzoites.

MYR1-dependent protein export plays a key role in host transcription modification in bradyzoites-containing host cells

Transcriptional changes can be imparted directly by pathogen effectors or as a result of downstream signalling after immune activation. We wished to specifically identify transcriptional changes induced by bradyzoites and to determine the overall effect of protein export on the host. To do this, we first determined whether MYR proteins, putative components of the PVM translocon and required for effector export, are present in bradyzoites[25, 28]. We assessed the relative expression of *myr1*, *2* and *3* in bradyzoites and tachyzoites from our RNAseq data (Fig. 3A). We found that *myr1, 2 and 3* are expressed in bradyzoites albeit at reduced levels (Fig. 3A). To functionally assess this complex in bradyzoites, we genetically tagged MYR1 with HA and could show that this protein is easily detectable and localises around the periphery of bradyzoites, similar to tachyzoites (see Fig. S2A), and is within the confines of the cyst wall, as marked by CST1 (Fig. 3B). We then knocked-out MYR1 in mCherry-expressing-Pru using CRISPR/Cas9 by targeting the first exon to ensure disruption. This resulted in a random 69bp insertion leading to three stop codons (see Fig. S2B) and was functionally confirmed by the inability of parasites to export transiently expressed GRA24-Myc (see Fig. S2C)[27]. Next, we assessed differentiation capacity and morphology of Δ*myr1* bradyzoites by inducing bradyzoite formation *in vitro*. There was no obvious differences in morphology indicated by an intact cyst wall, compact parasites expressing SRS9, and the presence of amylopectin granules (Fig. 3C (i)). The number of cyst-containing host cells was significantly less in Δ*myr1* samples (Fig. 3C (ii)) (see below for potential explanation of this); however, the size of the cysts was not altered by the absence of MYR1 (Fig. 3C (iii)). Overall, this suggests that cyst development is not critically reliant on MYR1, at least in tissue culture. This is in contrast to deletion of ASP5, which results in defects in cyst wall biosynthesis[30].

The ability to form healthy Δ*myr1* cysts then enabled us to determine what transcriptional changes are specifically caused by potential bradyzoite effectors in the early stages of chronic infection (7 days), compared to indirect effects such as immune

bioRxiv preprint doi: https://doi.org/10.1101/669689. The copyright holder for this preprint (which was not peer-reviewed) is the author/funder. It is made available under a CC-BY 4.0 International license.

signalling. Following the procedure laid out in Figure 1, uninfected, bradyzoite-containing and uninfected bystander cells were collected. When WT-infected cells were compared with Δ*myr1*-infected cells, we observed dramatic differences in gene expression in the absence of MYR1. A heat map generated of the top 100 DEG identified between WT-infected and Δ*myr1*-infected cells shows that the loss of MYR1 results in a transcriptional profile that closely mirrors the transcriptional changes seen in bystander cells (Fig. 3D, see Table S4). Reinforcing this concept, Δ*myr1*-infected cells were more closely related in the hierarchical heatmap with bystander cells rather than WT-infected cells (whereas bradyzoite-WT-containing and uninfected cells are excluded from this cluster). Moreover, bystander cells are vastly different to uninfected cells, implying that uninfected bystander cells are impacted by the presence of bradyzoites in culture. Together these data suggests that transcriptional changes observed in the presence of bradyzoites are actively modulated and that protein export via MYR1 plays a role in altering the transcriptional program during chronic infection.

We then assessed what impact MYR1-dependent protein export plays in altering host biological pathways of bradyzoite-containing cells. We first compared the DEG analysis of WT-infected vs uninfected with Δ*myr1*-infected vs uninfected and found the expression of 3068 host genes (~42%) was dependent on MYR1 (Fig. 3E). The remaining genes (4312) were altered in the same direction in both comparisons; however, a limitation with this type of analysis is that it does not distinguish between the degree of change. For an example, XIAP is significantly upregulated in both WT infected cells and Δ*myr1* infected cells when compared to uninfected host, but to different degrees which is seemingly dependent on MYR1 (see Fig. S3C). Nevertheless, it is evident that MYR1 has an impact on the host transcriptional response to the presence of bradyzoites.

We performed over-representation analyses using the Hallmark gene sets on each group and observed that bradyzoites depend on MYR1 in order to alter these pathways. In accordance with the first data set, it is evident that the presences of bradyzoites results in a multitude of changes in the host transcriptome, which impact all the Hallmark pathways. All the pathways examined contain a significant number of genes that change in expression following the loss of MYR1; however, the modulation

bioRxiv preprint doi: https://doi.org/10.1101/669689. The copyright holder for this preprint (which was not peer-reviewed) is the author/funder. It is made available under a CC-BY 4.0 International license.

of some pathways is less dependent on MYR1 than others. For example, pathways *TNF-alpha signalling via NFKB* and *Epithelial Mesenchymal Transition* are highly enriched in the MYR1 independent gene set (see Fig. S3B and Table S5), whereas the manipulation of other pathways such as *Adipogenesis* and *Glycolysis* are more dependent on MYR1 (see Fig. S3A and Table S5). Nevertheless, differentially expressed genes dependent on MYR1 are present in the majority of the pathways to a significant degree.

These data represents all the gene expression changes upon bradyzoite infection, including those that are present during tachyzoite infection. To determine what role protein export plays specifically in bradyzoite host manipulation, we examined the Hallmark pathways that saw a significant enrichment of DEGs specific to bradyzoites (Fig. 1E) and determined the proportion of the pathway that was dependent on MYR1. We found that all pathways were significantly altered by the absence of MYR1 (Fig. 4, see Table S5). This shows that a large proportion of bradyzoite induced host transcriptome manipulation requires the presence of MYR1, and further implicates the importance of active export of effector proteins in bradyzoites.

IST is expressed and exported in bradyzoites

Given our findings above, we hypothesised that bradyzoites have a repertoire of effector proteins that are exported into the host, some of which may also be exported in tachyzoites. After several unsuccessful attempts at determining, in an unbiased fashion, bradyzoite specific effector proteins, we focused on known effector proteins, GRA16, GRA24 and IST[17-20]. We first compared the proportion of reads between the infected bradyzoite and tachyzoites samples, from the data in our original RNAseq analysis. We saw a significant drop in the expression of GRA16 (Log_2 fold change -2.681) and GRA24 (Log_2 fold change -2.159) in bradyzoite samples, whereas IST appears to be slightly more expressed (Log_2 fold change +0.374) (Fig. 5A). To validate that mRNA expression changes were translatable to protein expression, we HA tagged these proteins in PruΔ*ku80* and probed for their expression via western blot. GRA16, GRA24 and IST were all expressed in tachyzoites, whereas bradyzoites (classified by SRS9 expression and SAG1 absence) expressed GRA16 and IST (Fig. 5B). This indicated that at least two known effectors are present in bradyzoites.

bioRxiv preprint doi: https://doi.org/10.1101/669689. The copyright holder for this preprint (which was not peer-reviewed) is the author/funder. It is made available under a CC-BY 4.0 International license.

In order to establish if GRA16 and IST are found in the host nucleus in bradyzoite-containing cells, we quantitated their expression and localisation by microscopy (Fig. 5C). GRA24 is consistently not expressed in 7-day-old bradyzoites; accordingly, the presence of GRA24 in the host nucleus is comparable to un-tagged WT controls (Fig. 5C and S4A). Interestingly, there appears to be some GRA16 present within the bradyzoite PV, but it is undetectable in the host nucleus (Fig. 5C and S4A). In contrast, we observed the export of IST into the host nucleus by bradyzoites (Fig. 5C and S4A) in equivalent amounts to tachyzoites (Fig. 5D). Therefore the increase of expression does not directly indicate an increase in the amount of protein exported into the host cell. To resolve whether the presence of IST in the host nucleus is residual protein from tachyzoite stages or is synthesised and exported in bradyzoites, we differentiated bradyzoites for a week, before extracting via needle passage and inoculating new host cells. Both 24 hours and one week after inoculation, we continue to see IST export in bradyzoites (Fig. 5E(i) and (ii)). This strongly suggests that IST is produced in and exported by bradyzoites.

Following the identification of IST as a bradyzoite exported effector protein, we sought to determine whether MYR1 was also responsible for IST export in bradyzoite stages and whether this effector was functional in controlling IFNγ-dependent responses. To investigate this, we created knockouts of both *myr1* and *ist* in the PruΔ*ku80* IST-HA line by coupling CRISPR/Cas9 with an homologous template containing the DHFR selectable marker followed by verification via western blot and microscopy, respectively (see Fig. S5A and B). Upon *myr1* disruption, the export of IST in bradyzoites is significantly inhibited (Fig. 6A(i) and (iiI)) and is comparable to background levels of cells infected with Δ*ist* and WT PruΔ*ku80* levels (Fig. 6A(i) and (ii)). Together, these data show that bradyzoites differentially express and actively export known effector protein, IST, via MYR1 during infection.

Bradyzoites supress the Interferon gamma pathway through MYR1-dependent IST export

In tachyzoite infection, IST has been shown to inhibit the host cell response to IFNγ stimulation[19, 20]. To determine if this holds true for bradyzoite infection, we

bioRxiv preprint doi: https://doi.org/10.1101/669689. The copyright holder for this preprint (which was not peer-reviewed) is the author/funder. It is made available under a CC-BY 4.0 International license.

stimulated bradyzoite-containing cells with IFNγ and probed for IRF1, a downstream protein which is upregulated upon IFNγ stimulation and pSTAT1-GAS binding[76]. As is the case in tachyzoites, IRF1 expression is significantly inhibited in cells containing WT cysts as compared to bystander cells (Fig. 6B(i) and (ii)). On the other hand Δ*myr1* and Δ*ist* parasites are unable to inhibit IRF1 expression and are comparable to uninfected bystander cells (Fig. 6B(i) and (ii)). The significant lower levels of IRF1 expression in Δ*myr1* as compared to Δ*ist* could be explained by an underestimation due to host cell death, as discussed below. Interestingly, we noticed that the ability for a cyst to inhibit IRF1 expression varied widely between host cells, from having no effect to complete inhibition (Fig. 6B(ii) and S5C(i); range 1.069-0.133). We checked whether this variation could be explained by the correlation between the amount of IST in the nucleus and the subsequent expression of IRF1. Our observations could be explained by fitting a hyperbolic curve (blue; see Fig. S5C(ii)) ($p = 1.042 \times 10^{-12}$). As the hyperbolic curve indicates, the level of IRF1 decreases as amount of IST-HA in the nucleus increases; however, there is a point at which high levels of IST cannot further decrease IRF1 expression. The variability in parasite induced IRF1 inhibition was also noted in the tachyzoite stages of the PruΔ*ku80* strain, with no significant difference in the degree of inhibition between the two stages (see Fig. S5D). Interestingly, RHΔ*ku80* strains showed a stronger ability to suppress IRF1 with less variability (see Fig. S5D).

To further analyse the role of MYR1 (and therefore indirectly IST) in the host cell's response to bradyzoite infection, we returned to our dataset derived from Δ*myr1* bradyzoites (Fig. 3 and 4). Despite the absence of IFNγ stimulation in our RNA sequencing data, we observed a difference in the expression of IRF1 between WT infected and Δ*myr1* infected cells. In the absence of *myr1*, the transcript levels of IRF1 is comparable to that of uninfected bystander cells, as previously shown by Olias et al., (2016) (Fig. 6C). This pattern is consistent in several genes previously identified via CHIP-Seq analysis as IFNγ-induced pSTAT1-GAS transcripts, including GBPs (see Fig. S6)[77]. A gene expression heat map of the Hallmark gene set: *Interferon gamma response* (Fig. 6D, see Table S6) illustrates that Δ*myr1* infected cells cluster more closely with uninfected bystander cells than with WT infected cells, suggesting that the majority of transcriptional changes that occur within the *Interferon gamma response* pathway are dependent on MYR1 in bradyzoites. Overall, this work indicates

bioRxiv preprint doi: https://doi.org/10.1101/669689. The copyright holder for this preprint (which was not peer-reviewed) is the author/funder. It is made available under a CC-BY 4.0 International license.

that bradyzoites are altering the host cells response to IFNγ stimulation via the export of IST through the MYR1 pathway.

Protein export is important for survival of bradyzoite-containing cells upon IFNγ challenge

During our experiments, we noticed that the number of intact Δ*myr1* cysts was greatly reduced after IFNγ treatment, suggesting this cytokine may cause death of infected host cells. To understand this in detail, we performed live imaging of WT, Δ*myr1* and Δ*ist* over 15 hours following IFNγ treatment (Fig. 7A (i); see examples movies S1 (WT), S2 (Δ*myr1*) and S3(Δ*ist*)) and monitored host cell death by Propidium Iodide (PI) uptake. Upon IFNγ treatment we observed that there was a significant decrease in the survival of infected host cells when compared to negative controls (Fig. 7A(ii)). Cells containing Δ*myr1* cysts had the largest decrease in cell survival (87%), whereas WT and Δ*ist* saw a drop of only 28% and 37%, respectively. This equated to no significant difference between IFNγ treated WT and Δ*ist* cyst numbers at the end of the 15 hour period, whilst loss of MYR1 was significantly different from both WT and Δ*ist*, suggesting a role for other unknown MYR1-dependent exported protein/s in blocking IFNγ-induced host cell death (Fig. 7A(ii)). Analysing the same samples using FACS and monitoring GFP expressed from the bradyzoite-specific LDH2 promoter also showed a similar outcome (Fig. 7B(i) & (ii))[75]. In stark contrast, IFNγ treatment of cells infected with Δ*myr1*-tachyzoites did not have a significant cell death phenotype, strongly supporting the notion that our bradyzoite-infected cells are functionally different from tachyzoite-infected cells (see Fig S7A). These data suggest that IST alone is not accountable for the large volume of cell loss seen by Δ*myr1*-bradyzoite-containing cells, implying other factors contribute to prevent cell death.

We then observed the morphology of cysts over the filming period and tracked how long it took for cell death to occur. Here we could see that cell death was accompanied by PI uptake, which was observed as staining of the host nucleus and debris. During cell death, host cells contracted before cell blebbing occurred (Fig. 7A(i), and SV1, SV2, SV3 in the supplementary material), a typical sign of programmed cell death. For Δ*myr1* infected cells, cell death occurred earlier, at

bioRxiv preprint doi: https://doi.org/10.1101/669689. The copyright holder for this preprint (which was not peer-reviewed) is the author/funder. It is made available under a CC-BY 4.0 International license.

approximately 9 hours post IFNγ stimulation, and was significantly earlier than those WT-infected cells that died (13.65 hours) (Fig. 7C). Interestingly, the time of death for Δ*ist*-infected cells was between Δ*myr1*- and WT-infected cells (at approximately 11 hours), further implying that IST alone cannot account for the host cell response to IFNγ during infection. We also observed that although some bradyzoites are released from the cyst, a majority remain within the dying cell and in some cases parasites are also observed taking up PI (Fig. 7A(i); white arrows).

We wanted to determine if this phenomenon was host cell driven or if it was caused by the egress of parasites from host cells. The latter would suggest bradyzoites can sense a change in the environment upon IFNγ treatment resulting in egress activation, whereas the former implies the host cell initiates cell death in the absence of parasite modulation. To disentangle these two pathways we used compound 1, which has been shown to prevent egress by inhibiting PKG[61, 78]. We hypothesised that if parasite egress was responsible for the cell death, then the addition of compound 1 would result in the recovery of the phenotype. Bradyzoite samples were incubated with compound 1 for an hour prior to the addition of IFNγ and 15 hours later checked for the levels of bradyzoite-containing host cells. Compound 1 was able to inhibit bradyzoite egress (see Fig. S7C); however, there was no significant difference in cell survival between cells treated with and without compound 1 upon IFNγ treatment (Fig. 7D). Furthermore, PI uptake was observed in bradyzoite-containing cells treated with compound 1 and IFNγ suggesting cell death was still occurring in the absence of parasite lysis (see Fig. S7B; white arrows indicate PI-positive parasites). These data indicate that one or more MYR1-dependent effectors protect bradyzoite-containing host cells from undergoing IFNγ-mediated cell death, demonstrating the importance of host cell modification during immune challenge, at least in early bradyzoite forms.

bioRxiv preprint doi: https://doi.org/10.1101/669689. The copyright holder for this preprint (which was not peer-reviewed) is the author/funder. It is made available under a CC-BY 4.0 International license.

Discussion

Chronic *Toxoplasma* infection can result in progressive blindness, act as a reservoir for disease reactivation, is a source of transmission in the food chain[1] and more recently has been associated with several psychiatric disorders[4]. The interactions between *Toxoplasma* and its host cell are likely critical to the parasites ability to persist for life and alter the physiology of the brain. Our study shows, for the first time, that bradyzoites actively manipulate their host cell, which is functionally relevant to persistence upon immune challenge. We have established that host cells containing 7 day-old bradyzoites have a transcriptional profile that is different from acute-stage tachyzoite forms. We show that MYR1 (a likely component of the export machinery) is expressed in bradyzoites and that its absence leads to an inability to induce transcriptional changes in bradyzoites containing cells. Furthermore, we show that IST, expressed from its native promoter, is exported by bradyzoites into host cells in a MYR1-dependent fashion, thus strongly suggesting that bradyzoites are capable of protein export into and modification of their host cell. Given that IST represses STAT1 signalling during IFNγ stimulation[20], our data suggests that IST could be important for bradyzoite persistence in muscle and CNS tissue, a line of enquiry future *in vivo* studies could focus on.

Our data is somewhat at odds with a recent study by Krishnamurthy and Saeij (2018)[79], which shows that the enforced expression of two tachyzoites effectors in bradyzoites (GRA16 and GRA24) does not result in export. Instead these effectors accumulated within the cyst wall, therefore suggesting that protein export might not occur at these stages. The authors suggest this could be because these proteins are not required during chronic stages, and either the cyst wall creates a physical barrier to protein export or that bradyzoites lack a translocation complex (i.e. MYR1). We, on the other hand, monitor all protein export from native promoters and we show here that GRA24 is not expressed, whilst GRA16 appears to be expressed but not exported. In the case of GRA16, the experiments reported here are in line with Krishnamurthy and Saeij's study and the reason for production of this protein without export is yet underdetermined. Interestingly, in bradyzoites we see an increase in IST expression as well as a similar level of export, when compared to tachyzoites. IST was detected in host cells that were both infected with tachyzoites and subsequently differentiated

bioRxiv preprint doi: https://doi.org/10.1101/669689. The copyright holder for this preprint (which was not peer-reviewed) is the author/funder. It is made available under a CC-BY 4.0 International license.

into bradyzoites for 7 days, and in samples where isolated bradyzoites were re-infected onto new host cells. Together with our transcriptional data showing increased expression of this effector we are confident that bradyzoites are capable of exporting IST into the host cell nucleus. What our data does not address is whether translocation across the cyst wall occurs. It remains possible from our study that all IST observed in the host cell nucleus of 7 day old bradyzoites is exported before the production of the cyst wall. For this to be true IST would have to be extremely stable and have a very low turnover rate; this would enable IST to stay at the levels we observed in tachyzoites after 7 days of differentiation. The other possibility is that there is something unique about IST that allows for its export across the cyst wall in bradyzoites but not GRA16 and GRA24. The only known trafficking element in exported proteins is the TEXEL motif[27, 29], but this cannot explain the export differences observed given this motif is present in both GRA16 and IST[17, 19]. If this was the case then IST should be able to be exported when expressed under the inducible promoter that Krishnamurthy and Saeij use[79].

We further show that the transcription factor IRF1, which is expressed in a IFNγ dependent fashion, is blocked by the presence of IST. This suggests that, at least at the early timepoints (7 days), bradyzoites do have the ability to block IFNγ signalling just as well as tachyzoites. However, our data also indicates that IST alone does not appear to protect bradyzoite-containing host cells from IFNγ-mediated cell death.

The lifestyles of tachyzoites and bradyzoites are vastly different and thus they have distinct requirements of their host cell. Tachyzoites are fast growing and aim to spread through tissue and around the body. Bradyzoites, on the other hand, are slow growing and aim to persist for the life of their host, seemingly avoiding immune detection. Here we show that bradyzoite-containing host cells have a distinct transcriptional landscape, which differs from acute stage tachyzoites perhaps reflecting specific survival requirements. Tachyzoites appear to impact the host's cell cycle and survival pathways (such as Myc targets, PI3K/AKT/mTOR signalling, p53, mitotic spindle, G2M checkpoints, E2F targets, DNA repair, apoptosis), and metabolism (unfolded protein response, mTORC1 signalling, glycolysis, heme metabolism). In contrast, bradyzoite infection appears to more heavily impact immune pathways (complement, IL6/JAK/STAT3 signalling, inflammatory response, interferon

bioRxiv preprint doi: https://doi.org/10.1101/669689. The copyright holder for this preprint (which was not peer-reviewed) is the author/funder. It is made available under a CC-BY 4.0 International license.

gamma response, interferon alpha response), in addition to some pathways that are also altered by tachyzoites. Others have used microarrays to analyse the expression of bradyzoite-containing host cells and concluded that, when the effects of the stress on the host were taken into account, there was little to no transcriptional differences to tachyzoite infected host cells[70]. However, in this study bradyzoite samples were taken 44 hours post infection as compared to our study that took samples after 7 days. The enhanced sensitivity of RNAseq vs microarray, or residual tachyzoite effects at this early time point may explain the differences in our findings[70].

It is interesting to note that known targets of GRA16[17] and the newly identified HCE1/TEEGR effector[23, 24] are differentially affected between bradyzoite and tachyzoite-infected cells. HCE1/TEEGR targets E2F-dependent genes (including cyclins and NF-kB targets) and these are clearly not affected in bradyzoite infected cells, thus we would predict that this effector is not expressed or exported in latent forms. GRA16 is known to be a key player in host cell cycle regulation by modulating p53 signalling, DNA replication, and DNA repair[17]. In our data, these pathways appear to be regulated to a lower degree in bradyzoites when compared to tachyzoites, in accordance with our observation that GRA16 is not exported in these stages[79]. Furthermore, tachyzoites are known to induce DNA replication but block the G2M transition preventing mitosis in host cells, thus increasing the ploidy of the host cells[80, 81]. These observations complement our data which shows the regulation of both the G2M and mitosis pathways in tachyzoites but not bradyzoites. The differential ability for *Toxoplasma* zoites to control cycle cell pathways could reflect the type of host cell the parasites reside in. Tachyzoites can replicate in rapidly dividing cells, whilst bradyzoites appear to develop predominantly reside in post-mitotic cells, such as neurons, myocytes and cardiomyocytes, and thus may have no need to modulate the cell cycle[82].

Our work also suggests that MYR1-dependent manipulation of host cells containing bradyzoites allows for their survival during immune attack. The loss of MYR1 causes the expression of many genes to revert to the transcriptomic pattern of uninfected bystander cells, suggesting that bradyzoites actively supress many genes which would normally become active in an inflammatory environment. A good example of this pattern from our data is the IFNγ pathway. The expression of IFNγ related genes

bioRxiv preprint doi: https://doi.org/10.1101/669689. The copyright holder for this preprint (which was not peer-reviewed) is the author/funder. It is made available under a CC-BY 4.0 International license.

globally decreases in bradyzoite-containing cells when compared to uninfected bystanders (presumably by exported IST). Upon the loss of MYR1, the manipulation of IFNγ-mediated gene expression is lost, and bradyzoite-containing cells mimic uninfected cells from the same culture.

A parasite's ability to interfere with the IFNγ-axis is important because it is the host's key mechanism in controlling *Toxoplasma* infection *in vivo*[46]. The mechanism by which IFNγ does this *in vivo* is not fully understood. Through *in vitro* analysis of human and murine cells, it's been suggested that IFNγ induced cell death or nutrient depletion might play a role during acute stages[41, 83]. Our data suggests that during chronic infection IFNγ may also play a role initiating cell death as an anti-microbial tool. We have shown that fibroblasts containing MYR1-knockout bradyzoites undergo cell death upon IFNγ stimulation, whereas this is not the case in tachyzoites stimulated with IFNγ post infection. This suggests that bradyzoite protein effectors may work to block IFNγ mediated death. Furthermore, we show cell death occurs in the absence of parasite egress. It is speculated that in tachyzoite-infected macrophages cell death may occur by pyroptosis initiated by the release of PAMPs following GBP-induced PVM breakdown in human cells[41], but the type of cell death observed in IFNγ-primed HFFs remains undetermined[84] and apoptosis could be equally likely. Although type II tachyzoites lacking IST are more susceptible to clearance after and before the addition of IFNγ in murine macrophages[19, 20], we have shown that cell death upon IFNγ of bradyzoite-containing HFF cells is not solely controlled by IST, suggesting that there could be other parasite effectors in play in chronic stages. Together, these data implies that bradyzoites actively modulate cell pathways that control cell death and that this phenomenon is different between latent and acute forms.

Uncovering the cell death pathway initiated upon IFNγ stimulation and how the parasite inhibits this is important in understanding how the chronic stages persistent. Further studies should look into whether IFNγ-induced cell death occurs in physiologically important bradyzoite reservoirs such as neurons[85]. Unfortunately, the current limitations in *in vitro* bradyzoite-neuron tissue culture models makes this a difficult course. Alternatively, *in vivo* studies could shed light on whether MYR1 is required for bradyzoite persistence, but will require a conditional system as MYR1

bioRxiv preprint doi: https://doi.org/10.1101/669689. The copyright holder for this preprint (which was not peer-reviewed) is the author/funder. It is made available under a CC-BY 4.0 International license.

knockouts are avirulent in acute stages *in vivo*[28]. Overall, this data suggests that targeting protein export with small drug molecules, or augmenting cell death pathways (as has been used in for clearance of other pathogens)[86] could be an effective way to treat chronic *Toxoplasma* infection.

bioRxiv preprint doi: https://doi.org/10.1101/669689. The copyright holder for this preprint (which was not peer-reviewed) is the author/funder. It is made available under a CC-BY 4.0 International license.

Acknowledgments

We'd like to acknowledge to Niall Geohegan and Cindy Evelyn from WEHI's Centre of Dynamic Imaging. We're thankful to Timothy McCulloch and Stacey Jeffrey for assistance with flow cytometry. We are grateful to Anita Koshy for providing us with the Pru-Cre parasite line used and John Boothroyd for providing us with the SRS9 and CST1 antibodies. We'd like to thank Stephen Wilcox from the Ian Potter Centre for Genomics and Personalised Medicine at WEHI for assistance with RNA sequencing and Roberto Bonelli for assistance with R modelling. SS is supported by the Australian Government as a recipient of the Research Training Program Stipend Scholarship. We're grateful for institutional support from the Victorian State Government Operational Infrastructure Support and the Australian Government NHMRC IRIISS. Finally, we would like to acknowledge The David Winston Turner Endowment Fund for supporting this work.

Author Contributions

SS designed and performed the experiments, analysed the data, and generated the figures. MJC preformed experiments. LWW produced code to analyse imaging data. ALG analysed RNA sequencing data and generated figures. CJT supervised all work. SS and CJT wrote the manuscript with input from all authors.

Data availability

The RNA sequencing dataset produced during this study have been deposited in Gene Expression Omnibus (GEO), accession code GSE125122, reviewer code: ahspsaaanfqpjyn. Further data is available from the corresponding author upon reasonable request.

Declaration of Interests

The authors declare no competing interests.

bioRxiv preprint doi: https://doi.org/10.1101/669689. The copyright holder for this preprint (which was not peer-reviewed) is the author/funder. It is made available under a CC-BY 4.0 International license.

References

1. Hill, D. & Dubey, J.P. Toxoplasma gondii: transmission, diagnosis and prevention. *Clinical microbiology and infection* **8**, 634-640 %@ 1198-1743X (2002).
2. Furtado, J.M., Smith, J.R., Belfort Jr, R., Gattey, D. & Winthrop, K.L. Toxoplasmosis: a global threat. *Journal of global infectious diseases* **3**, 281 (2011).
3. Grigg, M.E., Ganatra, J., Boothroyd, J.C. & Margolis, T.P. Unusual abundance of atypical strains associated with human ocular toxoplasmosis. *The Journal of infectious diseases* **184**, 633-639 %@ 1537-6613 (2001).
4. Tyebji, S., Seizova, S., Hannan, A.J. & Tonkin, C.J. Toxoplasmosis: A pathway to neuropsychiatric disorders. *Neuroscience & Biobehavioral Reviews %@ 0149-7634* (2018).
5. Melo, M.B., Jensen, K.D.C. & Saeij, J.P.J. Toxoplasma gondii effectors are master regulators of the inflammatory response. *Trends in parasitology* **27**, 487-495 %@ 1471-4922 (2011).
6. Hakimi, M.-A., Olias, P. & Sibley, L.D. Toxoplasma effectors targeting host signaling and transcription. *Clinical microbiology reviews* **30**, 615-645 %@ 0893-8512 (2017).
7. Etheridge, R.D. *et al.* The Toxoplasma pseudokinase ROP5 forms complexes with ROP18 and ROP17 kinases that synergize to control acute virulence in mice. *Cell host & microbe* **15**, 537-550 %@ 1931-3128 (2014).
8. Yamamoto, M. *et al.* A single polymorphic amino acid on Toxoplasma gondii kinase ROP16 determines the direct and strain-specific activation of Stat3. *Journal of Experimental Medicine* **206**, 2747-2760 %@ 0022-1007 (2009).
9. Saeij, J.P.J. *et al.* Toxoplasma co-opts host gene expression by injection of a polymorphic kinase homologue. *Nature* **445**, 324 %@ 1476-4687 (2007).
10. Butcher, B.A. *et al.* Toxoplasma gondii rhoptry kinase ROP16 activates STAT3 and STAT6 resulting in cytokine inhibition and arginase-1-dependent growth control. *PLoS pathogens* **7**, e1002236 %@ 1001553-1007374 (2011).
11. Ong, Y.-C., Reese, M.L. & Boothroyd, J.C. Toxoplasma rhoptry protein 16 (ROP16) subverts host function by direct tyrosine phosphorylation of STAT6. *Journal of Biological Chemistry* **285**, 28731-28740 %@ 20021-29258 (2010).
12. Niedelman, W. *et al.* The rhoptry proteins ROP18 and ROP5 mediate Toxoplasma gondii evasion of the murine, but not the human, interferon-gamma response. *PLoS pathogens* **8**, e1002784 %@ 1001553-1007374 (2012).
13. Reese, M.L., Shah, N. & Boothroyd, J.C. The Toxoplasma pseudokinase ROP5 is an allosteric inhibitor of the immunity-related GTPases. *Journal of Biological Chemistry*, jbc. M114. 567057 %@ 560021-569258 (2014).
14. Rosowski, E.E. *et al.* Strain-specific activation of the NF-κB pathway by GRA15, a novel Toxoplasma gondii dense granule protein. *Journal of Experimental Medicine* **208**, 195-212 %@ 0022-1007 (2011).
15. Pernas, L. *et al.* Toxoplasma effector MAF1 mediates recruitment of host mitochondria and impacts the host response. *PLoS biology* **12**, e1001845 %@ 1001545-1007885 (2014).
16. Ma, J.S. *et al.* Selective and strain-specific NFAT4 activation by the Toxoplasma gondii polymorphic dense granule protein GRA6. *Journal of Experimental Medicine* **211**, 2013-2032 %@ 0022-1007 (2014).
17. Bougdour, A. *et al.* Host cell subversion by Toxoplasma GRA16, an exported dense granule protein that targets the host cell nucleus and alters gene expression. *Cell host & microbe* **13**, 489-500 %@ 1931-3128 (2013).

bioRxiv preprint doi: https://doi.org/10.1101/669689. The copyright holder for this preprint (which was not peer-reviewed) is the author/funder. It is made available under a CC-BY 4.0 International license.

18. Braun, L. *et al.* A Toxoplasma dense granule protein, GRA24, modulates the early immune response to infection by promoting a direct and sustained host p38 MAPK activation. *Journal of Experimental Medicine* **210**, 2071-2086 %@ 0022-1007 (2013).
19. Gay, G. *et al.* Toxoplasma gondii TgIST co-opts host chromatin repressors dampening STAT1-dependent gene regulation and IFN-γ–mediated host defenses. *Journal of Experimental Medicine*, jem. 20160340 %@ 20160022-20161007 (2016).
20. Olias, P., Etheridge, R.D., Zhang, Y., Holtzman, M.J. & Sibley, L.D. Toxoplasma effector recruits the Mi-2/NuRD complex to repress STAT1 transcription and block IFN-γ-dependent gene expression. *Cell host & microbe* **20**, 72-82 %@ 1931-3128 (2016).
21. Nadipuram, S.M. *et al.* In vivo biotinylation of the Toxoplasma parasitophorous vacuole reveals novel dense granule proteins important for parasite growth and pathogenesis. *MBio* **7**, e00808-00816 %@ 02150-07511 (2016).
22. He, H. *et al.* Characterization of a Toxoplasma effector uncovers an alternative GSK3/β-catenin-regulatory pathway of inflammation. *eLife* **7**, e39887 %@ 32050-39084X (2018).
23. Panas, M.W., Naor, A., Cygan, A. & Boothroyd, J. Toxoplasma controls host cyclin E expression through the use of a novel MYR1-dependent effector protein, HCE1. *bioRxiv*, 573618 (2019).
24. Braun, L. *et al.* The Toxoplasma effector TEEGR promotes parasite persistence by modulating NF-κB signalling via EZH2. *Nature microbiology*, 1 %@ 2058-5276 (2019).
25. Marino, N.D. *et al.* Identification of a novel protein complex essential for effector translocation across the parasitophorous vacuole membrane of Toxoplasma gondii. *PLoS pathogens* **14**, e1006828 %@ 1001553-1007374 (2018).
26. Coffey, M.J., Jennison, C., Tonkin, C.J. & Boddey, J.A. Role of the ER and Golgi in protein export by Apicomplexa. *Current opinion in cell biology* **41**, 18-24 %@ 0955-0674 (2016).
27. Coffey, M.J. *et al.* An aspartyl protease defines a novel pathway for export of Toxoplasma proteins into the host cell. *Elife* **4**, e10809 %@ 12050-10084X (2015).
28. Franco, M. *et al.* A novel secreted protein, MYR1, is central to Toxoplasma's manipulation of host cells. *MBio* **7**, e02231-02215 %@ 02150-07511 (2016).
29. Curt-Varesano, A., Braun, L., Ranquet, C., Hakimi, M.A. & Bougdour, A. The aspartyl protease TgASP5 mediates the export of the Toxoplasma GRA16 and GRA24 effectors into host cells. *Cellular microbiology* **18**, 151-167 %@ 1462-5814 (2016).
30. Hammoudi, P.-M. *et al.* Fundamental roles of the Golgi-associated Toxoplasma aspartyl protease, ASP5, at the host-parasite interface. *PLoS pathogens* **11**, e1005211 %@ 1001553-1007374 (2015).
31. Hiller, N.L. *et al.* A host-targeting signal in virulence proteins reveals a secretome in malarial infection. *Science* **306**, 1934-1937 %@ 0036-8075 (2004).
32. Marti, M., Good, R.T., Rug, M., Knuepfer, E. & Cowman, A.F. Targeting malaria virulence and remodeling proteins to the host erythrocyte. *Science* **306**, 1930-1933 %@ 0036-8075 (2004).
33. Boddey, J.A. *et al.* An aspartyl protease directs malaria effector proteins to the host cell. *Nature* **463**, 627 %@ 1476-4687 (2010).
34. Russo, I. *et al.* Plasmepsin V licenses Plasmodium proteins for export into the host erythrocyte. *Nature* **463**, 632 %@ 1476-4687 (2010).
35. Coffey, M.J. *et al.* Aspartyl Protease 5 Matures Dense Granule Proteins That Reside at the Host-Parasite Interface in Toxoplasma gondii. *mBio* **9**, e01796-01718 %@ 02150-07511 (2018).

bioRxiv preprint doi: https://doi.org/10.1101/669689. The copyright holder for this preprint (which was not peer-reviewed) is the author/funder. It is made available under a CC-BY 4.0 International license.

36. Naor, A. *et al.* MYR1-Dependent Effectors Are the Major Drivers of a Host Cell's Early Response to Toxoplasma, Including Counteracting MYR1-Independent Effects. *mBio* **9**, e02401-02417 %@ 02150-07511 (2018).
37. Yarovinsky, F. Innate immunity to Toxoplasma gondii infection. *Nature Reviews Immunology* **14**, 109 %@ 1474-1741 (2014).
38. Winter, S.V. *et al.* Determinants of GBP recruitment to Toxoplasma gondii vacuoles and the parasitic factors that control it. *PloS one* **6**, e24434 %@ 21932-26203 (2011).
39. Yamamoto, M. *et al.* A cluster of interferon-γ-inducible p65 GTPases plays a critical role in host defense against Toxoplasma gondii. *Immunity* **37**, 302-313 %@ 1074-7613 (2012).
40. Martens, S. *et al.* Disruption of Toxoplasma gondii parasitophorous vacuoles by the mouse p47-resistance GTPases. *PLoS pathogens* **1**, e24 %@ 1553-7374 (2005).
41. Saeij, J.P. & Frickel, E.-M. Exposing Toxoplasma gondii hiding inside the vacuole: a role for GBPs, autophagy and host cell death. *Current opinion in microbiology* **40**, 72-80 %@ 1369-5274 (2017).
42. Rosowski, E.E. & Saeij, J.P.J. Toxoplasma gondii clonal strains all inhibit STAT1 transcriptional activity but polymorphic effectors differentially modulate IFNγ induced gene expression and STAT1 phosphorylation. *PLoS One* **7**, e51448 %@ 51932-56203 (2012).
43. Rosowski, E.E., Nguyen, Q.P., Camejo, A., Spooner, E. & Saeij, J.P.J. Toxoplasma gondii inhibits gamma interferon (IFN-γ)-and IFN-β-induced host cell STAT1 transcriptional activity by increasing the association of STAT1 with DNA. *Infection and immunity* **82**, 706-719 %@ 0019-9567 (2014).
44. Gazzinelli, R.T. *et al.* Parasite-induced IL-12 stimulates early IFN-gamma synthesis and resistance during acute infection with Toxoplasma gondii. *The Journal of Immunology* **153**, 2533-2543 %@ 0022-1767 (1994).
45. Scharton-Kersten, T.M. *et al.* In the absence of endogenous IFN-gamma, mice develop unimpaired IL-12 responses to Toxoplasma gondii while failing to control acute infection. *The Journal of Immunology* **157**, 4045-4054 %@ 0022-1767 (1996).
46. Suzuki, Y., Orellana, M.A., Schreiber, R.D. & Remington, J.S. Interferon-gamma: the major mediator of resistance against Toxoplasma gondii. *Science* **240**, 516-518 %@ 0036-8075 (1988).
47. Koshy, A.A. *et al.* Toxoplasma secreting Cre recombinase for analysis of host-parasite interactions. *Nature methods* **7**, 307 %@ 1548-7105 (2010).
48. Fox, B.A. *et al.* Type II Toxoplasma gondii KU80 knockout strains enable functional analysis of genes required for cyst development and latent infection. *Eukaryotic cell*, EC. 00297-00210 %@ 01535-09778 (2011).
49. Weiss, L.M. *et al.* A cell culture system for study of the development of Toxoplasma gondii bradyzoites. *Journal of Eukaryotic Microbiology* **42**, 150-157 %@ 1066-5234 (1995).
50. Shen, B., Brown, K.M., Lee, T.D. & Sibley, L.D. Efficient gene disruption in diverse strains of Toxoplasma gondii using CRISPR/CAS9. *MBio* **5**, e01114-01114 %@ 02150-07511 (2014).
51. Sidik, S.M., Hackett, C.G., Tran, F., Westwood, N.J. & Lourido, S. Efficient genome engineering of Toxoplasma gondii using CRISPR/Cas9. *PloS one* **9**, e100450 %@ 101932-106203 (2014).
52. Peng, D. & Tarleton, R. EuPaGDT: a web tool tailored to design CRISPR guide RNAs for eukaryotic pathogens. *Microbial genomics* **1** (2015).
53. Huynh, M.-H. & Carruthers, V.B. Tagging of endogenous genes in a Toxoplasma gondii strain lacking Ku80. *Eukaryotic cell* **8**, 530-539 %@ 1535-9778 (2009).

bioRxiv preprint doi: https://doi.org/10.1101/669689. The copyright holder for this preprint (which was not peer-reviewed) is the author/funder. It is made available under a CC-BY 4.0 International license.

54. Long, S., Wang, Q. & Sibley, L.D. Analysis of non-canonical calcium dependent protein kinases in Toxoplasma gondii by targeted gene deletion using CRISPR/Cas9. *Infection and immunity*, IAI. 01173-01115 %@ 00019-09567 (2016).
55. Donald, R.G. & Roos, D.S. Stable molecular transformation of Toxoplasma gondii: a selectable dihydrofolate reductase-thymidylate synthase marker based on drug-resistance mutations in malaria. *Proceedings of the National Academy of Sciences* **90**, 11703-11707 %@ 10027-18424 (1993).
56. Donald, R.G.K., Carter, D., Ullman, B. & Roos, D.S. Insertional tagging, cloning, and expression of the Toxoplasma gondii hypoxanthine-xanthine-guanine phosphoribosyltransferase gene Use as a selectable marker for stable transformation. *Journal of Biological Chemistry* **271**, 14010-14019 %@ 10021-19258 (1996).
57. Gaskins, E. *et al.* Identification of the membrane receptor of a class XIV myosin in Toxoplasma gondii. *The Journal of cell biology* **165**, 383-393 %@ 0021-9525 (2004).
58. Burg, J.L., Perelman, D., Kasper, L.H., Ware, P.L. & Boothroyd, J.C. Molecular analysis of the gene encoding the major surface antigen of Toxoplasma gondii. *The Journal of Immunology* **141**, 3584-3591 %@ 0022-1767 (1988).
59. Kim, S.-K., Karasov, A. & Boothroyd, J.C. Bradyzoite-specific surface antigen SRS9 plays a role in maintaining Toxoplasma gondii persistence in the brain and in host control of parasite replication in the intestine. *Infection and immunity* **75**, 1626-1634 %@ 0019-9567 (2007).
60. McCoy, J.M. *et al.* A forward genetic screen identifies a negative regulator of rapid Ca2+-dependent cell egress (MS1) in the intracellular parasite Toxoplasma gondii. *Journal of Biological Chemistry* **292**, 7662-7674 %@ 0021-9258 (2017).
61. Donald, R.G.K. *et al.* Toxoplasma gondii cyclic GMP-dependent kinase: chemotherapeutic targeting of an essential parasite protein kinase. *Eukaryotic cell* **1**, 317-328 %@ 1535-9778 (2002).
62. Howard, B.L. *et al.* Identification of potent phosphodiesterase inhibitors that demonstrate cyclic nucleotide-dependent functions in apicomplexan parasites. *ACS chemical biology* **10**, 1145-1154 %@ 1554-8929 (2015).
63. Liao, Y., Smyth, G.K. & Shi, W. The Subread aligner: fast, accurate and scalable read mapping by seed-and-vote. *Nucleic acids research* **41**, e108-e108 %@ 1362-4962 (2013).
64. Liao, Y., Smyth, G.K. & Shi, W. featureCounts: an efficient general purpose program for assigning sequence reads to genomic features. *Bioinformatics* **30**, 923-930 %@ 1460-2059 (2013).
65. Robinson, M.D., McCarthy, D.J. & Smyth, G.K. edgeR: a Bioconductor package for differential expression analysis of digital gene expression data. *Bioinformatics* **26**, 139-140 %@ 1367-4803 (2010).
66. Ritchie, M.E. *et al.* limma powers differential expression analyses for RNA-sequencing and microarray studies. *Nucleic acids research* **43**, e47-e47 %@ 0305-1048 (2015).
67. Robinson, M.D. & Oshlack, A. A scaling normalization method for differential expression analysis of RNA-seq data. *Genome biology* **11**, R25 %@ 1474-1760X (2010).
68. McCarthy, D.J. & Smyth, G.K. Testing significance relative to a fold-change threshold is a TREAT. *Bioinformatics* **25**, 765-771 %@ 1460-2059 (2009).
69. Phipson, B., Lee, S., Majewski, I.J., Alexander, W.S. & Smyth, G.K. Robust hyperparameter estimation protects against hypervariable genes and improves power to detect differential expression. *The annals of applied statistics* **10**, 946 (2016).

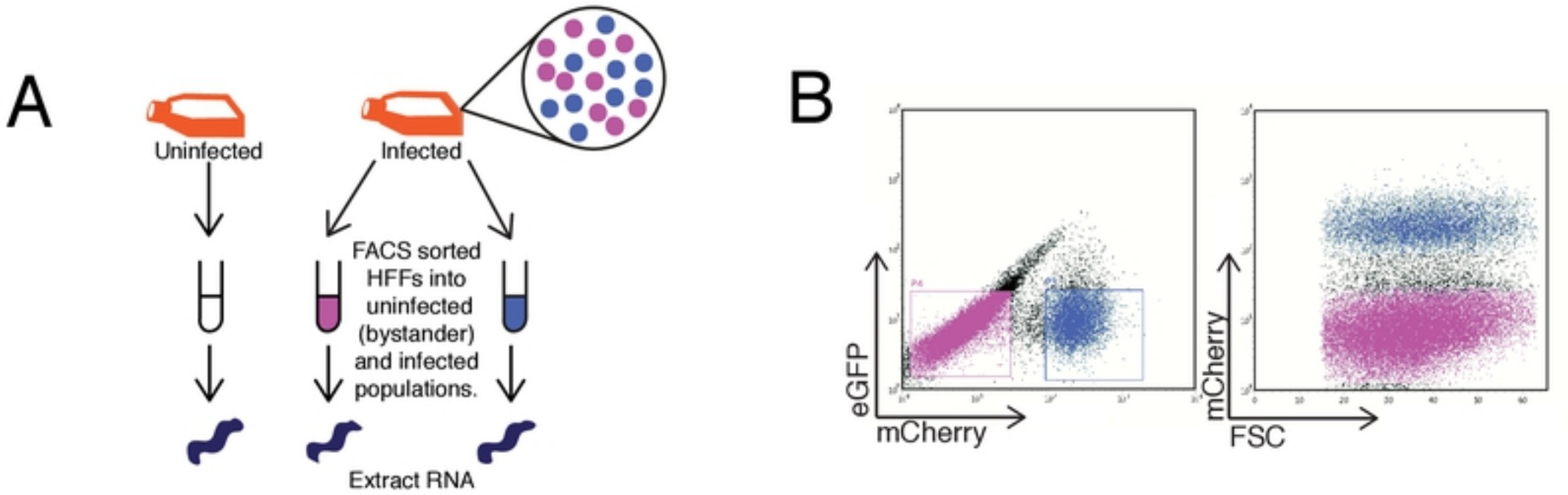
bioRxiv preprint doi: https://doi.org/10.1101/669689. The copyright holder for this preprint (which was not peer-reviewed) is the author/funder. It is made available under a CC-BY 4.0 International license.

70. Fouts, A.E. & Boothroyd, J.C. Infection with Toxoplasma gondii bradyzoites has a diminished impact on host transcript levels relative to tachyzoite infection. *Infection and immunity* **75**, 634-642 %@ 0019-9567 (2007).
71. Parmley, S.F., Weiss, L.M. & Yang, S. Cloning of a bradyzoite-specific gene of Toxoplasma gondii encoding a cytoplasmic antigen. *Molecular and biochemical parasitology* **73**, 253-257 %@ 0166-6851 (1995).
72. Manger, I.D., Hehl, A.B. & Boothroyd, J.C. The surface of Toxoplasma tachyzoites is dominated by a family of glycosylphosphatidylinositol-anchored antigens related to SAG1. *Infection and immunity* **66**, 2237-2244 %@ 0019-9567 (1998).
73. Lyons, R.E., McLeod, R. & Roberts, C.W. Toxoplasma gondii tachyzoite–bradyzoite interconversion. *Trends in parasitology* **18**, 198-201 %@ 1471-4922 (2002).
74. Dzierszinski, F., Mortuaire, M., Dendouga, N., Popescu, O. & Tomavo, S. Differential expression of two plant-like enolases with distinct enzymatic and antigenic properties during stage conversion of the protozoan parasite Toxoplasma gondii. *Journal of molecular biology* **309**, 1017-1027 %@ 0022-2836 (2001).
75. Yang, S. & Parmley, S.F. Toxoplasma gondii expresses two distinct lactate dehydrogenase homologous genes during its life cycle in intermediate hosts. *Gene* **184**, 1-12 %@ 0378-1119 (1997).
76. Sims, S.H. *et al.* A novel interferon-inducible domain: structural and functional analysis of the human interferon regulatory factor 1 gene promoter. *Molecular and Cellular Biology* **13**, 690-702 %@ 0270-7306 (1993).
77. Satoh, J.-i. & Tabunoki, H. A comprehensive profile of ChIP-Seq-based STAT1 target genes suggests the complexity of STAT1-mediated gene regulatory mechanisms. *Gene regulation and systems biology* **7**, GRSB. S11433 %@ 11177-16250 (2013).
78. Lourido, S., Tang, K. & Sibley, L.D. Distinct signalling pathways control Toxoplasma egress and host-cell invasion. *The EMBO journal* **31**, 4524-4534 %@ 0261-4189 (2012).
79. Krishnamurthy, S. & Saeij, J. Toxoplasma does not secrete the GRA16 and GRA24 effectors beyond the parasitophorous vacuole membrane of tissue cysts. *Frontiers in cellular and infection microbiology* **8**, 366 %@ 2235-2988 (2018).
80. Brunet, J. *et al.* Toxoplasma gondii exploits UHRF1 and induces host cell cycle arrest at G2 to enable its proliferation. *Cellular microbiology* **10**, 908-920 %@ 1462-5814 (2008).
81. Molestina, R.E., El-Guendy, N. & Sinai, A.P. Infection with Toxoplasma gondii results in dysregulation of the host cell cycle. *Cellular microbiology* **10**, 1153-1165 %@ 1462-5814 (2008).
82. Dubey, J.P., Lindsay, D.S. & Speer, C.A. Structures of Toxoplasma gondiitachyzoites, bradyzoites, and sporozoites and biology and development of tissue cysts. *Clinical microbiology reviews* **11**, 267-299 %@ 0893-8512 (1998).
83. Pfefferkorn, E.R. Interferon gamma blocks the growth of Toxoplasma gondii in human fibroblasts by inducing the host cells to degrade tryptophan. *Proceedings of the National Academy of Sciences* **81**, 908-912 %@ 0027-8424 (1984).
84. Niedelman, W., Sprokholt, J.K., Clough, B., Frickel, E.-M. & Saeij, J.P.J. Cell death of gamma interferon-stimulated human fibroblasts upon Toxoplasma gondii infection induces early parasite egress and limits parasite replication. *Infection and immunity* **81**, 4341-4349 %@ 0019-9567 (2013).
85. Cabral, C.M. *et al.* Neurons are the primary target cell for the brain-tropic intracellular parasite Toxoplasma gondii. *PLoS pathogens* **12**, e1005447 %@ 1001553-1007374 (2016).

bioRxiv preprint doi: https://doi.org/10.1101/669689. The copyright holder for this preprint (which was not peer-reviewed) is the author/funder. It is made available under a CC-BY 4.0 International license.

86. Jorgensen, I., Rayamajhi, M. & Miao, E.A. Programmed cell death as a defence against infection. *Nature reviews immunology* **17**, 151 %@ 1474-1741 (2017).

Figure 1



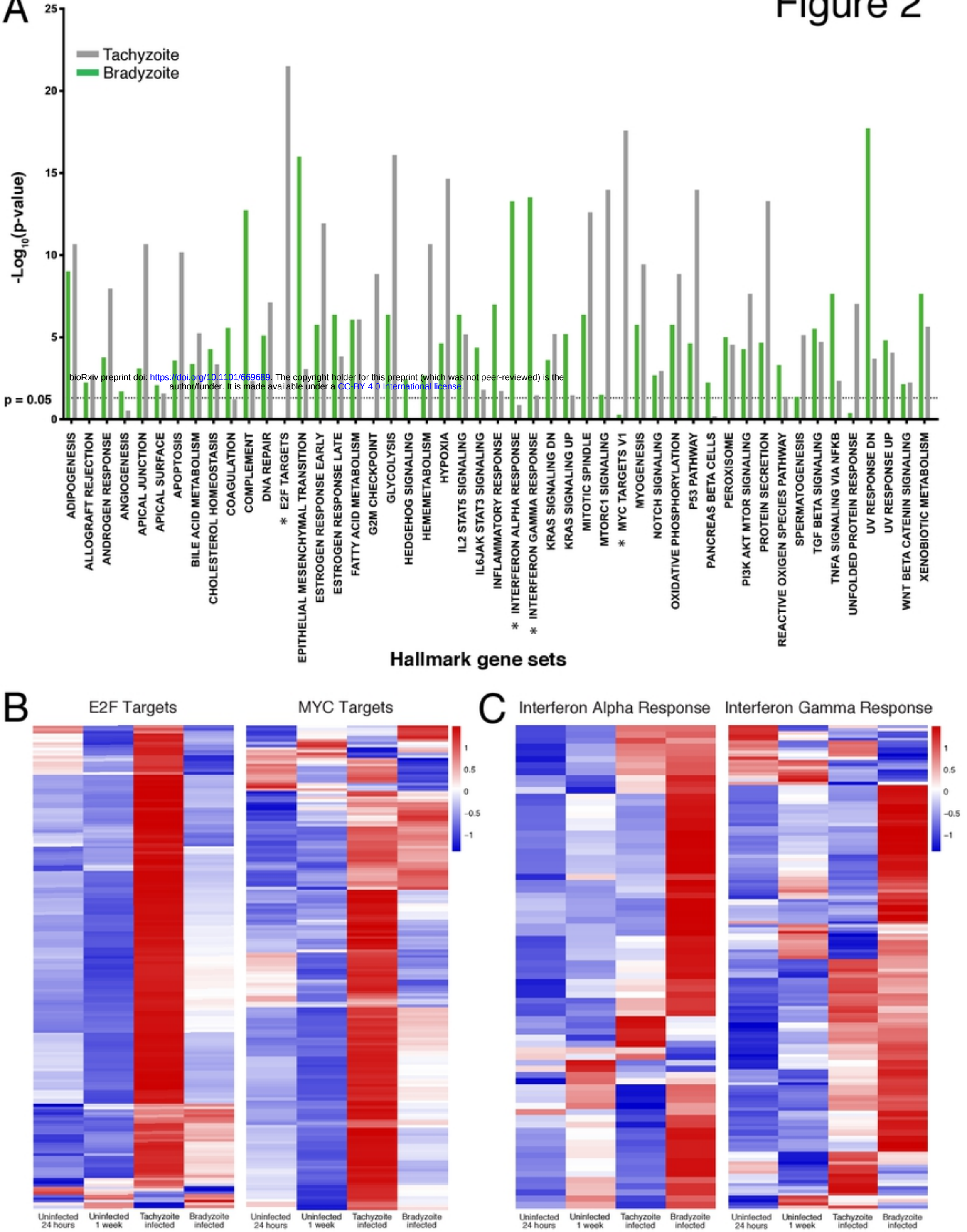
bioRxiv preprint doi: https://doi.org/10.1101/669689. The copyright holder for this preprint (which was not peer-reviewed) is the author/... made available under a CC-BY 4.0 International license.

bioRxiv preprint doi: https://doi.org/10.1101/669689. The copyright holder for this preprint (which was not peer-reviewed) is the author/funder. It is made available under a CC-BY 4.0 International license.

Figure Legends

Figure 1. Transcriptional landscape of bradyzoite-containing host cells is different to tachyzoite infection. (**A**) Schematic of sample collection for RNA sequencing indicating uninfected, infected, and bystander populations. (**B**, *left*) a representative FACS plot of the sorting gates used to sort infected and bystander host cells defined as $mCherry^{+}eGFP^{-}$ (blue) and $mCherry^{-}eGFP^{-}$ (magenta) respectively; discarded cells indicated in black. (**B**, *right*) a FACS plot showing a shift towards a $mCherry^{+}$ population after inoculation (**C**) (i) The proportion of $SRS9^{+}$ (grey) and $SRS9^{-}$ (black) parasites in bradyzoite samples. (ii) The levels of SAG1 and BAG1 reads (RPKM) in tachyzoite and bradyzoite samples. (iii) The negative Log_{10} of the P-value for known bradyzoite (grey) and tachyzoite (black) protein markers. (**D**) Inoculated HFF cells (human foreskin fibroblast) were FACS sorted into infected and uninfected samples before RNA extraction and sequencing (as per figure 1A) (n = 3 experiments, each with 3 replicates). Heat map of expression values for the top 100 differentially regulated genes between bradyzoite-infected (7 days *in vitro*) vs uninfected host cells (7 days). Top 100 DEGs expression are also shown for the tachyzoite-infected (24 hours) and uninfected host cells (24 hours) samples. Expression values are Log_2 reads per kilobase per million (RPKM), scaled to have mean 0 and standard deviation 1 for each gene. The plots show that bradyzoites change the transcriptional profile of the host cell, and this appears to be somewhat different to the profile of tachyzoite infected host cells. See Table S1 for gene names. (**E**) Venn diagram of tachyzoite vs uninfected DEGs (24 hours post infection; grey) and bradyzoite vs uninfected DEGs (7 days post infection; green); the number of up-regulated genes are identified in red and down-regulated genes in blue.

bioRxiv preprint doi: https://doi.org/10.1101/669689. The copyright holder for this preprint (which was not peer-reviewed) is the author/funder. It is made available under a CC-BY 4.0 International license.



bioRxiv preprint doi: https://doi.org/10.1101/669689. The copyright holder for this preprint (which was not peer-reviewed) is the author/funder. It is made available under a CC-BY 4.0 International license.

Figure 2. Tachyzoites and Bradyzoites modulate different host pathways. (**A**) Tachyzoites (grey) and bradyzoite (green) over-representation analysis results for each Hallmark gene set displayed as the negative Log_{10} of the P-value, dotted line p = 0.05. Stars indicate pathways with largely different profiles between tachyzoite and bradyzoites, which are shown in Figure 2B and C. (**B**) Pathways enriched during tachyzoite infection. Heat map of expression values for the genes that make up the *E2F target* and *MYC target* pathways. Expression values are Log_2 RPKM, scaled to have mean 0 and standard deviation 1 for each gene. The plots show that tachyzoites alter the transcriptional profile of pathways *E2F target* and *MYC target* more so than bradyzoites. (**C**) Pathways enriched during bradyzoites infection. Heat map of expression values for the genes that make up the *Interferon Alpha Response* and *Interferon Gamma Response* pathways. Expression values are Log_2 RPKM, scaled to have mean 0 and standard deviation 1 for each gene. The plots show that bradyzoite infections alters the transcriptional profile of pathways these two pathways more than bradyzoites. See also Figure S1, and Table S2 and Table S3 for gene lists.

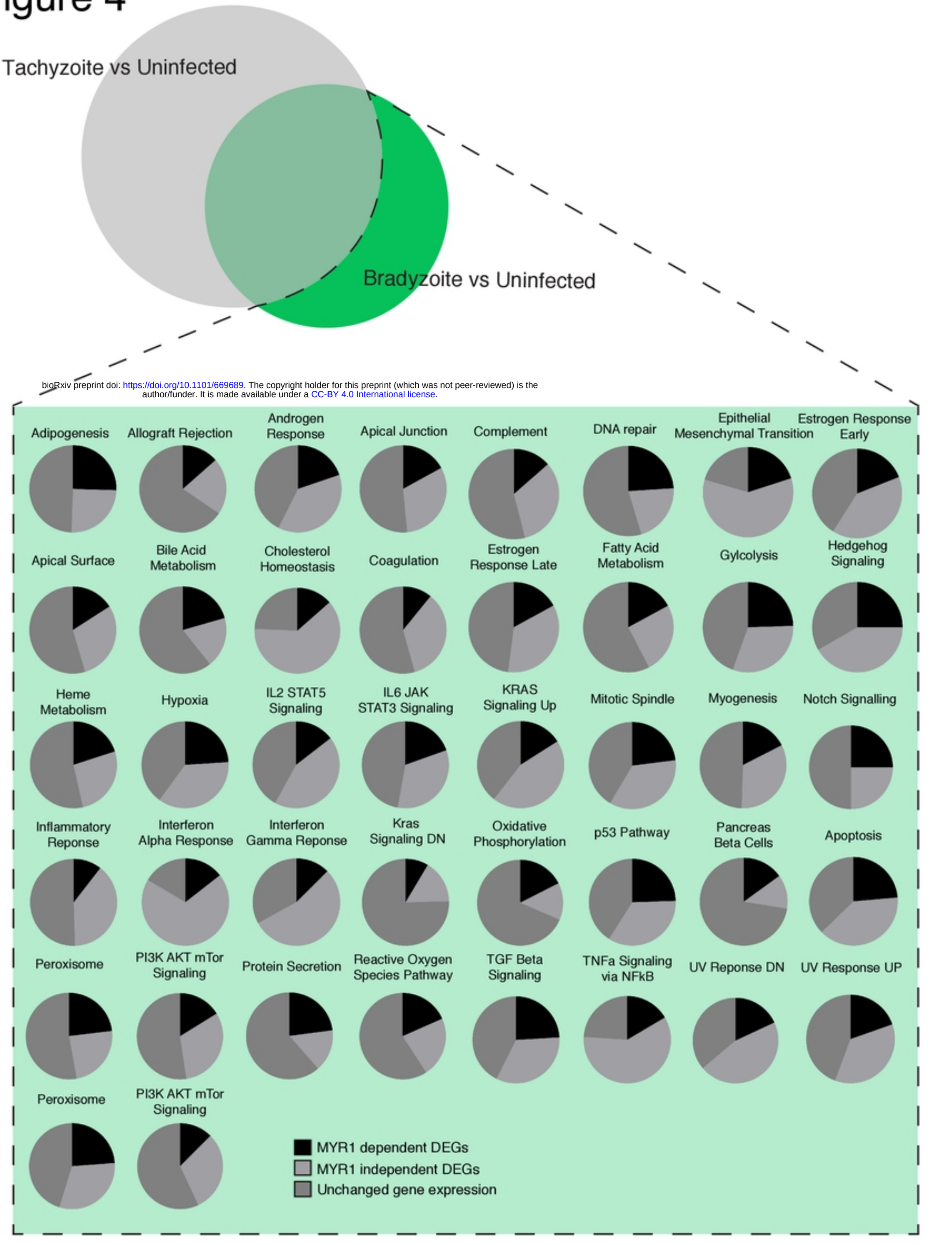
Figure 3

bioRxiv preprint https://doi.org/10.1101/669689. The copyright holder for this preprint (which was not peer-reviewed) is the author/funder. It is made available under a CC-BY 4.0 International license.

bioRxiv preprint doi: https://doi.org/10.1101/669689. The copyright holder for this preprint (which was not peer-reviewed) is the author/funder. It is made available under a CC-BY 4.0 International license.

Figure 3. MYR1 plays a role regulating host cell transcriptional changes in bradyzoites containing cells. (**A**) Differences in the expressional profile (Log_2CPM) of MYR1, MYR2, and MYR3 between tachyzoites (24 hours) and bradyzoites (7 days *in vitro*). Expression drops during bradyzoite stages for all proteins. (**B**) PruΔ*ku80* and PruΔ*ku80* MYR1-HA parasites were induced under alkaline conditions for 7 days before fixation. MYR1-HA (αHA; white) in bradyzoites (pLDH2-eGFP; green) is localised to the PV space and co-localises to cyst wall marker CST1 (αCST1; magenta). Brightness and contrast was edited on single colour channels prior to merging. (**C**) (i) WT and Δ*myr1* parasites were fixed after 7 days of differentiation under alkaline conditions. Both WT and Δ*myr1* were able to form intact cysts (DBA; green) containing health bradyzoites (αSRS9; magenta) and showed the presence of amylopectin granules (black arrows). Scale bar = 10μM; MYR, Myc Regulationr; PV, parasitophorous vacuole; DAPI, 4',6-diamidino-2-phenylindole; DBA, fluorescein conjugated Dolichos biflorus agglutinin. Brightness and contrast was edited on single colour channels prior to merging. (ii) The number of bradyzoite containing cells after 7 days of differentiation between WT (Pru) and Δ*myr1* was analysed by FACS (mean ± SD, n = 3 experiments, unpaired, two-sided Student's t-test with Welch's correction; **p=0.0058). (iii). The size of PruΔ*ku80* Δ*myr1* cysts were compared to WT by quantification of from immuno-fluorescence images (mean ± SD, n = 3 experiments, each experiment analysed on average between 20-40 bradyzoite cysts, unpaired, two-sided Student's t-test with Mann-Whitney correction; p=0.156) (**D**) WT (Pru) and Δ*myr1* inoculated human foreskin fibroblast (HFF) cells were FACS sorted into infected and uninfected samples before RNA extraction and sequencing (as per Fig. 1A). Heat map of log_2RPKM expression for the top 100 differentially regulated genes between WT bradyzoite infected and Δ*myr1* bradyzoite infected cells. Expression has been scaled to have mean 0 and standard deviation 1 for each gene. In the absence of MYR1, bradyzoite specific host expression appears to somewhat mimic the bystander cell population (from both WT and Δ*myr1*). See also Figure S2 and Table S4 for gene list. (**E**) Venn diagram of bradyzoite WT infected vs uninfected DEGs (grey) and bradyzoite Δ*myr1* infected vs uninfected DEGs (green); the number of up-regulated genes are identified in red and down-regulated genes in blue. Dotted lines indicated shared DEGs deemed as independent of MYR1.

Figure 4



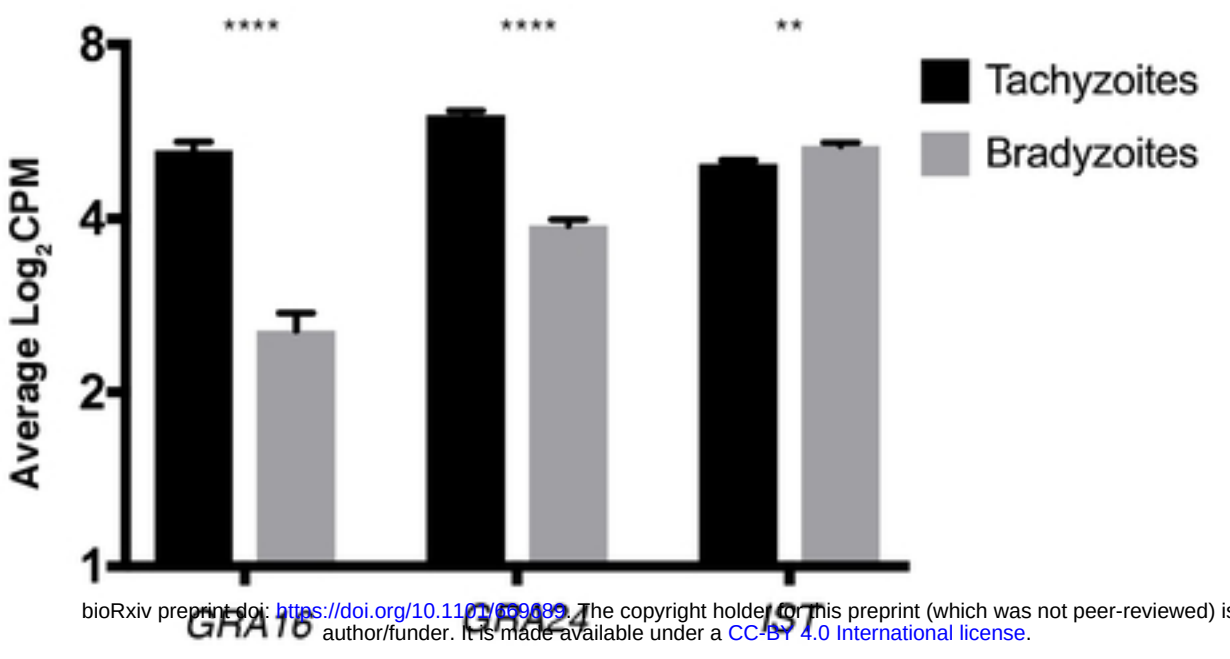
bioRxiv preprint doi: https://doi.org/10.1101/669689. The copyright holder for this preprint (which was not peer-reviewed) is the author/funder. It is made available under a CC-BY 4.0 International license.

Figure 4

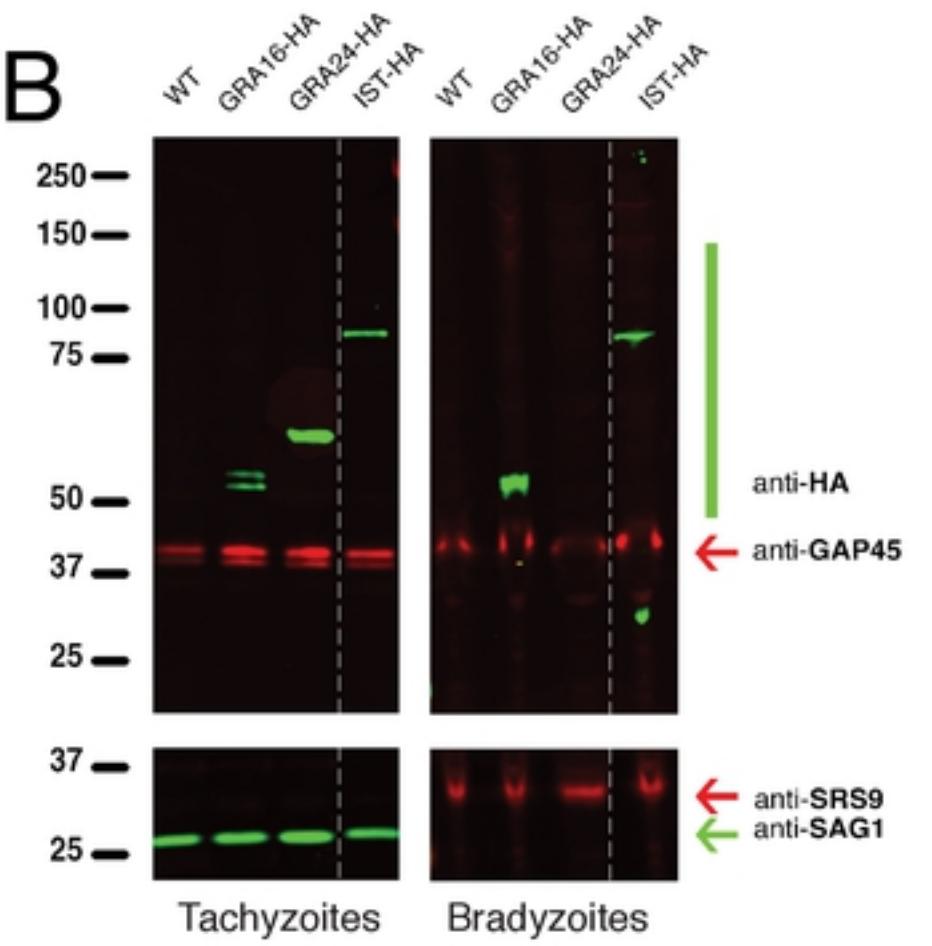
bioRxiv preprint doi: https://doi.org/10.1101/669689. The copyright holder for this preprint (which was not peer-reviewed) is the author/funder. It is made available under a CC-BY 4.0 International license.

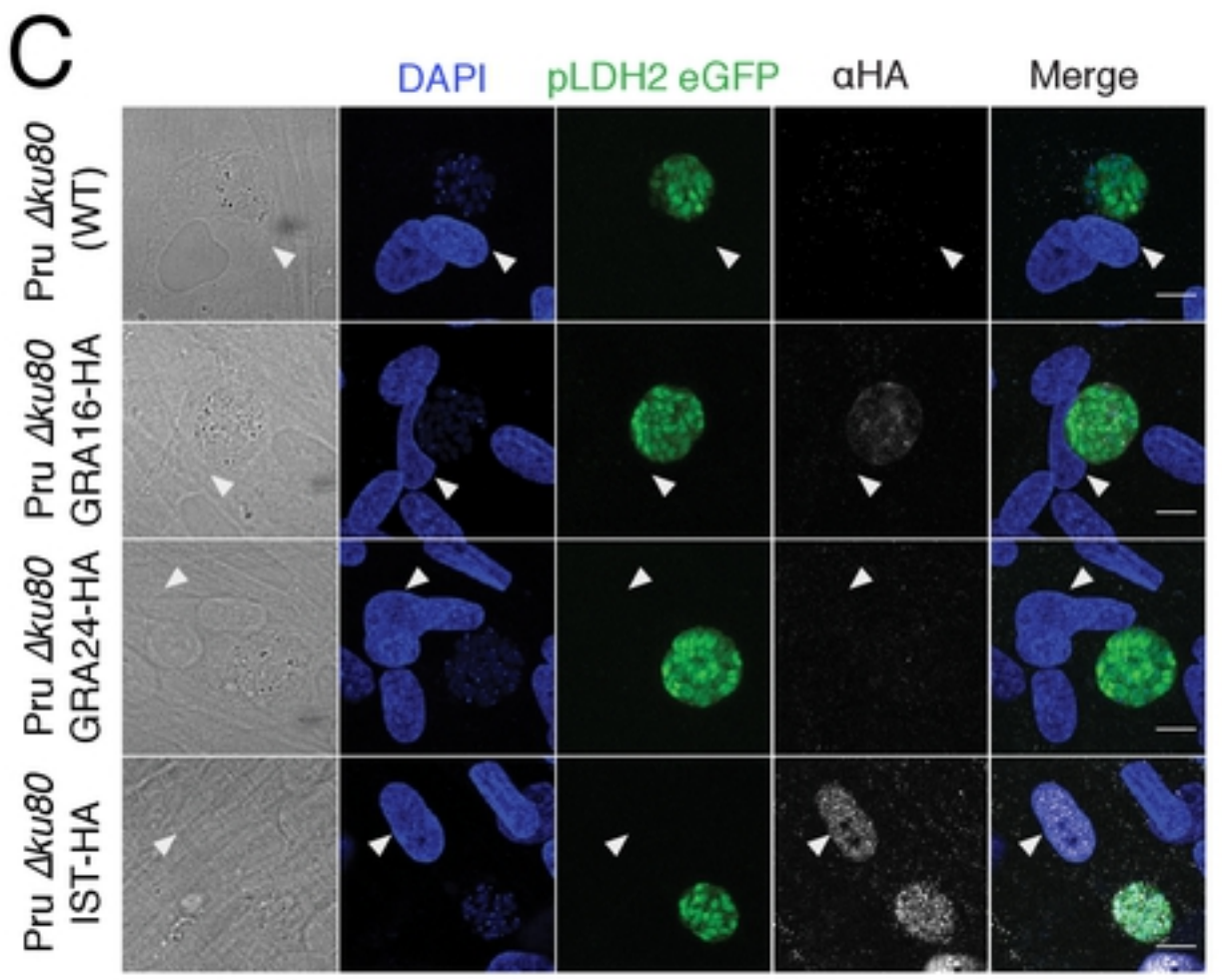
Figure 4. Proportion of bradyzoite specific pathways changes are dependent on MYR1. Bradyzoite specific DEGs shown in Fig. 2 was used for GSEA Hallmark gene set pathway analysis. The proportion of DEGs that were dependent on MYR1 (as determined by Fig. 4B) were then shown in those pathways that were significantly altered in bradyzoites (from Fig. 2B). Black, MYR1 dependent DEGs; Light grey, MYR1 independent DEGs; Dark grey, unchanged DEGs. See also Figure S3 and Table S5 for gene list.

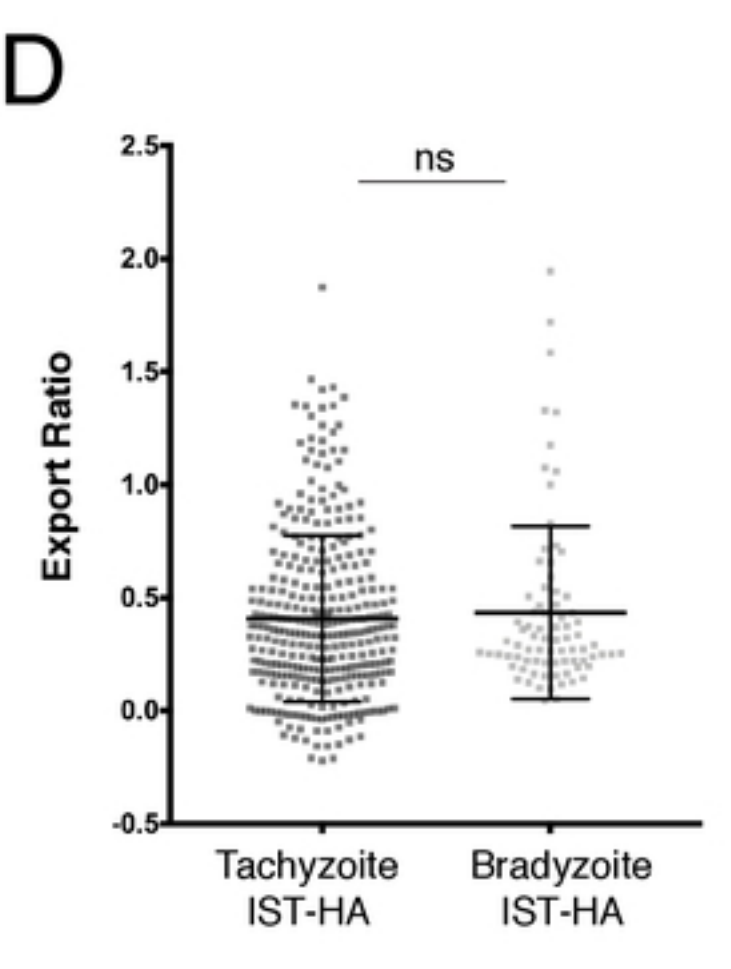
Figure 5



bioRxiv preprint doi: https://doi.org/10.1101/659698. The copyright holder for this preprint (which was not peer-reviewed) is the author/funder. It is made available under a CC-BY 4.0 International license.







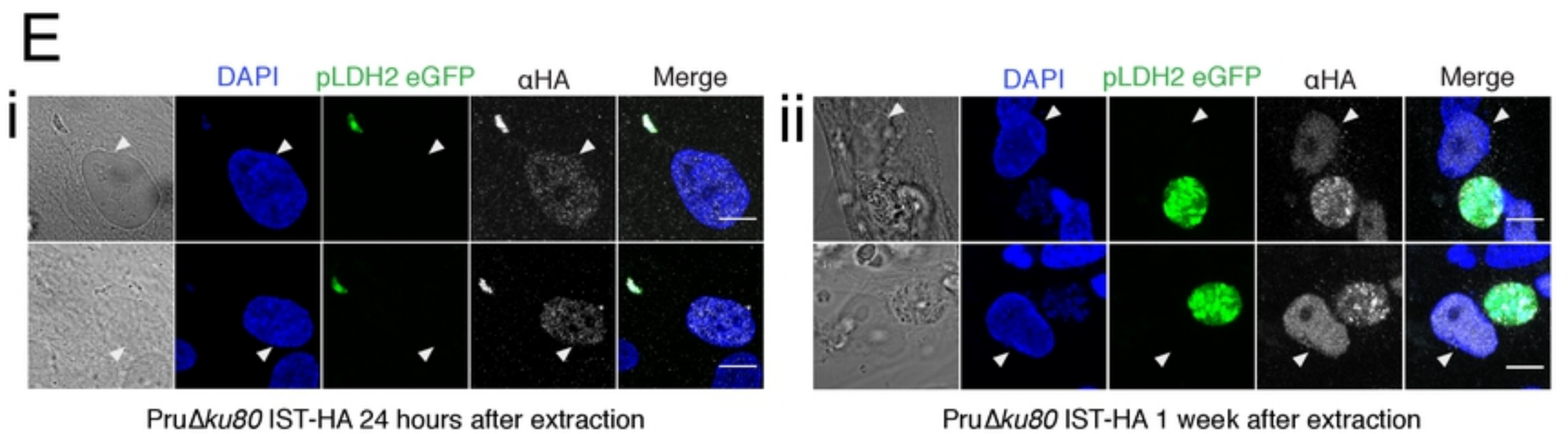
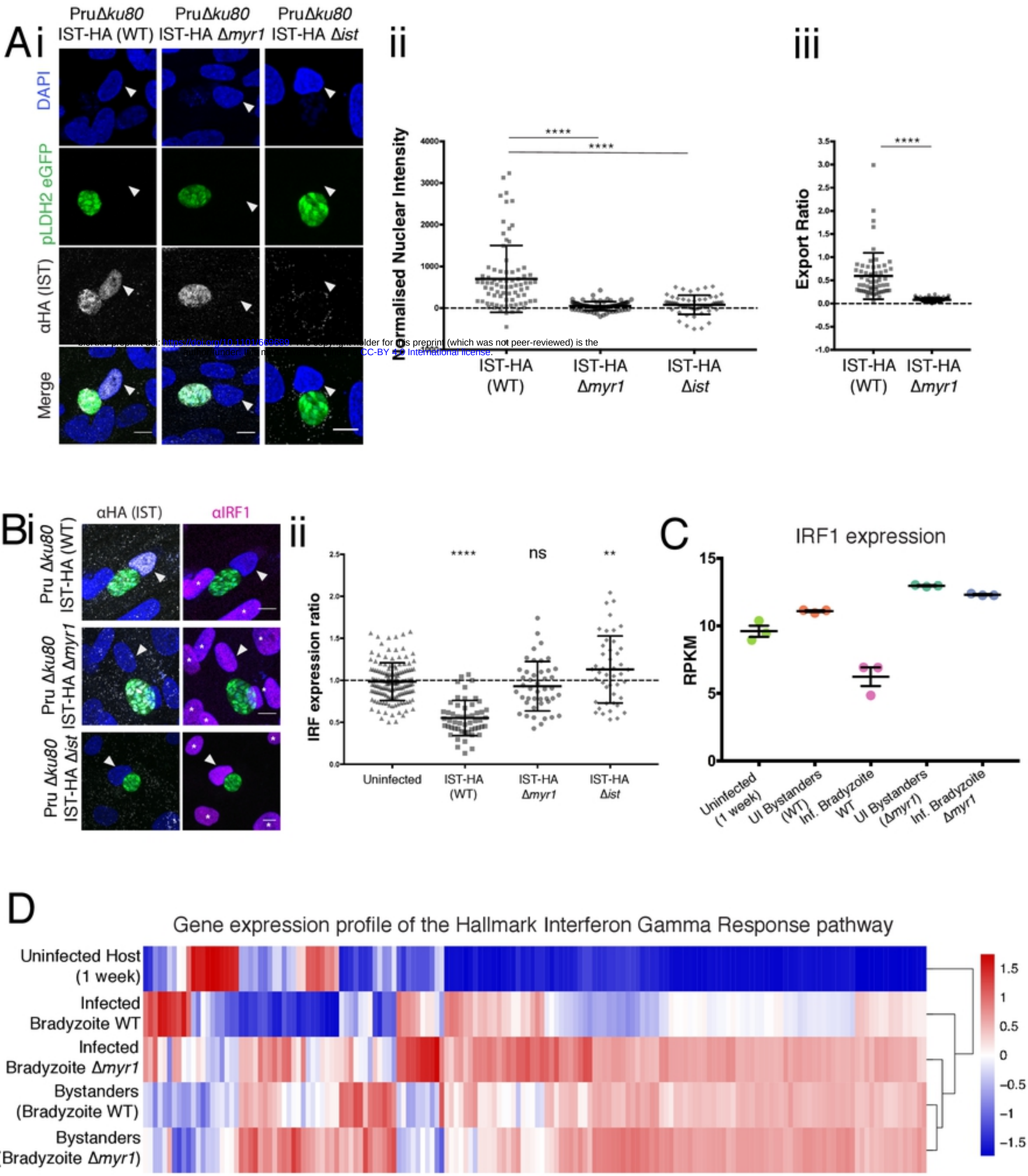


Figure 5

bioRxiv preprint doi: https://doi.org/10.1101/669689. The copyright holder for this preprint (which was not peer-reviewed) is the author/funder. It is made available under a CC-BY 4.0 International license.

Figure 5. Bradyzoites produce and export IST. (**A**) Differences in the expressional profile (Log_2CPM) of *GRA16*, *GRA24*, and *IST* between tachyzoites (24 hours) and bradyzoites (7 days *in vitro*). *GRA16* and *GRA24* reads drop during bradyzoite stages, whereas *IST* levels slightly increase (n = 3 experiments, each with 3 replicates; ****p<0.0001) (**B**) Western blot indicates GRA16-HA, GRA24-HA and IST-HA (PruΔ*ku80* background) are expressed in tachyzoites (lysed), whereas only GRA16-HA and IST-HA are expressed in bradyzoites (7 days in vitro). αGAP45 is used as a loading control, αSAG1 and αSRS9 are used as tachyzoite and bradyzoite controls respectively. (**C**) PruΔ*ku80* WT, GRA16-HA, GRA24-HA and IST-HA parasites were differentiated under alkaline conditions for 7 days before fixation. GRA24-HA (αHA; white) was not produced by bradyzoites (pLDH2-eGFP; green) or exported into the host nucleus. In contrast, bradyzoites were able to produce GRA16-HA and IST-HA; however, only IST-HA was exported into the host nucleus. White arrows indicate location of host nucleus (DAPI; blue). (**D**) No change in the ratio (nuclear intensity/vacuolar intensity) of IST export between tachyzoites and bradyzoites from immuno-fluorescence imaging (Figure 6c) (mean ± SD, n = 3 experiments, each experiment analysed on average between 20-40 bradyzoite cysts and 60-200 tachyzoite vacuoles; unpaired, two-sided Student's t-test; ****p<0.0001). (**E**) PruΔ*ku80*IST-HA parasites were differentiated under alkaline conditions for 7 days before extracted and reinoculated. Samples were either fixed 24hours (i) or 1 week post infection (ii). IST is consistently exported during bradyzoites infection. Scale bar = 10μM. Brightness and contrast was edited on single colour channels prior to merging. Scale bar = 10μM; GRA, dense granule; IST, inhibitor of STAT1 transcriptional activity; PV, parasitophorous vacuole; DAPI, 4',6-diamidino-2-phenylindole. Brightness and contrast was edited on single colour channels prior to merging. See also Figure S4.

Figure 6

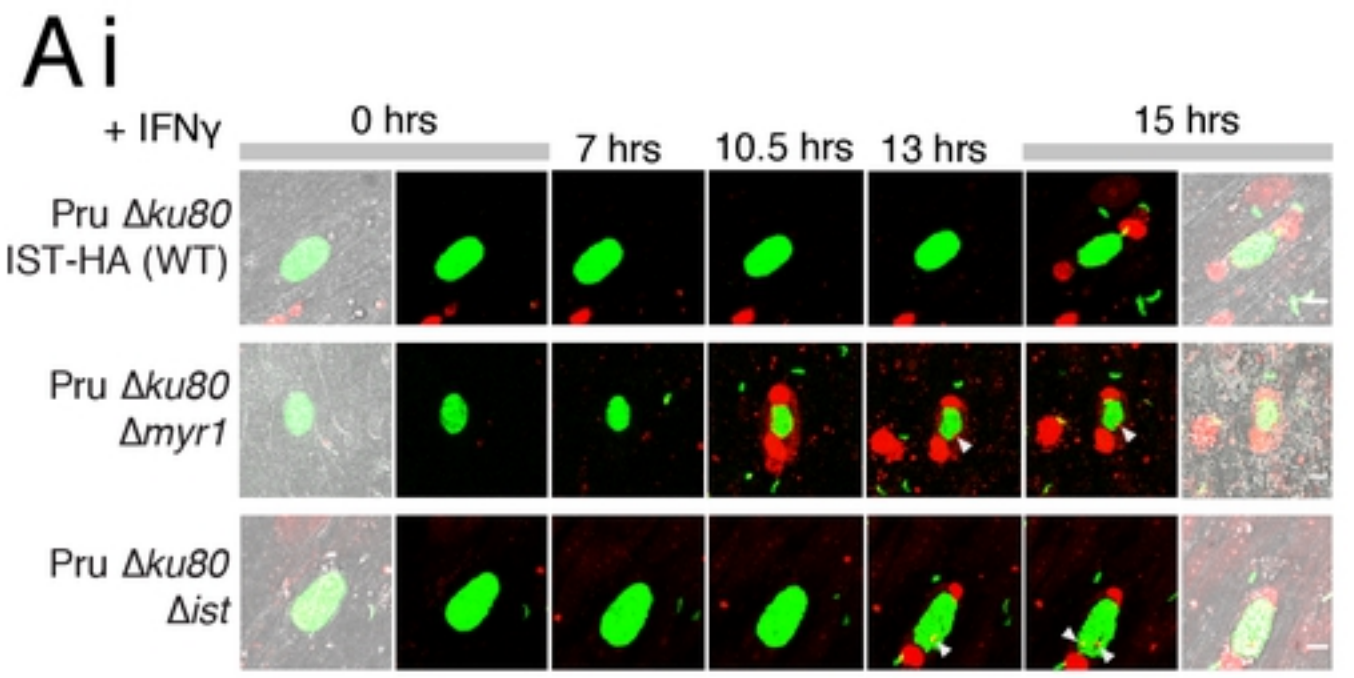


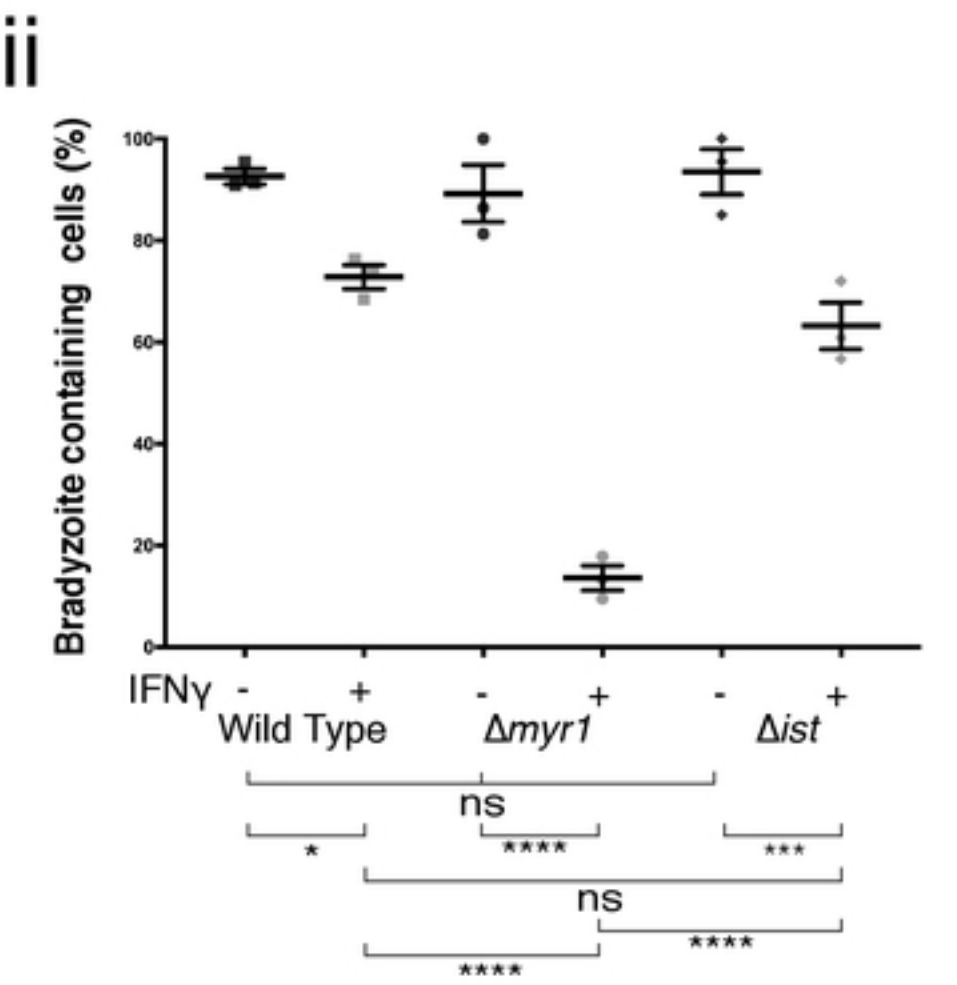
bioRxiv preprint doi: https://doi.org/10.1101/669689. The copyright holder for this preprint (which was not peer-reviewed) is the author/funder. It is made available under a CC-BY 4.0 International license.

bioRxiv preprint doi: https://doi.org/10.1101/669689. The copyright holder for this preprint (which was not peer-reviewed) is the author/funder. It is made available under a CC-BY 4.0 International license.

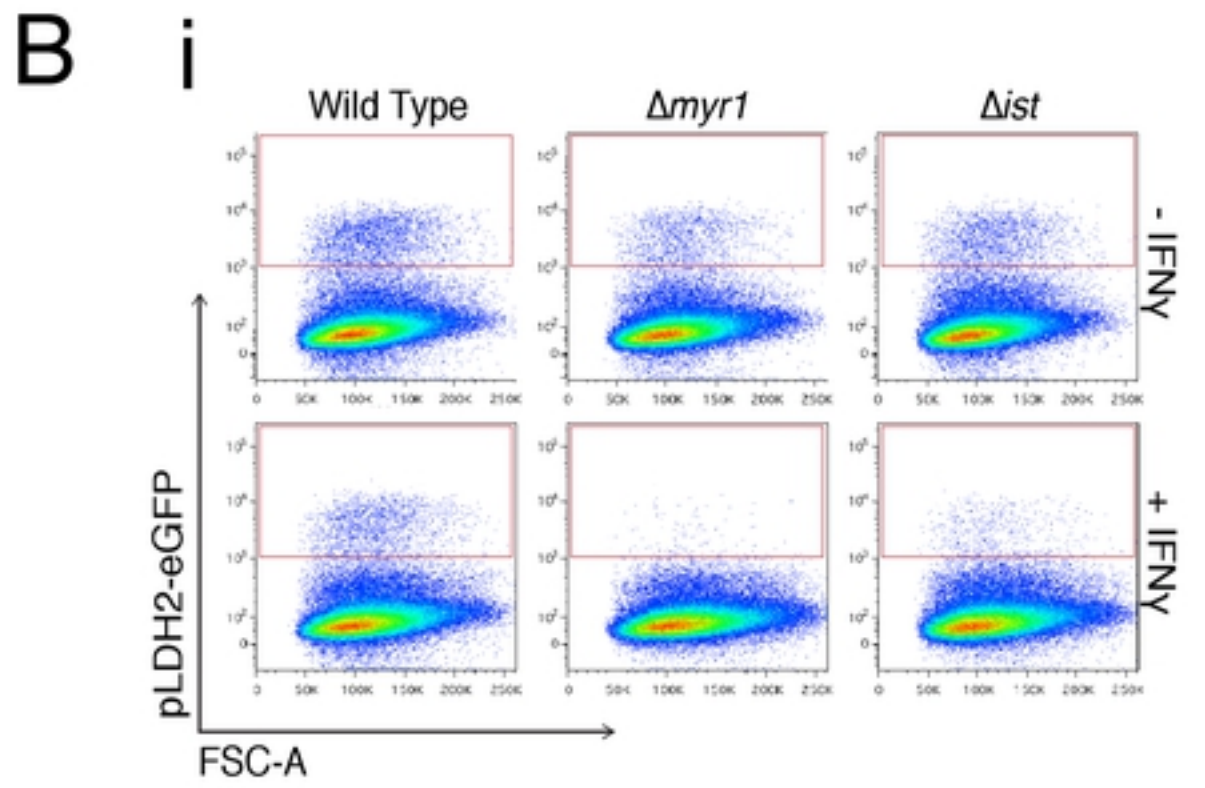
Figure 6. Bradyzoites alter the Interferon gamma pathway. (**A**) (i) PruΔ*ku80* IST-HA (WT), PruΔ*ku80* IST-HA Δ*myr1*, and PruΔ*ku80* IST-HA Δ*ist* parasites were differentiated under alkaline conditions for 7 days before fixation. The absence of MYR1 in bradyzoites (pLDH2-eGFP; green) inhibits the export of IST-HA (αHA; white) into the host nucleus. White arrows indicate location of infected host nucleus (DAPI; blue). White stars indicate location of un-infected host nuclei. Scale bar = 10μM. Brightness and contrast was edited on single colour channels prior to merging. (ii) The increase in IST-HA mean fluorescence intensity in the host nuclei of WT infected cells is lost in Δ*myr1* and Δ*ist* infected host cells (normalised to PruΔ*ku80* untagged controls). Analysed from immuno-fluorescence imaging (Figure 7ai) (mean ± SD, n = 3 experiments, each experiment analysed on average between 20-30 bradyzoite cysts; unpaired, parametric one-way ANOVA test with Dunn's multiple comparison; ****p<0.0001). (iii) The ratio (nuclear intensity/vacuolar intensity) of IST drops in Δ*myr1* when compared to WT. Analysed from immuno-fluorescence imaging (Figure 7ai) (mean ± SD, n = 3 experiments, each experiment analysed on average between 20-30 bradyzoite cysts; unpaired, two-sided Student's t-test; ****p<0.0001). (**B**) (i) PruΔ*ku80* IST-HA (WT), Δ*myr1*, and Δ*ist* parasites were differentiated under alkaline conditions for 7 days before being treated with 50ng/ml of human-IFNγ for 15hrs and fixed. Nuclear IRF1 (αIRF1; magenta) protein levels drop to varying degrees in WT infected cells, and this inhibition is lost in Δ*myr1* and Δ*ist* bradyzoite (pLDH2-eGFP; green) infected host cells. White arrows indicate location of host nucleus (DAPI; blue). White stars indicate location of un-infected host nuclei. Scale bar = 10μM. Brightness and contrast was edited on single colour channels prior to merging. (ii) The inhibition of IRF1 by WT bradyzoites is reversed by the knockout of *myr1* and IRF1 levels return to similar levels when compared to uninfected and Δ*ist* infected cells. Analysed from immuno-fluorescence imaging and normalised to surrounding uninfected cells (Figure 7bi) (mean ± SD, n = 3 experiments, each experiment analysed on average between 20-30 bradyzoite infected host cells; unpaired, parametric one-way ANOVA test with Dunn's multiple comparison; **p<0.01, ****p<0.0001). (**C**) RPKM values for IRF1 from Figure 3 data set. (**D**) A gene heat map of $\log_2$RPKM expression for the Hallmark gene set *IFN gamma response* showing all samples from the Figure 3 analysis. Expression has been scaled to have mean 0 and standard deviation 1 for each gene. See also Figure S5, S6 and Table S6 for gene list.

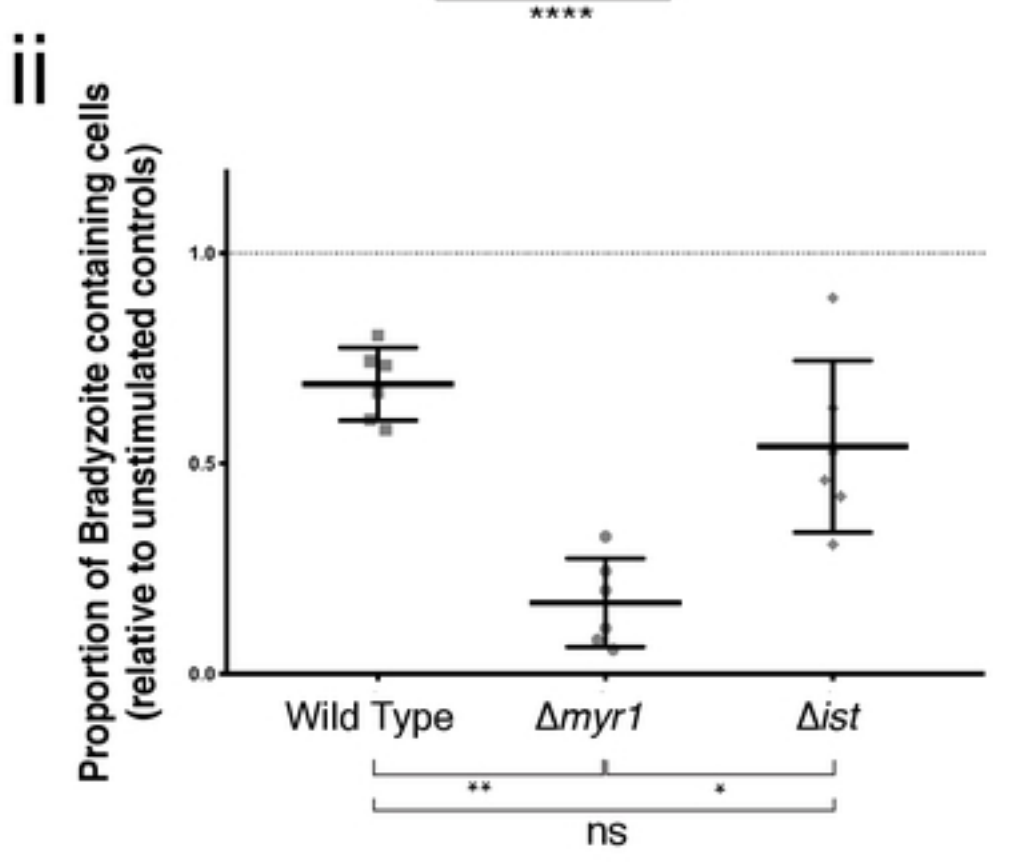
Figure 7

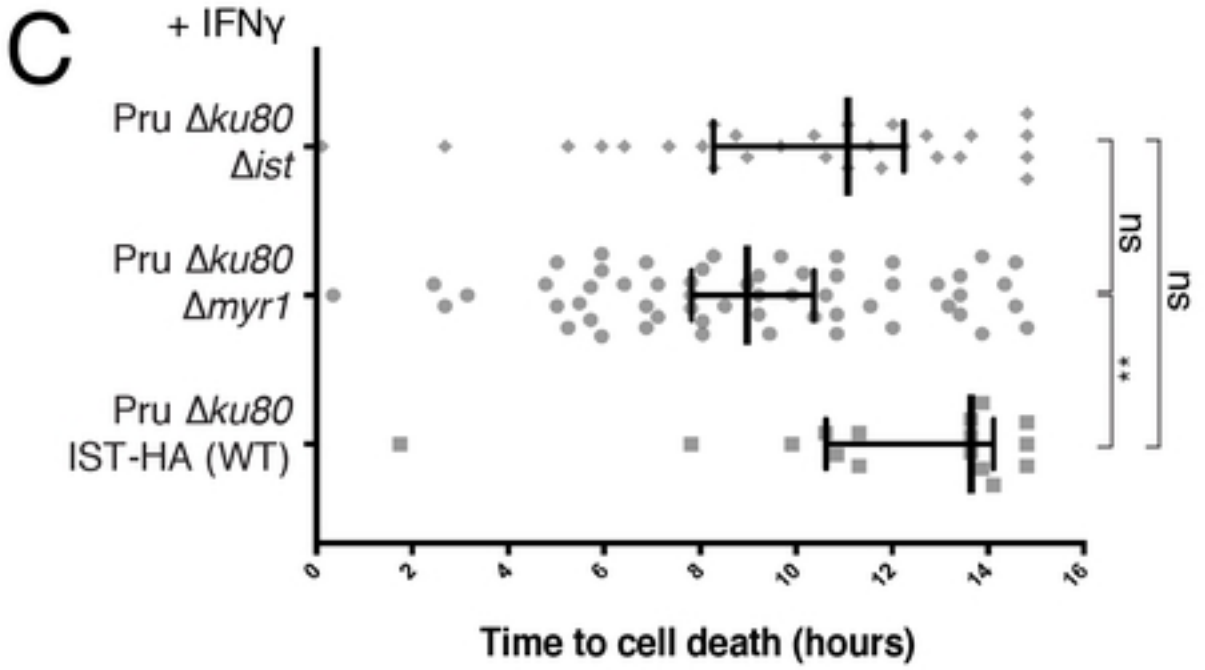


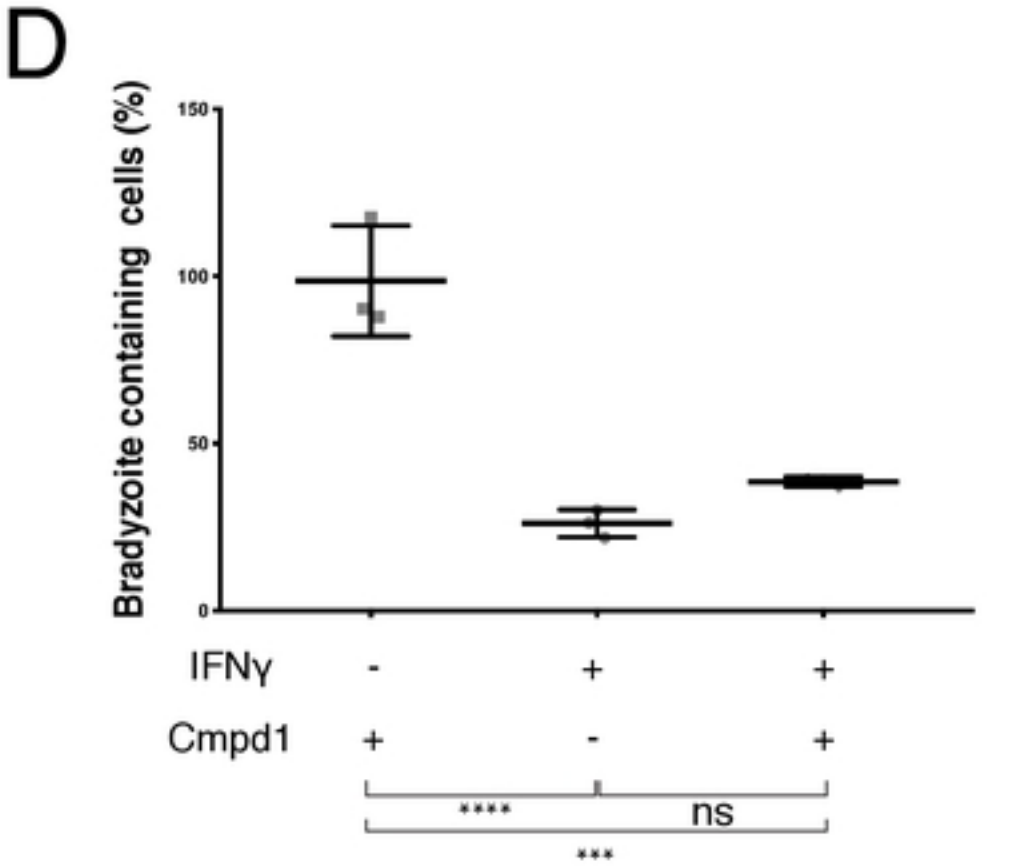


bioRxiv preprint doi: https://doi.org/10.1101/669689. The copyright holder for this preprint (which was not peer-reviewed) is the author/funder. It is made available under a CC-BY 4.0 International license.





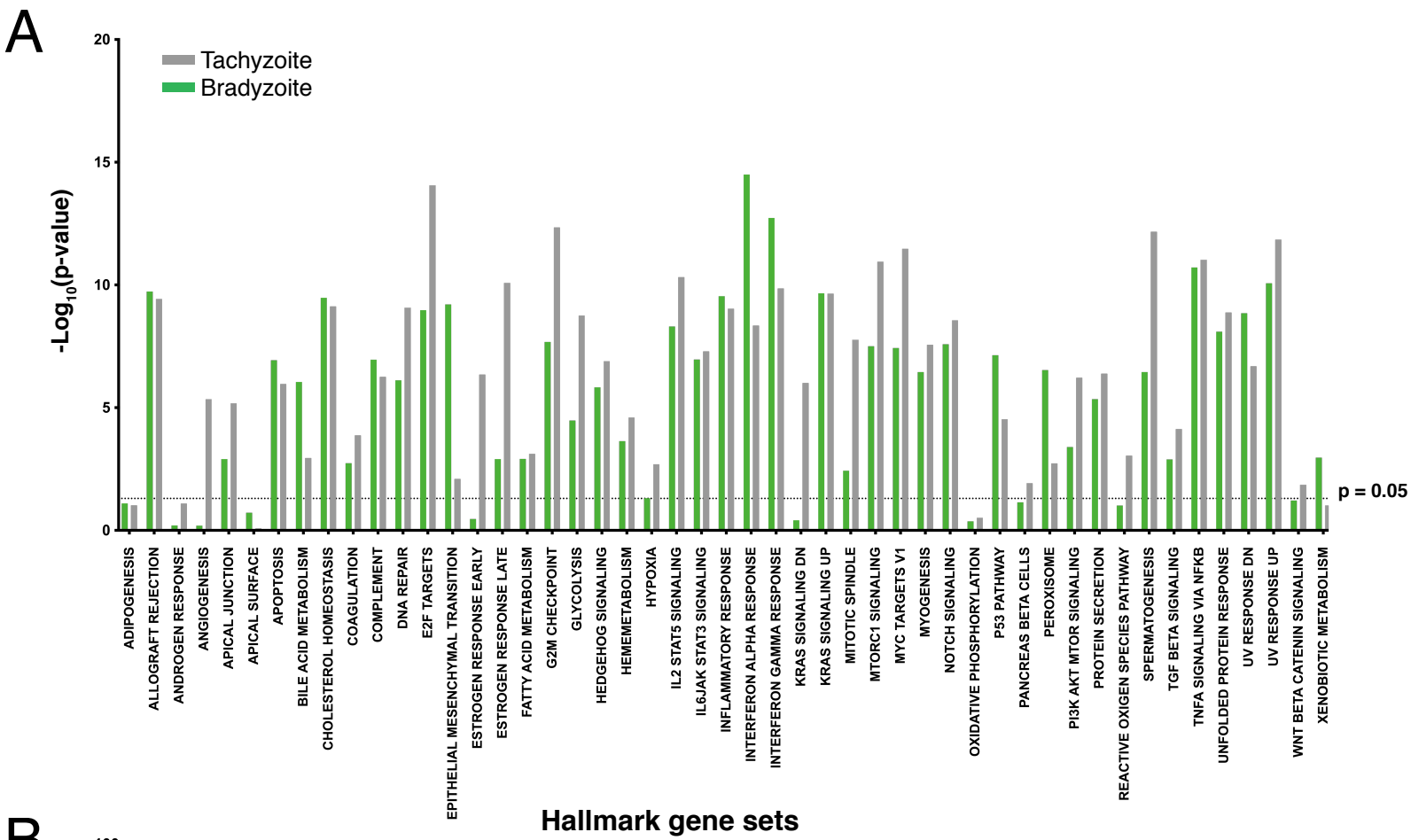


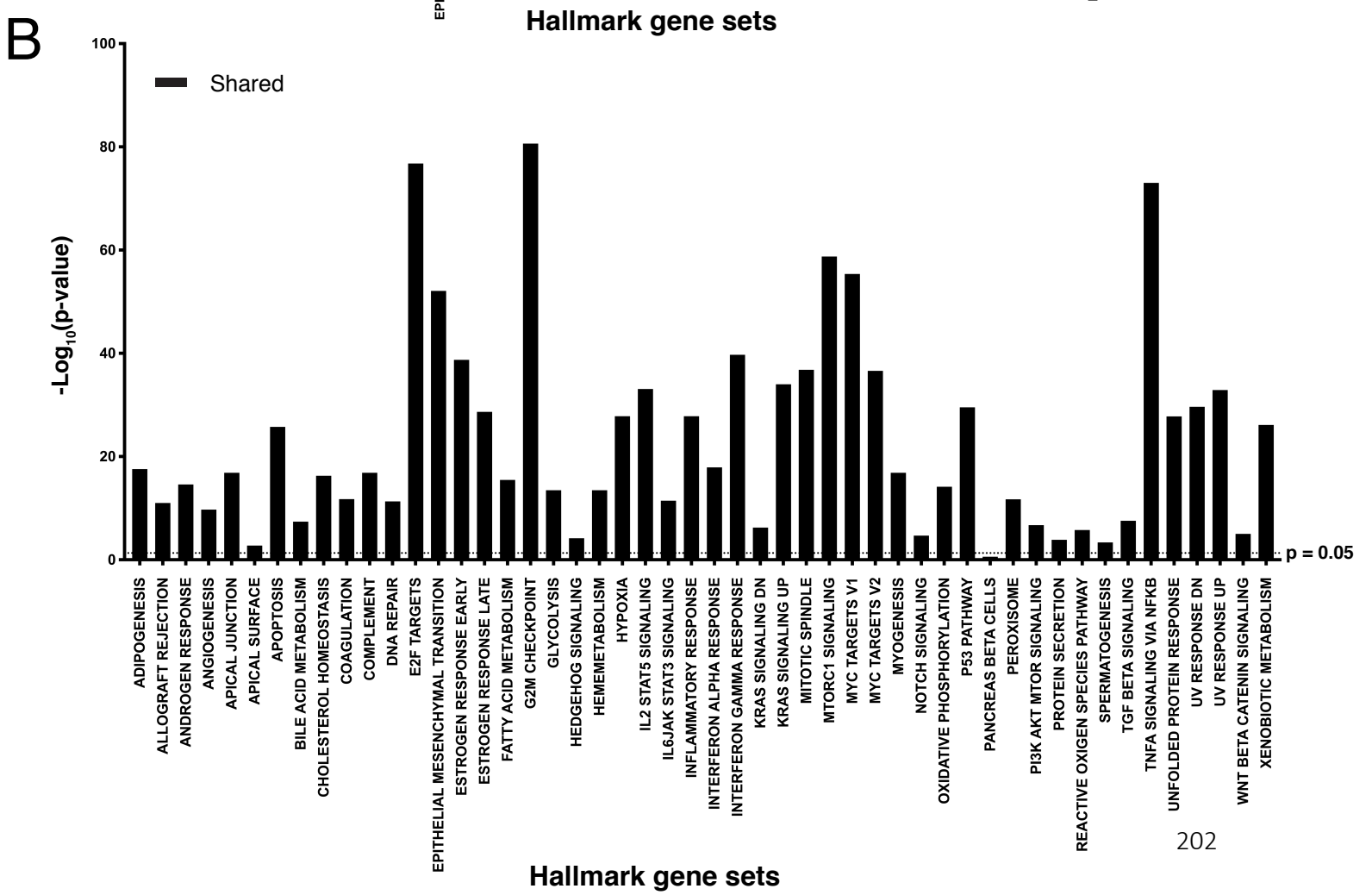


bioRxiv preprint doi: https://doi.org/10.1101/669689. The copyright holder for this preprint (which was not peer-reviewed) is the author/funder. It is made available under a CC-BY 4.0 International license.

Figure 7. Depletion of MYR1 prevents cyst persistence and induces host cell death upon IFNγ stimulation. (**A**) (i) PruΔ*ku80* IST-HA (WT), PruΔ*ku80* IST-HA Δ*myr1*, and PruΔ*ku80* IST-HA Δ*ist* parasites were differentiated under alkaline conditions for 7 days before imaging. During each experiment (n=3), between 15-35 parasite cysts were imaged every 14 mins for 15 hours after the addition of PI (red) and 50ng/ml of IFNγ. PI can be seen entering the host cell and bradyzoites (pLDH2-eGFP; green; white arrow) are released. Scale bar = 10μM. Brightness and contrast was edited on single colour channels prior to merging. (ii) The percentage of cyst infected cells that survived the 15 hours treatment of IFNγ drops by almost 90% in Δ*myr1* infected cells, significantly more than both WT and Δ*ist* (mean ± SD, n = 3 experiments, each experiment tracked between 15-30 bradyzoite cysts; unpaired, one-way ANOVA test with Sidak's multiple comparison test; *p<0.05, ***p<0.001, ****p<0.0001). (**B**) (i) PruΔ*ku80* IST-HA (WT), Δ*myr1*, and Δ*ist* parasites were differentiated under alkaline conditions for 7 days before being treated with 50ng/ml of human-IFNγ for 15hrs, trypinised and FACS sorted. FACS plot showing gating of eGFP$^+$ cells (red) of WT, Δ*myr1*, and Δ*ist* bradyzoite infected host cells. (ii) Proportion of bradyzoite -eGFP$^+$ cells compared to unstimulated samples shows a similar pattern to the live imaging data from Figure 8a. (mean ± SD, n = 6 experiments, unpaired, one-way ANOVA test with Sidak's multiple comparison test; *p<0.05, **p<0.01). (**C**) Time to cell death in hours; Δ*myr1* infected cells died earlier than both WT and Δ*ist* (median ± 95% CI, n = 3 experiments, each experiment tracked between 15-30 bradyzoite cysts; unpaired, nonparametric one-way Kruskal-Wallis ANOVA test with Dunn's multiple comparison; **p<0.01). (**D**) Compound 1 (2μM) was added to 7-day-old bradyzoites for an hour prior to the IFNγ addition for 15 hours. Samples were fixed, FACS analysed, and the proportion of bradyzoite-eGFP$^+$ cells compared to untreated samples (mean ± SD, n = 3 experiments, unpaired, one-way ANOVA test with Sidak's multiple comparison test; ***p<0.001, ****p<0.0001, p=0.510).

Supplementary Figure 1

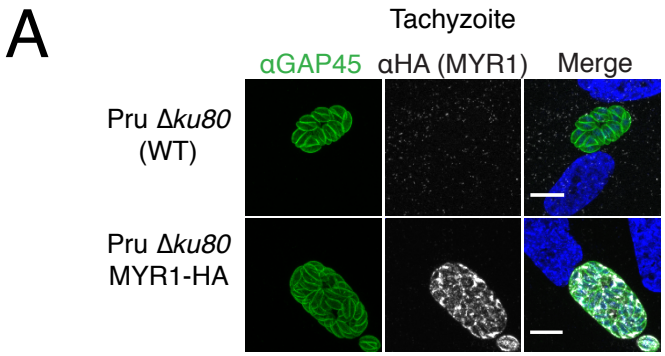


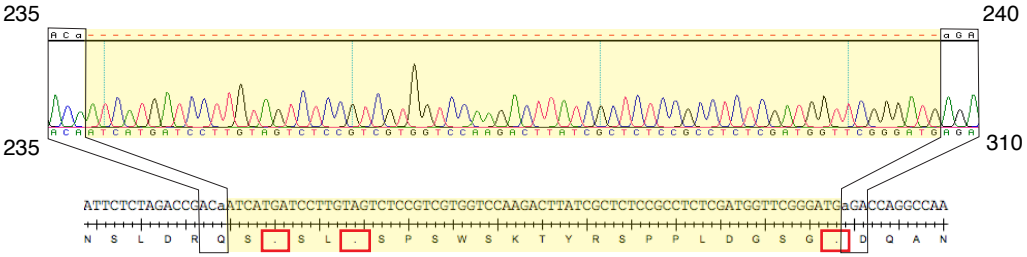


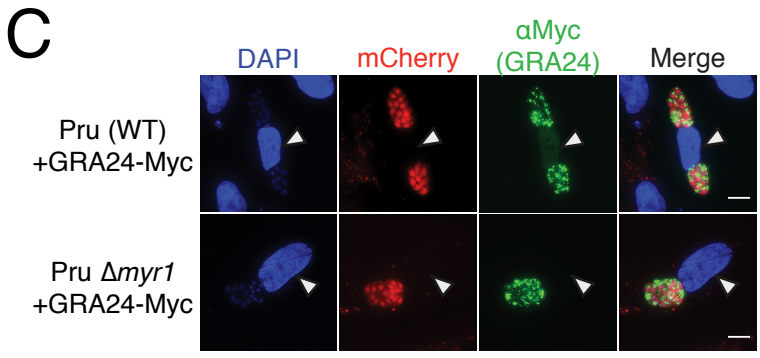
bioRxiv preprint doi: https://doi.org/10.1101/669689. The copyright holder for this preprint (which was not peer-reviewed) is the author/funder. It is made available under a CC-BY 4.0 International license.

Figure S1, related to Figure 2. Pathways enriched during both tachyzoite and bradyzoite infection (**A**) Over-representation analysis results for tachyzoite vs uninfected (grey) and vs uninfected DEGs (green) for each Hallmark gene set displayed as the negative Log_{10} of the p-value, dotted line p = 0.05. (**B**) Over-representation analysis results for tachyzoite and bradyzoite shared DEGs (black) for each Hallmark gene set displayed as the negative Log_{10} of the P-value, dotted line p = 0.05. See also Table S2.

Supplementary Figure 2



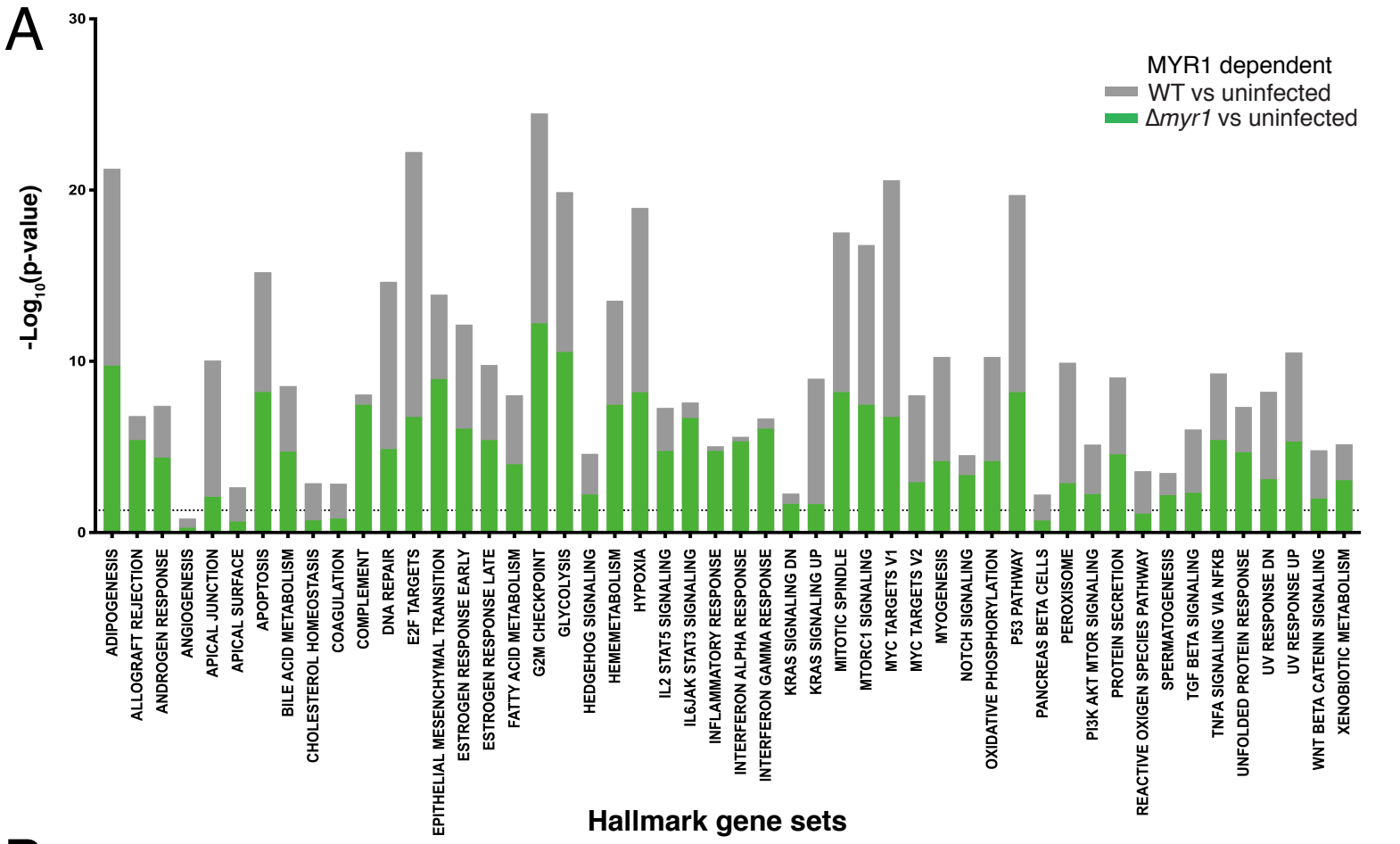


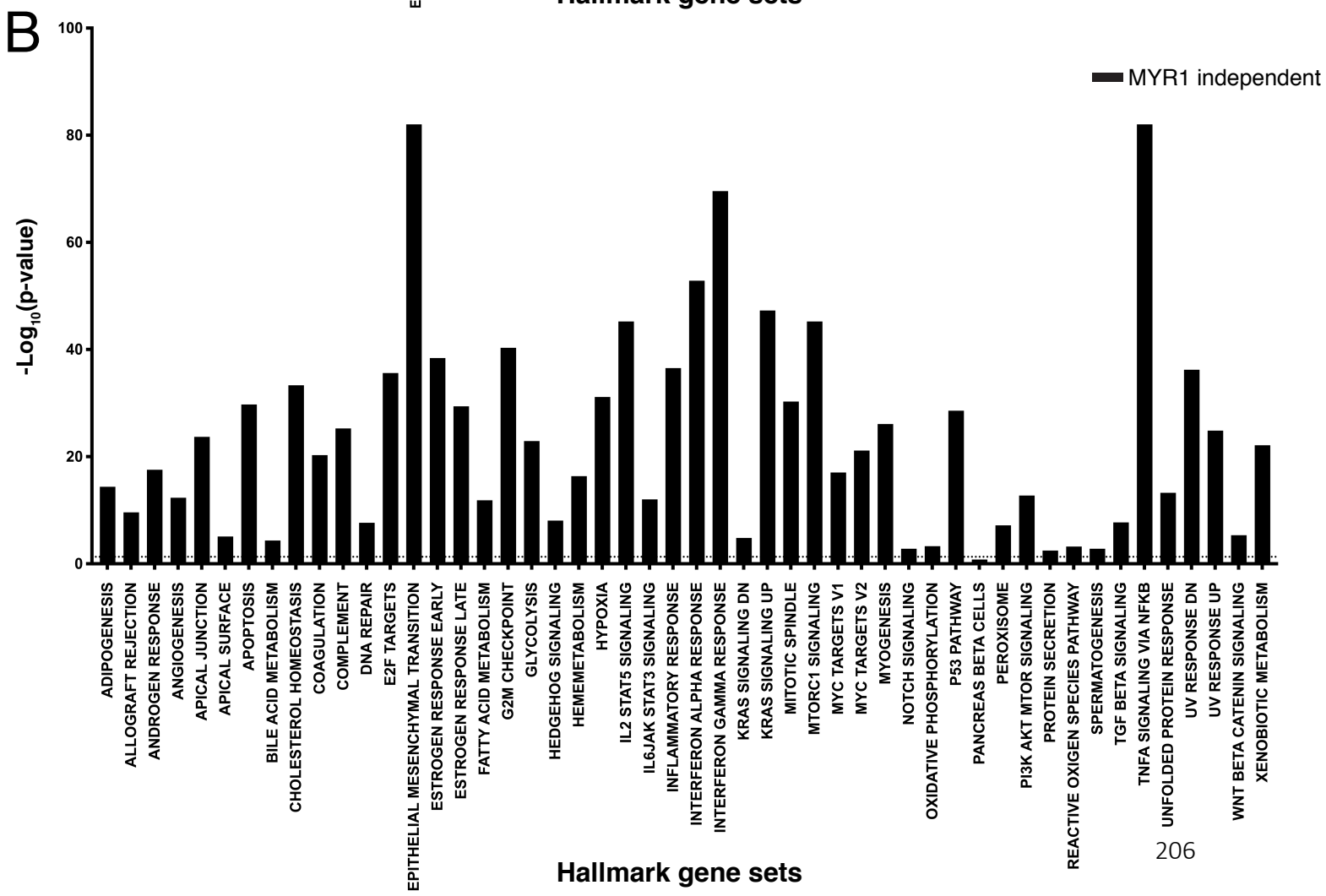


bioRxiv preprint doi: https://doi.org/10.1101/669689. The copyright holder for this preprint (which was not peer-reviewed) is the author/funder. It is made available under a CC-BY 4.0 International license.

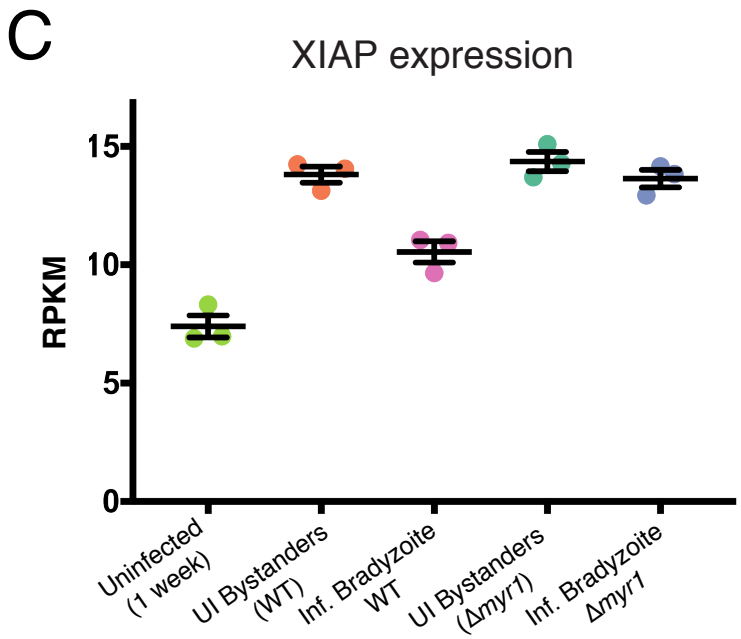
Figure S2, related to Figure 3. Expression and knockout of MYR1 (**A**) Tachyzoites (αGAP45; green) express MYR1 (αHA; white) at the PV and within the PV space. Scale bar = 10μM (**B**) A random 69 bp insertion between 237-238 results in three stop codons (**C**) Transiently transfected GRA24-myc3 (αMyc; green) export into the host nucleus (DAPI; blue) is inhibited in Δ*myr1* tachyzoites (mCherry; red). White arrows indicate location of host nucleus. Scale bar = 10μM. Brightness and contrast was edited on single colour channels prior to merging.

Supplementary Figure 3





Supplementary Figure 3 continued

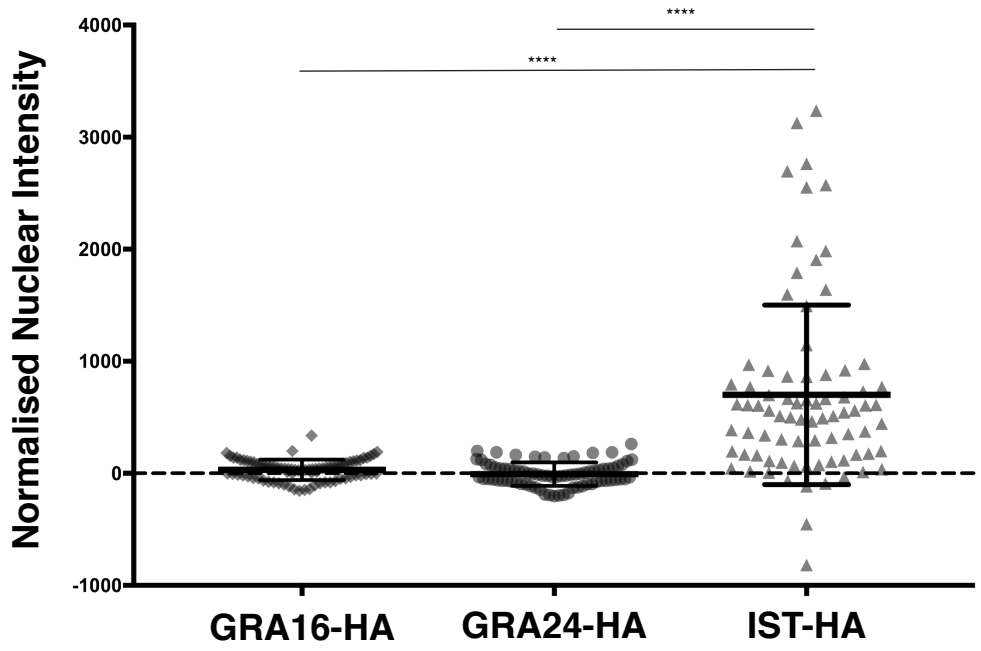


bioRxiv preprint doi: https://doi.org/10.1101/669689. The copyright holder for this preprint (which was not peer-reviewed) is the author/funder. It is made available under a CC-BY 4.0 International license.

Figure S3, related to Figure 3. MYR1 dependent DEGs play a significant role in pathways regulated by bradyzoites infection. (**A**) Over-representation analysis results for the MYR1 dependent DEGs for each Hallmark gene set displayed as the negative Log_{10} of the P-value, dotted line p = 0.05. (**B**) Over-representation analysis results for the MYR1 independent DEGs (black) for each Hallmark gene set displayed as the negative Log_{10} of the P-value, dotted line p = 0.05. (**C**) RPKM values for XIAP protein expression Figure 4 data set. See also Table S5 for gene lists.

Supplementary Figure 4

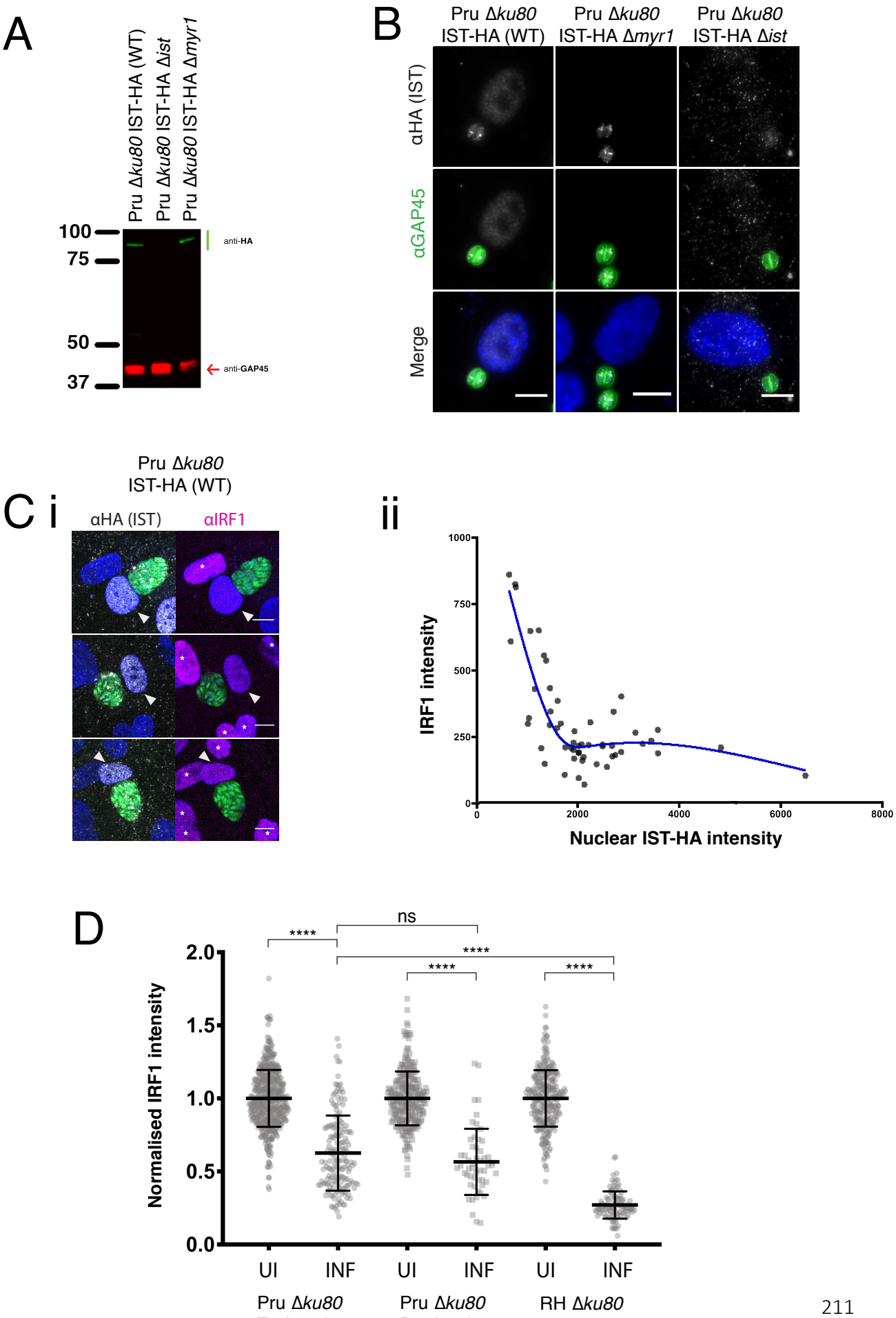
A



bioRxiv preprint doi: https://doi.org/10.1101/669689. The copyright holder for this preprint (which was not peer-reviewed) is the author/funder. It is made available under a CC-BY 4.0 International license.

Figure S4, related to Figure 5. Bradyzoites export IST. (**D**) Quantification of the intensity of nuclear GRA16-HA, GRA24-HA and IST-HA (normalised to PruΔ*ku80* WT controls) of bradyzoites infected host cells from immuno-fluorescence imaging (Figure 6c) (mean ± SD, n = 3 experiments, each experiment analysed on average between 20-40 bradyzoite cysts and 60-200 tachyzoite vacuoles; unpaired, parametric one-way ANOVA test with Dunn's multiple comparison; ****p<0.0001)

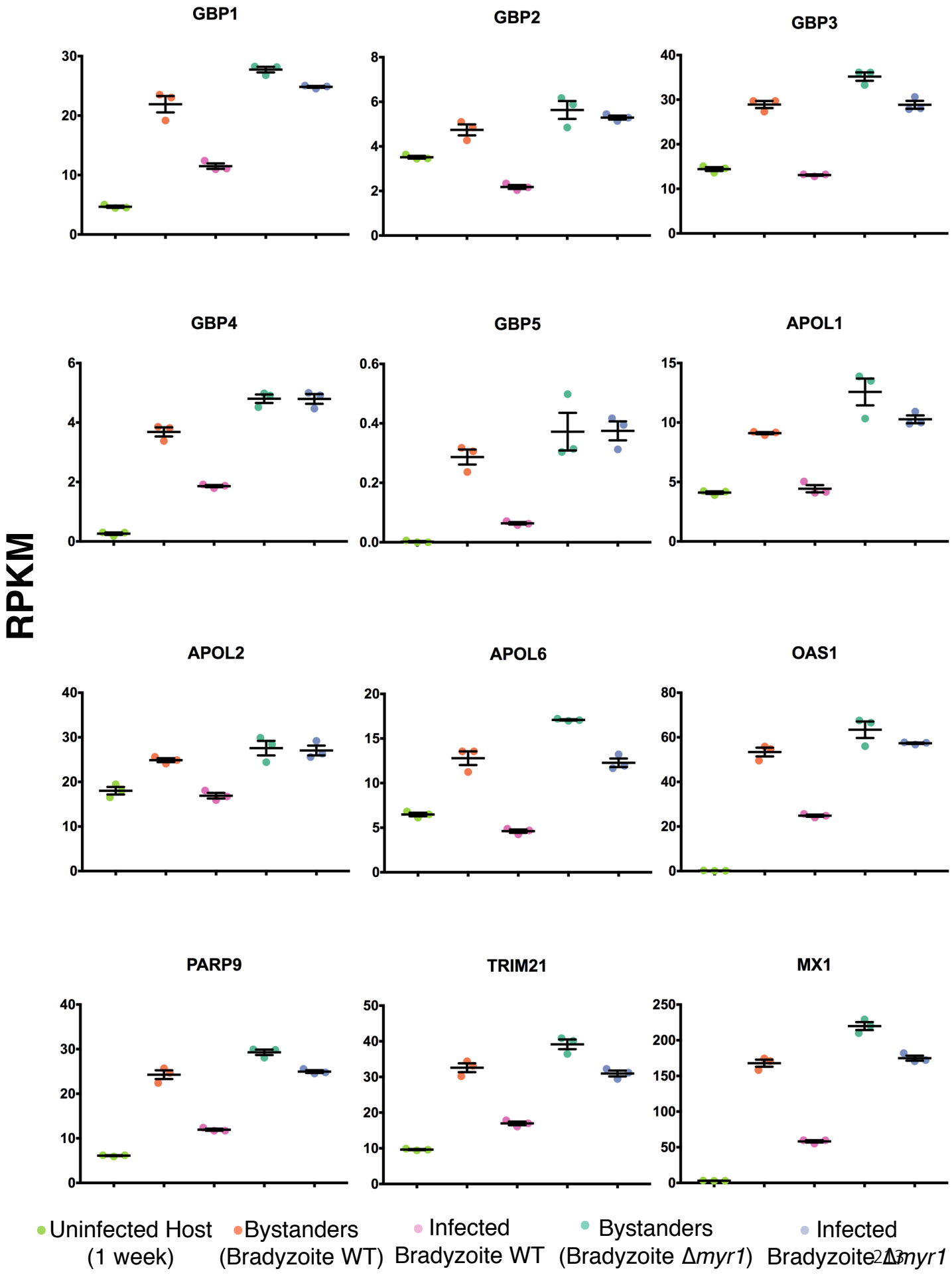
Supplementary Figure 5



bioRxiv preprint doi: https://doi.org/10.1101/669689. The copyright holder for this preprint (which was not peer-reviewed) is the author/funder. It is made available under a CC-BY 4.0 International license.

Figure S5, related to Figure 6. MYR1 knockouts effects on IRF1 (**A**) Western blot indicates IST (αHA) is expressed in WT and Δ*myr1* tachyzoites but is absent in Δ*ist*. αGAP45 is used as a loading control. (**B**) Immuno-fluorescence images of tachyzoite (αGAP45; green) PruΔ*ku80* IST-HA (WT), PruΔ*ku80* IST-HA Δ*myr1*, and PruΔ*ku80* IST-HA Δ*ist* infected cells. WT can export IST-HA (αHA; white) in to the host nucleus (DAPI; blue), whereas there is a loss of export in Δ*myr1* and no expression in Δ*ist* infected cells. Scale bar = 10μM. Brightness and contrast was edited on single colour channels prior to merging. (**C**) (i) PruΔ*ku80* IST-HA (WT), PruΔ*ku80* IST-HA Δ*myr1*, and PruΔ*ku80* IST-HA Δ*ist* bradyzoites (green) were treated with 50ng/ml of human-IFNγ for 15hrs and before being fixed and probed for IST (anti-HA; white) and IRF1 (magenta). There is a range of IRF1 inhibition. (iii) The relationship between the intensity of IRF1 and the intensity of nuclear IST-HA was modelled with a non-linear curve (blue) using natural splines with 3 degrees of freedom. This could significantly explain the relationship between IST-HA and IRFI ($p=1.042x10^{-12}$) (**D**) RHΔ*ku80* IST-HA tachyzoites and PruΔ*ku80* IST-HA parasites, that were either differentiated under alkaline conditions for 7 days (bradyzoites) or grown in D1 for 15 hours (tachyzoites), were treated with 50ng/ml of human-IFNγ for 15hrs. Samples were fixed and probed with αIRF1 and DAPI. Nuclear IRF1 protein intensity levels were measure as a proportion of surrounding uninfected cell intensity for both uninfected and infected cells. There was no difference in IRF1 expression between PruΔ*ku80* tachyzoites and bradyzoites (mean ± SD, n = 3 experiments, p=0.306). However there is a significant difference between PruΔ*ku80* and RHΔ*ku80* tachyzoites (****p<0.0001). Each experiment analysed on average between 20-30 bradyzoite infected host cells and 60-200 tachyzoite vacuoles (unpaired, one-way ANOVA test with Sidak's multiple comparison test).

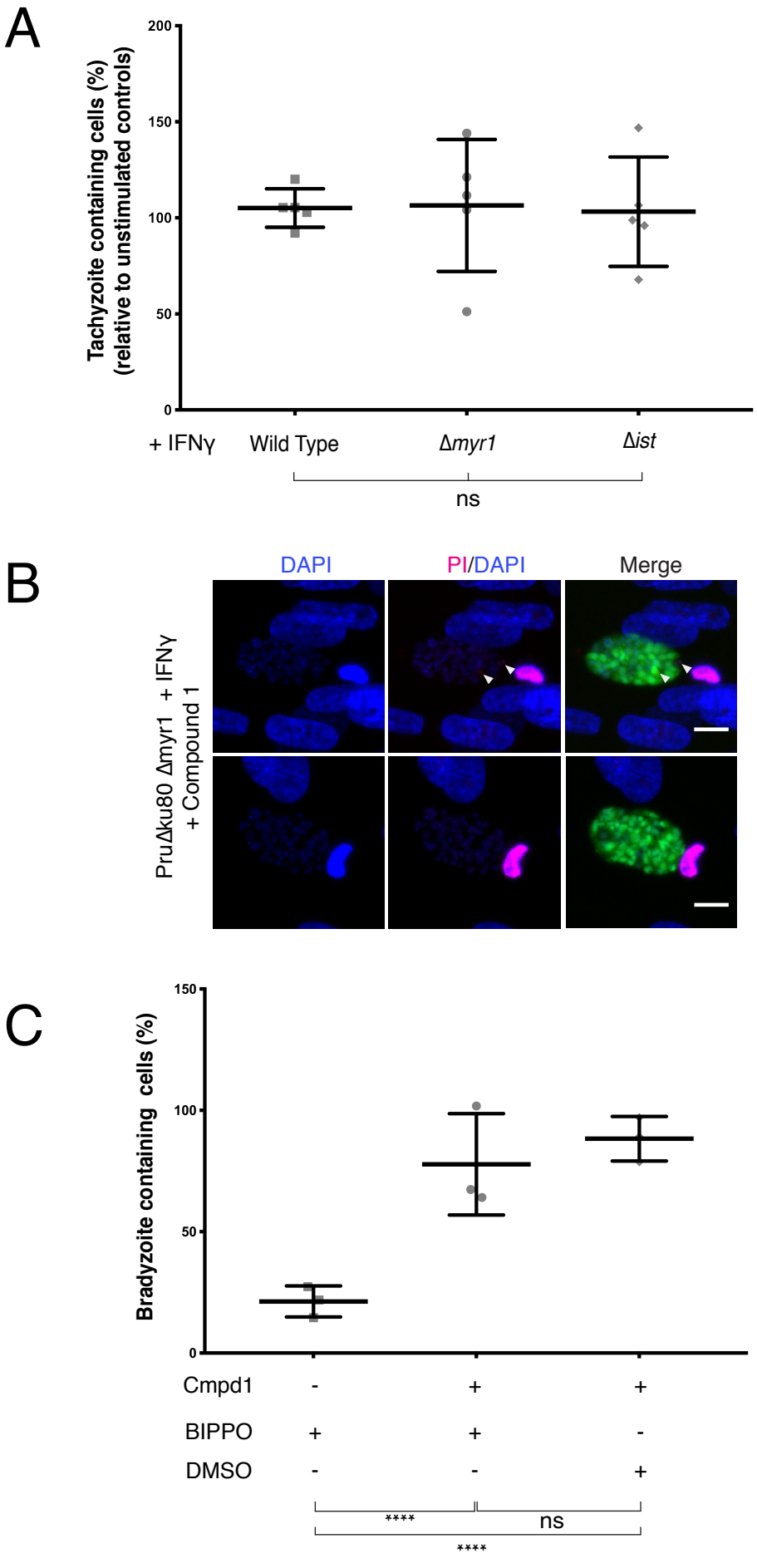
Supplementary Figure 6



bioRxiv preprint doi: https://doi.org/10.1101/669689. The copyright holder for this preprint (which was not peer-reviewed) is the author/funder. It is made available under a CC-BY 4.0 International license.

Figure S6, related to Figure 6. RPKM values for protein expression of IFNγ-pSTAT1-GAS induced transcripts from Figure 4 data set. Samples include: uninfected (green), bradyzoite WT-infected (pink) and bystander (orange), bradyzoite Δ*myr1*-infected (indigo) and bystander (aqua) cells.

Supplementary Figure 7



bioRxiv preprint doi: https://doi.org/10.1101/669689. The copyright holder for this preprint (which was not peer-reviewed) is the author/funder. It is made available under a CC-BY 4.0 International license.

Figure S7, related to Figure 7. IFNγ induced cell death of bradyzoite containing HFF cells. (**A**) PruΔ*ku80* IST-HA (WT), Δ*myr1*, and Δ*ist* tachyzoites were treated with IFNγ for 15 hours. HFFs were washed, trypinised and fixed, before probed with αGAP45. Samples were analysed using FACS (mean ± SD, n = 5 experiments, unpaired, one-way ANOVA test with Sidak's multiple comparison test; p>0.98) (**B**) Compound 1 (2μM) was added to 7-day-old PruΔ*ku80* IST-HA Δ*myr1* bradyzoites (green) for an hour prior to the IFNγ addition for 15 hours. PI (red) was added for 10 mins before being washed and fixed, white arrows indicated PI positive parasites. (**C**) Compound 1 (2μM) was added to 7-day-old PruΔ*ku80* IST-HA Δ*myr1* bradyzoites for 16 hours prior to the addition of BIPPO or vehicle (DMSO). Samples were trypinised and fixed, FACS analysed, and the proportion of bradyzoite-eGFP^{+} cells compared to untreated samples (mean ± SD, n = 3 experiments, unpaired, one-way ANOVA test with Sidak's multiple comparison test; p<0.0001, p=0.889).

bioRxiv preprint doi: https://doi.org/10.1101/669689. The copyright holder for this preprint (which was not peer-reviewed) is the author/funder. It is made available under a CC-BY 4.0 International license.

Video S1, related to Figure 7. Wildtype bradyzoite lysis during IFNγ stimulation. Parasites were differentiated for 7 days (bradyzoites express pLDH2-eGFP, green), before the addition of Propidium Iodide (red) and IFNγ and imaged every 14 mins for 15 hours.

Video S2, related to Figure 7. Δ*myr1* bradyzoite lysis during IFNγ stimulation. Parasites were differentiated for 7 days (bradyzoites express pLDH2-eGFP, green), before the addition of Propidium Iodide (red) and IFNγ and imaged every 14 mins for 15 hours.

Video S3, related to Figure 7. Δ*ist* bradyzoite lysis during IFNγ stimulation. Parasites were differentiated for 7 days (bradyzoites express pLDH2-eGFP, green), before the addition of Propidium Iodide (red) and IFNγ and imaged every 14 mins for 15 hours.

Table S1. Log RPKM values for the top 100 differentially regulated genes between uninfected host cells and bradyzoite infected host cell related to Figure 1D.

Table S2. Table of DEG and their corresponding Hallmark Pathways for tachyzoite specific, bradyzoite specific and shared genes related to Figure 2A and S1.

bioRxiv preprint doi: https://doi.org/10.1101/669689. The copyright holder for this preprint (which was not peer-reviewed) is the author/funder. It is made available under a CC-BY 4.0 International license.

Table S3. Log RPKM values for genes expressed in the E2F, Myc, IFNα and IFNγ Hallmark pathways for tachyzoite (related to Fig. 2B) and bradyzoite (related to Fig. 2C) comparisons.

Table S4. Log RPKM values for the top 100 differentially regulated genes between bradyzoite WT-infected and Δ*myr1*-infected host cells related to Figure 3D.

Table S5. Table of DEG and their corresponding Hallmark Pathways for MYR1 dependent (WT and Δ*myr1* specific) genes and MYR1-independent (shared) genes related to Figure 4 and S3.

Table S6. Log RPKM values for genes expressed in the IFNγ (related to Fig. 6) Hallmark pathways for MYR1 knockout comparisons.

Appendix B -

Data set 1: Data alignment, normalisation, filtering, and exploration .
Code and processing was completed by Dr. Alexandra Garnham from WEHI

1 Background

This report provides the analysis of RNA sequencing data provided by Simona Seizova and Chris Tonkin (Tonkin Lab, Infection and Immunity). These data comprise 18 samples of human fibroblasts. The fibroblasts are from a single donor. The samples are either un-infected (UI), treated with toxoplasma but the cells remain un-infected, treated with toxoplasma that results in infection (Inf). Two different stages of toxoplasma are separately used - tachyzoites and bradyzoites. The tachyzoites and bradyzoites require difference media and conditions for growth. The tachyzoites require D1 media and 24h infection time, while the bradyzoites need iM media and 1 week infection time. We therefore have 6 separate groups each with 3 biological replicates, described in the table below.

Group	Description
UI_Host_24h	Host Uninfected 24 hours D1
UI_Tachy_24h	Uninfected Tachy 24 hours D1
Inf_Tachy_24h	Infected Tachy 24 hours D1
UI_Host_1week	Host Uninfected 1 week iM
UI_Brady_1week	Uninfected Brady 1 week iM
Inf_Brady_1week	Infected Brady 1 week iM

Within each time point, Simona would like to identify differentially expressed genes between the following groups:

- Samples treated with toxoplasma but are un-infected and the un-infected host samples
- Infected samples and the un-infected host samples
- Infected samples and the un-infected treated samples

In addition to the above, Simona would also like to determine which genes are differentially expressed between the infected tachy and infected brady samples. However, the biological differences between these samples are confounded with the incubation time difference between them. Simona would still like to go ahead with the analysis anyway. Therefore, in order to determine genes that are potentially changing between these groups due to biological differences only and not incubation time, we also look at genes that are differentially expressed between the uninfected sample groups.

Finally, Simona would like to know if parasite RNA can be detected in her samples. To this end, the data will be aligned to both the human and toxoplasma (strain ME49) genomes. The toxoplasma genome plus annotation is available at http://toxodb.org/common/downloads/release-31/TgondiiME49/.

2 The targets file

The targets file contains all experimental information regarding each sample. The targets file for these data:

```
> targets <- read.delim("Human_toxo_fibro_targets.txt", stringsAsFactors = FALSE)
> targets[targets$Read == 1, -2]
```

	FileName	Replicate	InfectionTime	Media	InfectionStatus	Toxoplasma	Group	SampleID
1	Host-uninf-24h-D1-R-1_S1_R1.fastq.gz	1	24hour	D1	Un-infected	Host	UI_Host_24h	UI_Host_24h_1
3	Host-uninf-24h-D1-R-2_S2_R1.fastq.gz	2	24hour	D1	Un-infected	Host	UI_Host_24h	UI_Host_24h_2
5	Host-uninf-24h-D1-R-3_S3_R1.fastq.gz	3	24hour	D1	Un-infected	Host	UI_Host_24h	
7	uninf-Tachy-24h-D1-R-1_S4_R1.fastq.gz	1	24hour	D1	Un-infected	Tachy	UI_Tachy_24h	
9	uninf-Tachy-24h-D1-R-2_S5_R1.fastq.gz	2	24hour	D1	Un-infected	Tachy	UI_Tachy_24h	
11	uninf-Tachy-24h-D1-R-3_S6_R1.fastq.gz	3	24hour	D1	Un-infected	Tachy	UI_Tachy_24h	
13	inf-Tachy-24h-D1-R-1_S7_R1.fastq.gz	1	24hour	D1	Infected	Tachy	Inf_Tachy_24h	
15	inf-Tachy-24h-D1-R-2_S8_R1.fastq.gz	2	24hour	D1	Infected	Tachy	Inf_Tachy_24h	
17	inf-Tachy-24h-D1-R-3_S9_R1.fastq.gz	3	24hour	D1	Infected	Tachy	Inf_Tachy_24h	
19	Host-uninf-1wk-iM-R-1_S10_R1.fastq.gz	1	1week	iM	Un-infected	Host	UI_Host_1week	
21	Host-uninf-1wk-iM-R-2_S11_R1.fastq.gz	2	1week	iM	Un-infected	Host	UI_Host_1week	
23	Host-uninf-1wk-iM-R-3_S12_R1.fastq.gz	3	1week	iM	Un-infected	Host	UI_Host_1week	
25	uninf-Brady-1wk-iM-R-1_S13_R1.fastq.gz	1	1week	iM	Un-infected	Brady	UI_Brady_1week	
27	uninf-Brady-1wk-iM-R-2_S14_R1.fastq.gz	2	1week	iM	Un-infected	Brady	UI_Brady_1week	
29	uninf-Brady-1wk-iM-R-3_S15_R1.fastq.gz	3	1week	iM	Un-infected	Brady	UI_Brady_1week	
31	inf-Brady-1wk-iM-R-1_S16_R1.fastq.gz	1	1week	iM	Infected	Brady	Inf_Brady_1week	
33	inf-Brady-1wk-iM-R-2_S17_R1.fastq.gz	2	1week	iM	Infected	Brady	Inf_Brady_1week	
35	inf-Brady-1wk-iM-R-3_S18_R1.fastq.gz	3	1week	iM	Infected	Brady	Inf_Brady_1week	

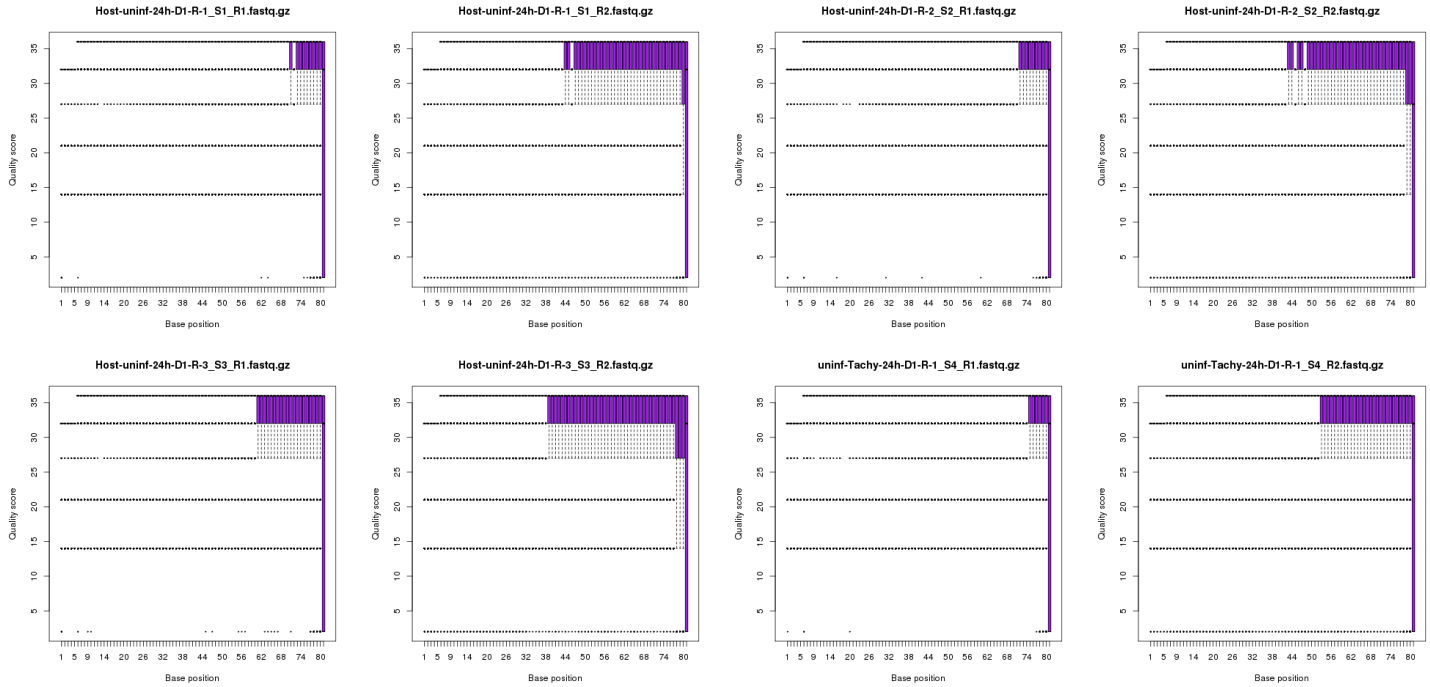
```
5      UI_Host_24h_3
7     UI_Tachy_24h_1
9     UI_Tachy_24h_2
11    UI_Tachy_24h_3
13   Inf_Tachy_24h_1
15   Inf_Tachy_24h_2
17   Inf_Tachy_24h_3
19   UI_Host_1week_1
21   UI_Host_1week_2
23   UI_Host_1week_3
25  UI_Brady_1week_1
27  UI_Brady_1week_2
29  UI_Brady_1week_3
31 Inf_Brady_1week_1
33 Inf_Brady_1week_2
35 Inf_Brady_1week_3
```

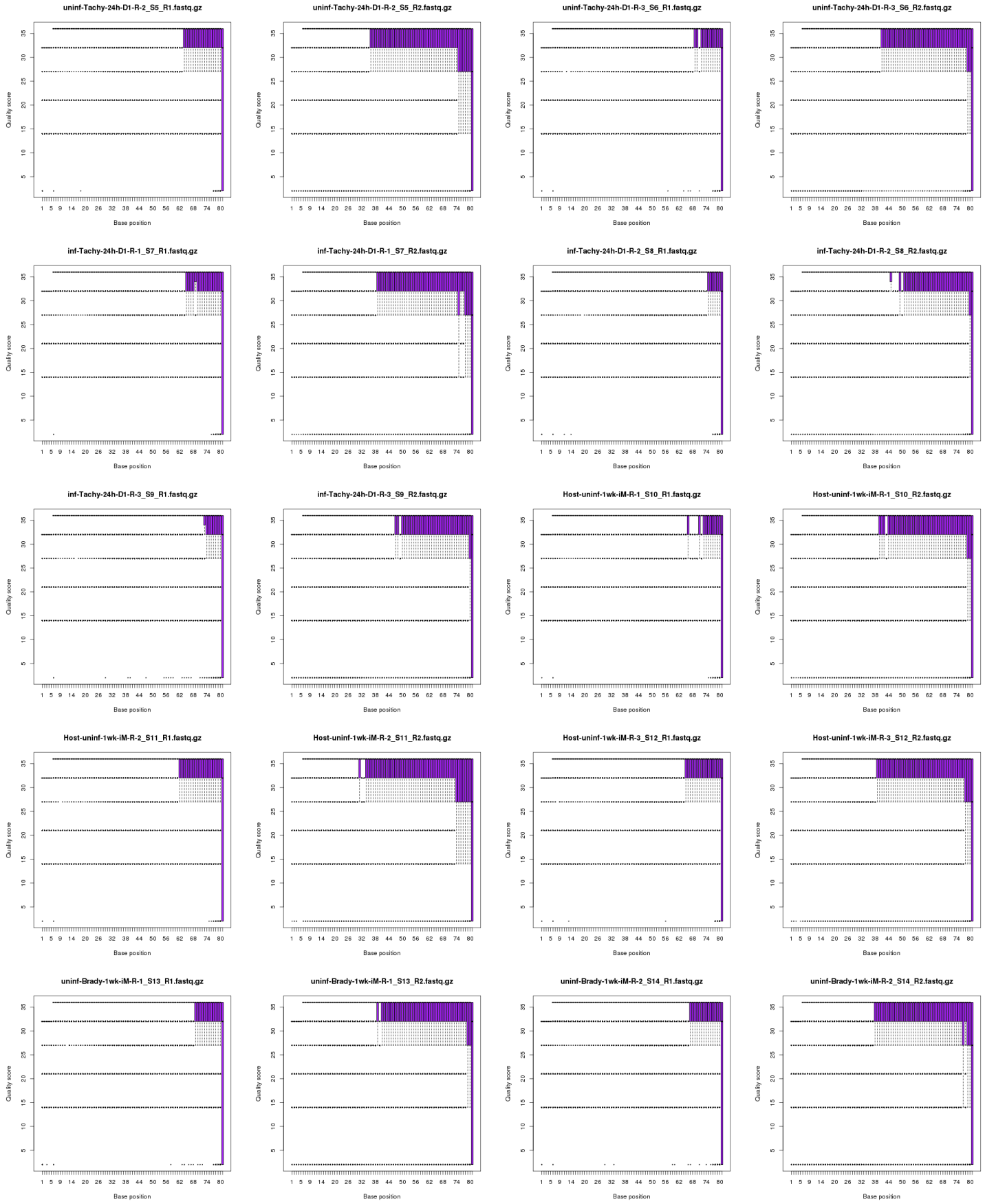
3 Alignment to the human and toxoplasma genomes

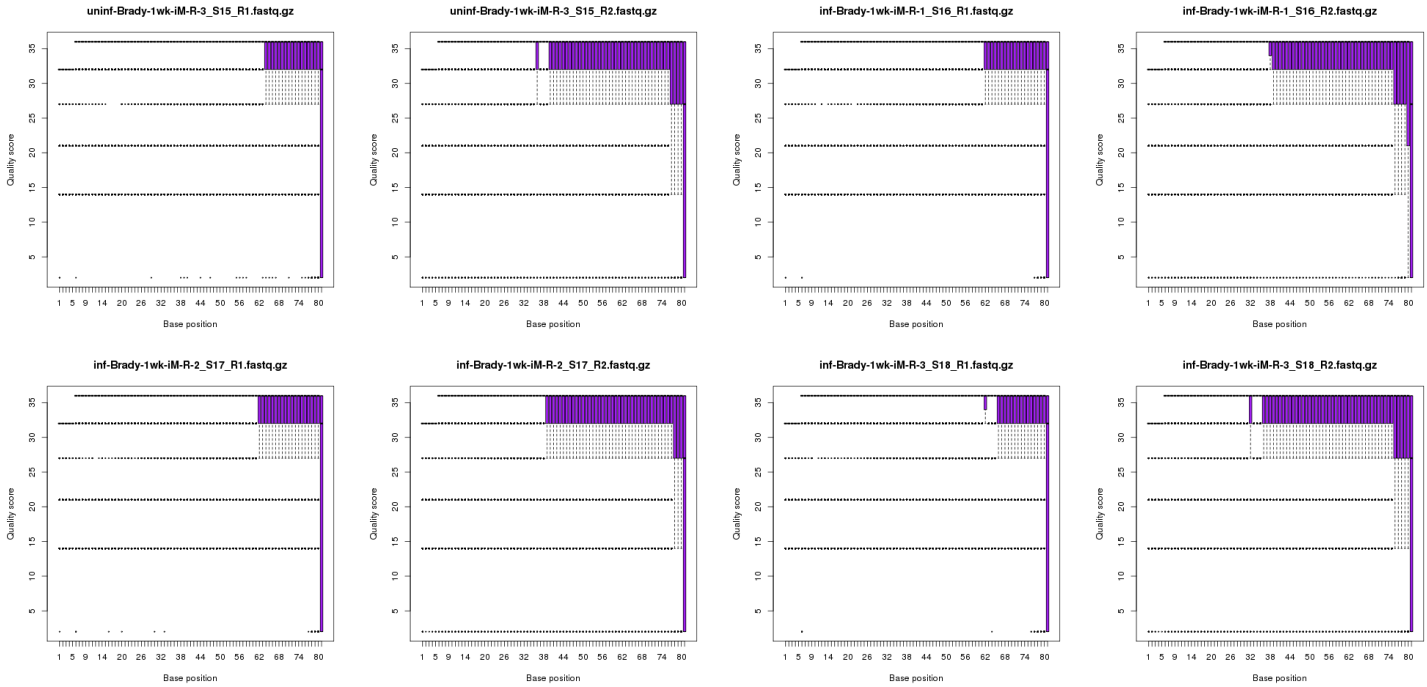
3.1 FastQ files

All samples were sequenced by Stephen Wilcox (O'Connor Lab, Systems Biology and Personalized Medicine) on the Illumina NextSeq platform. The reads are 80bp paired end. Before aligning the samples to the genomes, the quality of the sequencing is assessed by examining the quality scores associated with each read. A quality score is an indication of the probability of error when assigning a base to a read. Each base within each each read is given a quality score. A high quality score implies low probability of error, meaning the higher the quality score, the better quality the sequence. Boxplots of the quality scores for each fastq file are shown below.

```
> library(Rsubread)
> FastQ <- paste0("simona140317/", targets$FileName)
> for (i in 1:length(FastQ)) {
+     png(paste0("Plots/", paste0(targets$FileName[i], "_QS.png")))
+     boxplot(qualityScores(FastQ[i]), ylab = "Quality score", xlab = "Base position", main = targets$FileName[i],
+         cex = 0.25, col = "purple")
+     dev.off()
+ }
```




uninf-Tachy-24h-D1-R-2_S5_R1.fastq.gz
uninf-Tachy-24h-D1-R-2_S5_R2.fastq.gz
uninf-Tachy-24h-D1-R-3_S6_R1.fastq.gz
uninf-Tachy-24h-D1-R-3_S6_R2.fastq.gz
inf-Tachy-24h-D1-R-1_S7_R1.fastq.gz
inf-Tachy-24h-D1-R-1_S7_R2.fastq.gz
inf-Tachy-24h-D1-R-2_S8_R1.fastq.gz
inf-Tachy-24h-D1-R-2_S8_R2.fastq.gz
inf-Tachy-24h-D1-R-3_S9_R1.fastq.gz
inf-Tachy-24h-D1-R-3_S9_R2.fastq.gz
Host-uninf-1wk-iM-R-1_S10_R1.fastq.gz
Host-uninf-1wk-iM-R-1_S10_R2.fastq.gz
Host-uninf-1wk-iM-R-2_S11_R1.fastq.gz
Host-uninf-1wk-iM-R-2_S11_R2.fastq.gz
Host-uninf-1wk-iM-R-3_S12_R1.fastq.gz
Host-uninf-1wk-iM-R-3_S12_R2.fastq.gz
uninf-Brady-1wk-iM-R-1_S13_R1.fastq.gz
uninf-Brady-1wk-iM-R-1_S13_R2.fastq.gz
uninf-Brady-1wk-iM-R-2_S14_R1.fastq.gz
uninf-Brady-1wk-iM-R-2_S14_R2.fastq.gz
Quality score
Base position



3.2 Genome index

To detect parasite RNA in the samples, they need to be aligned to the human and toxoplasma genomes simultaneously. There a genome index needs to be built that contains both genomes. To this end, the toxoplasma genome is placed at the end of the human genome as artificial chromosomes. Here the human genome build hg38 is used together with the current genome for toxoplasma ME49.

```
> system("cat ~/Genome/hg38/hg38.fa ToxoDB-CURRENT_TgondiiME49_Genome.fasta > hg38_toxoME49.fasta")
```

An index for the alignment is built using this combined genome.

```
> buildindex("hg38_toxoME49_index", reference = "hg38_toxoME49.fasta", indexSplit = FALSE, gappedIndex = FALSE)
```

3.3 Read alignment

All samples are aligned to the previously built index.

```
> read1 <- FastQ[targets$Read == 1]
> read2 <- FastQ[targets$Read == 2]
> subjunc(index = "hg38_toxoME49_index", readfile1 = read1, readfile2 = read2, nthreads = 15)

> targets <- targets[targets$Read == 1, -2]
```

The quality of the alignment is assessed by checking the proportion of reads that successfully mapped to the genome. This includes reads that map to coding and non-coding regions. The table below gives the following for each sample:

NumTotal total number of reads

NumMapped number of mapped reads

PropMapped proportion of mapped reads

```
> bam.files <- paste0(read1, ".subjunc.BAM")
> prop.mapped <- propmapped(bam.files)
> prop.mapped$Samples <- targets$SampleID
> prop.mapped
```

```
             Samples NumTotal NumMapped PropMapped
1      UI_Host_24h_1 32568940  30035750   0.922221
2      UI_Host_24h_2 50615278  46249722   0.913750
3      UI_Host_24h_3 18324117  16822512   0.918053
4     UI_Tachy_24h_1 25378335  23583553   0.929279
5     UI_Tachy_24h_2 24990833  23105649   0.924565
6     UI_Tachy_24h_3 26642818  24650239   0.925211
7    Inf_Tachy_24h_1 14515030  13433140   0.925464
8    Inf_Tachy_24h_2 20382137  18910545   0.927800
9    Inf_Tachy_24h_3 17396222  16152863   0.928527
10   UI_Host_1week_1 23734363  21897257   0.922597
11   UI_Host_1week_2 45077493  41093066   0.911609
12   UI_Host_1week_3 31421202  28364751   0.902726
13  UI_Brady_1week_1 14814013  13541606   0.914108
14  UI_Brady_1week_2 31702156  28959501   0.913487
15  UI_Brady_1week_3 33780906  30668689   0.907871
16 Inf_Brady_1week_1 25532620  23298091   0.912483
17 Inf_Brady_1week_2 23181811  21207180   0.914820
18 Inf_Brady_1week_3 24356630  22303883   0.915721
```

3.4 Genome annotation

Human and toxoplasma gene annotation is combined.

```
> library(limma)
> library(GenomicRanges)
> toxo_anno <- read.delim("ToxoDB-31_TgondiiME49.gff", stringsAsFactors = FALSE, comment.char = "#",
+     header = FALSE)
> toxo_anno <- toxo_anno[, ]
> toxo_anno <- toxo_anno[grepl("gene", toxo_anno[, 3]), -c(6, 8)]
> toxo_anno <- cbind(toxo_anno, strsplit2(toxo_anno$V9, ";|=")[, c(2, 4)])
> toxo_anno <- toxo_anno[, c(1, 4, 5, 6, 8, 9)]
> colnames(toxo_anno) <- c("Chr", "Start", "End", "Strand", "GeneID", "description")

> hg38_anno <- getInBuiltAnnotation("hg38")
> all.exons <- hg38_anno[grepl("chr", hg38_anno$Chr), ]
> by.geneid <- split(all.exons$Chr, all.exons$GeneID)
> gene.body <- GRanges(sapply(by.geneid, function(x) {
+     x[1]
+ }), IRanges(sapply(split(all.exons$Start, all.exons$GeneID), min), sapply(split(all.exons$End,
+     all.exons$GeneID), max)), strand = sapply(split(all.exons$Strand, all.exons$GeneID), function(x) {
+     x[1]
+ }))
> names(gene.body) <- names(by.geneid)
> hg38_anno <- data.frame(GeneID = names(by.geneid), as.data.frame(gene.body))
> colnames(hg38_anno)[2:6] <- c("Chr", "Start", "End", "Width", "Strand")
> anno_comb <- rbind(hg38_anno[, c("GeneID", "Chr", "Start", "End", "Strand")], toxo_anno[, c("GeneID",
+     "Chr", "Start", "End", "Strand")])
```

3.5 Gene counts

The number of reads mapping to genes are summarized into counts.

```
> FC <- featureCounts(bam.files, annot.ext = anno_comb, nthreads = 15, isPairedEnd = TRUE)
> colnames(FC$counts) <- targets$SampleID
```

The total number of reads aligning to genes - both human and parasite; in each sample:

```
> data.frame(Library.size = colSums(FC$counts))

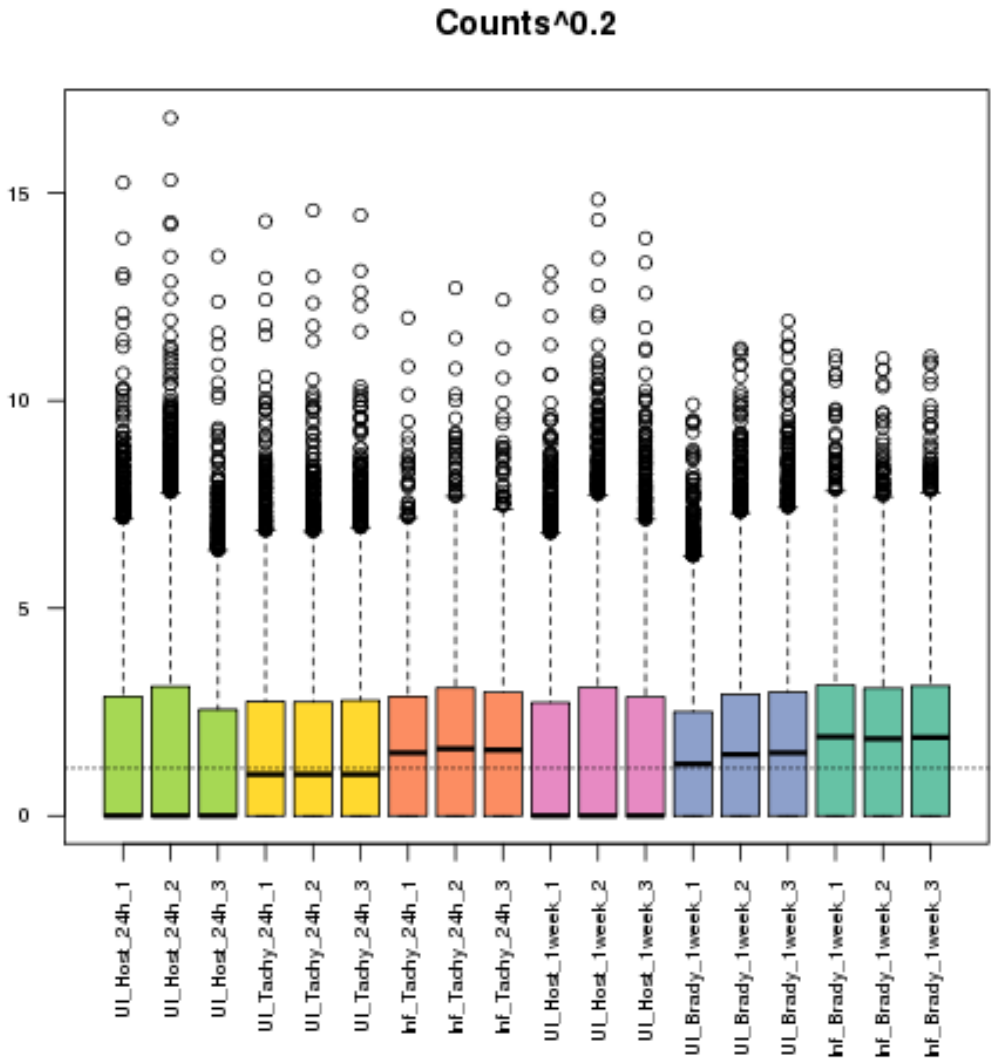
                 Library.size
UI_Host_24h_1         25281861
UI_Host_24h_2         38900004
UI_Host_24h_3         14161456
UI_Tachy_24h_1        19879074
UI_Tachy_24h_2        19346255
UI_Tachy_24h_3        20690533
Inf_Tachy_24h_1       11340211
Inf_Tachy_24h_2       15991765
Inf_Tachy_24h_3       13675103
```

```
UI_Host_1week_1       18525094
UI_Host_1week_2       34717406
UI_Host_1week_3       23917113
UI_Brady_1week_1      11334003
UI_Brady_1week_2      24172702
UI_Brady_1week_3      25592761
Inf_Brady_1week_1     19654815
Inf_Brady_1week_2     17868735
Inf_Brady_1week_3     18765231
```

Boxplots of the samples to the power of 0.2 are shown below. The median of all counts is indicated by the dotted line.

```
> library(RColorBrewer)
> group <- as.factor(targets$Group)
> group.col <- group
> levels(group.col) <- brewer.pal(6, "Set2")

> png("Plots/Boxplots_counts.png")
> par(cex.axis = 0.7, mar = c(7, 4, 4, 2))
> boxplot(FC$counts^0.2, main = "Counts^0.2", las = 2, col = as.character(group.col))
> abline(h = median(FC$counts^0.2), lty = 3)
> dev.off()
```



The counts and proportion mapped statistics are saved in the file '170323_RNAseq_subjunc_hg38parasite_toxoplasmaBradyTachy_SimonaS.RData'.

```
> Alignment_output <- list(FeatureCounts = FC, PropMapped = prop.mapped)
> save(Alignment_output, file = "170323_RNAseq_subjunc_hg38parasite_toxoplasmaBradyTachy_SimonaS.RData")
```

4 Proportion of parasite RNA

The counts for the parasite genes are extracted from the overall counts data.

```
> load("170323_RNAseq_subjunc_hg38parasite_toxoplasmaBradyTachy_SimonaS.RData")
> counts_comb <- Alignment_output$FeatureCounts$counts
> counts_toxo <- counts_comb[grepl("TGME49", row.names(counts_comb)), ]
> counts_human <- counts_comb[!grepl("TGME49", row.names(counts_comb)), ]
```

The total number of reads in each sample aligning to the toxoplasma genome:

```
> colSums(counts_toxo)
```

```
    UI_Host_24h_1     UI_Host_24h_2     UI_Host_24h_3    UI_Tachy_24h_1    UI_Tachy_24h_2    UI_Tachy_24h_3
              154               135               125             21357             20525             17282
  Inf_Tachy_24h_1   Inf_Tachy_24h_2   Inf_Tachy_24h_3   UI_Host_1week_1   UI_Host_1week_2   UI_Host_1week_3
          1353528           1940117           1555736                78               296               586
 UI_Brady_1week_1  UI_Brady_1week_2  UI_Brady_1week_3 Inf_Brady_1week_1 Inf_Brady_1week_2 Inf_Brady_1week_3
            78988            161861            191083           1645579           1419160           1628769
```

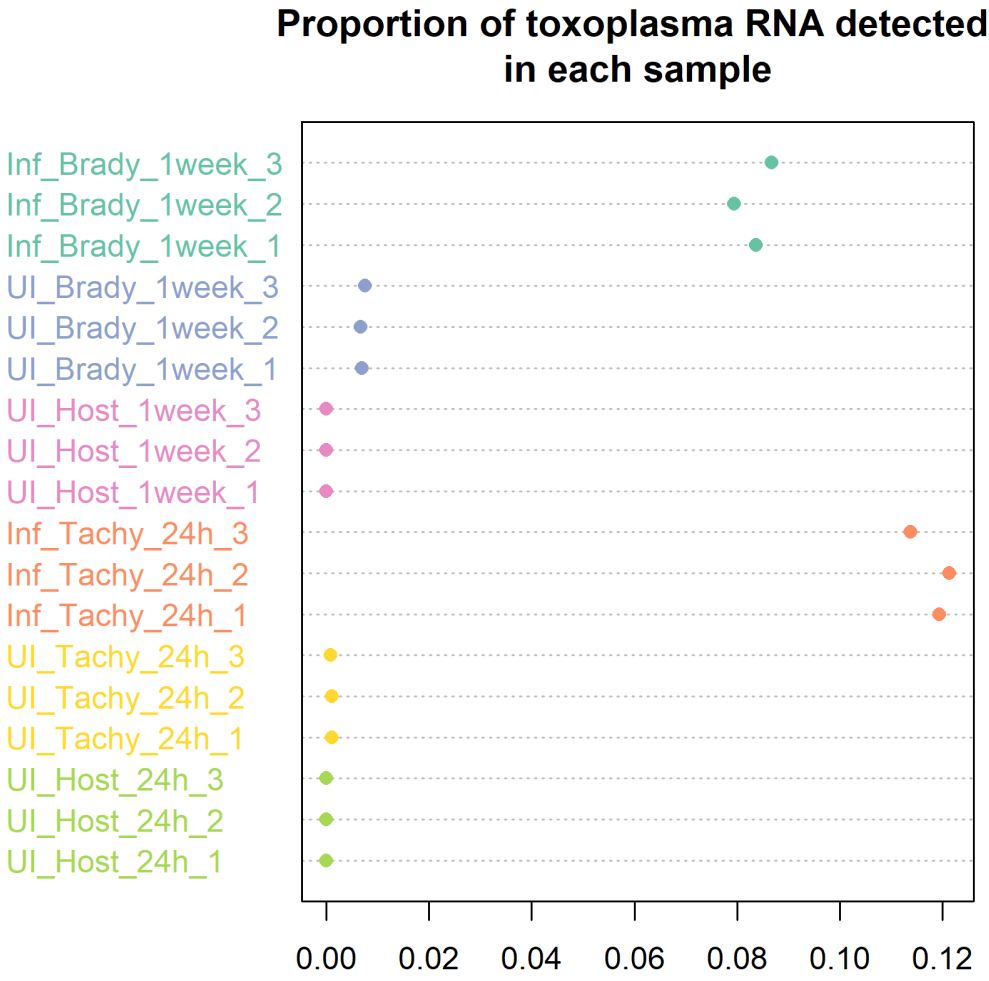
The proportion of reads mapping to toxoplasma in each sample:

```
> colSums(counts_toxo)/colSums(counts_comb)
```

```
    UI_Host_24h_1     UI_Host_24h_2     UI_Host_24h_3    UI_Tachy_24h_1    UI_Tachy_24h_2    UI_Tachy_24h_3
         6.09e-06          3.47e-06          8.83e-06          1.07e-03          1.06e-03          8.35e-04
  Inf_Tachy_24h_1   Inf_Tachy_24h_2   Inf_Tachy_24h_3   UI_Host_1week_1   UI_Host_1week_2   UI_Host_1week_3
         1.19e-01          1.21e-01          1.14e-01          4.21e-06          8.53e-06          2.45e-05
 UI_Brady_1week_1  UI_Brady_1week_2  UI_Brady_1week_3 Inf_Brady_1week_1 Inf_Brady_1week_2 Inf_Brady_1week_3
         6.97e-03          6.70e-03          7.47e-03          8.37e-02          7.94e-02          8.68e-02
```

A graphical representation of the above proportions:

```
> dotchart(colSums(counts_toxo)/colSums(counts_comb), col = as.character(group.col), pch = 16,
+     main = "Proportion of toxoplasma RNA detected \nin each sample")
```



Simona would like to know the expression of the following toxoplasma genes

- bradyzoite antigen BAG1 (TGME49_259020)
- SAG-related sequence SRS29B (TGME49_233460)
- GRA28 (TGME49_231960)
- GRA16 (TGME49_208830)
- GRA24 (TGME49_230180)
- IST (TGME49_240060)

Annotation for these genes:

```
> library(edgeR)
> toxo_anno <- toxo_anno[match(row.names(counts_toxo), toxo_anno$GeneID), ]
> toxo_anno <- cbind(toxo_anno, Length = Alignment_output$FeatureCounts$annotation[grepl("TGME49",
+     Alignment_output$FeatureCounts$annotation$GeneID), "Length"])
> DGE_toxo <- DGEList(counts_toxo, genes = toxo_anno, group = group)
> DGE_toxo$samples$lib.size <- colSums(counts_comb)
> RPKM_toxo <- rpkm(DGE_toxo)
> genes <- c("TGME49_259020", "TGME49_233460", "TGME49_231960", "TGME49_208830", "TGME49_230180",
+     "TGME49_240060")
```

```
> names(genes) <- c("BAG1", "SAG1", "GRA28", "GRA16", "GRA24", "IST")
> genes_anno <- DGE_toxo$genes[DGE_toxo$genes$GeneID %in% genes, ]
> genes_anno$Symbol <- names(genes[match(genes_anno$GeneID, genes)])
> genes_anno

                         Chr   Start     End Strand        GeneID                 description Length Symbol
TGME49_230180 TGME49_chrVIII  664211  670474      - TGME49_230180        hypothetical protein   6264  GRA24
TGME49_233460 TGME49_chrVIII 2664481 2665491      + TGME49_233460 SAG-related sequence SRS29B   1011   SAG1
TGME49_231960 TGME49_chrVIII 1670549 1677536      - TGME49_231960   omega secalin%2C putative   6988  GRA28
TGME49_259020 TGME49_chrVIIb 3023202 3025687      - TGME49_259020     bradyzoite antigen BAG1   2486   BAG1
TGME49_208830   TGME49_chrIb  888008  891283      - TGME49_208830        hypothetical protein   3276  GRA16
TGME49_240060   TGME49_chrVI 1035030 1038681      + TGME49_240060        hypothetical protein   3652    IST
```

The raw counts for these genes:

```
> y <- DGE_toxo$counts[row.names(DGE_toxo$counts) %in% genes_anno$GeneID, ]
> row.names(y) <- genes_anno$Symbol[match(row.names(y), genes_anno$GeneID)]
> y

      UI_Host_24h_1 UI_Host_24h_2 UI_Host_24h_3 UI_Tachy_24h_1 UI_Tachy_24h_2 UI_Tachy_24h_3 Inf_Tachy_24h_1
GRA24             0             0             0             15             26             12             855
SAG1              0             0             0             79             75             85            5402
GRA28             0             0             0              4              2              1             203
BAG1              0             0             0              0              0              0               0
GRA16             0             0             0             13              7             12             549
IST               0             0             0              3              6              7             407
      Inf_Tachy_24h_2 Inf_Tachy_24h_3 UI_Host_1week_1 UI_Host_1week_2 UI_Host_1week_3 UI_Brady_1week_1 UI_Brady_1week_2
GRA24            1264             965              0              0              0                9               23
SAG1             7657            6232              0              0              1               13               17
GRA28             305             282              0              0              0                4               17
BAG1                9               0              1              1              0              423              906
GRA16             670             531              0              0              0                1                7
IST               612             450              0              0              0               28               69
      UI_Brady_1week_3 Inf_Brady_1week_1 Inf_Brady_1week_2 Inf_Brady_1week_3
GRA24               16               288              184              271
SAG1                29               348              335              313
GRA28                9                94               72               78
BAG1              1141              7411             6595             6998
GRA16                4                65              102              132
IST                 65               692              617              716

> for (i in 1:nrow(y)) {
+     png(paste0("Plots/Counts_", row.names(y)[i], ".png"))
+     barplot(y[i, ], col = as.character(group.col), ylab = "count", main = row.names(y)[i],
+         las = 2)
+     dev.off()
+ }
```

The RPKM for the genes:

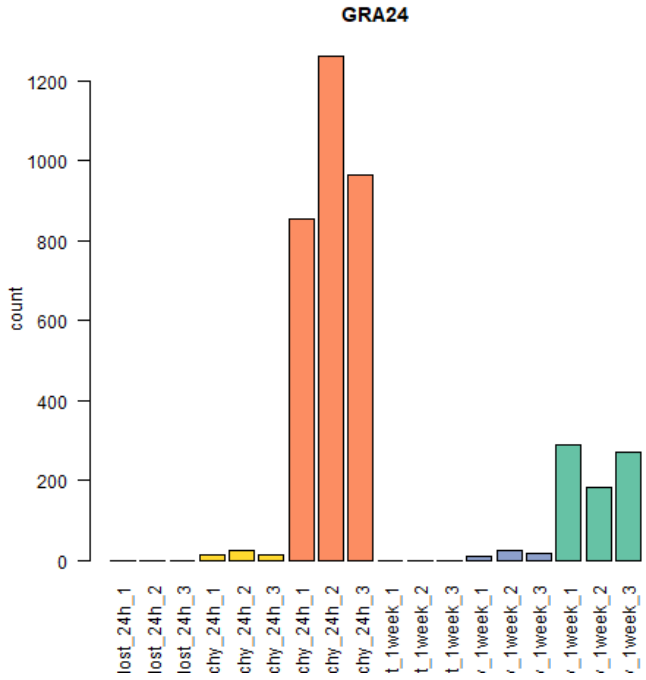
```
> x <- RPKM_toxo[row.names(RPKM_toxo) %in% genes_anno$GeneID, ]
> row.names(x) <- genes_anno$Symbol[match(row.names(x), genes_anno$GeneID)]
> x

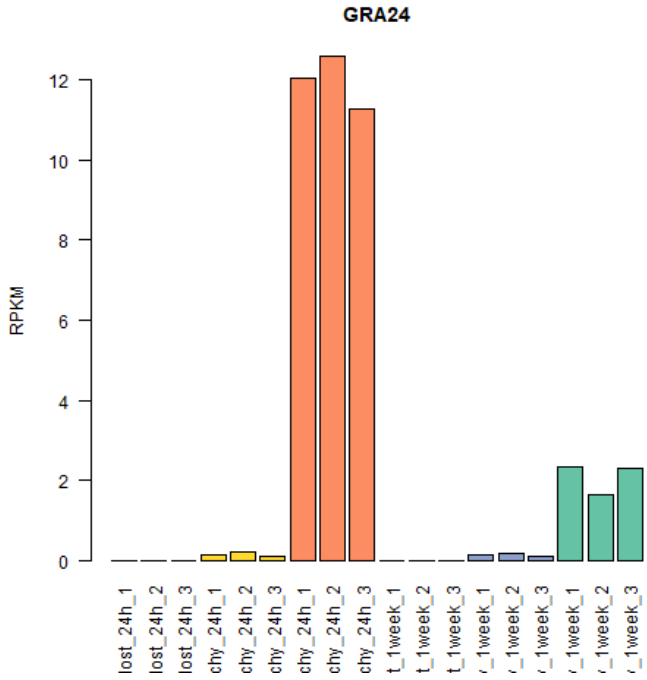
      UI_Host_24h_1 UI_Host_24h_2 UI_Host_24h_3 UI_Tachy_24h_1 UI_Tachy_24h_2 UI_Tachy_24h_3 Inf_Tachy_24h_1
GRA24             0             0             0         0.1205         0.2145        0.09259          12.04
SAG1              0             0             0         3.9308         3.8345        4.06346         471.18
GRA28             0             0             0         0.0288         0.0148        0.00692           2.56
BAG1              0             0             0         0.0000         0.0000        0.00000           0.00
GRA16             0             0             0         0.1996         0.1104        0.17704          14.78
IST               0             0             0         0.0413         0.0849        0.09264           9.83
      Inf_Tachy_24h_2 Inf_Tachy_24h_3 UI_Host_1week_1 UI_Host_1week_2 UI_Host_1week_3 UI_Brady_1week_1 UI_Brady_1week_2
GRA24          12.618          11.27          0.0000          0.0000          0.0000          0.1268          0.1519
SAG1          473.599         450.76          0.0000          0.0000          0.0414          1.1345          0.6956
GRA28           2.729           2.95          0.0000          0.0000          0.0000          0.0505          0.1006
BAG1            0.226           0.00          0.0217          0.0116          0.0000         15.0126         15.0765
GRA16          12.789          11.85          0.0000          0.0000          0.0000          0.0269          0.0884
IST            10.479           9.01          0.0000          0.0000          0.0000          0.6765          0.7816
      UI_Brady_1week_3 Inf_Brady_1week_1 Inf_Brady_1week_2 Inf_Brady_1week_3
GRA24           0.0998             2.339             1.644             2.305
SAG1            1.1208            17.513            18.544            16.498
```

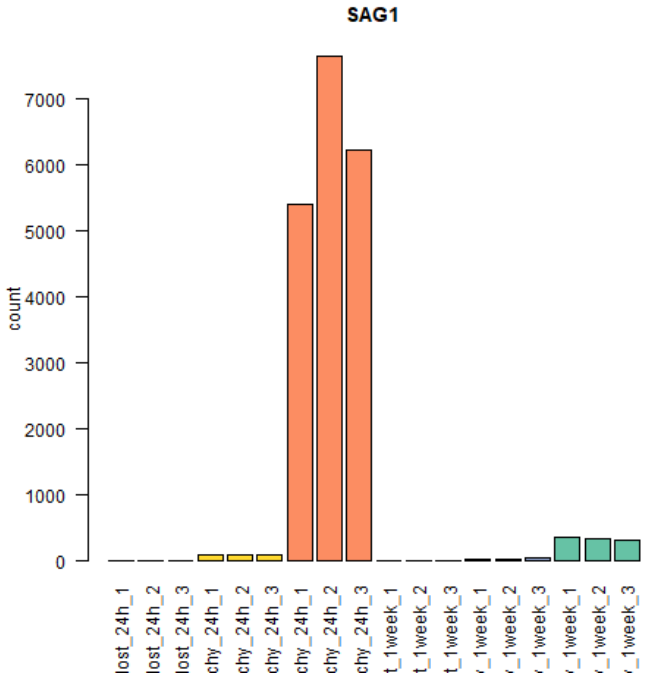
```
GRA28           0.0503           0.684           0.577           0.595
BAG1           17.9336         151.672         148.464         150.010
GRA16           0.0477           1.009           1.742           2.147
IST             0.6954           9.641           9.455          10.448

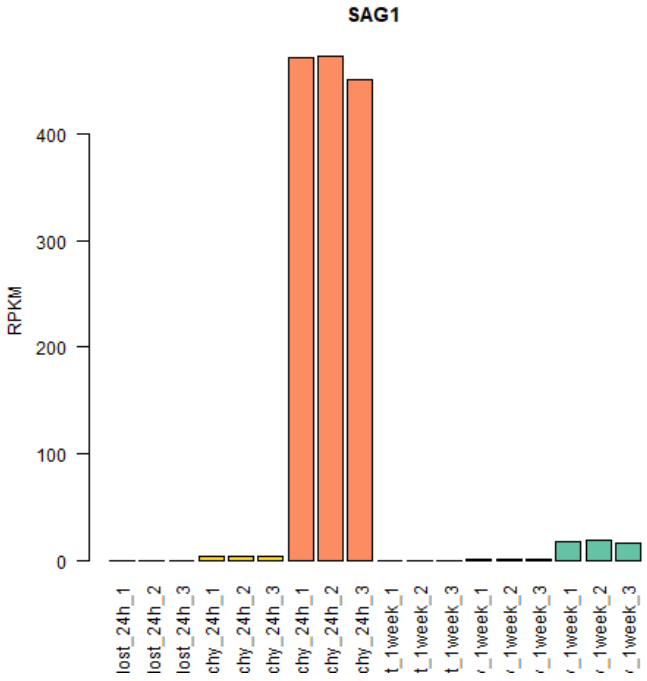
> for (i in 1:nrow(x)) {
+     png(paste0("Plots/RPKM_", row.names(x)[i], ".png"))
+     barplot(x[i, ], col = as.character(group.col), ylab = "RPKM", main = row.names(x)[i], las = 2)
+     dev.off()
+ }
```

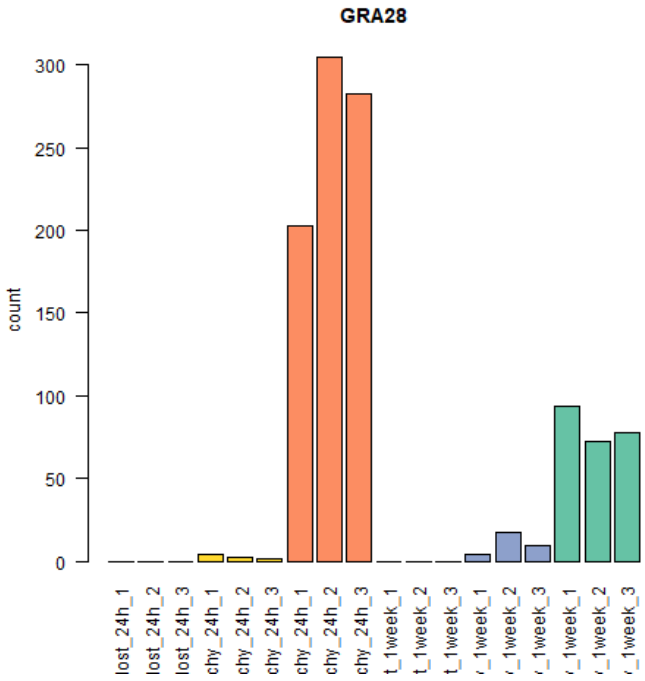
Plots of the counts and RPKMs:

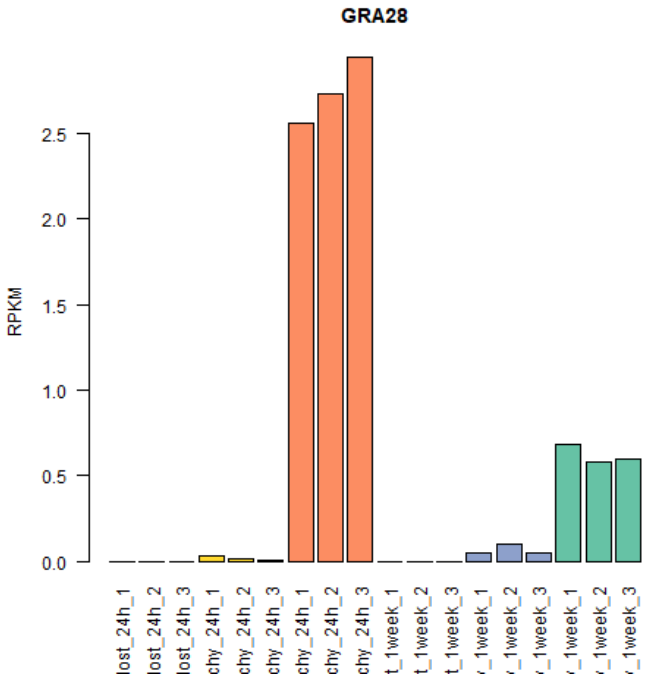


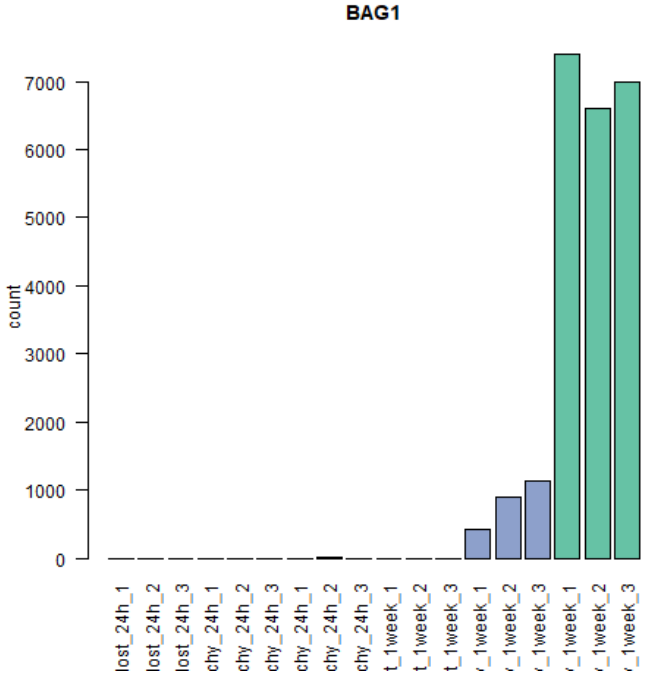


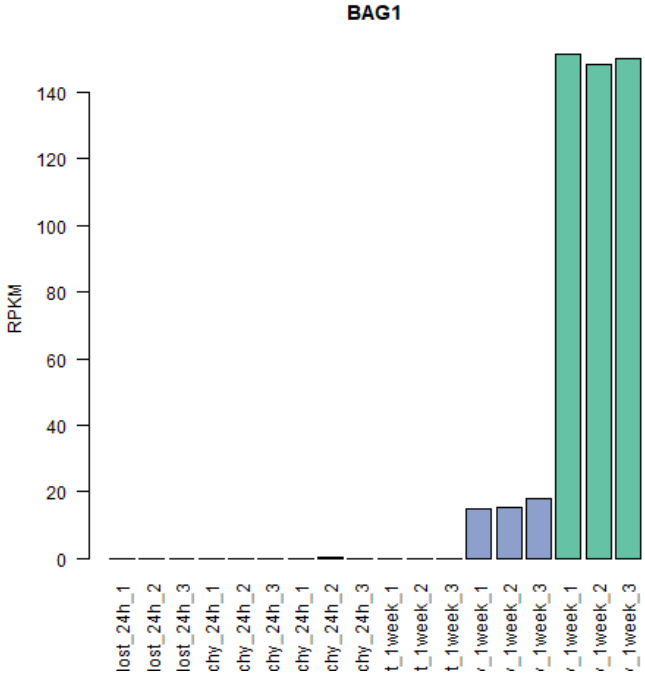


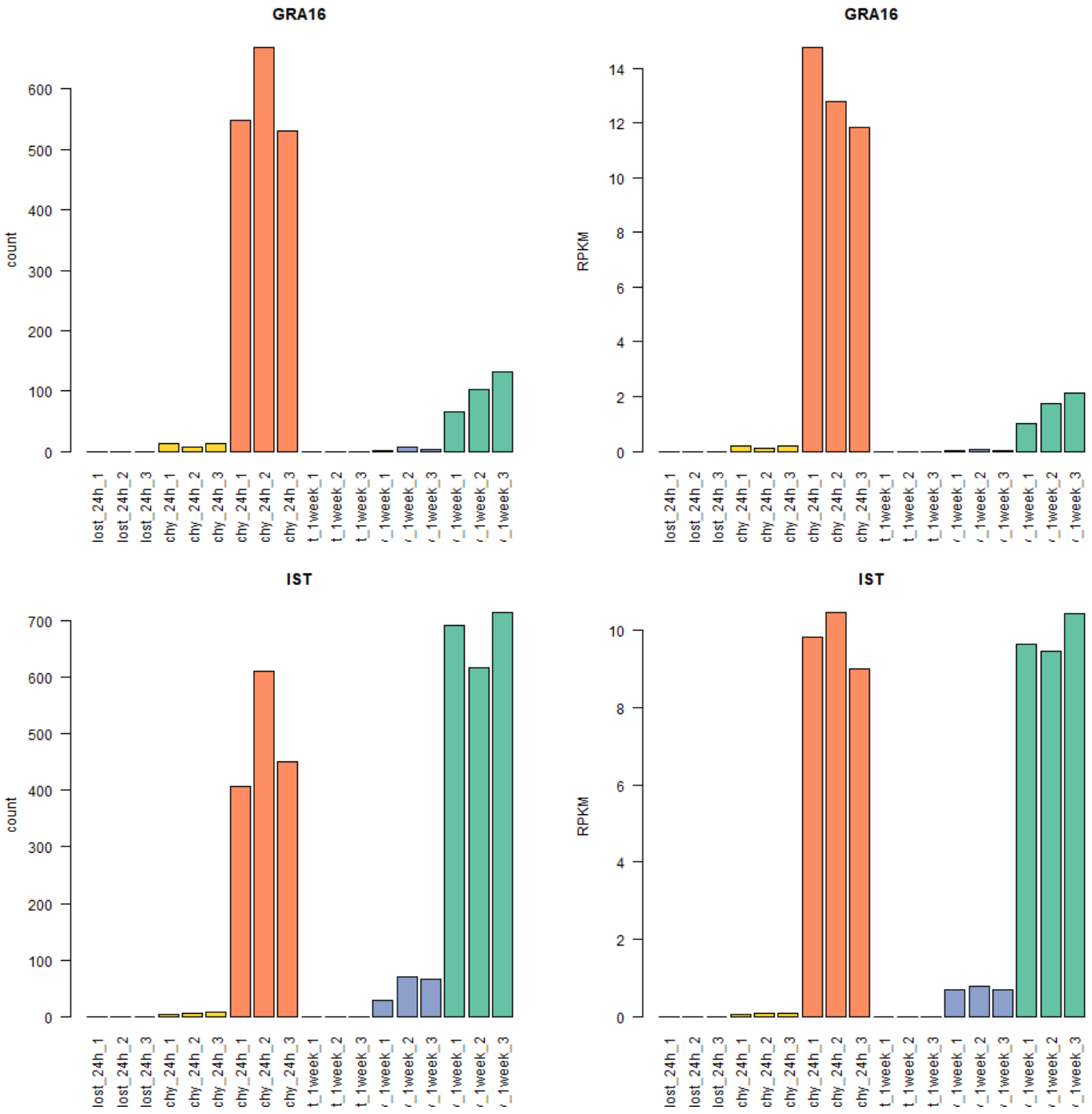



GRA28
count
0
50
100
150
200
250
300
lost_24h_1
lost_24h_2
lost_24h_3
chy_24h_1
chy_24h_2
chy_24h_3
chy_24h_1
chy_24h_2
chy_24h_3
t_1week_1
t_1week_2
t_1week_3
_1week_1
_1week_2
_1week_3
_1week_1
_1week_2
_1week_3


GRA28
RPKM
0.0
0.5
1.0
1.5
2.0
2.5
lost_24h_1
lost_24h_2
lost_24h_3
chy_24h_1
chy_24h_2
chy_24h_3
chy_24h_1
chy_24h_2
chy_24h_3
t_1week_1
t_1week_2
t_1week_3
_1week_1
_1week_2
_1week_3
_1week_1
_1week_2
_1week_3


BAG1
count
0
1000
2000
3000
4000
5000
6000
7000
lost_24h_1
lost_24h_2
lost_24h_3
chy_24h_1
chy_24h_2
chy_24h_3
chy_24h_1
chy_24h_2
chy_24h_3
t_1week_1
t_1week_2
t_1week_3
_1week_1
_1week_2
_1week_3
_1week_1
_1week_2
_1week_3


BAG1
RPKM
0
20
40
60
80
100
120
140
lost_24h_1
lost_24h_2
lost_24h_3
chy_24h_1
chy_24h_2
chy_24h_3
chy_24h_1
chy_24h_2
chy_24h_3
t_1week_1
t_1week_2
t_1week_3
_1week_1
_1week_2
_1week_3
_1week_1
_1week_2
_1week_3



5 Additional human gene annotation

Additional annotation for the human genes is added from the NCBI database, ftp://ftp.ncbi.nlm.nih.gov/gene/DATA/GENE_INFO/
The human annotation is stored in the Homo_sapiens.gene_info.gz file. Note the January 2017 version is used.

```
> lib <- "~/GeneInformationSets/HumanGenomeAnnotation/Homo_sapiens.gene_info_Jan17.gz"
> annotation.library <- read.delim(lib, stringsAsFactors = FALSE)
> annotation <- annotation.library[match(row.names(counts_human), annotation.library$GeneID),
+     c("GeneID", "Symbol", "description", "chromosome", "Synonyms", "type_of_gene")]
> annotation <- cbind(annotation, Length = Alignment_output$FeatureCounts$annotation[!grepl("TGME49",
+     Alignment_output$FeatureCounts$annotation$GeneID), "Length"])
```

The available annotation for each gene:

```
> colnames(annotation)

[1] "GeneID"       "Symbol"       "description"  "chromosome"   "Synonyms"     "type_of_gene" "Length"
```

6 Data filtering and normalization

6.1 Filtering

Genes should only be included in the analysis if they are truly expressed. Lowly expressed genes need to therefore be filtered from the data.

```
> DGE_human <- DGEList(counts_human, genes = annotation, group = group)
> CPM_human <- cpm(DGE_human)
> summary(CPM_human)

 UI_Host_24h_1   UI_Host_24h_2   UI_Host_24h_3   UI_Tachy_24h_1  UI_Tachy_24h_2  UI_Tachy_24h_3  Inf_Tachy_24h_1
 Min.   :    0   Min.   :    0   Min.   :    0   Min.   :    0   Min.   :    0   Min.   :    0   Min.   :    0
 1st Qu.:    0   1st Qu.:    0   1st Qu.:    0   1st Qu.:    0   1st Qu.:    0   1st Qu.:    0   1st Qu.:    0
 Median :    0   Median :    0   Median :    0   Median :    0   Median :    0   Median :    0   Median :    0
 Mean   :   35   Mean   :   35   Mean   :   35   Mean   :   35   Mean   :   35   Mean   :   35   Mean   :   35
 3rd Qu.:   20   3rd Qu.:   19   3rd Qu.:   20   3rd Qu.:   21   3rd Qu.:   21   3rd Qu.:   21   3rd Qu.:   23
 Max.   :32646   Max.   :34523   Max.   :31404   Max.   :30336   Max.   :34139   Max.   :30668   Max.   :24860
 Inf_Tachy_24h_2 Inf_Tachy_24h_3 UI_Host_1week_1 UI_Host_1week_2 UI_Host_1week_3 UI_Brady_1week_1 UI_Brady_1week_2
 Min.   :    0   Min.   :    0   Min.   :    0   Min.   :    0   Min.   :    0   Min.   :   0     Min.   :   0
 1st Qu.:    0   1st Qu.:    0   1st Qu.:    0   1st Qu.:    0   1st Qu.:    0   1st Qu.:   0     1st Qu.:   0
 Median :    0   Median :    0   Median :    0   Median :    0   Median :    0   Median :   0     Median :   0
 Mean   :   35   Mean   :   35   Mean   :   35   Mean   :   35   Mean   :   35   Mean   :  35     Mean   :  35
 3rd Qu.:   23   3rd Qu.:   23   3rd Qu.:   21   3rd Qu.:   21   3rd Qu.:   21   3rd Qu.:  22     3rd Qu.:  23
 Max.   :23643   Max.   :24472   Max.   :20820   Max.   :20771   Max.   :21798   Max.   :8498     Max.   :7554
 UI_Brady_1week_3 Inf_Brady_1week_1 Inf_Brady_1week_2 Inf_Brady_1week_3
 Min.   :   0     Min.   :   0      Min.   :   0      Min.   :   0
 1st Qu.:   0     1st Qu.:   0      1st Qu.:   0      1st Qu.:   0
 Median :   0     Median :   0      Median :   0      Median :   0
 Mean   :  35     Mean   :  35      Mean   :  35      Mean   :  35
 3rd Qu.:  23     3rd Qu.:  24      3rd Qu.:  24      3rd Qu.:  24
 Max.   :9473     Max.   :9305      Max.   :9876      Max.   :9671

> median(CPM_human)

[1] 0.193

> 10/(1e-06 * colSums(DGE_human$counts))

    UI_Host_24h_1     UI_Host_24h_2     UI_Host_24h_3    UI_Tachy_24h_1    UI_Tachy_24h_2    UI_Tachy_24h_3
            0.396             0.257             0.706             0.504             0.517             0.484
  Inf_Tachy_24h_1   Inf_Tachy_24h_2   Inf_Tachy_24h_3   UI_Host_1week_1   UI_Host_1week_2   UI_Host_1week_3
            1.001             0.712             0.825             0.540             0.288             0.418
 UI_Brady_1week_1  UI_Brady_1week_2  UI_Brady_1week_3 Inf_Brady_1week_1 Inf_Brady_1week_2 Inf_Brady_1week_3
            0.888             0.416             0.394             0.555             0.608             0.584

> table(group)

group
Inf_Brady_1week   Inf_Tachy_24h  UI_Brady_1week   UI_Host_1week     UI_Host_24h    UI_Tachy_24h
              3               3               3               3               3               3
```

Any gene that does not achieve a count per million reads (CPM) greater than 1 in at least 3 samples is filtered. Furthermore, any gene which does not have a symbol are also removed.

```
> is.exprs_human <- rowSums(CPM_human > 0.5) >= 3
> table(is.exprs_human)

is.exprs_human
FALSE  TRUE
14479 13846

> has.sym <- !is.na(DGE_human$genes$Symbol)
> table(has.sym)
```

```
has.sym
FALSE  TRUE
  316 28009

> DGE_human <- DGE_human[is.exprs_human & has.sym, , keep.lib.sizes = FALSE]
```

After filtering 13793 genes remain for downstream analysis.

6.2 Normalization

RNA composition within each sample is normalized using the TMM method. This method calculates a scaling factor for each sample using the weighted trimmed mean of log-expression ratios. This scaling factors aims to minimize the log-fold changes between the samples for the majority of genes. Ideally all scaling factors should be around 1.

```
> DGE_human <- calcNormFactors(DGE_human, method = "TMM")
> DGE_human$samples

                          group lib.size norm.factors
UI_Host_24h_1         UI_Host_24h 25270514        0.938
UI_Host_24h_2         UI_Host_24h 38879938        0.933
UI_Host_24h_3         UI_Host_24h 14154696        0.956
UI_Tachy_24h_1       UI_Tachy_24h 19849717        0.946
UI_Tachy_24h_2       UI_Tachy_24h 19317359        0.945
UI_Tachy_24h_3       UI_Tachy_24h 20664433        0.938
Inf_Tachy_24h_1     Inf_Tachy_24h  9982469        1.001
Inf_Tachy_24h_2     Inf_Tachy_24h 14045475        0.996
Inf_Tachy_24h_3     Inf_Tachy_24h 12113899        0.991
UI_Host_1week_1     UI_Host_1week 18515922        1.007
UI_Host_1week_2     UI_Host_1week 34699910        1.008
UI_Host_1week_3     UI_Host_1week 23904887        0.986
UI_Brady_1week_1   UI_Brady_1week 11249708        1.036
UI_Brady_1week_2   UI_Brady_1week 23998663        1.054
UI_Brady_1week_3   UI_Brady_1week 25387424        1.043
Inf_Brady_1week_1 Inf_Brady_1week 17998750        1.077
Inf_Brady_1week_2 Inf_Brady_1week 16439960        1.077
Inf_Brady_1week_3 Inf_Brady_1week 17125679        1.090
```

7 The design matrix

The design matrix mathematically represents the design of the experiment.

```
> design_human <- model.matrix(~0 + group)
> colnames(design_human) <- levels(group)
> row.names(design_human) <- targets$SampleID
> design_human

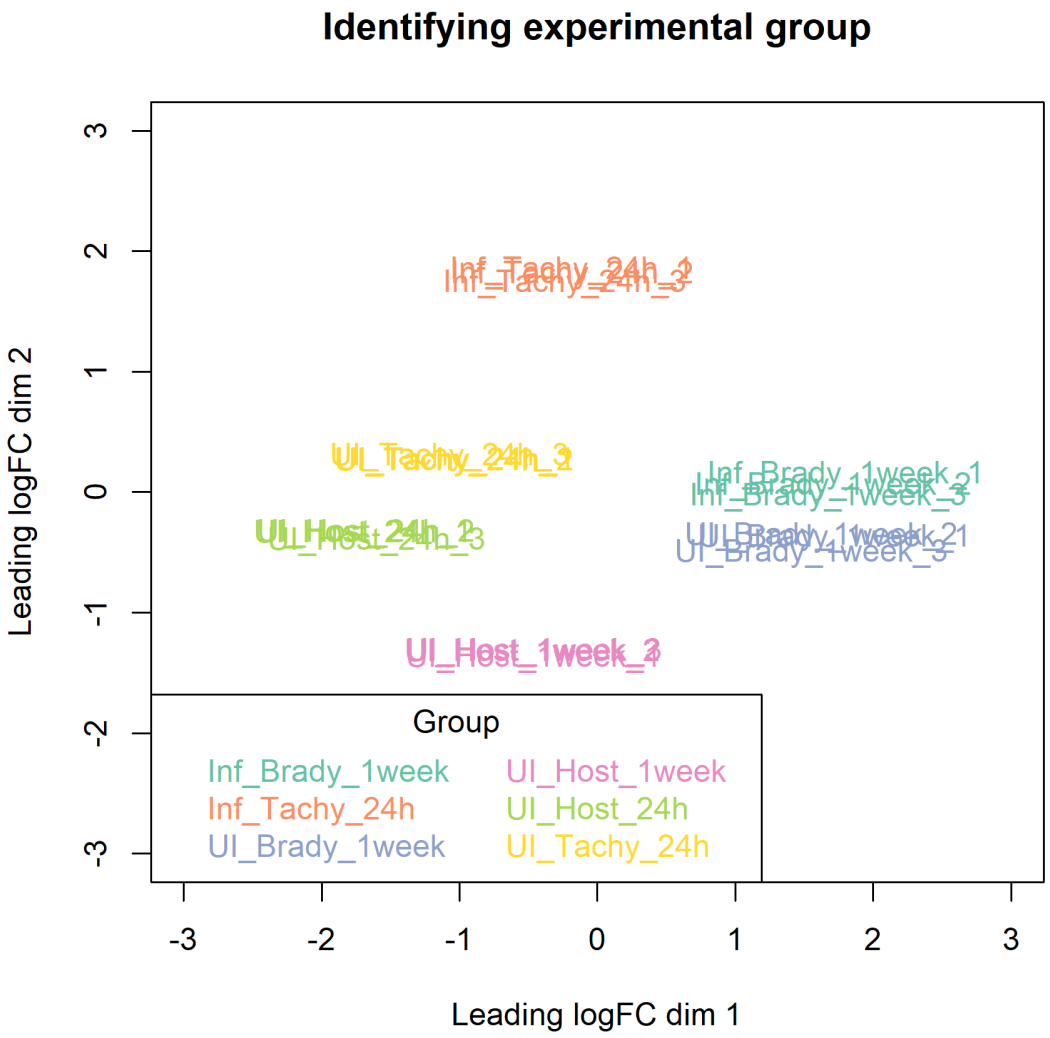
                 Inf_Brady_1week Inf_Tachy_24h UI_Brady_1week UI_Host_1week UI_Host_24h UI_Tachy_24h
UI_Host_24h_1                  0             0              0             0          1             0
UI_Host_24h_2                  0             0              0             0          1             0
UI_Host_24h_3                  0             0              0             0          1             0
UI_Tachy_24h_1                 0             0              0             0          0             1
UI_Tachy_24h_2                 0             0              0             0          0             1
UI_Tachy_24h_3                 0             0              0             0          0             1
Inf_Tachy_24h_1                0             1              0             0          0             0
Inf_Tachy_24h_2                0             1              0             0          0             0
Inf_Tachy_24h_3                0             1              0             0          0             0
UI_Host_1week_1                0             0              0             1          0             0
UI_Host_1week_2                0             0              0             1          0             0
UI_Host_1week_3                0             0              0             1          0             0
UI_Brady_1week_1               0             0              1             0          0             0
UI_Brady_1week_2               0             0              1             0          0             0
UI_Brady_1week_3               0             0              1             0          0             0
Inf_Brady_1week_1              1             0              0             0          0             0
Inf_Brady_1week_2              1             0              0             0          0             0
Inf_Brady_1week_3              1             0              0             0          0             0
attr(,"assign")
[1] 1 1 1 1 1 1
attr(,"contrasts")
attr(,"contrasts")$group
[1] "contr.treatment"
```

8 Data exploration

8.1 Sample clustering

The multi-dimensional scaling (MDS) plot below shows the unsupervised clustering of the samples. On an MDS plot, each sample is plotted according to the distance between it and all other samples. This distance is calculated using the top 500 most variable genes between each pair of samples. Therefore, samples that are more similar will appear closer together, while those that are more different will be further apart. The MDS plot below is coloured according to the experimental group of the samples.

```
> plotMDS(DGE_human, col = as.character(group.col), xlim = c(-3, 3), ylim = c(-3, 3), main = "Identifying experimental group")
> legend("bottomleft", legend = levels(group), text.col = levels(group.col), ncol = 2, title = "Group",
+     title.col = "black")
```



This plot shows that good clustering is achieved within each groups and all groups are nicely separated. Additionally, the tachy and brady samples are grouped together on opposite sides of the plot.

8.2 Biological variation

The biological variation between the samples is estimated.

```
> disp_human <- estimateDisp(DGE_human, design = design_human)
```

The biological coefficient of variation (BCV) is determined. The BCV indicates how the abundance of each gene varies between replicate samples. The common BCV:

```
> BCV_human <- sqrt(disp_human$common.dispersion)
> BCV_human

[1] 0.0611
```

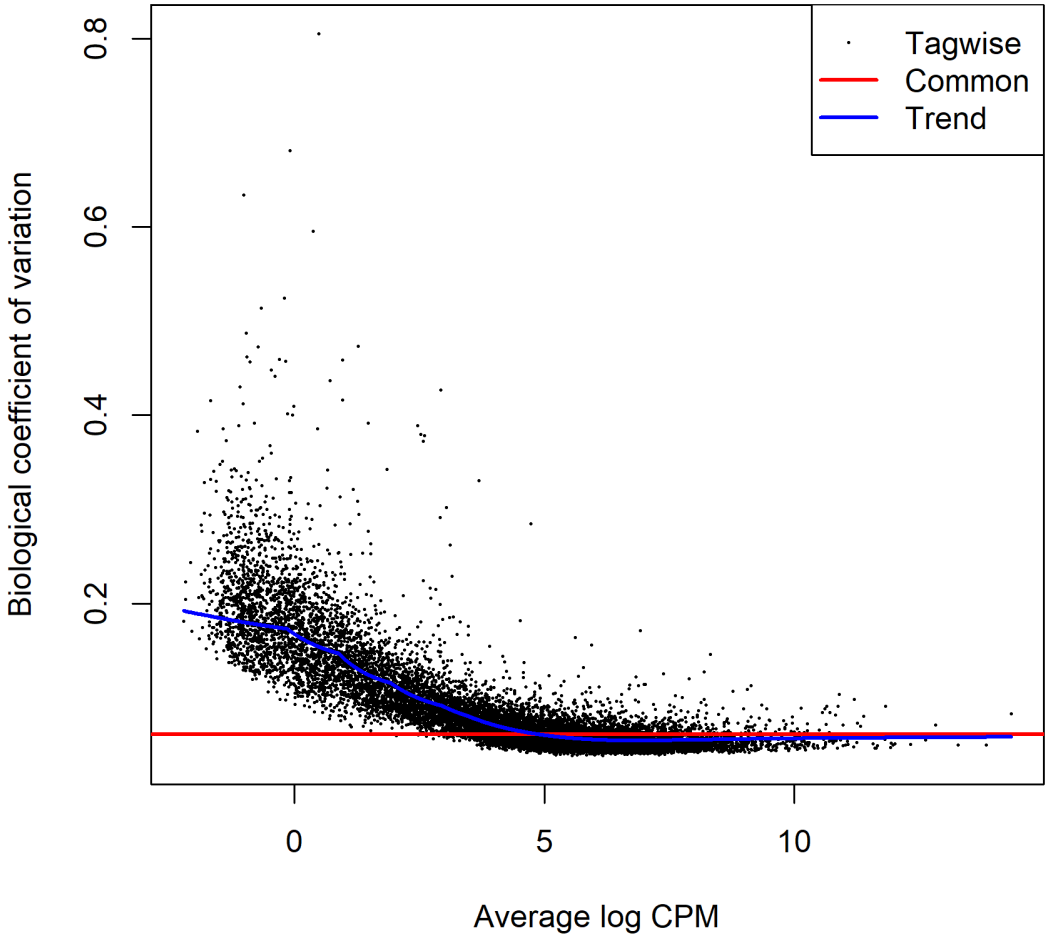
A summary of the gene specific BCVs:

```
> summary(sqrt(disp_human$tagwise.dispersion))

   Min. 1st Qu.  Median    Mean 3rd Qu.    Max.
  0.038   0.053   0.065   0.088   0.103   0.805
```

A plot of the average $\log_2$-CPM versus the BCV for each gene is shown. This plot visualises how gene variation (y-axis) between replicate samples changes as gene abundance (x-axis) increases. As you can see, gene variability decreases as abundance increases.

```
> plotBCV(disp_human)
```



9 Differential expression analysis

The data is transformed to $\log_2$-CPM.

Appendix C -

Data set 2: Data alignment, normalisation, filtering, and exploration
Code and processing was completed by Dr. Alexandra Garnham from WEHI

Code

RNAseq: Toxoplasma (bradyzoites) infected human fibroblasts KO and WT

Alexandra Garnham

2018-05-08

1 Background

The report details the analysis of RNA-sequencing data provided by Simona Seizova and Chris Tonkin (Tonkin lab, Infection and Immunity). These data consist of 15 samples of human fibroblasts taken from a single donor. The samples fall into one of 5 experimental groups with 3 samples per group. Each sample is a biological replicate. The groups are described in the table below.

Group	Description
UI Host	Un-infected (UI) host samples
UI Brady WT	Samples treated with wild type (WT) bradyzoites but remain un-infected
UI Myr1 KO Brady	Samples treated with Myr1 knock-out (KO) bradyzoites by remain un-infected
Infected Brady WT	Samples infected with WT bradyzoites
Infected Myr1 KO Brady	Samples infected with Myr1 KO bradyzoites

Simona would like to identify differentially expressed genes between all groups followed by pathway analysis if applicable.

Hide

```
library(Rsubread)
library(Rsamtools)
library(GenomicRanges)
```

Hide

```
library(EBImage)
library(RColorBrewer)
library(limma)
library(edgeR)
library(matrixStats)
library(Glimma)
```

2 Sample information

Experimental information regarding each sample is displayed below.

Hide

```
targets <- read.delim("Human_Toxo_Brady_WTvsKO_targets.txt", stringsAsFactors = FALSE)
targets[targets$Read == 1, ]
```

	FileName <chr>	Read <int>
1	Host-Uninf-Rep-1_S1_R1.fastq.gz	1
3	Host-Uninf-Rep-2_S2_R1.fastq.gz	1
5	Host-Uninf-Rep-3_S3_R1.fastq.gz	1
7	Uninf-PCA-Brady-Rep-1_S7_R1.fastq.gz	1
9	Uninf-PCA-Brady-Rep-2_S8_R1.fastq.gz	1
11	Uninf-PCA-Brady-Rep-3_S9_R1.fastq.gz	1
13	Uninf-PCAdelMyr1-Brady-Rep-1_S13_R1.fastq.gz	1
15	Uninf-PCAdelMyr1-Brady-Rep-2_S14_R1.fastq.gz	1
17	Uninf-PCAdelMyr1-Brady-Rep-3_S15_R1.fastq.gz	1
19	inf-PCA-Brady-Rep-1_S4_R1.fastq.gz	1

1-10 of 15 rows | 1-3 of 8 columns Previous 1 2 Next

Description <chr>	Infection <chr>	ToxoTreated <chr>
Host Uninfected 1wk iM Rep 1	UI	Host
Host Uninfected 1wk iM Rep 2	UI	Host
Host Uninfected 1wk iM Rep 3	UI	Host
Uninfected PCA Brady 1wk iM Rep 1	UI	Brady_WT
Uninfected PCA Brady 1wk iM Rep 2	UI	Brady_WT
Uninfected PCA Brady 1wk iM Rep 3	UI	Brady_WT
Uninfected PCA?Myr1 Brady 1wk iM Rep 1	UI	Brady_Myr1_KO
Uninfected PCA?Myr1 Brady 1wk iM Rep 2	UI	Brady_Myr1_KO
Uninfected PCA?Myr1 Brady 1wk iM Rep 3	UI	Brady_Myr1_KO
Infected PCA Brady 1wk iM Rep 1	Infected	Brady_WT

1-10 of 15 rows | 4-6 of 8 columns Previous 1 2 Next

Infection <chr>	ToxoTreated <chr>	Group <chr>	Replicate <int>	SampleID <chr>
UI	Host	UI_Host	1	UI_Host_1
UI	Host	UI_Host	2	UI_Host_2
UI	Host	UI_Host	3	UI_Host_3
UI	Brady_WT	UI_Brady_WT	1	UI_Brady_WT_1
UI	Brady_WT	UI_Brady_WT	2	UI_Brady_WT_2
UI	Brady_WT	UI_Brady_WT	3	UI_Brady_WT_3
UI	Brady_Myr1_KO	UI_Brady_Myr1_KO	1	UI_Brady_Myr1_KO_1
UI	Brady_Myr1_KO	UI_Brady_Myr1_KO	2	UI_Brady_Myr1_KO_2
UI	Brady_Myr1_KO	UI_Brady_Myr1_KO	3	UI_Brady_Myr1_KO_3
Infected	Brady_WT	Infected_Brady_WT	1	Infected_Brady_WT_1

1-10 of 15 rows | 5-9 of 8 columns Previous 1 2 Next

	FileName <chr>	Read <int>
21	inf-PCA-Brady-Rep-2_S5_R1.fastq.gz	1
23	inf-PCA-Brady-Rep-3_S6_R1.fastq.gz	1
25	inf-PCAdelMyr1-Brady-Rep-1_S10_R1.fastq.gz	1
27	inf-PCAdelMyr1-Brady-Rep-2_S11_R1.fastq.gz	1
29	inf-PCAdelMyr1-Brady-Rep-3_S12_R1.fastq.gz	1

11-15 of 15 rows | 1-3 of 8 columns Previous 1 2 Next

Description <chr>	Infection <chr>	ToxoTreated <chr>
Infected PCA Brady 1wk iM Rep 2	Infected	Brady_WT
Infected PCA Brady 1wk iM Rep 3	Infected	Brady_WT
Infected PCA?Myr1 Brady 1wk iM Rep 1	Infected	Brady_Myr1_KO
Infected PCA?Myr1 Brady 1wk iM Rep 2	Infected	Brady_Myr1_KO
Infected PCA?Myr1 Brady 1wk iM Rep 3	Infected	Brady_Myr1_KO

11-15 of 15 rows | 4-6 of 8 columns Previous 1 2 Next

Infection <chr>	ToxoTreated <chr>	Group <chr>	Replicate <int>	SampleID <chr>
Infected	Brady_WT	Infected_Brady_WT	2	Infected_Brady_WT_2
Infected	Brady_WT	Infected_Brady_WT	3	Infected_Brady_WT_3
Infected	Brady_Myr1_KO	Infected_Brady_Myr1_KO	1	Infected_Brady_Myr1_KO_1
Infected	Brady_Myr1_KO	Infected_Brady_Myr1_KO	2	Infected_Brady_Myr1_KO_2
Infected	Brady_Myr1_KO	Infected_Brady_Myr1_KO	3	Infected_Brady_Myr1_KO_3

11-15 of 15 rows | 5-9 of 8 columns Previous 1 2 Next

3 Data generation

3.1 FastQ files

All samples were sequenced by Stephen Wilcox (Systems Biology and Personalised Medicine, Genomics lab) on an Illumina NextSeq machine using 75bp paired end reads. The quality of the sequencing is checked by running the samples through the FastQC program. This program generates a report on every fastQ file. A summary of these reports can be found here.

Hide

```
system("fastqc simonaS140917/*.fastq.gz")
system("multiqc .")
```

3.2 Alignment

Simona would like to determine the level of parasite RNA present in the samples. To determine this, the samples are aligned to both the human and toxoplasma genomes simultaneously. For this alignment, the genome index for the combined genome used in Simona's previous RNAseq data (Human WT toxoplasma infected fibroblasts) is utilized. The proportion of reads successfully mapped to the genome is shown in the table below. The table gives for each sample:

- **NumTotal** total number of reads
- **NumMapped** number of mapped reads
- **PropMapped** proportion of mapped reads

Hide

```
read1 <- paste0("simonaS140917/", targets$FileName[targets$Read == 1])
read2 <- paste0("simonaS140917/", targets$FileName[targets$Read == 2])
subjunc(index = "/home/users/allstaff/garnham.a/Projects/InfectionAndImmunity/TokinLab/SimonaSeizov
a/Human_Toxoplasma_fibroblasts/hg38_toxoME49_index",
    readfile1 = read1, readfile2 = read2, nthreads = 10)
bam.files_subjunc <- paste0("simonaS140917/HumanToxoAlignment_subjunc/", targets$FileName[targets$Re
ad ==
    1], ".subjunc.BAM")
prop.mapped <- propmapped(bam.files_subjunc)
prop.mapped$Samples <- targets$SampleID[targets$Read == 1]
prop.mapped
```

Hide

```
targets <- targets[targets$Read == 1, ]
```

```
                  Samples NumTotal NumMapped PropMapped
1                UI_Host_1 37552992  33458714   0.890973
2                UI_Host_2 52832427  47230138   0.893961
3                UI_Host_3 53640369  47346690   0.882669
4             UI_Brady_WT_1 33833747  31407901   0.928301
5             UI_Brady_WT_2 57674999  53342558   0.924882
6             UI_Brady_WT_3 30866280  28673785   0.928968
7         UI_Brady_Myr1_KO_1 17990183  16474444   0.915746
8         UI_Brady_Myr1_KO_2 25106892  23299039   0.927994
9         UI_Brady_Myr1_KO_3 20217419  18636554   0.921807
10      Infected_Brady_WT_1 67479722  62581244   0.927408
11      Infected_Brady_WT_2 25312504  23404570   0.924625
12      Infected_Brady_WT_3 68276583  63444697   0.929231
13 Infected_Brady_Myr1_KO_1 23096819  21492393   0.930535
14 Infected_Brady_Myr1_KO_2 21963611  20456406   0.931377
15 Infected_Brady_Myr1_KO_3 28681287  26721213   0.931660
```

3.3 Summarization

The reads are summarized into counts over both human and viral genes. Genes are identified using RefSeq annotation to the human genome and annotation for the parasite genome downloaded from http://toxodb.org/toxo/. Below is a barplot of of the following proportions:

- reads assigned to genes (human or viral)
- reads unassigned due to lack of annotated features in mapped locations
- reads unassigned due to mapping ambiguity
- reads that are unmapped

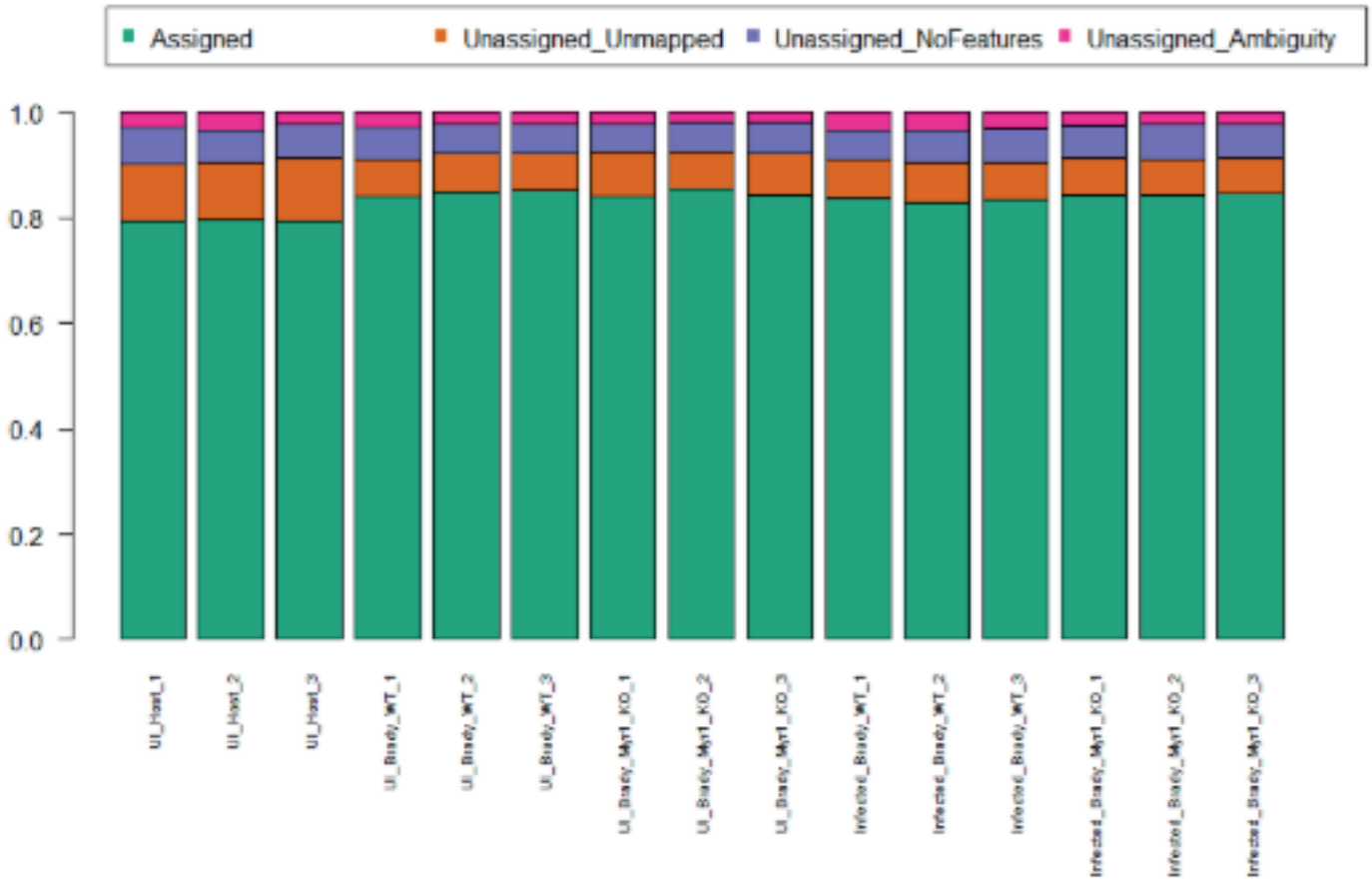
Hide

```
toxo_anno <- read.delim("~/Projects/InfectionAndImmunity/TokinLab/SimonaSeizova/Human_Toxoplasma_fib
roblasts/ToxoDB-31_TgondiiME49.gff",
    stringsAsFactors = FALSE, comment.char = "#", header = FALSE)
# toxo gene
toxo_anno_gene <- toxo_anno[grepl("gene", toxo_anno[, 3]), -c(6, 8)]
toxo_anno_gene <- cbind(toxo_anno_gene, strsplit2(toxo_anno_gene$V9, ";|=")[,
    c(2, 4)])
toxo_anno_gene <- toxo_anno_gene[, c(1, 4, 5, 6, 8, 9)]
colnames(toxo_anno_gene) <- c("Chr", "Start", "End", "Strand", "GeneID", "description")
# toxo exon
toxo_anno_exon <- toxo_anno[grepl("exon", toxo_anno[, 3]), -c(6, 8)]
toxo_anno_exon <- cbind(toxo_anno_exon, strsplit2(toxo_anno_exon$V9, ";|=")[,
    c(2, 4)])
toxo_anno_exon <- toxo_anno_exon[, c(1, 4, 5, 6, 8, 9)]
colnames(toxo_anno_exon) <- c("Chr", "Start", "End", "Strand", "ExonID", "ParentGeneID")
toxo_anno_exon$GeneID <- strsplit2(toxo_anno_exon$ParentGeneID, "-")[, 1]
# human
hg38_anno <- getInBuiltAnnotation("hg38")
hg38_anno <- hg38_anno[grepl("chr", hg38_anno$Chr), ]


anno_comb <- rbind(hg38_anno[, c("GeneID", "Chr", "Start", "End", "Strand")],
    toxo_anno_exon[, c("GeneID", "Chr", "Start", "End", "Strand")])
FC_hg38_toxo <- featureCounts(bam.files_subjunc, annot.ext = anno_comb, nthreads = 11,
    isPairedEnd = TRUE, useMetaFeatures = TRUE)
Alignment_output_toxohg38 <- list(FeatureCounts = FC_hg38_toxo)
save(Alignment_output_toxohg38, file = "171220_Alignment_hg38_toxo_Brady_KO_WT.RData")
```

Hide

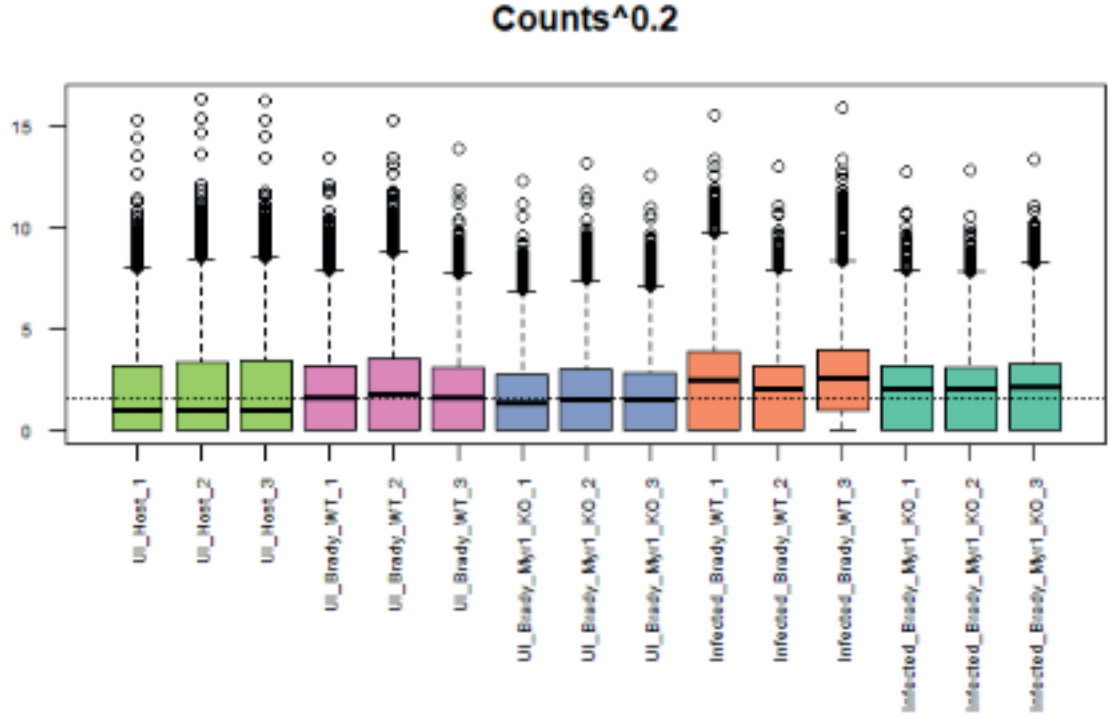
```
load("171220_Alignment_hg38_toxo_Brady_KO_WT.RData")
FC_hg38_toxo <- Alignment_output_toxohg38$FeatureCounts
colnames(FC_hg38_toxo$counts) <- targets$SampleID
align_stats <- Alignment_output_toxohg38$FeatureCounts$stat[, -1]
row.names(align_stats) <- Alignment_output_toxohg38$FeatureCounts$stat$Status
colnames(align_stats) <- targets$SampleID
align_stats <- align_stats[rowSums(align_stats) != 0, ]
par(mar = c(8, 4, 4, 2), xpd = TRUE)
barplot(t(t(align_stats)/colSums(align_stats)), las = 2, cex.names = 0.6, col = brewer.pal(4,
    "Dark2"))
legend(0, 1.2, row.names(align_stats), pch = 15, ncol = 4, col = brewer.pal(4,
    "Dark2"))
```



Boxplots of the counts to the power of 0.2 are shown below. The median of all counts is indicated by the dotted line.

Hide

```
group <- as.factor(targets$Group)
group.col <- group
levels(group.col) <- brewer.pal(5, "Set2")
par(cex.axis = 0.6, mar = c(8, 4, 4, 2))
boxplot(FC_hg38_toxo$counts^0.2, main = "Counts^0.2", col = as.character(group.col),
    las = 2)
abline(h = median(FC_hg38_toxo$counts^0.2), lty = 3)
```



4 Parasite RNA levels

The total number of reads aligning to human or viral genes:

Hide

```
counts_all <- FC_hg38_toxo$counts
counts_toxo <- counts_all[grepl("TGME49", row.names(counts_all)), ]
counts_human <- counts_all[!grepl("TGME49", row.names(counts_all)), ]
data.frame(CountsTotal = colSums(counts_all), CountsHuman = colSums(counts_human),
    CountsToxo = colSums(counts_toxo))
```

	CountsTotal <dbl>	CountsHuman <dbl>	CountsToxo <dbl>
UI_Host_1	29783946	29783719	227
UI_Host_2	42115064	42114843	221
UI_Host_3	42631292	42631022	270
UI_Brady_WT_1	28386494	28205245	181249
UI_Brady_WT_2	48911276	48617090	294186
UI_Brady_WT_3	26269068	26070056	199012
UI_Brady_Myr1_KO_1	15103095	15010707	92388
UI_Brady_Myr1_KO_2	21429355	21276428	152927
UI_Brady_Myr1_KO_3	17063421	16910643	152778
Infected_Brady_WT_1	56461204	52464133	3997071

1-10 of 15 rows Previous 1 2 Next

	CountsTotal <dbl>	CountsHuman <dbl>	CountsToxo <dbl>
Infected_Brady_WT_2	20957400	19608429	1348971
Infected_Brady_WT_3	56942463	52203673	4738790
Infected_Brady_Myr1_KO_1	19498276	17824838	1673438
Infected_Brady_Myr1_KO_2	18507642	16936042	1571600
Infected_Brady_Myr1_KO_3	24260015	22283600	1976415

11-15 of 15 rows Previous 1 2 Next

Proportion of reads that are human or viral:

Hide

```
data.frame(PropHuman = colSums(counts_human)/colSums(counts_all), PropToxo = colSums(counts_toxo)/co
lSums(counts_all))
```

	PropHuman <dbl>	PropToxo <dbl>
UI_Host_1	0.9999924	7.621556e-06
UI_Host_2	0.9999948	5.247529e-06
UI_Host_3	0.9999937	6.333376e-06
UI_Brady_WT_1	0.9936150	6.385044e-03
UI_Brady_WT_2	0.9939853	6.014687e-03
UI_Brady_WT_3	0.9924241	7.575906e-03
UI_Brady_Myr1_KO_1	0.9938828	6.117157e-03
UI_Brady_Myr1_KO_2	0.9928637	7.136332e-03
UI_Brady_Myr1_KO_3	0.9910465	8.953539e-03
Infected_Brady_WT_1	0.9292068	7.079323e-02

1-10 of 15 rows Previous 1 2 Next

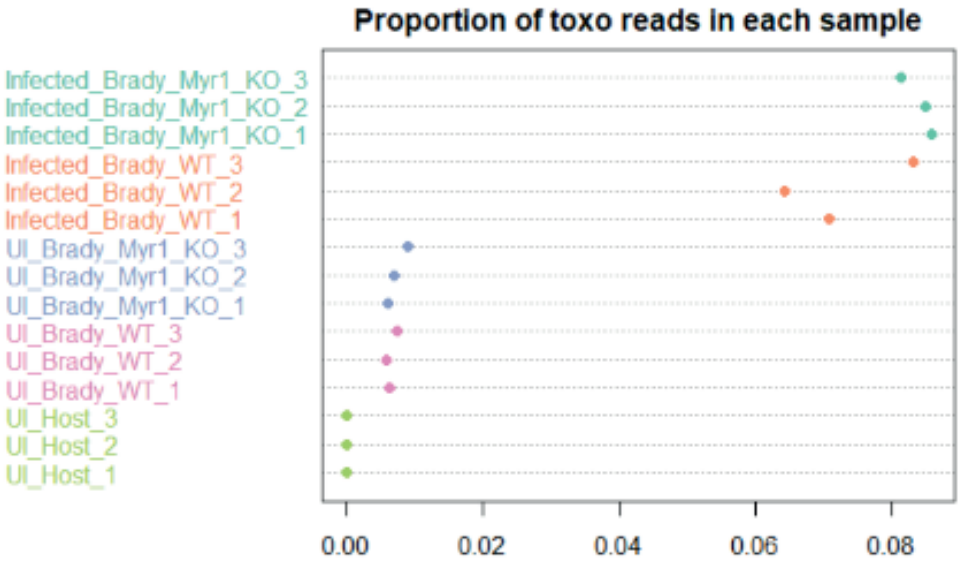
	PropHuman <dbl>	PropToxo <dbl>
Infected_Brady_WT_2	0.9356327	6.436729e-02
Infected_Brady_WT_3	0.9167793	8.322067e-02
Infected_Brady_Myr1_KO_1	0.9141751	8.582492e-02
Infected_Brady_Myr1_KO_2	0.9150837	8.491627e-02
Infected_Brady_Myr1_KO_3	0.9185320	8.146800e-02

11-15 of 15 rows Previous 1 2 Next

A dot chart of the toxo proportions:

Hide

```
dotchart(colSums(counts_toxo)/colSums(counts_all), col = as.character(group.col),
    pch = 16, main = "Proportion of toxo reads in each sample")
```



5 Analysis of human data: new

Within this section the human data will be analysed.

5.1 Annotation

Detailed annotation for each gene is available through the NCBI, ftp://ftp.ncbi.nlm.nih.gov/gene/DATA/GENE_INFO/. The October 2017 version of the human annotation is used for this analysis. The annotation available for each gene:

Hide

```
lib <- "~/GeneInformationSets/HumanGenomeAnnotation/Homo_sapiens.gene_info_Oct17.gz"
annotation.library <- read.delim(lib, stringsAsFactors = FALSE)
annotation <- annotation.library[match(row.names(counts_human), annotation.library$GeneID),
    c("GeneID", "Symbol", "description", "chromosome", "type_of_gene", "Synonyms")]
annotation <- cbind(annotation, Length = Alignment_output_toxohg38$FeatureCounts$annotation$Length[!
grepl("TGME49",
    Alignment_output_toxohg38$FeatureCounts$annotation$GeneID)])
colnames(annotation)
```

```
[1] "GeneID"      "Symbol"      "description"  "chromosome"   "type_of_gene" "Synonyms"     "Lengt
h"
```

5.2 Data filtering and normalization

5.2.1 Filtering

Genes should only by included if they are expressed at a reasonable level. Therefore, lowly expressed genes need to be filtered out. An appropriate filtering level is determined.

Hide

```
options(width = 90)
DGE <- DGEList(counts_human, genes = annotation, group = group)
CPM <- cpm(DGE)
summary(CPM)
```

```
   UI_Host_1          UI_Host_2          UI_Host_3         UI_Brady_WT_1
 Min.   :    0.00   Min.   :    0.000   Min.   :    0.000   Min.   :    0.000
 1st Qu.:    0.00   1st Qu.:    0.000   1st Qu.:    0.000   1st Qu.:    0.000
 Median :    0.47   Median :    0.451   Median :    0.422   Median :    0.425
 Mean   :   35.30   Mean   :   35.305   Mean   :   35.305   Mean   :   35.305
 3rd Qu.:   22.76   3rd Qu.:   22.652   3rd Qu.:   22.964   3rd Qu.:   24.357
 Max.   :27623.48   Max.   :27698.762   Max.   :26381.047   Max.   :15563.985
 UI_Brady_WT_2       UI_Brady_WT_3       UI_Brady_Myr1_KO_1 UI_Brady_Myr1_KO_2
 Min.   :    0.000   Min.   :    0.000   Min.   :    0.00   Min.   :    0.000
 1st Qu.:    0.000   1st Qu.:    0.000   1st Qu.:    0.00   1st Qu.:    0.000
 Median :    0.391   Median :    0.384   Median :    0.40   Median :    0.376
 Mean   :   35.305   Mean   :   35.305   Mean   :   35.30   Mean   :   35.305
 3rd Qu.:   24.230   3rd Qu.:   23.897   3rd Qu.:   23.18   3rd Qu.:   23.218
 Max.   :17215.489   Max.   :19745.412   Max.   :18455.36   Max.   :18418.458
 UI_Brady_Myr1_KO_3  Infected_Brady_WT_1 Infected_Brady_WT_2 Infected_Brady_WT_3
 Min.   :    0.000   Min.   :    0.000   Min.   :    0.000   Min.   :    0.000
 1st Qu.:    0.000   1st Qu.:    0.000   1st Qu.:    0.000   1st Qu.:    0.000
 Median :    0.414   Median :    0.534   Median :    0.561   Median :    0.575
 Mean   :   35.305   Mean   :   35.305   Mean   :   35.305   Mean   :   35.305
 3rd Qu.:   23.358   3rd Qu.:   25.656   3rd Qu.:   25.805   3rd Qu.:   25.669
 Max.   :18313.378   Max.   :17026.165   Max.   :19127.488   Max.   :19119.325
 Infected_Brady_Myr1_KO_1 Infected_Brady_Myr1_KO_2 Infected_Brady_Myr1_KO_3
 Min.   :    0.000        Min.   :    0.000        Min.   :    0.000
 1st Qu.:    0.000        1st Qu.:    0.000        1st Qu.:    0.000
 Median :    0.505        Median :    0.472        Median :    0.494
 Mean   :   35.305        Mean   :   35.305        Mean   :   35.305
 3rd Qu.:   24.572        3rd Qu.:   24.327        3rd Qu.:   24.368
 Max.   :18853.355        Max.   :20215.644        Max.   :18741.137
```

Hide

```
median(CPM)
```

```
[1] 0.4589863
```

Hide

```
10/(1e-06 * colSums(DGE$counts))
```

```
               UI_Host_1                UI_Host_2                UI_Host_3
               0.3357539                0.2374460                0.2345710
          UI_Brady_WT_1            UI_Brady_WT_2            UI_Brady_WT_3
               0.3545440                0.2056890                0.3835818
      UI_Brady_Myr1_KO_1       UI_Brady_Myr1_KO_2       UI_Brady_Myr1_KO_3
               0.6661911                0.4700037                0.5913436
     Infected_Brady_WT_1      Infected_Brady_WT_2      Infected_Brady_WT_3
               0.1906064                0.5099848                0.1915574
Infected_Brady_Myr1_KO_1 Infected_Brady_Myr1_KO_2 Infected_Brady_Myr1_KO_3
               0.5610149                0.5904567                0.4487605
```

Hide

```
table(group)
```

```
group
Infected_Brady_Myr1_KO       Infected_Brady_WT       UI_Brady_Myr1_KO
                     3                       3                      3
           UI_Brady_WT                 UI_Host
                     3                       3
```

Any gene which does achieve a count per million mapped reads (CPM) greater than 0.7 in at least 3 samples is filtered from the data together with all genes that do not have a symbol.

Hide

```
is.exprs <- rowSums(CPM > 0.7) >= 3
table(is.exprs)
```

```
is.exprs
FALSE  TRUE
14154 14171
```

Hide

```
has.sym <- !is.na(DGE$genes$Symbol)
table(has.sym)
```

```
has.sym
FALSE  TRUE
  366 27959
```

Hide

```
DGE <- DGE[is.exprs & has.sym, , keep.lib.sizes = FALSE]
```

After filtering there are 14128 genes remaining.

5.2.2 Normalization

RNA composition within each sample is normalized using the TMM method. This method calculates a scaling factor for each sample using the weighted trimmed mean of log-expression ratios. This factor aims to minimize the log-fold changes between the samples for the majority of genes. Ideally all scaling factors should be around 1.

Hide

```
DGE <- calcNormFactors(DGE, method = "TMM")
DGE$samples
```

	group <fctr>	lib.size <dbl>	norm.factors <dbl>
UI_Host_1	UI_Host	29757881	0.9644027
UI_Host_2	UI_Host	42079810	0.9624363
UI_Host_3	UI_Host	42597191	0.9711264
UI_Brady_WT_1	UI_Brady_WT	28183401	0.9992504
UI_Brady_WT_2	UI_Brady_WT	48583087	0.9964881
UI_Brady_WT_3	UI_Brady_WT	26051628	0.9839858
UI_Brady_Myr1_KO_1	UI_Brady_Myr1_KO	15000047	0.9751138
UI_Brady_Myr1_KO_2	UI_Brady_Myr1_KO	21262341	0.9610467
UI_Brady_Myr1_KO_3	UI_Brady_Myr1_KO	16898953	0.9669441
Infected_Brady_WT_1	Infected_Brady_WT	52415177	1.0615887

1-10 of 15 rows Previous 1 2 Next

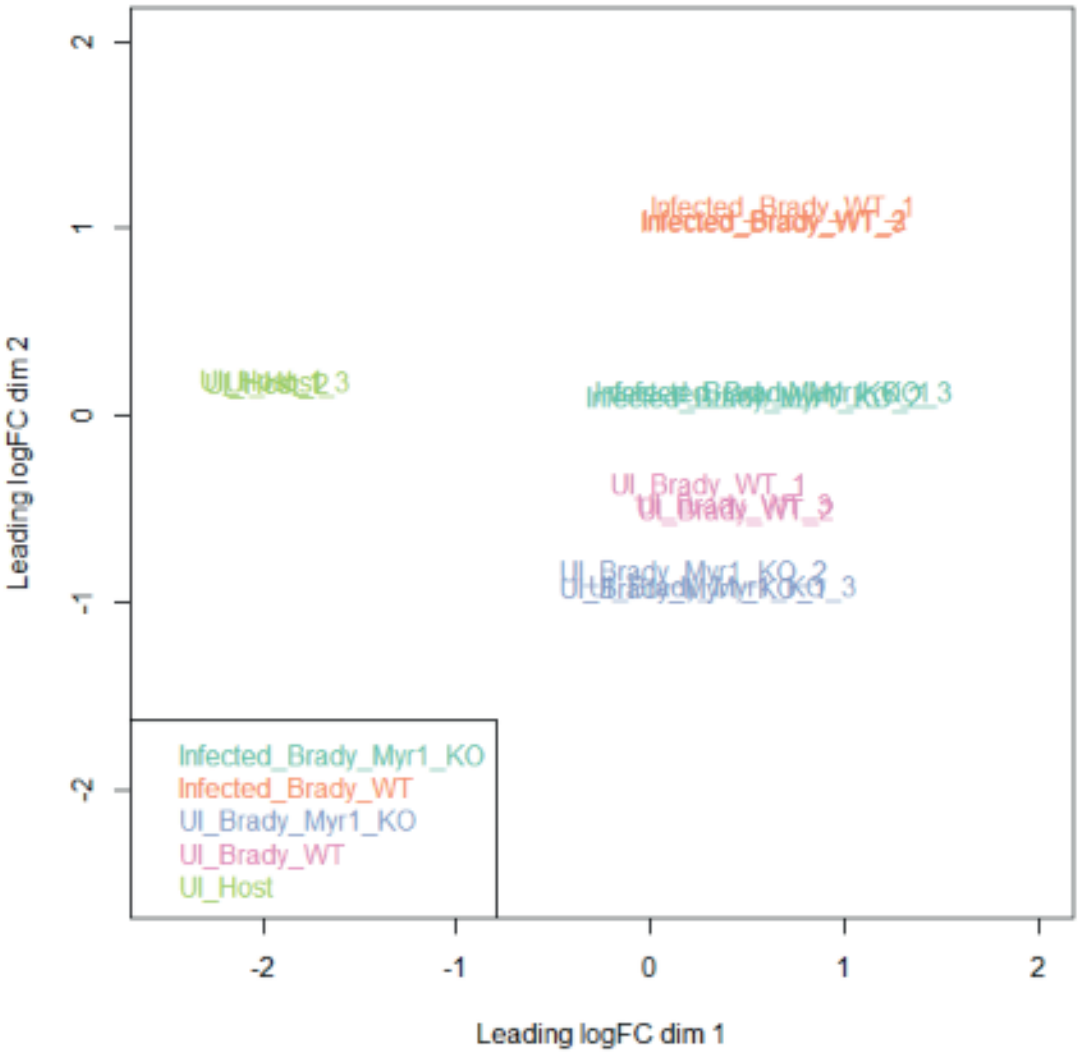
5.3 Data exploration

5.3.1 Sample clustering

The multi-dimensional scaling (MDS) plot below shows the unsupervised clustering of the samples. On an MDS plot each sample is plotted according to the distance between it and all other samples. This distance is calculated using the top 500 most variable genes between each pair of samples. The following plot colours the samples according to experimental group. You can see that all groups are nicely separated.

Hide

```
plotMDS(DGE, col = as.character(group.col), xlim = c(-2.5, 2), ylim = c(-2.5,
    2))
legend("bottomleft", levels(group), text.col = levels(group.col))
```



5.3.2 Biological variation

The biological variation between the samples is estimated and the biological coefficient of variation is determined. The BCV indicates how the abundance of each gene varies between replicate samples. The common BCV for the data set:

Hide

```
design <- model.matrix(~0 + group)
row.names(design) <- colnames(DGE)
colnames(design) <- levels(group)
disp <- estimateDisp(DGE, design = design, robust = TRUE)
sqrt(disp$common.dispersion)
```

```
[1] 0.06568963
```

A summary of the gene specific BCVs:

Hide

```
summary(sqrt(disp$tagwise.dispersion))
```

```
   Min. 1st Qu.  Median    Mean 3rd Qu.    Max. 
0.03560 0.05061 0.06176 0.07642 0.08541 0.89029 
```

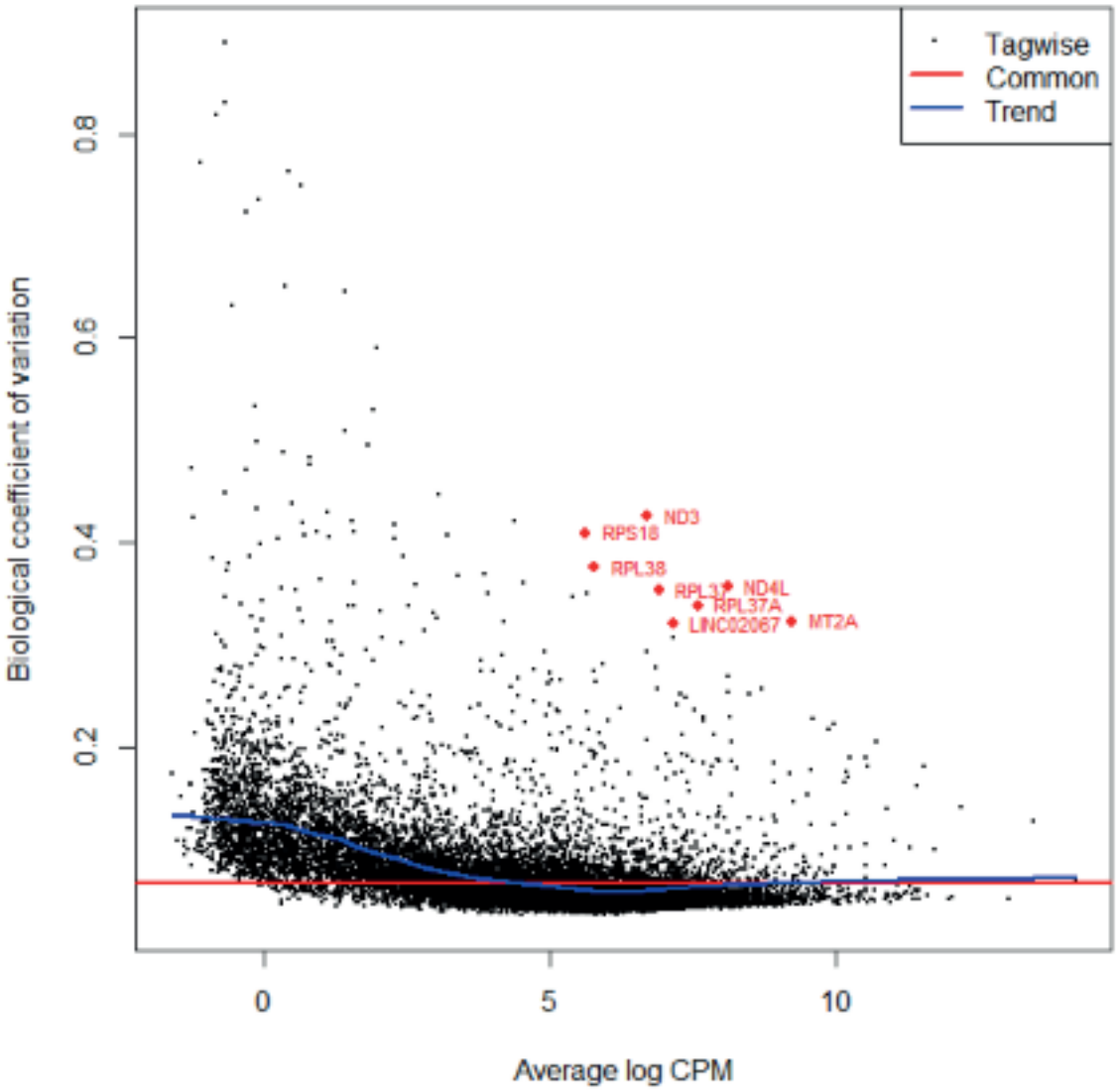
A plot of the average log2log2-CPM versus the BCV for each gene is shown below. This plot visualises how gene variation between replicate samples (y-axis) changes as gene abundance (x-axis) increases. You can see from this plot the gene variability typically decreases as gene abundance increases. However there are some genes which show high variability relative to their abundance, highlighted in red.

Hide

```
plotBCV(disp)
HV <- disp[disp$prior.df == min(disp$prior.df), ]
points(HV$AveLogCPM, sqrt(HV$tagwise.dispersion), pch = 16, col = "red", cex = 0.8)
```

Hide

```
text(HV$AveLogCPM, sqrt(HV$tagwise.dispersion), labels = HV$genes$Symbol, col = "red",
    cex = 0.7, pos = 4)
```



Hide

```
RPKM <- rpkm(DGE)
HV_HL <- as.factor(disp$genes$GeneID %in% HV$genes$GeneID)
levels(HV_HL) <- c(0, 1)
glXYPlot(x = disp$AveLogCPM, y = sqrt(disp$tagwise.dispersion), counts = RPKM,
    groups = group, samples = targets$SampleID, sample.cols = as.character(group.col),
    anno = DGE$genes, side.main = "Symbol", side.ylab = "RPKM", html = "glimma_BCV",
    status = as.numeric(as.character(HV_HL)), ylab = "Biological_coefficient_of_variation",
    xlab = "Average_logCPM", launch = FALSE)
```

Appendix D -

Data set 1 and 2, data combination process
Code and processing was completed by Dr. Alexandra Garnham from WEHI

6 Analysis of human data: incorporating new and previous data

Simona would like to know if her previous RNAseq data can be combined with the new data analysed here. The old data looks at uninfected and infected human foreskin fibroblasts where the infection is either wild type tachyzoite or bradyzoite. The fibroblasts were created from a different donor compared to the new data.

Hide

```
load("~/Projects/InfectionAndImmunity/TonkinLab/SimonaSeizova/Human_Toxo_fibroblasts/170323_RNAseq_subjunc_hg38parasite_toxoplasmaBradyTachy_SimonaS.RData")
counts_old <- Alignment_output$FeatureCounts$counts[!grepl("TGME49", row.names(Alignment_output$FeatureCounts$counts)),
    ]
counts_OldNew <- cbind(counts_human, counts_old[match(row.names(counts_human),
    row.names(counts_old)), ])
group_OldNew <- as.factor(c(rep("UI_Host", 3), rep("UI_Brady_WT", 3), rep("UI_Brady_Myr1KO",
    3), rep("Inf_Brady_WT", 3), rep("Inf_Brady_Myr1KO", 3), rep("UI_Host_24h",
    3), rep("UI_Tachy_WT", 3), rep("Inf_Tachy_WT", 3), rep("UI_Host", 3), rep("UI_Brady_WT",
    3), rep("Inf_Brady_WT", 3)))
OldNew <- as.factor(c(rep("New", ncol(counts_human)), rep("Old", ncol(counts_old))))
OldNew.col <- OldNew
levels(OldNew.col) <- brewer.pal(3, "Dark2")[1:2]
DGE_OldNew <- DGEList(counts_OldNew, genes = annotation, group = group_OldNew)
```

6.1 Filtering and normalization

6.1.1 Filtering

An appropriate filtering level is determined.

Hide

```
options(width = 90)
CPM_OldNew <- cpm(DGE_OldNew)
summary(CPM_OldNew)
```

```
  UI_Host_1          UI_Host_2           UI_Host_3          UI_Brady_WT_1
Min.   :    0.00   Min.   :    0.000   Min.   :    0.000   Min.   :    0.000
1st Qu.:    0.00   1st Qu.:    0.000   1st Qu.:    0.000   1st Qu.:    0.000
Median :    0.47   Median :    0.451   Median :    0.422   Median :    0.425
Mean   :   35.30   Mean   :   35.305   Mean   :   35.305   Mean   :   35.305
3rd Qu.:   22.76   3rd Qu.:   22.652   3rd Qu.:   22.964   3rd Qu.:   24.357
Max.   :27623.48   Max.   :27698.762   Max.   :26381.047   Max.   :15563.985
UI_Brady_WT_2       UI_Brady_WT_3       UI_Brady_Myr1_KO_1 UI_Brady_Myr1_KO_2
Min.   :    0.000   Min.   :    0.000   Min.   :    0.00   Min.   :    0.000
1st Qu.:    0.000   1st Qu.:    0.000   1st Qu.:    0.00   1st Qu.:    0.000
Median :    0.391   Median :    0.384   Median :    0.40   Median :    0.376
Mean   :   35.305   Mean   :   35.305   Mean   :   35.30   Mean   :   35.305
3rd Qu.:   24.230   3rd Qu.:   23.897   3rd Qu.:   23.18   3rd Qu.:   23.218
Max.   :17215.489   Max.   :19745.412   Max.   :18455.36   Max.   :18418.458
UI_Brady_Myr1_KO_3  Infected_Brady_WT_1 Infected_Brady_WT_2 Infected_Brady_WT_3
Min.   :    0.000   Min.   :    0.000   Min.   :    0.000   Min.   :    0.000
1st Qu.:    0.000   1st Qu.:    0.000   1st Qu.:    0.000   1st Qu.:    0.000
Median :    0.414   Median :    0.534   Median :    0.561   Median :    0.575
Mean   :   35.305   Mean   :   35.305   Mean   :   35.305   Mean   :   35.305
3rd Qu.:   23.358   3rd Qu.:   25.656   3rd Qu.:   25.805   3rd Qu.:   25.669
Max.   :18313.378   Max.   :17026.165   Max.   :19127.488   Max.   :19119.325
Infected_Brady_Myr1_KO_1 Infected_Brady_Myr1_KO_2 Infected_Brady_Myr1_KO_3
Min.   :    0.000       Min.   :    0.000       Min.   :    0.000
1st Qu.:    0.000       1st Qu.:    0.000       1st Qu.:    0.000
Median :    0.505       Median :    0.472       Median :    0.494
Mean   :   35.305       Mean   :   35.305       Mean   :   35.305
3rd Qu.:   24.572       3rd Qu.:   24.327       3rd Qu.:   24.368
Max.   :18853.355       Max.   :20215.644       Max.   :18741.137
UI_Host_24h_1       UI_Host_24h_2       UI_Host_24h_3       UI_Tachy_24h_1
Min.   :    0.00   Min.   :    0.00   Min.   :    0.000   Min.   :    0.000
1st Qu.:    0.00   1st Qu.:    0.00   1st Qu.:    0.000   1st Qu.:    0.000
Median :    0.16   Median :    0.18   Median :    0.141   Median :    0.151
Mean   :   35.30   Mean   :   35.30   Mean   :   35.305   Mean   :   35.305
3rd Qu.:   19.74   3rd Qu.:   19.41   3rd Qu.:   20.055   3rd Qu.:   20.999
Max.   :32645.66   Max.   :34523.25   Max.   :31404.393   Max.   :30336.267
UI_Tachy_24h_2      UI_Tachy_24h_3       Inf_Tachy_24h_1     Inf_Tachy_24h_2
Min.   :    0.00   Min.   :    0.000   Min.   :    0.00   Min.   :    0.000
1st Qu.:    0.00   1st Qu.:    0.000   1st Qu.:    0.00   1st Qu.:    0.000
Median :    0.16   Median :    0.145   Median :    0.10   Median :    0.142
Mean   :   35.30   Mean   :   35.305   Mean   :   35.30   Mean   :   35.305
3rd Qu.:   20.96   3rd Qu.:   20.655   3rd Qu.:   22.93   3rd Qu.:   22.987
Max.   :34139.25   Max.   :30668.036   Max.   :24860.41   Max.   :23642.992
Inf_Tachy_24h_3     UI_Host_1week_1     UI_Host_1week_2     UI_Host_1week_3
Min.   :    0.000   Min.   :    0.000   Min.   :    0.000   Min.   :0.00e+00
1st Qu.:    0.000   1st Qu.:    0.000   1st Qu.:    0.000   1st Qu.:0.00e+00
Median :    0.165   Median :    0.216   Median :    0.202   Median :2.09e-01
Mean   :   35.305   Mean   :   35.305   Mean   :   35.305   Mean   :3.53e+01
3rd Qu.:   22.856   3rd Qu.:   21.161   3rd Qu.:   21.171   3rd Qu.:2.07e+01
Max.   :24471.988   Max.   :20820.279   Max.   :20771.026   Max.   :2.18e+04
UI_Brady_1week_1   UI_Brady_1week_2   UI_Brady_1week_3   Inf_Brady_1week_1
Min.   :   0.000   Min.   :   0.000   Min.   :   0.000   Min.   :   0.000
1st Qu.:   0.000   1st Qu.:   0.000   1st Qu.:   0.000   1st Qu.:   0.000
Median :   0.178   Median :   0.208   Median :   0.236   Median :   0.222
Mean   :  35.305   Mean   :  35.305   Mean   :  35.305   Mean   :  35.305
3rd Qu.:  22.479   3rd Qu.:  22.906   3rd Qu.:  22.597   3rd Qu.:  23.766
Max.   :8498.434   Max.   :7553.671   Max.   :9473.114   Max.   :9304.948
Inf_Brady_1week_2  Inf_Brady_1week_3
Min.   :   0.000   Min.   :   0.000
1st Qu.:   0.000   1st Qu.:   0.000
Median :   0.243   Median :   0.292
Mean   :  35.305   Mean   :  35.305
3rd Qu.:  23.587   3rd Qu.:  23.926
Max.   :9876.243   Max.   :9671.366
```

Hide

```
median(CPM_OldNew)
```

```
[1] 0.2926846
```

Hide

```
10/(1e-06 * colSums(DGE_OldNew$counts))
```

```
               UI_Host_1                UI_Host_2                UI_Host_3
               0.3357539                0.2374460                0.2345710
           UI_Brady_WT_1            UI_Brady_WT_2            UI_Brady_WT_3
               0.3545440                0.2056890                0.3835818
      UI_Brady_Myr1_KO_1       UI_Brady_Myr1_KO_2       UI_Brady_Myr1_KO_3
               0.6661911                0.4700037                0.5913436
     Infected_Brady_WT_1      Infected_Brady_WT_2      Infected_Brady_WT_3
               0.1906064                0.5099848                0.1915574
Infected_Brady_Myr1_KO_1 Infected_Brady_Myr1_KO_2 Infected_Brady_Myr1_KO_3
               0.5610149                0.5904567                0.4487605
           UI_Host_24h_1            UI_Host_24h_2            UI_Host_24h_3
               0.3955429                0.2570703                0.7061483
          UI_Tachy_24h_1           UI_Tachy_24h_2           UI_Tachy_24h_3
               0.5035826                0.5174449                0.4837169
          Inf_Tachy_24h_1          Inf_Tachy_24h_2          Inf_Tachy_24h_3
               1.0013335                0.7116603                0.8251256
         UI_Host_1week_1          UI_Host_1week_2          UI_Host_1week_3
               0.5398106                0.2880424                0.4181209
        UI_Brady_1week_1         UI_Brady_1week_2         UI_Brady_1week_3
               0.8884928                0.4164785                0.3936748
        Inf_Brady_1week_1        Inf_Brady_1week_2        Inf_Brady_1week_3
               0.5552706                0.6079184                0.5835510
```

Hide

```
table(group_OldNew)
```

```
group_OldNew
Inf_Brady_Myr1KO     Inf_Brady_WT     Inf_Tachy_WT  UI_Brady_Myr1KO      UI_Brady_WT
               3                6                3                3                6
         UI_Host      UI_Host_24h      UI_Tachy_WT
               6                3                3
```

All genes with a CPM less than 1 in at least 3 samples are filtered from the data together with all genes with no annotation.

Hide

```
is.exprs_OldNew <- rowSums(CPM > 1) >= 3
table(is.exprs_OldNew)
```

```
is.exprs_OldNew
FALSE  TRUE
14698 13627
```

Hide

```
DGE_OldNew <- DGE_OldNew[is.exprs_OldNew & has.sym, , keep.lib.sizes = FALSE]
```

There are 13599 genes remaining.

6.1.2 Normalization

RNA composition is normalized. The scaling factor for each sample:

Hide

```
DGE_OldNew <- calcNormFactors(DGE_OldNew, method = "TMM")
DGE_OldNew$samples
```

	group <fctr>	lib.size <dbl>	norm.factors <dbl>
UI_Host_1	UI_Host	29747815	0.9041536
UI_Host_2	UI_Host	42066439	0.9012300
UI_Host_3	UI_Host	42584241	0.9136135
UI_Brady_WT_1	UI_Brady_WT	28174917	0.9488007
UI_Brady_WT_2	UI_Brady_WT	48570236	0.9368468
UI_Brady_WT_3	UI_Brady_WT	26044500	0.9288327
UI_Brady_Myr1_KO_1	UI_Brady_Myr1KO	14996091	0.9164016
UI_Brady_Myr1_KO_2	UI_Brady_Myr1KO	21257053	0.9071315
UI_Brady_Myr1_KO_3	UI_Brady_Myr1KO	16894627	0.9112830
Infected_Brady_WT_1	Inf_Brady_WT	52396221	0.9999939

1-10 of 33 rows Previous 1 2 3 4 Next

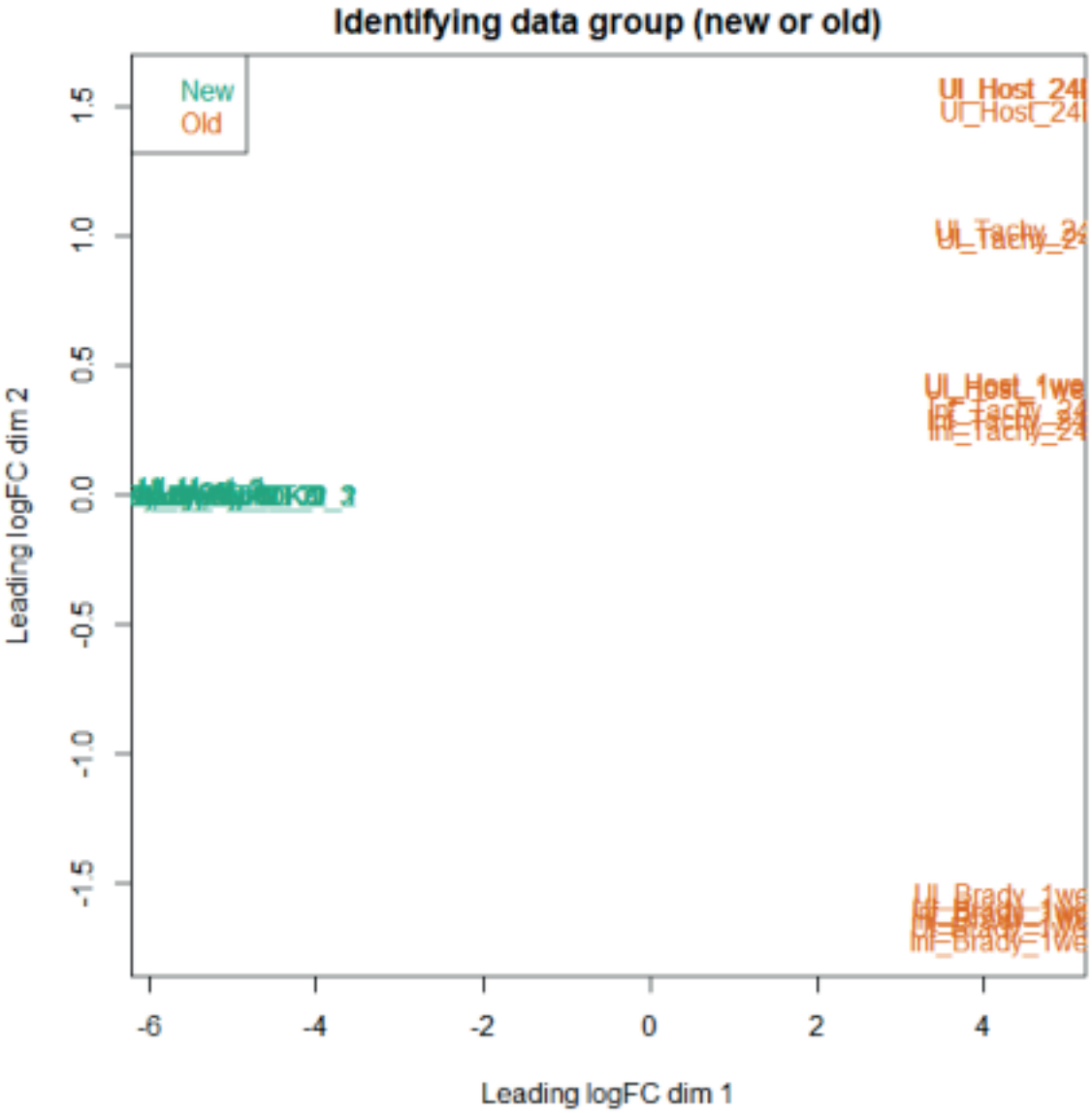
6.2 Data exploration

6.2.1 Sample clustering

An MDS plot of the data:

Hide

```
plotMDS(DGE_OldNew, col = as.character(OldNew.col), main = "Identifying data group (new or old)")
legend("topleft", levels(OldNew), text.col = levels(OldNew.col))
```



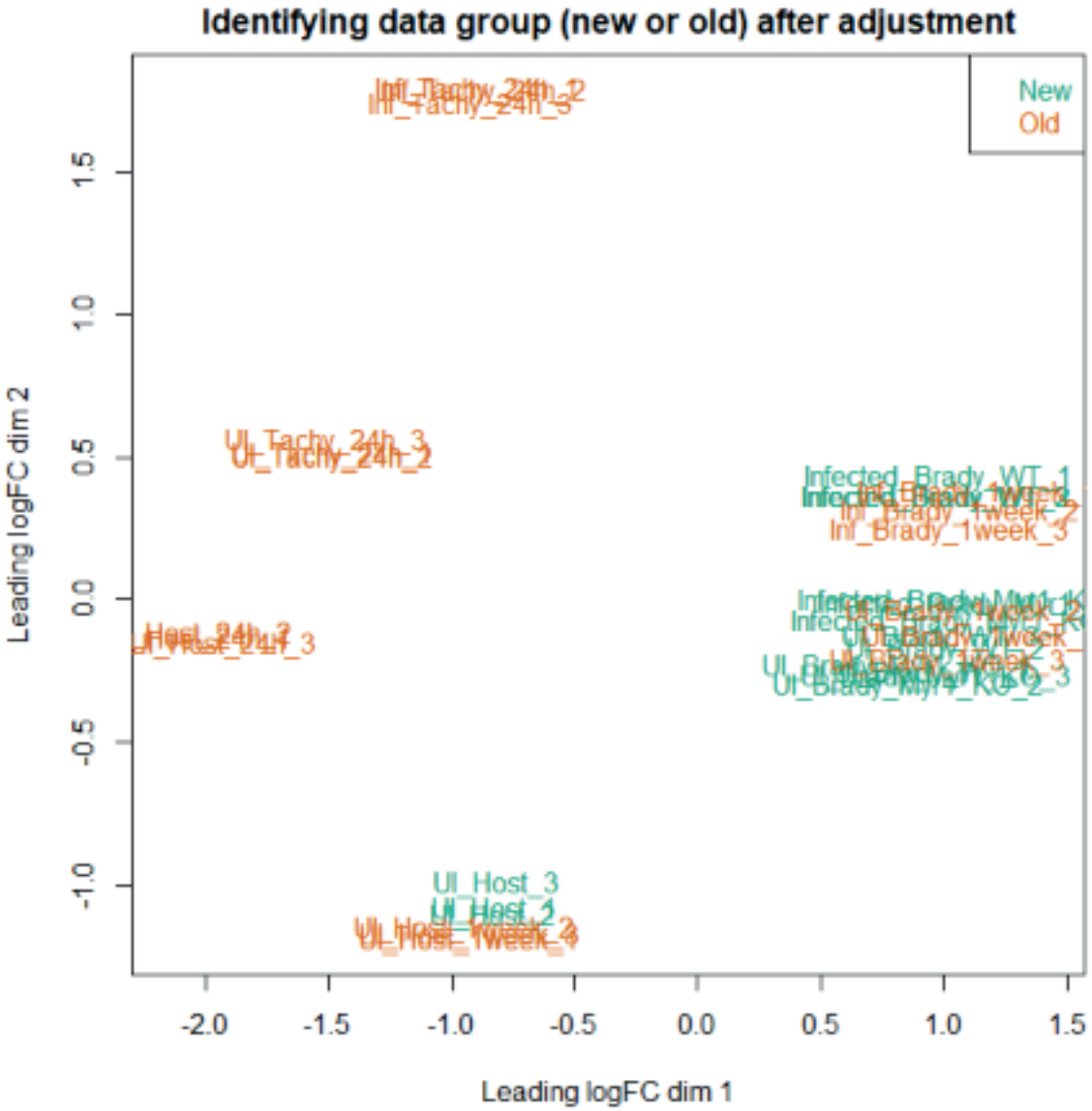
From the above plot you can see that the data clusters into two major groups - new and old data. The old data is also much more variable compared to the new data. We adjust for the differences between the data set using the following groups:

Group	Data set
Uninfected host (1 week)	Old
Uninfected host	New
Uninfected brady (1 week)	Old
Uninfected brady WT	New
Infected brady (1 week)	Old
Infected brady (1 week)	New

The MDS plot after adjustment

Hide

```
logCPM_OldNew <- cpm(DGE_OldNew, log = TRUE, prior.count = 2)
logCPM_OldNew_BC <- removeBatchEffect(logCPM_OldNew, design = model.matrix(~0 +
    group_OldNew), batch = OldNew)
plotMDS(logCPM_OldNew_BC, col = as.character(OldNew.col), main = "Identifying data group (new or ol
d) after adjustment")
legend("topright", levels(OldNew), text.col = levels(OldNew.col))
```

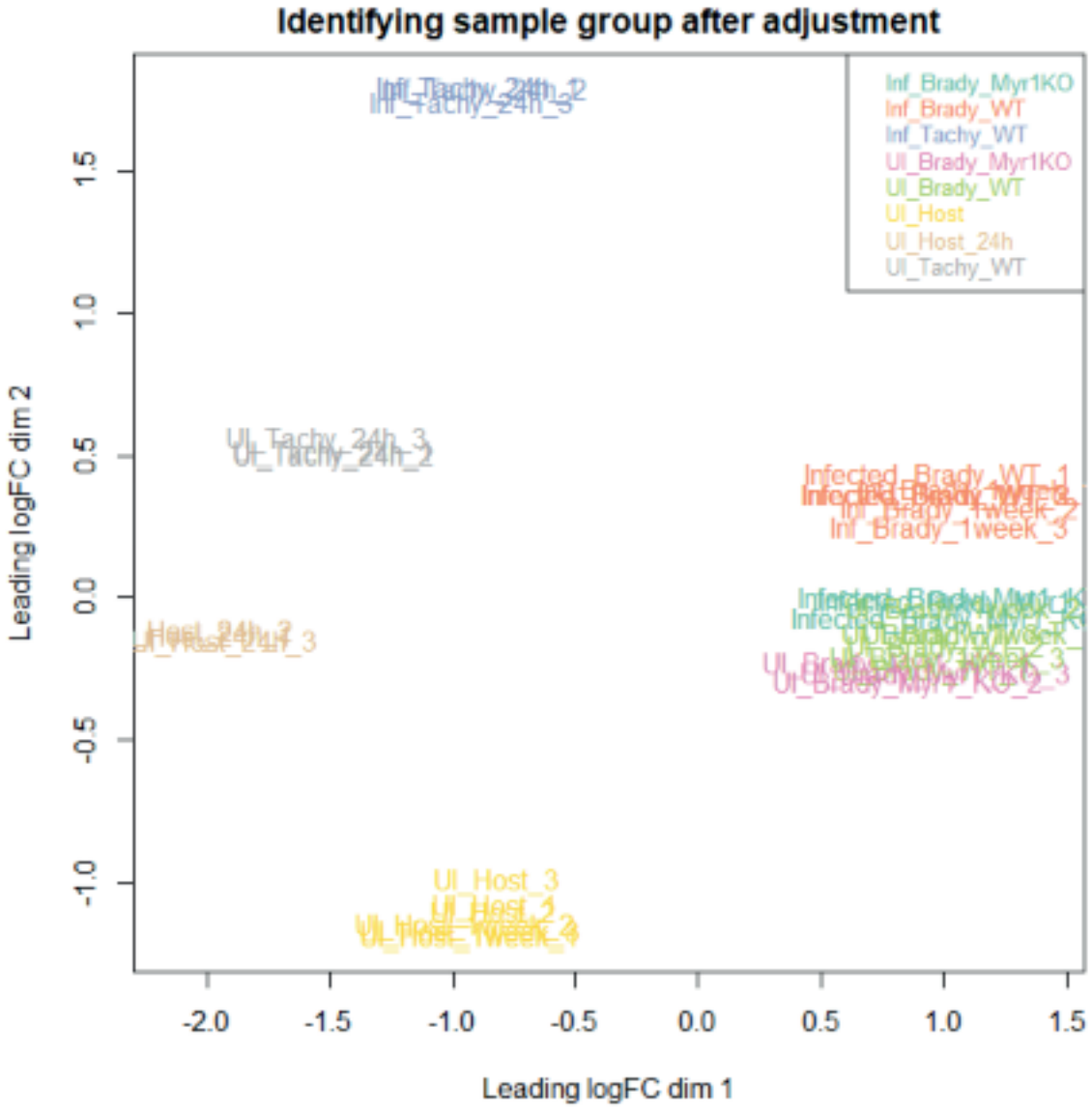


Hide

```
group_OldNew.col <- group_OldNew
levels(group_OldNew.col) <- brewer.pal(8, "Set2")
plotMDS(logCPM_OldNew_BC, col = as.character(group_OldNew.col), main = "Identifying sample group aft
er adjustment")
legend("topright", levels(group_OldNew), text.col = levels(group_OldNew.col),
    cex = 0.8)
```

Hide

```
group_OldNew.col <- group_OldNew
levels(group_OldNew.col) <- brewer.pal(8, "Set2")
plotMDS(logCPM_OldNew_BC, col = as.character(group_OldNew.col), main = "Identifying sample group aft
er adjustment")
legend("topright", levels(group_OldNew), text.col = levels(group_OldNew.col),
    cex = 0.8)
```



6.2.2 Biological variation

The common BCV for the data:

Hide

```
design_OldNew <- model.matrix(~0 + group_OldNew + OldNew)
row.names(design_OldNew) <- colnames(DGE_OldNew)
colnames(design_OldNew) <- c(levels(group_OldNew), "Old")
disp_OldNew <- estimateDisp(DGE_OldNew, design = design_OldNew, robust = TRUE)
sqrt(disp_OldNew$common.dispersion)
```

```
[1] 0.08635192
```

A summary of the gene specific dispersions:

Hide

```
summary(sqrt(disp_OldNew$tagwise.dispersion))
```

```
   Min. 1st Qu.  Median    Mean 3rd Qu.    Max. 
0.01595 0.05963 0.07774 0.09271 0.10912 0.80363 
```

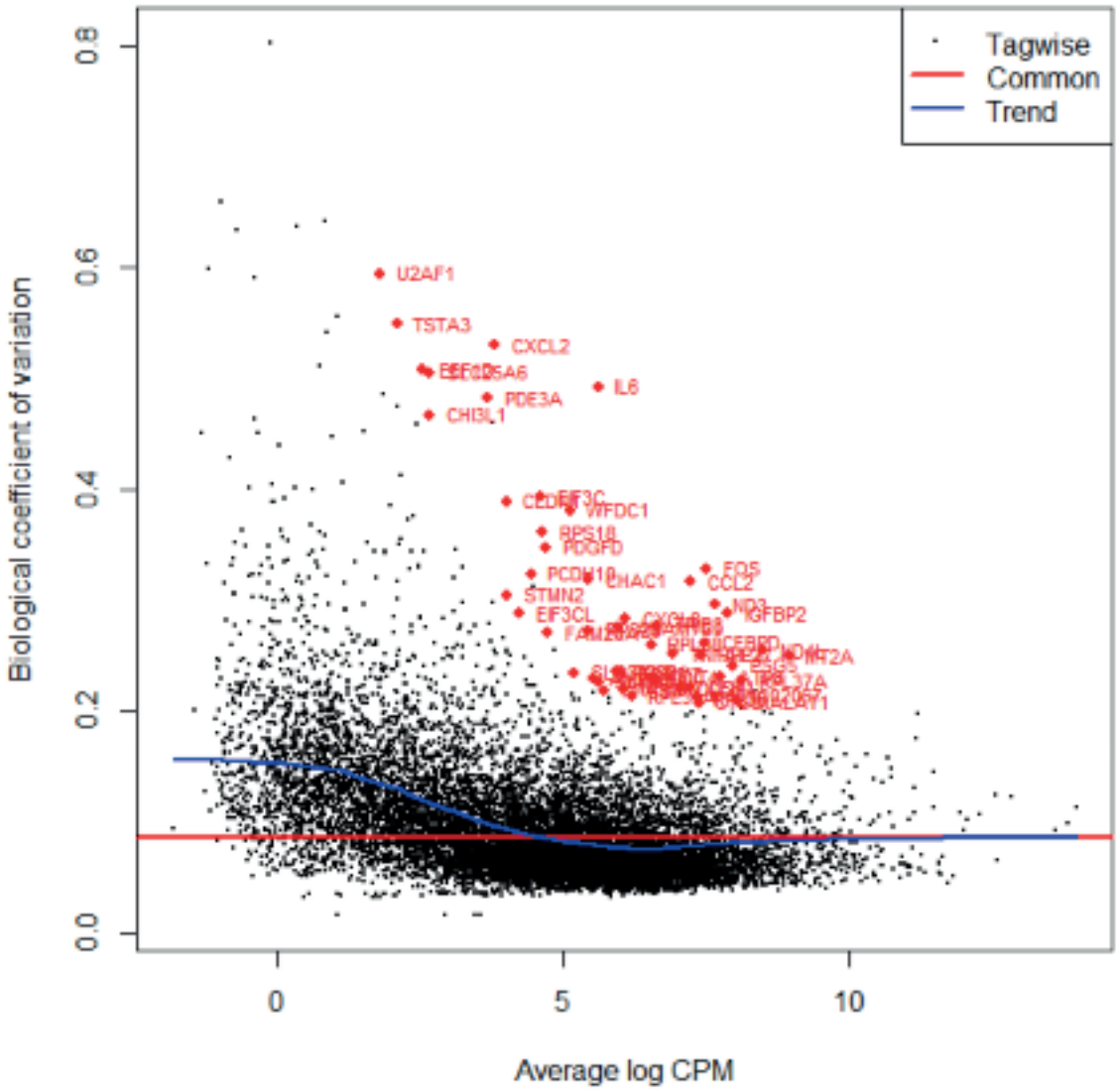
A plot of the average logCPM versus gene specific BCV is shown below. Variable genes are highlighted and labelled.

Hide

```
plotBCV(disp_OldNew)
HV_OldNew <- disp_OldNew[disp_OldNew$prior.df == min(disp_OldNew$prior.df),
    ]
points(HV_OldNew$AveLogCPM, sqrt(HV_OldNew$tagwise.dispersion), pch = 16, col = "red",
    cex = 0.8)
```

Hide

```
text(HV_OldNew$AveLogCPM, sqrt(HV_OldNew$tagwise.dispersion), labels = HV_OldNew$genes$Symbol,
    col = "red", pos = 4, cex = 0.7)
```



Hide

```
HV_OldNew_HL <- as.factor(disp_OldNew$genes$GeneID %in% HV_OldNew$genes$GeneID)
levels(HV_OldNew_HL) <- c(0, 1)
glXYPlot(x = disp_OldNew$AveLogCPM, y = sqrt(disp_OldNew$tagwise.dispersion),
    counts = logCPM_OldNew_BC, groups = group_OldNew, samples = colnames(DGE_OldNew),
    sample.cols = as.character(group_OldNew.col), anno = DGE_OldNew$genes, side.main = "Symbol",
    side.ylab = "logCPM (Batch Corrected)", html = "glimma_BCV_OldNew", status = as.numeric(as.chara
cter(HV_OldNew_HL)),
    ylab = "Biological_coefficient_of_variation", xlab = "Average_logCPM", launch = FALSE)
```

References

1 Seizova, S. *et al. Toxoplasma gondii* bradyzoites induce transcriptional changes to host cells and prevent IFNγ-mediated cell death. *bioRxiv*, 669689, doi:10.1101/669689 (2019).

2 Dubey, J. P. The history of *Toxoplasma gondii*—the first 100 years. *Journal of Eukaryotic Microbiology* **55**, 467-475 (2008).

3 Pappas, G., Roussos, N. & Falagas, M. E. Toxoplasmosis snapshots: global status of *Toxoplasma gondii* seroprevalence and implications for pregnancy and congenital toxoplasmosis. *International journal for parasitology* **39**, 1385-1394 (2009).

4 Flegr, J., Prandota, J., Sovičková, M. & Israili, Z. H. Toxoplasmosis–a global threat. Correlation of latent toxoplasmosis with specific disease burden in a set of 88 countries. *PloS one* **9** (2014).

5 Belluco, S. *et al.* Investigating the Determinants of *Toxoplasma gondii* Prevalence in Meat: A Systematic Review and Meta-Regression. *PloS one* **11**, e0153856-e0153856 (2016).

6 Bowie, W. R. *et al.* Outbreak of toxoplasmosis associated with municipal drinking water. *The Lancet* **350**, 173-177 (1997).

7 Wang, Z.-D. *et al.* Prevalence and burden of *Toxoplasma gondii* infection in HIV-infected people: a systematic review and meta-analysis. *The Lancet HIV* **4**, e177-e188 (2017).

8 Sonneville, R. *et al.* Neurological complications of HIV infection in critically ill patients: clinical features and outcomes. *Journal of Infection* **62**, 301-308 (2011).

9 Cong, W. *et al. Toxoplasma gondii* infection in cancer patients: prevalence, risk factors, genotypes and association with clinical diagnosis. *Cancer letters* **359**, 307-313 (2015).

10 Khurana, S. & Batra, N. Toxoplasmosis in organ transplant recipients: Evaluation, implication, and prevention. *Tropical parasitology* **6**, 123 (2016).

11 Furtado, J. M., Smith, J. R., Belfort Jr, R., Gattey, D. & Winthrop, K. L. Toxoplasmosis: a global threat. *Journal of global infectious diseases* **3**, 281 (2011).

12 Robert-Gangneux, F. & Dardé, M.-L. Epidemiology of and diagnostic strategies for toxoplasmosis. *Clinical microbiology reviews* **25**, 264-296 (2012).

13 McAuley, J. B. Congenital toxoplasmosis. *Journal of the Pediatric Infectious Diseases Society* **3**, S30-S35 (2014).

14 Elbez-Rubinstein, A. *et al.* Congenital toxoplasmosis and reinfection during pregnancy: case report, strain characterization, experimental model of reinfection, and review. *Journal of Infectious Diseases* **199**, 280-285 (2009).

15 Torgerson, P. R. & Mastroiacovo, P. The global burden of congenital toxoplasmosis: a systematic review. *Bulletin of the World Health Organization* **91**, 501-508 (2013).

16 Rougier, S., Montoya, J. G. & Peyron, F. Lifelong Persistence of *Toxoplasma* Cysts: A Questionable Dogma? *Trends in Parasitology* (2016).

17 Shwab, E. K. *et al.* Geographical patterns of *Toxoplasma gondii* genetic diversity revealed by multilocus PCR-RFLP genotyping. *Parasitology* **141**, 453-461 (2014).

18 Hassan, M. A., Olijnik, A.-A., Frickel, E.-M. & Saeij, J. P. Clonal and atypical *Toxoplasma* strain differences in virulence vary with mouse sub-species. *International journal for parasitology* **49**, 63-70 (2019).

19 Su, C. *et al.* Recent expansion of *Toxoplasma* through enhanced oral transmission. *Science* **299**, 414-416 (2003).

20 Howe, D. K. & Sibley, L. D. *Toxoplasma gondii* comprises three clonal lineages: correlation of parasite genotype with human disease. *Journal of infectious diseases* **172**, 1561-1566 (1995).

21 Howe, D. K., Honoré, S., Derouin, F. & Sibley, L. D. Determination of genotypes of *Toxoplasma gondii* strains isolated from patients with toxoplasmosis. *Journal of clinical microbiology* **35**, 1411-1414 (1997).

22 Sibley, L. D. & Boothroyd, J. C. Virulent strains of *Toxoplasma gondii* comprise a single clonal lineage. *Nature* **359**, 82 (1992).

23 Saeij, J. P. J., Boyle, J. P. & Boothroyd, J. C. Differences among the three major strains of *Toxoplasma gondii* and their specific interactions with the infected host. *Trends in Parasitology* **21**, 476-481 (2005).

24 Grigg, M. E., Bonnefoy, S., Hehl, A. B., Suzuki, Y. & Boothroyd, J. C. Success and virulence in *Toxoplasma* as the result of sexual recombination between two distinct ancestries. *Science* **294**, 161-165 (2001).

25 Su, C., Howe, D. K., Dubey, J., Ajioka, J. W. & Sibley, L. D. Identification of quantitative trait loci controlling acute virulence in *Toxoplasma gondii*. *Proceedings of the National Academy of Sciences* 99, 10753-10758 (2002).

26 Rosowski, E. E. *et al.* Strain-specific activation of the NF-κB pathway by GRA15, a novel *Toxoplasma gondii* dense granule protein. *Journal of Experimental Medicine* 208, 195-212, 0022-1007 (2011).

27 Saeij, J. *et al. Toxoplasma* co-opts host gene expression by injection of a polymorphic kinase homologue. *Nature* 445, 324-327 (2007).

28 Boyle, J. P., Saeij, J. P., Harada, S. Y., Ajioka, J. W. & Boothroyd, J. C. Expression QTL mapping of *Toxoplasma* genes reveals multiple mechanisms for strain-specific differences in gene expression. *Eukaryotic Cell* (2008).

29 Bertranpetit, E. *et al.* Phylogeography of *Toxoplasma gondii* points to a South American origin. *Infection, Genetics and Evolution* 48, 150-155 (2017).

30 Khan, A., Taylor, S., Ajioka, J. W., Rosenthal, B. M. & Sibley, L. D. Selection at a single locus leads to widespread expansion of *Toxoplasma gondii* lineages that are virulent in mice. *PLoS Genetics* 5 (2009).

31 Khan, A. *et al.* Recent transcontinental sweep of *Toxoplasma gondii* driven by a single monomorphic chromosome. *Proceedings of the National Academy of Sciences* 104, 14872-14877 (2007).

32 Minot, S. *et al.* Admixture and recombination among *Toxoplasma gondii* lineages explain global genome diversity. *Proceedings of the National Academy of Sciences* 109, 13458-13463 (2012).

33 Shwab, E. K. *et al.* Human impact on the diversity and virulence of the ubiquitous zoonotic parasite *Toxoplasma gondii*. *Proceedings of the National Academy of Sciences* 115, E6956-E6963 (2018).

34 Lehmann, T., Marcet, P. L., Graham, D. H., Dahl, E. R. & Dubey, J. P. Globalization and the population structure of *Toxoplasma gondii*. *Proceedings of the National Academy of Sciences* 103, 11423-11428 (2006).

35 Galal, L. *et al.* The introduction of new hosts with human trade shapes the extant distribution of *Toxoplasma gondii* lineages. *PLoS neglected tropical diseases* 13 (2019).

36 Su, C. *et al.* Globally diverse *Toxoplasma gondii* isolates comprise six major clades originating from a small number of distinct ancestral lineages. *Proceedings of the National Academy of Sciences* 109, 5844-5849 (2012).

37 Sibley, L. D. & Ajioka, J. W. Population structure of *Toxoplasma gondii*: clonal expansion driven by infrequent recombination and selective sweeps. *Annu. Rev. Microbiol.* 62, 329-351 (2008).

38 Dubey, J. P., Lindsay, D. S. & Speer, C. A. Structures of *Toxoplasma gondii*tachyzoites, bradyzoites, and sporozoites and biology and development of tissue cysts. *Clinical microbiology reviews* 11, 267-299, 0893-8512 (1998).

39 Dubey, J., Lindsay, D. & Speer, C. Structures of *Toxoplasma gondii*tachyzoites, bradyzoites, and sporozoites and biology and development of tissue cysts. *Clinical microbiology reviews* 11, 267-299 (1998).

40 Dubey, J. Duration of immunity to shedding of *Toxoplasma gondii* oocysts by cats. *The Journal of parasitology*, 410-415 (1995).

41 Dubey, J. Advances in the life cycle of *Toxoplasma gondii*. *International journal for parasitology* 28, 1019-1024 (1998).

42 Dubey, J. *et al.* Toxoplasmosis in captive dolphins (Tursiops truncatus) and walrus (Odobenus rosmarus). *The Journal of parasitology* 95, 82 (2009).

43 Stelzer, S. *et al. Toxoplasma gondii* infection and toxoplasmosis in farm animals: Risk factors and economic impact. *Food and Waterborne Parasitology* 15, e00037 (2019).

44 Watts, E. *et al.* Novel approaches reveal that *Toxoplasma gondii* bradyzoites within tissue cysts are dynamic and replicating entities in vivo. *MBio* 6, e01155-01115 (2015).

45 Melo, E., Attias, M. & De Souza, W. The single mitochondrion of tachyzoites of *Toxoplasma gondii*. *Journal of structural biology* 130, 27-33 (2000).

46 van Dooren, G. G. & Striepen, B. The algal past and parasite present of the apicoplast. *Annual review of microbiology* 67, 271-289 (2013).

47 Zhu, G., Marchewka, M. J. & Keithly, J. S. Cryptosporidium parvum appears to lack a plastid genome. *Microbiology* 146, 315-321 (2000).

48 Huang, J. *et al.* Phylogenomic evidence supports past endosymbiosis, intracellular and horizontal gene transfer in Cryptosporidium parvum. *Genome biology* 5, R88 (2004).

49 LEVINE, N. D. Progress in taxonomy of the Apicomplexan protozoa. *The Journal of protozoology* 35, 518-520 (1988).

50 Boothroyd, J. C. & Dubremetz, J.-F. Kiss and spit: the dual roles of *Toxoplasma* rhoptries. *Nature Reviews Microbiology* 6, 79-88 (2008).

51 Carruthers, V. B. & Tomley, F. M. in *Molecular Mechanisms of Parasite Invasion* 33-45 (Springer, 2008).

52 Mercier, C., Adjogble, K. D. Z., Däubener, W. & Delauw, M.-F.-C. Dense granules: Are they key organelles to help understand the parasitophorous vacuole of all apicomplexa parasites? *International Journal for Parasitology* **35**, 829-849 (2005).

53 Gaskins, E. *et al.* Identification of the membrane receptor of a class XIV myosin in *Toxoplasma gondii*. *The Journal of cell biology* **165**, 383-393, 0021-9525 (2004).

54 Keeley, A. & Soldati, D. The glideosome: a molecular machine powering motility and host-cell invasion by Apicomplexa. *Trends in cell biology* **14**, 528-532 (2004).

55 Morrissette, N. S. & Sibley, L. D. Cytoskeleton of Apicomplexan Parasites. *Microbiology and Molecular Biology Reviews* **66**, 21-38 (2002).

56 Morrissette, N. S., Murray, J. M. & Roos, D. S. Subpellicular microtubules associate with an intramembranous particle lattice in the protozoan parasite *Toxoplasma gondii*. *Journal of cell science* **110**, 35-42 (1997).

57 Nichols, B. A. & Chiappino, M. L. Cytoskeleton of *Toxoplasma gondii* 1. *The Journal of protozoology* **34**, 217-226 (1987).

58 Blader, I. J., Coleman, B. I., Chen, C.-T. & Gubbels, M.-J. Lytic Cycle of *Toxoplasma gondii*: 15 Years Later. *Annual review of microbiology* **69**, 463-485 (2015).

59 Meissner, M., Schlüter, D. & Soldati, D. Role of *Toxoplasma gondii* myosin A in powering parasite gliding and host cell invasion. *Science* **298**, 837-840 (2002).

60 Frénal, K., Dubremetz, J.-F., Lebrun, M. & Soldati-Favre, D. Gliding motility powers invasion and egress in Apicomplexa. *Nature Reviews Microbiology* **15**, 645 (2017).

61 Heintzelman, M. B. & Schwartzman, J. D. Characterization of Myosin-A and Myosin-C: Two class XIV unconventional myosins from *Toxoplasma gondii*. *Cell motility and the cytoskeleton* **44**, 58-67 (1999).

62 Herm-Götz, A. *et al. Toxoplasma gondii* myosin A and its light chain: a fast, single-headed, plus-end-directed motor. *The EMBO journal* **21**, 2149-2158 (2002).

63 Williams, M. J. *et al.* Two essential light chains regulate the MyoA lever arm to promote *Toxoplasma* gliding motility. *MBio* **6**, e00845-00815 (2015).

64 Frénal, K. *et al.* Functional dissection of the apicomplexan glideosome molecular architecture. *Cell host & microbe* **8**, 343-357 (2010).

65 Jacot, D. *et al.* An Apicomplexan Actin-Binding Protein Serves as a Connector and Lipid Sensor to Coordinate Motility and Invasion. *Cell Host & Microbe* **20**, 731-743 (2016).

66 Mueller, C. *et al.* The *Toxoplasma* protein ARO mediates the apical positioning of rhoptry organelles, a prerequisite for host cell invasion. *Cell host & microbe* **13**, 289-301 (2013).

67 Suarez, C. *et al.* A lipid-binding protein mediates rhoptry discharge and invasion in Plasmodium falciparum and *Toxoplasma gondii* parasites. *Nature communications* **10**, 1-14 (2019).

68 Kessler, H. *et al.* Microneme protein 8–a new essential invasion factor in *Toxoplasma gondii*. *Journal of cell science* **121**, 947-956 (2008).

69 Koshy, A. A. *et al. Toxoplasma* co-opts host cells it does not invade. *PLoS pathogens* **8**, e1002825, 1001553-1007374 (2012).

70 Clough, B. & Frickel, E.-M. The *Toxoplasma* parasitophorous vacuole: an evolving host–parasite frontier. *Trends in parasitology* **33**, 473-488 (2017).

71 Suss-Toby, E., Zimmerberg, J. & Ward, G. *Toxoplasma* invasion: the parasitophorous vacuole is formed from host cell plasma membrane and pinches off via a fission pore. *Proceedings of the National Academy of Sciences* **93**, 8413-8418 (1996).

72 Carruthers, V. B. & Sibley, L. Sequential protein secretion from three distinct organelles of *Toxoplasma gondii* accompanies invasion of human fibroblasts. *European journal of cell biology* **73**, 114-123 (1997).

73 Mercier, C. *et al.* Biogenesis of nanotubular network in *Toxoplasma* parasitophorous vacuole induced by parasite proteins. *Molecular biology of the cell* **13**, 2397-2409 (2002).

74 Sibley, L. D., Niesman, I. R., Parmley, S. F. & Cesbron-Delauw, M.-F. Regulated secretion of multi-lamellar vesicles leads to formation of a tubulo-vesicular network in host-cell vacuoles occupied by *Toxoplasma gondii*. *Journal of cell science* **108**, 1669-1677 (1995).

75 Magno, R. C., Lemgruber, L., Vommaro, R. C., De Souza, W. & Attias, M. Intravacuolar network may act as a mechanical support for *Toxoplasma gondii* inside the parasitophorous vacuole. *Microscopy research and technique* **67**, 45-52 (2005).

76 Francia, M. E. & Striepen, B. Cell division in apicomplexan parasites. *Nature Reviews Microbiology* **12**, 125-136 (2014).

77 Hu, K. *et al.* Daughter cell assembly in the protozoan parasite *Toxoplasma gondii*. *Molecular biology of the cell* **13**, 593-606 (2002).

78 Nishi, M., Hu, K., Murray, J. M. & Roos, D. S. Organellar dynamics during the cell cycle of *Toxoplasma gondii*. *Journal of cell science* **121**, 1559-1568 (2008).

79 Periz, J. *et al.* A highly dynamic F-actin network regulates transport and recycling of micronemes in *Toxoplasma gondii* vacuoles. *Nature Communications* **10**, 4183 (2019).

80 Muñiz-Hernández, S. *et al.* Contribution of the residual body in the spatial organization of *Toxoplasma gondii* tachyzoites within the parasitophorous vacuole. *BioMed Research International* **2011** (2011).

81 Morrissette, N. S. & Sibley, L. D. Disruption of microtubules uncouples budding and nuclear division in *Toxoplasma gondii*. *Journal of cell science* **115**, 1017-1025 (2002).

82 Endo, T., Sethi, K. & Piekarski, G. *Toxoplasma gondii*: Calcium Ionophore A23187-mediated exit of trophozoites from infected murine macrophages. *Experimental parasitology* **53**, 179-188 (1982).

83 Coppin, A. *et al.* Developmentally regulated biosynthesis of carbohydrate and storage polysaccharide during differentiation and tissue cyst formation in *Toxoplasma gondii*. *Biochimie* **85**, 353-361 (2003).

84 Denton, H., Roberts, C. W., Alexander, J., Thong, K.-w. & Coombs, G. H. Enzymes of energy metabolism in the bradyzoites and tachyzoites of *Toxoplasma gondii*. *FEMS microbiology letters* **137**, 103-108 (1996).

85 Ferguson, D. Use of molecular and ultrastructural markers to evaluate stage conversion of *Toxoplasma gondii* in both the intermediate and definitive host. *International journal for parasitology* **34**, 347-360 (2004).

86 Behnke, M. S., Radke, J. B., Smith, A. T., Sullivan Jr, W. J. & White, M. W. The transcription of bradyzoite genes in *Toxoplasma gondii* is controlled by autonomous promoter elements. *Molecular microbiology* **68**, 1502-1518 (2008).

87 Radke, J. R. *et al.* The transcriptome of *Toxoplasma gondii*. *BMC biology* **3**, 26 (2005).

88 Garfoot, A. L., Cervantes, P. W. & Knoll, L. J. Transcriptional analysis shows a robust host response to *Toxoplasma gondii* during early and late chronic infection in both male and female mice. *Infection and immunity* **87**, e00024-00019 (2019).

89 Fox, B. A. *et al.* Type II *Toxoplasma gondii* KU80 knockout strains enable functional analysis of genes required for cyst development and latent infection. *Eukaryotic cell*, EC. 00297-00210, 01535-09778 (2011).

90 Bohne, W. & Roos, D. S. Stage-specific expression of a selectable marker in *Toxoplasma gondii* permits selective inhibition of either tachyzoites or bradyzoites. *Molecular and Biochemical Parasitology* **88**, 115-126 (1997).

91 Bohne, W., Gross, U., Ferguson, D. J. & Heesemann, J. Cloning and characterization of a bradyzoite-specifically expressed gene (hsp30/bag1) of *Toxoplasma gondii*, related to genes encoding small heat-shock proteins of plants. *Molecular microbiology* **16**, 1221-1230 (1995).

92 Weiss, L. M., Ma, Y. F., Takvorian, P. M., Tanowitz, H. B. & Wittner, M. Bradyzoite development in *Toxoplasma gondii* and the hsp70 stress response. *Infection and immunity* **66**, 3295-3302 (1998).

93 Toursel, C., Dzierszinski, F., Bernigaud, A., Mortuaire, M. & Tomavo, S. Molecular cloning, organellar targeting and developmental expression of mitochondrial chaperone HSP60 in *Toxoplasma gondii*. *Molecular and biochemical parasitology* **111**, 319-332 (2000).

94 Echeverria, P. C. *et al. Toxoplasma gondii* Hsp90 is a potential drug target whose expression and subcellular localization are developmentally regulated. *Journal of molecular biology* **350**, 723-734 (2005).

95 Ueno, A. *et al. Toxoplasma gondii*: a bradyzoite-specific DnaK-tetratricopeptide repeat (DnaK-TPR) protein interacts with p23 co-chaperone protein. *Experimental parasitology* **127**, 795-803 (2011).

96 Zhang, Y. W. *et al.* Disruption of the *Toxoplasma gondii* bradyzoite-specific gene BAG1 decreases in vivo cyst formation. *Molecular microbiology* **31**, 691-701 (1999).

97 Lekutis, C., Ferguson, D. J., Grigg, M. E., Camps, M. & Boothroyd, J. C. Surface antigens of *Toxoplasma gondii*: variations on a theme. *International journal for parasitology* **31**, 1285-1292 (2001).

98 Van, T. T., Kim, S.-K., Camps, M., Boothroyd, J. C. & Knoll, L. J. The BSR4 protein is up-regulated in *Toxoplasma gondii* bradyzoites, however the dominant surface antigen recognised by the P36 monoclonal antibody is SRS9. *International journal for parasitology* **37**, 877-885 (2007).

99 Jung, C., Lee, C. Y.-F. & Grigg, M. E. The SRS superfamily of *Toxoplasma* surface proteins. *International journal for parasitology* **34**, 285-296 (2004).

100 Crawford, J. *et al.* Structural characterization of the bradyzoite surface antigen (BSR4) from *Toxoplasma gondii*, a unique addition to the surface antigen glycoprotein 1-related superfamily. *Journal of Biological Chemistry* **284**, 9192-9198 (2009).

101 Knoll, L. J. & Boothroyd, J. C. Isolation of Developmentally Regulated Genes from*Toxoplasma gondii* by a Gene Trap with the Positive and Negative Selectable Marker Hypoxanthine-Xanthine-Guanine Phosphoribosyltransferase. *Molecular and Cellular Biology* **18**, 807-814 (1998).

102 Kim, S.-K., Karasov, A. & Boothroyd, J. C. Bradyzoite-specific surface antigen SRS9 plays a role in maintaining *Toxoplasma gondii* persistence in the brain and in host control of parasite replication in the intestine. *Infection and immunity* **75**, 1626-1634, 0019-9567 (2007).

103 Yang, S. & Parmley, S. F. *Toxoplasma gondii* expresses two distinct lactate dehydrogenase homologous genes during its life cycle in intermediate hosts. *Gene* **184**, 1-12, 0378-1119 (1997).

104 Lunghi, M., Galizi, R., Magini, A., Carruthers, V. B. & Di Cristina, M. Expression of the glycolytic enzymes enolase and lactate dehydrogenase during the early phase of T oxoplasma differentiation is regulated by an intron retention mechanism. *Molecular microbiology* **96**, 1159-1175 (2015).

105 Dando, C. *et al.* The kinetic properties and sensitivities to inhibitors of lactate dehydrogenases (LDH1 and LDH2) from *Toxoplasma gondii*: comparisons with pLDH from Plasmodium falciparum. *Molecular and biochemical parasitology* **118**, 23-32 (2001).

106 Al-Anouti, F., Tomavo, S., Parmley, S. & Ananvoranich, S. The expression of lactate dehydrogenase is important for the cell cycle of *Toxoplasma gondii*. *Journal of Biological Chemistry* **279**, 52300-52311 (2004).

107 Abdelbaset, A. E. *et al.* Lactate dehydrogenase in *Toxoplasma gondii* controls virulence, bradyzoite differentiation, and chronic infection. *PloS one* **12** (2017).

108 Tu, V., Yakubu, R. & Weiss, L. M. Observations on bradyzoite biology. *Microbes Infect* **20**, 466-476 (2018).

109 Modrzynska, K. *et al.* A Knockout Screen of ApiAP2 Genes Reveals Networks of Interacting Transcriptional Regulators Controlling the Plasmodium Life Cycle. *Cell Host & Microbe* **21**, 11-22 (2017).

110 Jeninga, M. D., Quinn, J. E. & Petter, M. ApiAP2 transcription factors in apicomplexan parasites. *Pathogens* **8**, 47 (2019).

111 Balaji, S., Babu, M. M., Iyer, L. M. & Aravind, L. Discovery of the principal specific transcription factors of Apicomplexa and their implication for the evolution of the AP2-integrase DNA binding domains. *Nucleic acids research* **33**, 3994-4006 (2005).

112 Altschul, S. F., Wootton, J. C., Zaslavsky, E. & Yu, Y.-K. The construction and use of log-odds substitution scores for multiple sequence alignment. *PLoS Comput Biol* **6**, e1000852-e1000852 (2010).

113 Hong, D.-P., Radke, J. B. & White, M. W. Opposing transcriptional mechanisms regulate *Toxoplasma* development. *mSphere* **2**, e00347-00316 (2017).

114 Radke, J. B. *et al.* ApiAP2 transcription factor restricts development of the *Toxoplasma* tissue cyst. *Proceedings of the National Academy of Sciences* **110**, 6871-6876 (2013).

115 Huang, S. *et al. Toxoplasma gondii* AP2IX-4 regulates gene expression during bradyzoite development. *MSphere* **2**, e00054-00017 (2017).

116 Radke, J. B. *et al.* Transcriptional repression by ApiAP2 factors is central to chronic toxoplasmosis. *PLoS pathogens* **14**, e1007035 (2018).

117 Walker, R. *et al.* The T oxoplasma nuclear factor TgAP2XI-4 controls bradyzoite gene expression and cyst formation. *Molecular microbiology* **87**, 641-655 (2013).

118 Jeffers, V., Tampaki, Z., Kim, K. & Sullivan, W. J. A latent ability to persist: differentiation in *Toxoplasma gondii*. *Cellular and Molecular Life Sciences* **75**, 2355-2373 (2018).

119 Waldman, B. S. *et al.* Identification of a master regulator of differentiation in *Toxoplasma*. *Cell* (2020).

120 da Silva, M. d. F. F., Barbosa, H. S., Groß, U. & Lüder, C. G. Stress-related and spontaneous stage differentiation of *Toxoplasma gondii*. *Molecular Biosystems* **4**, 824-834 (2008).

121 Paredes-Santos, T. *et al.* Spontaneous cystogenesis in vitro of a Brazilian strain of *Toxoplasma gondii*. *Parasitology international* **62**, 181-188 (2013).

122 Fox, B. A., Gigley, J. P. & Bzik, D. J. *Toxoplasma gondii* lacks the enzymes required for de novo arginine biosynthesis and arginine starvation triggers cyst formation. *International journal for parasitology* **34**, 323-331 (2004).

123 Soete, M., Camus, D. & Dubrametz, J. Experimental induction of bradyzoite-specific antigen expression and cyst formation by the RH strain of *Toxoplasma gondii* in vitro. *Experimental parasitology* **78**, 361-370 (1994).

124 Donald, R. G. K. *et al. Toxoplasma gondii* cyclic GMP-dependent kinase: chemotherapeutic targeting of an essential parasite protein kinase. *Eukaryotic cell* **1**, 317-328, 1535-9778 (2002).

125 Suzuki, Y., Orellana, M. A., Schreiber, R. D. & Remington, J. S. Interferon-gamma: the major mediator of resistance against *Toxoplasma gondii*. *Science* **240**, 516-518, 0036-8075 (1988).

126 Swierzy, I. J. & Lüder, C. G. Withdrawal of skeletal muscle cells from cell cycle progression triggers differentiation of T oxoplasma gondii towards the bradyzoite stage. *Cellular microbiology* **17**, 2-17 (2015).

127 Lüder, C. G. & Rahman, T. Impact of the host on *Toxoplasma* stage differentiation. *Microbial Cell* **4**, 203 (2017).

128 Lüder, C. G., Giraldo-Velásquez, M., Sendtner, M. & Gross, U. *Toxoplasma gondii* in primary rat CNS cells: differential contribution of neurons, astrocytes, and microglial cells for the intracerebral development and stage differentiation. *Experimental parasitology* **93**, 23-32 (1999).

129 da Fonseca Ferreira-da-Silva, M., Takács, A. C., Barbosa, H. S., Gross, U. & Lüder, C. G. Primary skeletal muscle cells trigger spontaneous *Toxoplasma gondii* tachyzoite-to-bradyzoite conversion at higher rates than fibroblasts. *International Journal of Medical Microbiology* **299**, 381-388 (2009).

130 Kim, K. A Bradyzoite is a Bradyzoite is a Bradyzoite? *Trends in parasitology* **31**, 610-612 (2015).

131 Ferguson, D. J., Huskinson-Mark, J., Araujo, F. G. & Remington, J. S. A morphological study of chronic cerebral toxoplasmosis in mice: comparison of four different strains of*Toxoplasma gondii*. *Parasitology research* **80**, 493-501 (1994).

132 Lemgruber, L., Lupetti, P., Martins-Duarte, E. S., De Souza, W. & Vommaro, R. C. The organization of the wall filaments and characterization of the matrix structures of *Toxoplasma gondii* cyst form. *Cellular microbiology* **13**, 1920-1932 (2011).

133 Ferguson, D. & Hutchison, W. An ultrastructural study of the early development and tissue cyst formation of *Toxoplasma gondii* in the brains of mice. *Parasitology research* **73**, 483-491 (1987).

134 Tu, V. *et al.* Enrichment and proteomic characterization of the cyst wall from in vitro *Toxoplasma gondii* cysts. *MBio* **10**, e00469-00419 (2019).

135 Guevara, R. B., Fox, B. A., Falla, A. & Bzik, D. J. *Toxoplasma gondii* Intravacuolar-Network-Associated Dense Granule Proteins Regulate Maturation of the Cyst Matrix and Cyst Wall. *mSphere* **4**, e00487-00419 (2019).

136 Dzierszinski, F., Nishi, M., Ouko, L. & Roos, D. S. Dynamics of *Toxoplasma gondii* Differentiation. *Eukaryotic Cell* **3**, 992-1003 (2004).

137 Zhang, Y. W., Halonen, S. K., Ma, Y. F., Wittner, M. & Weiss, L. M. Initial Characterization of CST1, a*Toxoplasma gondii* Cyst Wall Glycoprotein. *Infection and immunity* **69**, 501-507, 0019-9567 (2001).

138 Caffaro, C. E. *et al.* A nucleotide sugar transporter involved in glycosylation of the *Toxoplasma* tissue cyst wall is required for efficient persistence of bradyzoites. *PLoS pathog* **9**, e1003331 (2013).

139 Tomita, T. *et al.* The *Toxoplasma gondii* cyst wall protein CST1 is critical for cyst wall integrity and promotes bradyzoite persistence. *PLoS Pathog* **9**, e1003823 (2013).

140 Tomita, T. *et al.* Making Home Sweet and Sturdy: *Toxoplasma gondii* ppGalNAc-Ts Glycosylate in Hierarchical Order and Confer Cyst Wall Rigidity. *mBio* **8**, e02048-02016 (2017).

141 Tomita, T. *et al.* The *Toxoplasma gondii* cyst wall protein CST1 is critical for cyst wall integrity and promotes bradyzoite persistence. *PLoS pathogens* **9** (2013).

142 Tomita, T., Ma, Y. & Weiss, L. Characterization of a SRS13: a new cyst wall mucin-like domain containing protein. *Parasitology research* **117**, 2457-2466 (2018).

143 Acquarone, M., Ferreira-da-Silva, M. d. F., Guimarães, E. V. & Barbosa, H. S. in *Toxoplasmosis* (IntechOpen, 2017).

144 Paredes Santos, T., Wang, Y., Waldman, B., Lourido, S. & Saeij, J. P. The GRA17 parasitophorous vacuole membrane permeability pore contributes to bradyzoite viability. *Frontiers in cellular and infection microbiology* **9**, 321 (2019).

145 Courret, N. *et al.* CD11c-and CD11b-expressing mouse leukocytes transport single *Toxoplasma gondii* tachyzoites to the brain. *Blood* **107**, 309-316 (2006).

146 Lambert, H., Hitziger, N., Dellacasa, I., Svensson, M. & Barragan, A. Induction of dendritic cell migration upon *Toxoplasma gondii* infection potentiates parasite dissemination. *Cellular microbiology* **8**, 1611-1623 (2006).

147 Lambert, H., Vutova, P. P., Adams, W. C., Loré, K. & Barragan, A. The *Toxoplasma gondii*-shuttling function of dendritic cells is linked to the parasite genotype. *Infection and immunity* **77**, 1679-1688 (2009).

148 Cai, Y. *et al. Toxoplasma gondii* inhibits apoptosis via a novel STAT3-miR-17–92-Bim pathway in macrophages. *Cellular signalling* **26**, 1204-1212 (2014).

149 Da Gama, L. M., Ribeiro-Gomes, F. L., Guimarães, U. & Arnholdt, A. C. V. Reduction in adhesiveness to extracellular matrix components, modulation of adhesion molecules and

in vivo migration of murine macrophages infected with *Toxoplasma gondii*. *Microbes and Infection* **6**, 1287-1296 (2004).

150 Weidner, J. M. & Barragan, A. Tightly regulated migratory subversion of immune cells promotes the dissemination of *Toxoplasma gondii*. *International journal for parasitology* **44**, 85-90 (2014).

151 Mendez, O. A. & Koshy, A. A. *Toxoplasma gondii*: Entry, association, and physiological influence on the central nervous system. *PLoS pathogens* **13** (2017).

152 Konradt, C. *et al.* Endothelial cells are a replicative niche for entry of *Toxoplasma gondii* to the central nervous system. *Nature microbiology* **1** (2016).

153 Barragan, A., Brossier, F. & Sibley, L. D. Transepithelial migration of *Toxoplasma gondii* involves an interaction of intercellular adhesion molecule 1 (ICAM-1) with the parasite adhesin MIC2. *Cellular microbiology* **7**, 561-568 (2005).

154 Barragan, A. & Sibley, L. D. Transepithelial migration of *Toxoplasma gondii* is linked to parasite motility and virulence. *The Journal of experimental medicine* **195**, 1625-1633 (2002).

155 Cabral, C. M. *et al.* Neurons are the primary target cell for the brain-tropic intracellular parasite *Toxoplasma gondii*. *PLoS Pathog* **12**, e1005447 (2016).

156 Dellacasa-Lindberg, I. *et al.* Migratory activation of primary cortical microglia upon infection with *Toxoplasma gondii*. *Infection and immunity* **79**, 3046-3052 (2011).

157 Melzer, T., Cranston, H., Weiss, L. & Halonen, S. Host cell preference of *Toxoplasma gondii* cysts in murine brain: a confocal study. *Journal of neuroparasitology* **1** (2010).

158 Koshy, A. A. *et al. Toxoplasma* co-opts host cells it does not invade. *PLoS pathog* **8**, e1002825 (2012).

159 Koshy, A. A. *et al. Toxoplasma* secreting Cre recombinase for analysis of host-parasite interactions. *Nature methods* **7**, 307-309 (2010).

160 Cabral, C. M. & Koshy, A. A. 3-D imaging and analysis of neurons infected in vivo with *Toxoplasma gondii*. *JoVE (Journal of Visualized Experiments)*, e52237-e52237 (2014).

161 Tyebji, S., Seizova, S., Hannan, A. J. & Tonkin, C. J. Toxoplasmosis: A pathway to neuropsychiatric disorders. *Neuroscience & Biobehavioral Reviews* **96**, 72-92 (2019).

162 Coppens, I. & Romano, J. D. Hostile intruder: *Toxoplasma* holds host organelles captive. *PLoS pathogens* **14** (2018).

163 Hakimi, M.-A., Olias, P. & Sibley, L. D. *Toxoplasma* effectors targeting host signaling and transcription. *Clinical microbiology reviews* **30**, 615-645, 0893-8512 (2017).

164 Lambert, H. & Barragan, A. Modelling parasite dissemination: host cell subversion and immune evasion by *Toxoplasma gondii*. *Cellular microbiology* **12**, 292-300 (2010).

165 Pernas, L. *et al. Toxoplasma* effector MAF1 mediates recruitment of host mitochondria and impacts the host response. *PLoS biology* **12**, e1001845, 1001545-1007885 (2014).

166 Fuks, J. M. *et al.* GABAergic signaling is linked to a hypermigratory phenotype in dendritic cells infected by *Toxoplasma gondii*. *PLoS pathogens* **8** (2012).

167 Blader, I. J., Manger, I. D. & Boothroyd, J. C. Microarray analysis reveals previously unknown changes in *Toxoplasma gondii*-infected human cells. *Journal of Biological Chemistry* **276**, 24223-24231 (2001).

168 Swierzy, I. J. *et al.* Divergent co-transcriptomes of different host cells infected with *Toxoplasma gondii* reveal cell type-specific host-parasite interactions. *Scientific reports* **7**, 1-14 (2017).

169 Taylor, S. *et al.* A Secreted Serine-Threonine Kinase Determines Virulence in the Eukaryotic Pathogen *Toxoplasma gondii*. *Science* **314**, 1776-1780 (2006).

170 Behnke, M. S. *et al.* Virulence differences in *Toxoplasma* mediated by amplification of a family of polymorphic pseudokinases. *Proceedings of the National Academy of Sciences* **108**, 9631-9636 (2011).

171 Saeij, J. *et al.* Polymorphic secreted kinases are key virulence factors in toxoplasmosis. *Science* **314**, 1780-1783 (2006).

172 Saeij, J. P. J. *et al. Toxoplasma* co-opts host gene expression by injection of a polymorphic kinase homologue. *Nature* **445**, 324, 1476-4687 (2007).

173 Braun, L. *et al.* A *Toxoplasma* dense granule protein, GRA24, modulates the early immune response to infection by promoting a direct and sustained host p38 MAPK activation. *Journal of Experimental Medicine* **210**, 2071-2086, 0022-1007 (2013).

174 Olias, P., Etheridge, R. D., Zhang, Y., Holtzman, M. J. & Sibley, L. D. *Toxoplasma* effector recruits the Mi-2/NuRD complex to repress STAT1 transcription and block IFN-γ-dependent gene expression. *Cell host & microbe* **20**, 72-82, 1931-3128 (2016).

175 Gay, G. *et al. Toxoplasma gondii* TgIST co-opts host chromatin repressors dampening STAT1-dependent gene regulation and IFN-γ–mediated host defenses. *Journal of Experimental Medicine*,. 20160340, 20160022-20161007 (2016).

176 Bougdour, A. *et al.* Host cell subversion by *Toxoplasma* GRA16, an exported dense granule protein that targets the host cell nucleus and alters gene expression. *Cell host & microbe* **13**, 489-500, 1931-3128 (2013).

177 Fouts, A. E. & Boothroyd, J. C. Infection with *Toxoplasma gondii* bradyzoites has a diminished impact on host transcript levels relative to tachyzoite infection. *Infection and immunity* **75**, 634-642, 0019-9567 (2007).

178 McGettigan, P. A. Transcriptomics in the RNA-seq era. *Current opinion in chemical biology* **17**, 4-11 (2013).

179 Jia, B. *et al.* Genome-wide comparative analysis revealed significant transcriptome changes in mice after *Toxoplasma gondii* infection. *Parasites & vectors* **6**, 161 (2013).

180 Tanaka, S. *et al.* Transcriptome analysis of mouse brain infected with *Toxoplasma gondii*. *Infection and immunity* **81**, 3609-3619 (2013).

181 Pittman, K. J., Aliota, M. T. & Knoll, L. J. Dual transcriptional profiling of mice and *Toxoplasma gondii* during acute and chronic infection. *BMC genomics* **15**, 806, 1471-2164 (2014).

182 Chen, L. *et al.* The *Toxoplasma gondii* virulence factor ROP16 acts in cis and trans, and suppresses T cell responses. *Journal of Experimental Medicine* **217** (2020).

183 Rastogi, S., Xue, Y., Quake, S. R. & Boothroyd, J. C. Differential Impacts on Host Transcription by ROP and GRA Effectors from the Intracellular Parasite *Toxoplasma gondii*. *bioRxiv*, 2020.2002.2004.934570, doi:10.1101/2020.02.04.934570 (2020).

184 Naor, A. *et al.* MYR1-Dependent Effectors Are the Major Drivers of a Host Cell's Early Response to *Toxoplasma*, Including Counteracting MYR1-Independent Effects. *mBio* **9**, e02401-02417, 02150-07511 (2018).

185 Bradley, P. J. *et al.* Proteomic analysis of rhoptry organelles reveals many novel constituents for host-parasite interactions in *Toxoplasma gondii*. *Journal of Biological Chemistry* **280**, 34245-34258 (2005).

186 El Hajj, H. *et al.* ROP18 is a rhoptry kinase controlling the intracellular proliferation of *Toxoplasma gondii*. *PLoS pathogens* **3** (2007).

187 Etheridge, R. D. *et al.* The *Toxoplasma* pseudokinase ROP5 forms complexes with ROP18 and ROP17 kinases that synergize to control acute virulence in mice. *Cell host & microbe* **15**, 537-550, 1931-3128 (2014).

188 Saeij, J. P. & Frickel, E.-M. Exposing *Toxoplasma gondii* hiding inside the vacuole: a role for GBPs, autophagy and host cell death. *Current opinion in microbiology* **40**, 72-80, 1369-5274 (2017).

189 Etheridge, R. D. *et al.* The *Toxoplasma* pseudokinase ROP5 forms complexes with ROP18 and ROP17 kinases that synergize to control acute virulence in mice. *Cell host & microbe* **15**, 537-550 (2014).

190 Melo, M. B., Jensen, K. D. & Saeij, J. P. *Toxoplasma gondii* effectors are master regulators of the inflammatory response. *Trends in parasitology* **27**, 487-495 (2011).

191 Fleckenstein, M. C. *et al.* A *Toxoplasma gondii* pseudokinase inhibits host IRG resistance proteins. *PLoS Biol* **10**, e1001358 (2012).

192 Steinfeldt, T. *et al.* Phosphorylation of mouse immunity-related GTPase (IRG) resistance proteins is an evasion strategy for virulent *Toxoplasma gondii*. *PLoS Biol* **8**, e1000576 (2010).

193 Reese, M. L., Shah, N. & Boothroyd, J. C. The *Toxoplasma* pseudokinase ROP5 is an allosteric inhibitor of the immunity-related GTPases. *Journal of Biological Chemistry*, jbc. M114. 567057, 560021-569258 (2014).

194 Behnke, M. S. *et al.* The polymorphic pseudokinase ROP5 controls virulence in *Toxoplasma gondii* by regulating the active kinase ROP18. *PLoS pathogens* **8** (2012).

195 Niedelman, W. *et al.* The rhoptry proteins ROP18 and ROP5 mediate *Toxoplasma gondii* evasion of the murine, but not the human, interferon-gamma response. *PLoS pathogens* **8**, e1002784, 1001553-1007374 (2012).

196 Behnke, M. S. *et al.* Rhoptry proteins ROP5 and ROP18 are major murine virulence factors in genetically divergent South American strains of *Toxoplasma gondii*. *PLoS genetics* **11** (2015).

197 Fox, B. A. *et al.* The *Toxoplasma gondii* rhoptry kinome is essential for chronic infection. *mBio* **7**, e00193-00116 (2016).

198 Peixoto, L. *et al.* Integrative genomic approaches highlight a family of parasite-specific kinases that regulate host responses. *Cell host & microbe* **8**, 208-218 (2010).

199 Sidik, S. M., Hackett, C. G., Tran, F., Westwood, N. J. & Lourido, S. Efficient genome engineering of *Toxoplasma gondii* using CRISPR/Cas9. *PloS one* **9**, e100450, 101932-106203 (2014).

200 Shen, B., Brown, K. M., Lee, T. D. & Sibley, L. D. Efficient gene disruption in diverse strains of *Toxoplasma gondii* using CRISPR/CAS9. *MBio* **5**, e01114-01114, 02150-07511 (2014).

201 Long, S., Wang, Q. & Sibley, L. D. Analysis of non-canonical calcium dependent protein kinases in *Toxoplasma gondii* by targeted gene deletion using CRISPR/Cas9. *Infection and immunity*, IAI. 01173-01115, 00019-09567 (2016).

202 Sidik, S. M. *et al.* A genome-wide CRISPR screen in *Toxoplasma* identifies essential apicomplexan genes. *Cell* **166**, 1423-1435. e1412 (2016).

203 Wang, Y. *et al.* A genome-wide loss-of-function screen identifies *Toxoplasma gondii* genes that determine fitness in interferon gamma-activated murine macrophages. *bioRxiv*, 867705, doi:10.1101/867705 (2019).

204 Sangaré, L. O. *et al.* In Vivo CRISPR Screen Identifies TgWIP as a *Toxoplasma* Modulator of Dendritic Cell Migration. *Cell host & microbe* **26**, 478-492. e478 (2019).

205 Young, J. *et al.* A CRISPR platform for targeted in vivo screens identifies *Toxoplasma gondii* virulence factors in mice. *Nature communications* **10**, 1-11 (2019).

206 Chen, Z. *et al.* Structure and control of the actin regulatory WAVE complex. *Nature* **468**, 533-538 (2010).

207 Mercier, C. & Cesbron-Delauw, M.-F. *Toxoplasma* secretory granules: one population or more? *Trends in parasitology* **31**, 60-71 (2015).

208 Ma, J. S. *et al.* Selective and strain-specific NFAT4 activation by the *Toxoplasma gondii* polymorphic dense granule protein GRA6. *Journal of Experimental Medicine* **211**, 2013-2032, 0022-1007 (2014).

209 Fox, B. A. *et al. Toxoplasma gondii* parasitophorous vacuole membrane-associated dense granule proteins orchestrate chronic infection and GRA12 underpins resistance to host gamma interferon. *MBio* **10**, e00589-00519 (2019).

210 Alaganan, A., Fentress, S. J., Tang, K., Wang, Q. & Sibley, L. D. *Toxoplasma* GRA7 effector increases turnover of immunity-related GTPases and contributes to acute virulence in the mouse. *Proceedings of the National Academy of Sciences* **111**, 1126-1131 (2014).

211 Hermanns, T., Müller, U. B., Könen-Waisman, S., Howard, J. C. & Steinfeldt, T. The *Toxoplasma gondii* rhoptry protein ROP18 is an Irga6-specific kinase and regulated by the dense granule protein GRA7. *Cellular microbiology* **18**, 244-259 (2016).

212 Nadipuram, S. M. *et al.* In vivo biotinylation of the *Toxoplasma* parasitophorous vacuole reveals novel dense granule proteins important for parasite growth and pathogenesis. *MBio* **7**, e00808-00816, 02150-07511 (2016).

213 Tiku, V., Tan, M.-W. & Dikic, I. Mitochondrial functions in infection and immunity. *Trends in Cell Biology* **30**, 263-275 (2020).

214 Adomako-Ankomah, Y. *et al.* Host mitochondrial association evolved in the human parasite *Toxoplasma gondii* via neofunctionalization of a gene duplicate. *Genetics* **203**, 283-298 (2016).

215 Blank, M. L. *et al.* A *Toxoplasma gondii* locus required for the direct manipulation of host mitochondria has maintained multiple ancestral functions. *Molecular microbiology* **108**, 519-535 (2018).

216 Seth, R. B., Sun, L., Ea, C.-K. & Chen, Z. J. Identification and characterization of MAVS, a mitochondrial antiviral signaling protein that activates NF-κB and IRF3. *Cell* **122**, 669-682 (2005).

217 Pernas, L., Bean, C., Boothroyd, J. C. & Scorrano, L. Mitochondria restrict growth of the intracellular parasite *Toxoplasma gondii* by limiting its uptake of fatty acids. *Cell metabolism* **27**, 886-897. e884 (2018).

218 Robben, P. M. *et al.* Production of IL-12 by macrophages infected with *Toxoplasma gondii* depends on the parasite genotype. *The Journal of Immunology* **172**, 3686-3694 (2004).

219 Liu, Q. *et al.* Transcriptomic analysis reveals *Toxoplasma gondii* strain-specific differences in host cell response to dense granule protein GRA15. *Parasitology research* **117**, 2785-2793 (2018).

220 Sangaré, L. O. *et al. Toxoplasma* GRA15 Activates the NF-κB Pathway through Interactions with TNF Receptor-Associated Factors. *mBio* **10**, e00808-00819 (2019).

221 Hinz, M. & Scheidereit, C. The IκB kinase complex in NF-κB regulation and beyond. *EMBO reports* **15**, 46-61 (2014).

222 Hunter, C. A., Subauste, C. S., Van Cleave, V. & Remington, J. S. Production of gamma interferon by natural killer cells from *Toxoplasma gondii*-infected SCID mice: regulation by interleukin-10, interleukin-12, and tumor necrosis factor alpha. *Infection and immunity* **62**, 2818-2824 (1994).

223 Scharton-Kersten, T. M. *et al.* In the absence of endogenous IFN-gamma, mice develop unimpaired IL-12 responses to *Toxoplasma gondii* while failing to control acute infection. *The Journal of Immunology* **157**, 4045-4054, 0022-1767 (1996).

224 Gov, L., Karimzadeh, A., Ueno, N. & Lodoen, M. B. Human innate immunity to *Toxoplasma gondii* is mediated by host caspase-1 and ASC and parasite GRA15. *MBio* **4**, e00255-00213 (2013).

225 Yamamoto, M. *et al. Toxoplasma* effector GRA15-dependent suppression of IFN-γ-induced antiparasitic response in human neurons. *Frontiers in cellular and infection microbiology* **9**, 140 (2019).

226 Bando, H. *et al.* Inducible nitric oxide synthase is a key host factor for *Toxoplasma* GRA15-dependent disruption of the gamma interferon-induced antiparasitic human response. *MBio* **9**, e01738-01718 (2018).

227 Pfefferkorn, E. R., Eckel, M. & Rebhun, S. Interferon-γ suppresses the growth of *Toxoplasma gondii* in human fibroblasts through starvation for tryptophan. *Molecular and biochemical parasitology* **20**, 215-224 (1986).

228 Pfefferkorn, E. R. Interferon gamma blocks the growth of *Toxoplasma gondii* in human fibroblasts by inducing the host cells to degrade tryptophan. *Proceedings of the National Academy of Sciences* **81**, 908-912, 0027-8424 (1984).

229 Melo, M. B., Jensen, K. D. C. & Saeij, J. P. J. *Toxoplasma gondii* effectors are master regulators of the inflammatory response. *Trends in parasitology* **27**, 487-495, 1471-4922 (2011).

230 Li, M. *et al.* Deubiquitination of p53 by HAUSP is an important pathway for p53 stabilization. *Nature* **416**, 648-653 (2002).

231 Kim, S. G. *et al.* Increase in the nuclear localization of PTEN by the *Toxoplasma* GRA16 protein and subsequent induction of p53-dependent apoptosis and anticancer effect. *Journal of cellular and molecular medicine* **23**, 3234-3245 (2019).

232 Brunet, J. *et al. Toxoplasma gondii* exploits UHRF1 and induces host cell cycle arrest at G2 to enable its proliferation. *Cellular microbiology* **10**, 908-920, 1462-5814 (2008).

233 Molestina, R. E., El-Guendy, N. & Sinai, A. P. Infection with *Toxoplasma gondii* results in dysregulation of the host cell cycle. *Cellular microbiology* **10**, 1153-1165, 1462-5814 (2008).

234 Shaw, P. *et al.* Induction of apoptosis by wild-type p53 in a human colon tumor-derived cell line. *Proceedings of the National Academy of Sciences* **89**, 4495-4499 (1992).

235 Yonish-Rouach, E. *et al.* Wild-type p53 induces apoptosis of myeloid leukaemic cells that is inhibited by interleukin-6. *Nature* **352**, 345-347 (1991).

236 Braun, L. *et al.* A *Toxoplasma* dense granule protein, GRA24, modulates the early immune response to infection by promoting a direct and sustained host p38 MAPK activation. *Journal of Experimental Medicine*, jem. 20130103 (2013).

237 Coulthard, L. R., White, D. E., Jones, D. L., McDermott, M. F. & Burchill, S. A. p38MAPK: stress responses from molecular mechanisms to therapeutics. *Trends in molecular medicine* **15**, 369-379 (2009).

238 Pellegrini, E. *et al.* Structural basis for the subversion of MAP kinase signaling by an intrinsically disordered parasite secreted agonist. *Structure* **25**, 16-26 (2017).

239 Gazzinelli, R. T. *et al.* Parasite-induced IL-12 stimulates early IFN-gamma synthesis and resistance during acute infection with *Toxoplasma gondii*. *The Journal of Immunology* **153**, 2533-2543, 0022-1767 (1994).

240 Majoros, A. *et al.* Canonical and non-canonical aspects of JAK–STAT signaling: lessons from interferons for cytokine responses. *Frontiers in immunology* **8**, 29 (2017).

241 Rosowski, E. E., Nguyen, Q. P., Camejo, A., Spooner, E. & Saeij, J. P. J. *Toxoplasma gondii* inhibits gamma interferon (IFN-γ)-and IFN-β-induced host cell STAT1 transcriptional activity by increasing the association of STAT1 with DNA. *Infection and immunity* **82**, 706-719, 0019-9567 (2014).

242 Rosowski, E. E. & Saeij, J. P. J. *Toxoplasma gondii* clonal strains all inhibit STAT1 transcriptional activity but polymorphic effectors differentially modulate IFNγ induced gene expression and STAT1 phosphorylation. *PLoS One* **7**, e51448, 51932-56203 (2012).

243 Kim, S.-K., Fouts, A. E. & Boothroyd, J. C. *Toxoplasma gondii* dysregulates IFN-γ-inducible gene expression in human fibroblasts: insights from a genome-wide transcriptional profiling. *The Journal of Immunology* **178**, 5154-5165 (2007).

244 Lüder, C. G., Algner, M., Lang, C., Bleicher, N. & Groβ, U. Reduced expression of the inducible nitric oxide synthase after infection with *Toxoplasma gondii* facilitates parasite replication in activated murine macrophages. *International journal for parasitology* **33**, 833-844 (2003).

245 Lüder, C. G., Walter, W., Beuerle, B., Maeurer, M. J. & Gross, U. *Toxoplasma gondii* down-regulates MHC class II gene expression and antigen presentation by murine macrophages via interference with nuclear translocation of STAT1α. *European journal of immunology* **31**, 1475-1484 (2001).

246 Rosowski, E. E., Nguyen, Q. P., Camejo, A., Spooner, E. & Saeij, J. P. *Toxoplasma gondii* inhibits gamma interferon (IFN-γ)-and IFN-β-induced host cell STAT1 transcriptional activity by increasing the association of STAT1 with DNA. *Infection and immunity* **82**, 706-719 (2014).

247 Gay, G. *et al. Toxoplasma gondii* TgIST co-opts host chromatin repressors dampening STAT1-dependent gene regulation and IFN-γ–mediated host defenses. *Journal of Experimental Medicine*, jem. 20160340 (2016).

248 Olias, P., Etheridge, R. D., Zhang, Y., Holtzman, M. J. & Sibley, L. D. *Toxoplasma effector* recruits the mi-2/NuRD complex to repress STAT1 transcription and block IFN-γ-dependent gene expression. *Cell Host & Microbe* **20**, 72-82 (2016).

249 Lang, C. *et al.* Impaired chromatin remodelling at STAT1-regulated promoters leads to global unresponsiveness of *Toxoplasma gondii*-infected macrophages to IFN-γ. *PLoS pathogens* **8** (2012).

250 Rosowski, E. E. & Saeij, J. P. *Toxoplasma gondii* clonal strains all inhibit STAT1 transcriptional activity but polymorphic effectors differentially modulate IFNγ induced gene expression and STAT1 phosphorylation. *PLoS One* **7**, e51448 (2012).

251 Butcher, B. A. *et al. Toxoplasma gondii* rhoptry kinase ROP16 activates STAT3 and STAT6 resulting in cytokine inhibition and arginase-1-dependent growth control. *PLoS Pathog* **7**, e1002236 (2011).

252 Rosowski, E. E. *et al.* Strain-specific activation of the NF-κB pathway by GRA15, a novel *Toxoplasma gondii* dense granule protein. *Journal of Experimental Medicine* **208**, 195-212 (2011).

253 Pittman, K. J. & Knoll, L. J. Long-term relationships: the complicated interplay between the host and the developmental stages of *Toxoplasma gondii* during acute and chronic infections. *Microbiology and Molecular Biology Reviews* **79**, 387-401 (2015).

254 Matta, S. K. *et al. Toxoplasma gondii* effector TgIST blocks type I interferon signaling to promote infection. *Proceedings of the National Academy of Sciences* **116**, 17480-17491 (2019).

255 Orellana, M., Suzuki, Y., Araujo, F. & Remington, J. Role of beta interferon in resistance to *Toxoplasma gondii* infection. *Infection and immunity* **59**, 3287-3290 (1991).

256 Schmitz, J., Carlin, J., Borden, E. & Byrne, G. Beta interferon inhibits *Toxoplasma gondii* growth in human monocyte-derived macrophages. *Infection and immunity* **57**, 3254-3256 (1989).

257 Han, S. J. *et al.* Internalization and TLR-dependent type I interferon production by monocytes in response to *Toxoplasma gondii*. *Immunology and cell biology* **92**, 872-881 (2014).

258 He, H. *et al.* Characterization of a *Toxoplasma effector* uncovers an alternative GSK3/β-catenin-regulatory pathway of inflammation. *eLife* **7**, e39887, 32050-39084X (2018).

259 Stamos, J. L. & Weis, W. I. The β-catenin destruction complex. *Cold Spring Harbor perspectives in biology* **5**, a007898 (2013).

260 Li, V. S. *et al.* Wnt signaling through inhibition of β-catenin degradation in an intact Axin1 complex. *Cell* **149**, 1245-1256 (2012).

261 Taelman, V. F. *et al.* Wnt signaling requires sequestration of glycogen synthase kinase 3 inside multivesicular endosomes. *Cell* **143**, 1136-1148 (2010).

262 Hillesheim, A., Nordhoff, C., Boergeling, Y., Ludwig, S. & Wixler, V. β-catenin promotes the type I IFN synthesis and the IFN-dependent signaling response but is suppressed by influenza A virus-induced RIG-I/NF-κB signaling. *Cell communication and signaling* **12**, 29 (2014).

263 Baril, M. *et al.* Genome-wide RNAi screen reveals a new role of a WNT/CTNNB1 signaling pathway as negative regulator of virus-induced innate immune responses. *PLoS pathogens* **9** (2013).

264 Kang, S. *et al.* Targeted knock down of CCL22 and CCL17 by siRNA during DC differentiation and maturation affects the recruitment of T subsets. *Immunobiology* **215**, 153-162 (2010).

265 Panas, M. W., Naor, A., Cygan, A. & Boothroyd, J. *Toxoplasma* controls host cyclin E expression through the use of a novel MYR1-dependent effector protein, HCE1. *bioRxiv*, 573618 (2019).

266 Braun, L. *et al.* The *Toxoplasma* effector TEEGR promotes parasite persistence by modulating NF-κB signalling via EZH2. *Nature microbiology*, 1, 2058-5276 (2019).

267 Margueron, R. & Reinberg, D. The Polycomb complex PRC2 and its mark in life. *Nature* **469**, 343-349 (2011).

268 Coffey, M. J., Jennison, C., Tonkin, C. J. & Boddey, J. A. Role of the ER and Golgi in protein export by Apicomplexa. *Current opinion in cell biology* **41**, 18-24, 0955-0674 (2016).

269 Boddey, J. A. *et al.* An aspartyl protease directs malaria effector proteins to the host cell. *Nature* **463**, 627-631 (2010).

270 Hiller, N. L. *et al.* A host-targeting signal in virulence proteins reveals a secretome in malarial infection. *Science* **306**, 1934-1937 (2004).

271 Marti, M., Good, R. T., Rug, M., Knuepfer, E. & Cowman, A. F. Targeting malaria virulence and remodeling proteins to the host erythrocyte. *Science* **306**, 1930-1933 (2004).

272 de Koning-Ward, T. F. *et al.* A newly discovered protein export machine in malaria parasites. *Nature* **459**, 945-949 (2009).

273 Elsworth, B. *et al.* PTEX is an essential nexus for protein export in malaria parasites. *Nature* **511**, 587-591 (2014).

274 Coffey, M. J. *et al.* An aspartyl protease defines a novel pathway for export of *Toxoplasma* proteins into the host cell. *Elife* **4**, e10809 (2015).

275 Curt-Varesano, A., Braun, L., Ranquet, C., Hakimi, M. A. & Bougdour, A. The aspartyl protease TgASP5 mediates the export of the *Toxoplasma* GRA16 and GRA24 effectors into host cells. *Cellular microbiology* **18**, 151-167 (2016).

276 Hammoudi, P.-M. *et al.* Fundamental roles of the Golgi-associated *Toxoplasma* aspartyl protease, ASP5, at the host-parasite interface. *PLoS Pathog* **11**, e1005211 (2015).

277 Hsiao, C. H. C., Luisa Hiller, N., Haldar, K. & Knoll, L. J. A HT/PEXEL motif in *Toxoplasma* dense granule proteins is a signal for protein cleavage but not export into the host cell. *Traffic* **14**, 519-531 (2013).

278 Cygan, A. M. *et al.* Co-immunoprecipitation with MYR1 identifies three additional proteins within the *Toxoplasma* parasitophorous vacuole required for translocation of dense granule effectors into host cells. *bioRxiv*, 867788, doi:10.1101/867788 (2019).

279 Franco, M. *et al.* A novel secreted protein, MYR1, is central to *Toxoplasma's* manipulation of host cells. *MBio* **7**, e02231-02215, 02150-07511 (2016).

280 Coffey, M. J. *et al.* An aspartyl protease defines a novel pathway for export of *Toxoplasma* proteins into the host cell. *Elife* **4**, e10809, 12050-10084X (2015).

281 Blakely, W. J., Holmes, M. J. & Arrizabalaga, G. The Secreted Acid Phosphatase Domain-Containing GRA44 from *Toxoplasma gondii* is required for c-Myc Induction in Infected Cells. *mSphere* **5**, e00877-00819 (2020).

282 Coffey, M. J. *et al.* Aspartyl Protease 5 Matures Dense Granule Proteins That Reside at the Host-Parasite Interface in *Toxoplasma gondii*. *mBio* **9**, e01796-01718, 02150-07511 (2018).

283 Matthews, K. M., Pitman, E. L. & de Koning-Ward, T. F. Illuminating how malaria parasites export proteins into host erythrocytes. *Cellular microbiology* **21**, e13009 (2019).

284 Hakimi, M.-A. & Bougdour, A. *Toxoplasma's* ways of manipulating the host transcriptome via secreted effectors. *Current Opinion in Microbiology* **26**, 24-31 (2015).

285 Hagai, T., Azia, A., Babu, M. M. & Andino, R. Use of host-like peptide motifs in viral proteins is a prevalent strategy in host-virus interactions. *Cell reports* **7**, 1729-1739 (2014).

286 Davey, N. E., Cyert, M. S. & Moses, A. M. Short linear motifs–ex nihilo evolution of protein regulation. *Cell Communication and Signaling* **13**, 43 (2015).

287 Davey, N. E. *et al.* Attributes of short linear motifs. *Molecular BioSystems* **8**, 268-281 (2012).

288 Fuxreiter, M., Tompa, P. & Simon, I. Local structural disorder imparts plasticity on linear motifs. *Bioinformatics* **23**, 950-956 (2007).

289 Hertz, E. P. T. *et al.* A conserved motif provides binding specificity to the PP2A-B56 phosphatase. *Molecular cell* **63**, 686-695 (2016).

290 Marino, N. D. *et al.* Identification of a novel protein complex essential for effector translocation across the parasitophorous vacuole membrane of *Toxoplasma gondii*. *PLoS pathogens* **14**, e1006828, 1001553-1007374 (2018).

291 Bracha, S. *et al.* Engineering brain parasites for intracellular delivery of therapeutic proteins. *BioRxiv*, 481192 (2018).

292 Panas, M. W. *et al.* Translocation of dense granule effectors across the parasitophorous vacuole membrane in *Toxoplasma*-infected cells requires the activity of ROP17, a rhoptry protein kinase. *mSphere* **4**, e00276-00219 (2019).

293 Franco, M. *et al.* A novel secreted protein, MYR1, is central to *Toxoplasma's* manipulation of host cells. *MBio* **7**, e02231-02215 (2016).

294 Lee, P. A., Tullman-Ercek, D. & Georgiou, G. The bacterial twin-arginine translocation pathway. *Annu. Rev. Microbiol.* **60**, 373-395 (2006).

295 Gold, D. A. *et al.* The *Toxoplasma* dense granule proteins GRA17 and GRA23 mediate the movement of small molecules between the host and the parasitophorous vacuole. *Cell host & microbe* **17**, 642-652 (2015).

296 Masatani, T. *et al.* TgGRA23, a novel *Toxoplasma gondii* dense granule protein associated with the parasitophorous vacuole membrane and intravacuolar network. *Parasitology international* **62**, 372-379 (2013).

297 Garten, M. *et al.* EXP2 is a nutrient-permeable channel in the vacuolar membrane of *Plasmodium* and is essential for protein export via PTEX. *Nature microbiology* **3**, 1090-1098 (2018).

298 Krishnamurthy, S. & Saeij, J. *Toxoplasma* does not secrete the GRA16 and GRA24 effectors beyond the parasitophorous vacuole membrane of tissue cysts. *Frontiers in cellular and infection microbiology* **8**, 366, 2235-2988 (2018).

299 Weiss, L. M. *et al.* A cell culture system for study of the development of *Toxoplasma gondii* bradyzoites. *Journal of Eukaryotic Microbiology* **42**, 150-157, 1066-5234 (1995).

300 Schindelin, J. *et al.* Fiji: an open-source platform for biological-image analysis. *Nature methods* **9**, 676-682 (2012).

301 Koshy, A. A. *et al. Toxoplasma* secreting Cre recombinase for analysis of host-parasite interactions. *Nature methods* **7**, 307, 1548-7105 (2010).

302 Liberzon, A. *et al.* The molecular signatures database hallmark gene set collection. *Cell systems* **1**, 417-425 (2015).

303 Hammoudi, P.-M. *et al.* Fundamental roles of the Golgi-associated *Toxoplasma* aspartyl protease, ASP5, at the host-parasite interface. *PLoS pathogens* **11**, e1005211, 1001553-1007374 (2015).

304 Bowen, N. J., Fujita, N., Kajita, M. & Wade, P. A. Mi-2/NuRD: multiple complexes for many purposes. *Biochimica et Biophysica Acta (BBA) - Gene Structure and Expression* **1677**, 52-57 (2004).

305 Ruijter, A. J. D., Gennip, A. H. V., Caron, H. N., Kemp, S. & Kuilenburg, A. B. V. Histone deacetylases (HDACs): characterization of the classical HDAC family. *Biochemical Journal* **370**, 737-749 (2003).

306 Pearson, J. S. *et al.* A type III effector antagonizes death receptor signalling during bacterial gut infection. *Nature* **501**, 247-251 (2013).

307 Newson, J. P. *et al. Salmonella* effectors SseK1 and SseK3 target death domain proteins in the TNF and TRAIL signaling pathways. *Molecular & Cellular Proteomics* **18**, 1138-1156 (2019).

308 Bélanger, C. *et al.* Human herpesvirus 8 viral FLICE-inhibitory protein inhibits Fas-mediated apoptosis through binding and prevention of procaspase-8 maturation. *Journal of human virology* **4**, 62-73 (2001).

309 Thome, M. *et al.* Viral FLICE-inhibitory proteins (FLIPs) prevent apoptosis induced by death receptors. *Nature* **386**, 517-521 (1997).

310 Price, A. M. *et al.* Epstein-Barr virus ensures B cell survival by uniquely modulating apoptosis at early and late times after infection. *Elife* **6**, e22509 (2017).

311 Boillat, M. *et al.* Neuroinflammation-Associated Aspecific Manipulation of Mouse Predator Fear by *Toxoplasma gondii*. *Cell Reports* **30**, 320-334. e326 (2020).

312 Gajria, B. *et al.* ToxoDB: an integrated *Toxoplasma gondii* database resource. *Nucleic acids research* **36**, D553-D556 (2007).

313 Peng, D. & Tarleton, R. EuPaGDT: a web tool tailored to design CRISPR guide RNAs for eukaryotic pathogens. *Microbial genomics* **1** (2015).

314 McCoy, J. M., Whitehead, L., van Dooren, G. G. & Tonkin, C. J. TgCDPK3 regulates calcium-dependent egress of *Toxoplasma gondii* from host cells. *PLoS pathogens* **8** (2012).

315 Donald, R. G. K., Carter, D., Ullman, B. & Roos, D. S. Insertional tagging, cloning, and expression of the *Toxoplasma gondii* hypoxanthine-xanthine-guanine phosphoribosyltransferase gene Use as a selectable marker for stable transformation. *Journal of Biological Chemistry* **271**, 14010-14019, 10021-19258 (1996).

316 Di Cristina, M. *et al. Toxoplasma* depends on lysosomal consumption of autophagosomes for persistent infection. *Nature microbiology* **2**, 17096 (2017).

317 Reischl, U., Bretagne, S., Krüger, D., Ernault, P. & Costa, J.-M. Comparison of two DNA targets for the diagnosis of Toxoplasmosis by real-time PCR using fluorescence resonance energy transfer hybridization probes. *BMC infectious diseases* **3**, 7 (2003).

318 Liao, Y., Smyth, G. K. & Shi, W. The Subread aligner: fast, accurate and scalable read mapping by seed-and-vote. *Nucleic acids research* **41**, e108-e108, 1362-4962 (2013).

319 Robinson, M. D., McCarthy, D. J. & Smyth, G. K. edgeR: a Bioconductor package for differential expression analysis of digital gene expression data. *Bioinformatics* **26**, 139-140, 1367-4803 (2010).

320 Ritchie, M. E. *et al.* limma powers differential expression analyses for RNA-sequencing and microarray studies. *Nucleic acids research* **43**, e47-e47, 0305-1048 (2015).

321 Robinson, M. D. & Oshlack, A. A scaling normalization method for differential expression analysis of RNA-seq data. *Genome biology* **11**, R25, 1474-1760X (2010).

322 McCarthy, D. J. & Smyth, G. K. Testing significance relative to a fold-change threshold is a TREAT. *Bioinformatics* **25**, 765-771, 1460-2059 (2009).

323 Phipson, B., Lee, S., Majewski, I. J., Alexander, W. S. & Smyth, G. K. Robust hyperparameter estimation protects against hypervariable genes and improves power to detect differential expression. *The annals of applied statistics* **10**, 946 (2016).

324 Yarovinsky, F. Innate immunity to *Toxoplasma gondii* infection. *Nature Reviews Immunology* **14**, 109, 1474-1741 (2014).

325 Winter, S. V. *et al.* Determinants of GBP recruitment to *Toxoplasma gondii* vacuoles and the parasitic factors that control it. *PloS one* **6**, e24434, 21932-26203 (2011).

326 Martens, S. *et al.* Disruption of *Toxoplasma gondii* parasitophorous vacuoles by the mouse p47-resistance GTPases. *PLoS pathogens* **1**, e24, 1553-7374 (2005).

327 Seidi, A. *et al.* Elucidating the mitochondrial proteome of *Toxoplasma gondii* reveals the presence of a divergent cytochrome c oxidase. *Elife* **7**, e38131 (2018).

328 Chen, A. L. *et al.* Novel components of the *Toxoplasma* inner membrane complex revealed by BioID. *MBio* **6**, e02357-02314 (2015).

329 Long, S., Anthony, B., Drewry, L. & Sibley, L. A conserved ankyrin repeat-containing protein regulated conoid stability, motility and cell invasion in *Toxoplasma gondii*. *Nature Communications* **8 (1),** 2236 (2017).

330 Liu, Y., Xue, F., Huang, M., Gan, S. & Gu, J. Separation and identification of the surface and secreted proteins in *Toxoplasma gondii* by biotin labeling and proteomics methods. *Zhongguo ji sheng chong xue yu ji sheng chong bing za zhi= Chinese journal of parasitology & parasitic diseases* **31**, 6-11 (2013).

331 Roux, K. J., Kim, D. I., Raida, M. & Burke, B. A promiscuous biotin ligase fusion protein identifies proximal and interacting proteins in mammalian cells. *Journal of Cell Biology* **196**, 801-810 (2012).

332 Hung, V. *et al.* Spatially resolved proteomic mapping in living cells with the engineered peroxidase APEX2. *Nature protocols* **11**, 456 (2016).

333 Rhee, H.-W. *et al.* Proteomic mapping of mitochondria in living cells via spatially restricted enzymatic tagging. *Science* **339**, 1328-1331 (2013).

334 van Dooren, G. G., Tomova, C., Agrawal, S., Humbel, B. M. & Striepen, B. *Toxoplasma gondii* Tic20 is essential for apicoplast protein import. *Proceedings of the National Academy of Sciences* **105**, 13574-13579 (2008).

335 Satoh, J.-i. & Tabunoki, H. A comprehensive profile of ChIP-Seq-based STAT1 target genes suggests the complexity of STAT1-mediated gene regulatory mechanisms. *Gene regulation and systems biology* **7**, GRSB. S11433, 11177-16250 (2013).

336 Lourido, S., Tang, K. & Sibley, L. D. Distinct signalling pathways control *Toxoplasma egress* and host-cell invasion. *The EMBO journal* **31**, 4524-4534, 0261-4189 (2012).

337 Mayoral, J. A., Shamamian, P. & Weiss, L. M. In vitro characterization of protein effector export in the bradyzoite stage of *Toxoplasma gondii*. *bioRxiv* (2020).

338 Toyama, B. H. *et al.* Identification of long-lived proteins reveals exceptional stability of essential cellular structures. *Cell* **154**, 971-982 (2013).

339 Toyama, B. H. & Hetzer, M. W. Protein homeostasis: live long, won't prosper. *Nat Rev Mol Cell Biol* **14**, 55-61 (2013).

340 van der Lee, R. *et al.* Intrinsically disordered segments affect protein half-life in the cell and during evolution. *Cell reports* **8**, 1832-1844 (2014).

341 Mallik, S. & Kundu, S. Topology and oligomerization of mono-and oligomeric proteins regulate their half-lives in the cell. *Structure* **26**, 869-878. e863 (2018).

342 Seeber, F., Dubremetz, J.-F. & Boothroyd, J. C. Analysis of *Toxoplasma gondii* stably transfected with a transmembrane variant of its major surface protein, SAG1. *Journal of cell science* **111**, 23-29 (1998).

343 Eden, E. *et al.* Proteome half-life dynamics in living human cells. *Science* **331**, 764-768 (2011).

344 Niedelman, W., Sprokholt, J. K., Clough, B., Frickel, E.-M. & Saeij, J. P. J. Cell death of gamma interferon-stimulated human fibroblasts upon *Toxoplasma gondii* infection induces early parasite egress and limits parasite replication. *Infection and immunity* **81**, 4341-4349, 0019-9567 (2013).

345 Kulkarni, A., Ganesan, P. & O'Donnell, L. A. Interferon gamma: influence on neural stem cell function in neurodegenerative and neuroinflammatory disease. *Clinical Medicine Insights: Pathology* **9**, CPath. S40497 (2016).

346 O'Donnell, L. A. *et al.* Interferon gamma induces protective non-canonical signaling pathways in primary neurons. *Journal of neurochemistry* **135**, 309-322 (2015).

347 O'Donnell, L. A. *et al.* STAT1-independent control of a neurotropic measles virus challenge in primary neurons and infected mice. *The Journal of Immunology* **188**, 1915-1923 (2012).

348 Burdeinick-Kerr, R., Govindarajan, D. & Griffin, D. E. Noncytolytic clearance of sindbis virus infection from neurons by gamma interferon is dependent on Jak/STAT signaling. *Journal of virology* **83**, 3429-3435 (2009).

349 Burdeinick-Kerr, R. & Griffin, D. E. Gamma interferon-dependent, noncytolytic clearance of sindbis virus infection from neurons in vitro. *Journal of virology* **79**, 5374-5385 (2005).

350 Donald, R. G. & Roos, D. S. Stable molecular transformation of *Toxoplasma gondii*: a selectable dihydrofolate reductase-thymidylate synthase marker based on drug-resistance mutations in malaria. *Proceedings of the National Academy of Sciences* **90**, 11703-11707, 10027-18424 (1993).

351 Messina, M., Niesman, I., Mercier, C. & Sibley, L. D. Stable DNA transformation of *Toxoplasma gondii* using phleomycin selection. *Gene* **165**, 213-217 (1995).

352 Livak, K. J. & Schmittgen, T. D. Analysis of relative gene expression data using real-time quantitative PCR and the 2− ΔΔCT method. *methods* **25**, 402-408 (2001).

353 McCoy, J. M. *et al.* A forward genetic screen identifies a negative regulator of rapid Ca^{2+}-dependent cell egress (MS1) in the intracellular parasite *Toxoplasma gondii*. *Journal of Biological Chemistry* **292**, 7662-7674, 0021-9258 (2017).

354 Howard, B. L. *et al.* Identification of potent phosphodiesterase inhibitors that demonstrate cyclic nucleotide-dependent functions in apicomplexan parasites. *ACS chemical biology* **10**, 1145-1154, 1554-8929 (2015).

355 Hakimi, M.-A., Olias, P. & Sibley, L. D. *Toxoplasma* Effectors Targeting Host Signaling and Transcription. *Clinical microbiology reviews* **30**, 615-645 (2017).

356 Drewry, L. L. & Sibley, L. D. The hitchhiker's guide to parasite dissemination. *Cellular microbiology* **21**, e13070 (2019).

357 Dzierszinski, F., Mortuaire, M., Dendouga, N., Popescu, O. & Tomavo, S. Differential expression of two plant-like enolases with distinct enzymatic and antigenic properties during stage conversion of the protozoan parasite *Toxoplasma gondii*. *Journal of molecular biology* **309**, 1017-1027, 0022-2836 (2001).

358 Ferguson, D., Hutchison, W. & Pettersen, E. Tissue cyst rupture in mice chronically infected *with Toxoplasma gondii*. *Parasitology research* **75**, 599-603 (1989).